DNA 5741T

FIRE, AIRBLAST, AND UNDERGROUND EFFECTS FROM NUCLEAR EXPLOSIONS-SOME CURRENT PROGRESS

[redacted]

Harold L. Brode
Dale A. Larson
Richard D. Small
Stephen J. Speicher
Frank J. Thomas

Pacific - Sierra Research Corporation
1456 Cloverleaf Boulevard
Santa Monica, California 90404

1 January 1981

Topical Report for Period 1 December 1979—1 January 1981

CONTRACT No. DNA 001-80-C-0065

Distribution limited to U.S. Government agencies only (Proprietary Information), 25 November 1981. Other requests for this document must be referred to the Director, Defense Nuclear Agency, Washington, D.C. 20305.

THIS WORK SPONSORED BY THE DEFENSE NUCLEAR AGENCY UNDER RDT&E RMSS CODE B310080464 P99QAXDB00154 H2590D.

Prepared for
Director
DEFENSE NUCLEAR AGENCY
Washington, D. C. 20305

UNCLASSIFIED

SECURITY CLASSIFICATION OF THIS PAGE (When Data Entered)

REPORT DOCUMENTATION PAGE

READ INSTRUCTIONS BEFORE COMPLETING FORM

1. REPORT NUMBER: DNA 5741T	2. GOVT ACCESSION NO.
3. RECIPIENT'S CATALOG NUMBER	
4. TITLE (and Subtitle): FIRE, AIRBLAST, AND UNDERGROUND EFFECTS FROM NUCLEAR EXPLOSIONS—SOME CURRENT PROGRESS	5. TYPE OF REPORT & PERIOD COVERED: Topical Report for Period 1 Dec 79—1 Jan 81
	6. PERFORMING ORG. REPORT NUMBER: PSR Report 1109
7. AUTHOR(s): Harold L. Brode, Stephen J. Speicher, Dale A. Larson, Frank J. Thomas, Richard D. Small	8. CONTRACT OR GRANT NUMBER(s): DNA 001-80-C-0065
9. PERFORMING ORGANIZATION NAME AND ADDRESS: Pacific-Sierra Research Corporation, 1456 Cloverfield Boulevard, Santa Monica, California 90404	10. PROGRAM ELEMENT, PROJECT, TASK AREA & WORK UNIT NUMBERS: Subtask P99QAXDB001-54
11. CONTROLLING OFFICE NAME AND ADDRESS: Director, Defense Nuclear Agency, Washington, D.C. 20305	12. REPORT DATE: 1 January 1981
	13. NUMBER OF PAGES: 244
14. MONITORING AGENCY NAME & ADDRESS (if different from Controlling Office)	15. SECURITY CLASS (of this report): UNCLASSIFIED
	15a. DECLASSIFICATION/DOWNGRADING SCHEDULE

16. DISTRIBUTION STATEMENT (of this Report)

Distribution limited to U.S. government agencies only (Proprietary Information), 25 November 1981. Other requests for this document must be referred to Director, Defense Nuclear Agency, Washington, D.C. 20305.

17. DISTRIBUTION STATEMENT (of the abstract entered in Block 20, if different from Report)

18. SUPPLEMENTARY NOTES

This work sponsored by the Defense Nuclear Agency under RDT&E RMSS Code B310080464 P99QAXDB00154 H2590D.

19. KEY WORDS (Continue on reverse side if necessary and identify by block number)

Peak Overpressure	Firestorms	Underground Testing
Dynamic Pressure	Cavity Decoupling	Shock Tube
Height of Burst	Time of arrival	Civil Defense
Nuclear Effects	Fire Damage	Nuclear Detection
Large-scale Fires	Fireball	Seismic Detection

20. ABSTRACT (Continue on reverse side if necessary and identify by block number)

This report covers research on nuclear-effects-related topics, such as airblast, large area fires, and underground testing. Analytic approximations are provided for the peak overpressure, including the double peak phenomenon, and for dynamic pressure as a function of height of burst and time. Fires accompanying nuclear warfare are covered from three perspectives. The first is a general review of urban superfires. This is followed by an analytic modeling study of such fires as they pertain to fire-generated winds, air

19. KEY WORDS (Continued)

Containment
Mach Reflection
Blast Impulse
Blast Duration
Thermal Radiation
Simulation of Nuclear Effects
Blast Waves in Tubes

20. ABSTRACT (Continued)

temperatures, and atmospheric effects; the model derives simplified differential expressions for the gas dynamics of large-scale fires. Finally, a methodology for predicting fire damage is outlined, and a flow diagram for a fire-damage prediction program is presented. Current information on cavity decoupling of underground nuclear tests from distant seismic signals is reviewed, and the potential contribution from additional underground testing is evaluated. Also discussed is the application of nuclear explosives to drive a large shock tube, allowing high overpressure and fireball exposures. The fireball phenomena to be simulated are detailed; questions regarding instrumentation and structural response in this hostile environment are explored. Other alternatives for simulating high-pressure flows are examined, and some details of a nuclear-shock-tube concept are discussed, including a method for reducing radioactive contamination in the test section.

PREFACE

This final report summarizes 1980 results for a number of studies conducted under contract DNA001-80-C-0065 for the Defense Nuclear Agency (DNA). Most of the subjects addressed under this contract have found appropriate extensions in continuing research. Nevertheless, each chapter in the present report stands independently as a useful contribution to research on nuclear effects.

Many of our results have already been disseminated beyond the immediate DNA nuclear effects community. The fire research is of interest to the Federal Emergency Management Agency and others concerned with civil defense. The airblast fits are already being used by several federal agencies. The cavity decoupling issue is of concern to the Defense Advanced Research Projects Agency, and the nuclear-driven shock tube has long been of interest to the U.S. Air Force.

Robert M. Henson, Eugene T. Herrin, and William E. Ogle, who coauthored Chap. 8, are associated with Energy Systems, Inc., Anchorage, Alaska.

TABLE OF CONTENTS

CHAPTER 1

INTRODUCTION AND SUMMARY

This report comprises eight topical reports dealing with different aspects of fire, airblast, and underground effects of nuclear explosions. Three concentrate on fire research. The first gives an overview of large-scale urban fires and reviews the outstanding questions and unresolved issues relevant to such fires, which are very likely in the event of nuclear attack. The second considers the construction of a program for predicting the probable damage from massive fires as well as the probability of fire spread, and outlines a computer program that includes some generalized flow diagrams. The third presents a simplified analytic model of the major features of gas dynamics during large-scale fires, focusing on a mathematical formulation for the flow field that permits predictions of winds, temperatures, and burn rates.

The latter two reports should be considered progress reports rather than final statements. The program for fire prediction has not progressed beyond the flow diagram and logic organization stage. Likewise, the analytic model does not yet include specific examples with quantitative results. Further useful information is anticipated from the current follow-on effort in both fire-damage-prediction modeling and analytic modeling.

Another three reports concentrate on airblast. The first presents an analytic approximation to the peak overpressure height-of-burst curves for ideal surfaces as defined by the revisions currently being incorporated into DNA handbooks. The second and third provide analytic approximations to the dynamic pressure from nuclear explosions. The latter two reports, while depending on the peak overpressure to fix the peak dynamic pressure, also provide an approximation to the time-history of the dynamic pressure and, therefore, the dynamic pressure impulse. Although much has been accomplished in the development of analytic approximations to the overpressure time-history and overpressure impulse fits for range and heights of burst, the final version of that fit is being completed under the current follow-on contract.

The final two reports are contributions to the underground-test-concept working group. The first discusses cavity decoupling of underground nuclear explosions and the relevance of research on this subject to underground testing. The second examines the rationale for and problems in developing a nuclear-driven shock tube. It does not include the details of preliminary designs or certain quantitative results of early calculations. Consequently, a revised report is in progress under the current contract.

Considerable additional effort was expended in areas that did not result in topical reports--notably, in support of the cratering and airblast working groups, on subjects of "other" nuclear hazards, on naval nuclear effects, in connection with a cavity underground experiment to investigate crater coupling, in various areas of strategic or tactical applications, and in some support of preparations for SAGE meetings.

CHAPTER 2

LARGE-SCALE URBAN FIRES

Harold L. Brode

It is fortunate that large-scale fires are rare events, since they are very destructive and a serious threat to life. Our concern with massive fires is restricted in this instance to large urban area fires, fires that involve many structures burning simultaneously. There are some features of such large area fires that are not important in the more frequent localized city fire, which may present new and unanticipated hazards to life and property during a large-scale fire. It is in the hope that a better understanding of the nature of such large-scale fires can lead to measures for minimizing casualties and damage that the current research is being pursued.

Tragic experience has taught us that a variety of major disturbances can lead to large-scale fires:

- Earthquakes--as in San Francisco, 1906.
- Civil disorder--as in the Watts riots, 1965.
- Explosions or crashes of ships, aircraft, trains, or trucks--as in the Texas City ship explosion, 1947.
- Accidental ignitions associated with no serious disruption--as in the great Chicago fire, 1871, said to have been started by an overturned lantern in a shed. (Interestingly, eight blocks of Chicago had burned the day before, due to another accidental ignition.)
- Warfare--as in the sacking of Rome, Napoleon's occupation of Moscow, or World War II.

Massive fires can and do occur under such a wide range of disruptive circumstances that their characteristics and consequences are of grave concern to those responsible for public safety and protection.

A massive fire has several unique and interrelated characteristics, all of which necessarily derive from the enormous size of the burning area--it could cover hundreds of square miles. Perhaps most significant, the air drawn in by such a fire could lead to winds exceeding hurricane speed--more than two hundred miles per hour. The winds in turn fan the flames, driving temperatures in the superfire above those normally associated with isolated building fires, or even the most serious forest fires. Temperatures are further increased by radiation entrapment in the large area covered by the flames. Such magnitude and intensity greatly accelerate the progress of the fire. It may peak in an hour or less, but then, having heated most fuels to combusion levels, may keep burning for days. Finally, the vast amounts of gas, smoke, hot air, and ashes generated by the fire may cause high casualties. The very size of the burning region precludes escape for most of those caught within the area. In World War II, for example, many casualties were attributed to carbon monoxide poisoning and heat exhaustion in the larger firestorms. Those factors are less significant in smaller fires, where escape or rescue are easier. Because of the unfamiliar aspects of the superfire, and its unusual intensity and magnitude, we must reevaluate the adequacy of emergency plans to deal with such fires.

NATURE AND CONSEQUENCES OF SUPERFIRES

The dynamics of a large area fire involve physical and chemical phenomena--and hence dangers--that simply do not exist in more conventional fires, or exist only to a minor degree. For example, the loss of life in World War II firestorms proved to be much higher than that in isolated building fires started by scattered bombing raids. Not only were many people injured by collapsing structures, but many, while trying to escape, were caught in the holocaust in the streets and burning areas outside their failing structures. Due to the higher burning rates, high winds, and higher temperatures, property damage is much more severe and complete in large-scale fires. In addition, such signs of disorganization as ineffective firefighting, poor evacuation control, looting, civil disorder, loss of other services, and disruption of utilities are likely to be severe and widespread. Finally, deleterious psychological factors arise when large groups of people experience the simultaneous loss of living quarters, possessions, and loved ones. In short, we should be concerned about superfires because

- Sources or causes of such fires are both probable enough and serious enough to affect public safety.
- Experience with such fires is almost nonexistent, and promises to be sufficiently different from that with conventional fires to merit special attention.
- The consequences of such fires are very costly in both life and property loss, making measures to mitigate them well worthwhile.

The special hazards of a large-scale fire derive from its unique characteristics. Figure 1 suggests the involvement of the atmosphere in such a fire. Picture a burning area many miles in diameter, the flames reaching hundreds of feet into the air. A plume rises above the flames, carrying burn products: smoke, ash, brands, carbon dioxide, carbon monoxide, and water vapor. Unlike the plume from a smaller, more conventional fire, this one is perhaps as wide as it is tall, and it may well up above the atmosphere in a fountain of burn products. This great upsurge of mass and energy generates a huge toroidal circulation, the rising plume feeding a flood of gases outward at some high altitude, which in turn cool and cause a subsiding fallout and a downflow of air toward the outskirts of the fire at ground level.

Perhaps the most unusual and important consequence is the extremely high winds rushing into the burning region, further increasing burning rates.(1) Such winds may exceed any experienced in natural meteorology. Indeed, the flames near the periphery may be laid nearly flat by the inrushing winds. Exceedingly fierce burning rates may result in the total combustion of all fuels within the fire area and the melting or destruction of many noncombustible structural materials. The wind alone may cause extensive damage to structures outside the burning area.

A detailed analysis of large-scale fires would include many of the pertinent variables listed in Table 1. Although the size of the

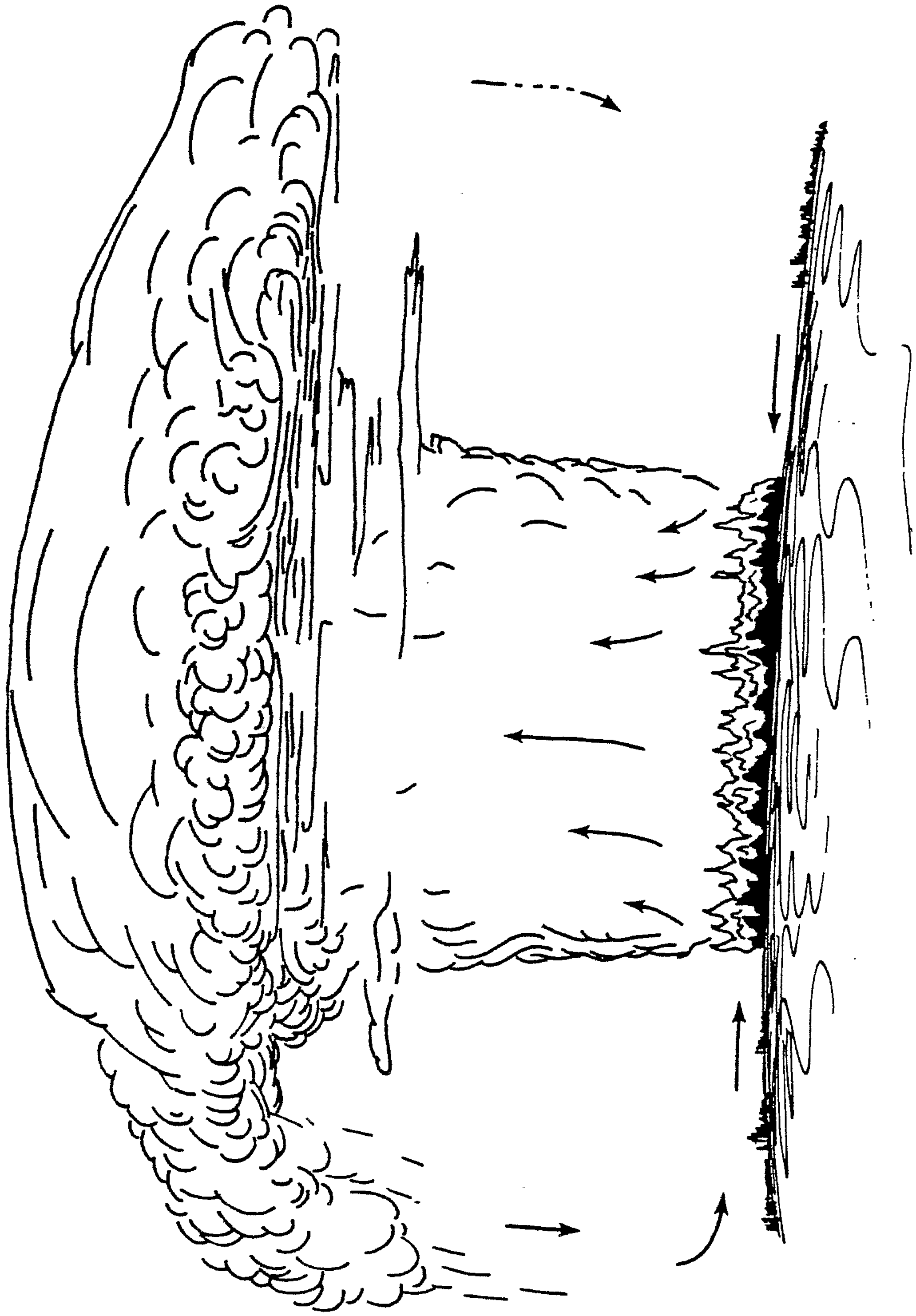

Figure 1. Plume and involvement of atmosphere in massive fire.

Table 1. Physical characteristics of burning zone.

Size of burning area	Topography
Size of potential burnable area	Fuel types
Flame height	Fuel density
Combustion rates	Fuel combustibility
Total heat released	Firebreaks and fuel distribution
Gas generation	Construction continuity
Temperatures	Combustibility of building contents
Expansion and buoyancy of plume	Building sizes

actively burning area is most crucial, the extent and nature of the smoke column is also important: its rate of rise; the altitude to which it rises (i.e., the degree of buoyancy of plume components); the smoke, ash, and brands carried aloft; the amount of spreading or growth of the plume; the degree of mixing with the atmosphere; and the various physical components and reaction rates of combustion products within the plume, and their influence upon the local meteorology (for example, large fires often generate rain).

As noted in connection with atmospheric recirculation, we are particularly interested in the development of hurricane-force surface winds feeding the fire, the influence of such winds on fire spread, the generation of fire whirls, and the distribution of firebrands and ash.

PAST LARGE-SCALE FIRES

Table 2 lists some well-known large-scale urban fires/disasters of the past, two of which illustrate very different dynamics and consequences. The great London fire of 1666 destroyed a large area of the old city, yet very few lives were lost. Like the Chicago fire of 1871, this one spread slowly enough from a single ignition point that people were able to escape the flames. The 1906 earthquake in San Francisco, on the other hand, generated some 30 separate ignitions that burned a great deal of the city, with considerable loss of life. The earthquake

Table 2. Some past large-scale urban fires.

City	Year	Deaths	Burned Area (km^2)	Comments
London	1666	8	1.8	Burned 5 days, 13,000 homes lost
New York City	1835			
Charleston, South Carolina	1838			
Pittsburgh	1845			
Philadelphia	1865			
Portland, Maine	1866			
Chicago	1871	50	8.6	Burned 1 day, 98,500 homeless (17,500 homes lost)
Boston	1872			
San Francisco	1906	452	12	Earthquake-generated explosions and fires, 30 ignitions, burned 3 days, 100,000 homeless
Halifax	1917	2000		
Tokyo	1923			
	1925			
	1932			
Nigata	1925			
Yamanaka	1931			
Hakodate	1934	2000		Generated firestorm
Takaoka	1938			
Boston	1942	1000		Explosion and fire, burned 3 days, 3000 injured, 300 missing
Muramatsu	~1946			
Texas City	1947	510		Fertilizer ship explosion
Chungking	1949	1000		
Brussels	1967	250		Burned 6 hours
Chelsea	1973			400 homes lost--many firemen involved

interrupted normal firefighting capabilities and broke water mains, so the fires spread and burned essentially uncontrolled.

During World War II, many bombing raids were designed to start fires, because in industrial or urban areas, fire could cause more damage than could comparable loads of high-explosive bombs. Firebombing occurred in some 71 German cities or urban centers; Table 3 gives a partial list of centers in which significant loss of life occurred.[2,3,4]

As the table indicates, some of those cities suffered a kind of firestorm action, with very fierce burning. In most such cases, the loss of life was much higher than in cities where individual fires did not coalesce.

Table 3. Casualties in German cities firebombed during World War II.

City	Population (in thousands)	Deaths[a] (in thousands)	Burned Area (ha)	Comments
Dresden	300[b]	135-250 (42%)	1950	Firestorm
Hamburg	90[b]	35-100 (45%)	1180	Firestorm
Berlin	4420	52 (1%)	--	Many small fires, many raids, no firestorm
Darmstadt	17[b]	8-15 (49%)	390	Firestorm, deaths due 90% to asphyxiation
Kassel	56[b]	6-9 (13%)	760	Firestorm
Heilborn	78	6-8 (10%)	--	Firestorm
Cologne	757	3.8-5.6 (<1%)	--	--
Wuppertal-Barmen	9[b]	2.6-5.2 (34%)	260	Deaths due 65% to fire
Augsburg	12[b]	3.1 (16%)	160	--
Duisburg	410	1.5-2.6 (<1%)	--	--
Bremen	434	1.2 (0.3%)	--	--
Schweinfurt	1[b]	1.0 (100%)	--	--
Pirmasens	50	0.6 (1%)	--	--
Brunswick	216	0.56 (0.3%)	--	Firestorm, 23,000 rescued
Braunswig	241	0.52 (0.2%)	--	Firestorm

NOTE: A total of 71 German cities were attacked with firebombs. This table lists 15 in which significant loss of life occurred. In total, German cities suffered 500,000 to 800,000 deaths. Some 49 of the 71 cities lost at least 39 percent of all residential units.

[a]The numbers in parentheses indicate the percentage of the population at risk (in the vicinity of the fire) who died; or, if that statistic is unknown, the percentage of the total population of the city.

[b]Population at risk.

Figure 2, an aerial view of burned-out buildings in the center of Hamburg, discloses the extent of the destruction from the firestorm in that city. The photograph shows that the flames burned on both sides of a very wide street. Only the shells of some of the buildings were

Reproduced from Fire and the Air War. Copyright © 1946, National Fire Protection Assn.

Figure 2. Aerial view of burned-out residential area of Hamburg.

left standing, a tribute to their massive masonry construction. Ordinary fires could burn out a single such building, leaving the abutting structures unscathed. Only in firestorm circumstances were all structures consumed. Large segments of the population succumbed (about 45 percent of those at risk--see Table 3). Figure 3 shows the desiccated corpses of victims of heat prostration and carbon monoxide poisoning--the most common causes of death in basement shelters. Figure 4 shows the corpse of a man who had been caught in the flames, heat, and high winds in the streets of Hamburg during the firestorm. Figure 5--a view of the burned-out center (old part) of Dresden--shows similar consequences. Here the three- to five-story buildings were mostly centuries old. The high density of structures loaded with combustibles contributed to the intensity of the fire. Note that many old masonry walls collapsed. Loss of life in this fire may have been the largest in history--135,000 to 250,000 dead.

In all the European bombing, the most intense damage and the greatest civilian loss of life--as well as the greatest impact on the

Reproduced from Fire and the Air War, Copyright© 1946, National Fire Protection Assn.

Figure 3. Desiccated corpses, Hamburg.

Reproduced from Fire and the Air War, Copyright© 1946, National Fire Protection Assn.

Figure 4. Body of man caught in street, Hamburg.

Reproduced from The Destruction of Dresden, London, 1963.

Figure 5. Aerial view of burned-out buildings at center of Old Dresden.

German war effort--resulted from these firestorms. The Allied planning staffs found that creating such fires was neither simple nor easy. A multitude of crews manning hundreds upon hundreds of bombers dropped high explosives as well as firebombs, in order to break up tile roofs and deter firefighters, while lighting fires within the buildings.

In most cities, the German defense was well organized, including effective air defenses with both fighter aircraft and antiaircraft batteries. They could generally harass the Allied bombers enough that their bomb drops were inaccurate or missed the targets completely, thus reducing the density of ignitions. Such defense measures were augmented with extensive firebreaks to inhibit the spread of fire. In addition, European building policy had long dictated firewalls between adjacent structures, to prevent the spread of fire from building to building. The Germans also built elaborate shelter systems--both basement shelters and, where water tables were too high to permit underground construction, large above-ground bunkers. Finally, they had fairly sophisticated firefighting equipment, ample water supplies, and well-trained firefighting crews. They had thousands of trained firefighters to combat some of the worst fires, often quite successfully limiting the damage and providing extensive rescue and medical aid. Throughout most of the war, the Germans were busy with repair and rehabilitation.

In Germany, the firebombing and the consequent firefighting developed over a period of several years (1941 through 1945). In Japan, on the other hand, the bombing attacks began in 1945 and peaked in a matter of a few months. Japanese defenses were more primitive at that late stage in the war, and their air defenses were relatively ineffective. Moreover, Japanese cities had primitive or antiquated firefighting equipment and quite inadequate training for firemen. To make matters worse, Japanese construction practices did not emphasize built-in fire containment. Structures tended to be close together, with few intervening firewalls or firebreaks, although by 1945 many Japanese cities--including Hiroshima--were busy creating firebreaks. Despite the value of firebreaks in containing fires with well-defined origins, however, they are less effective in impeding fires started by "area" sources, such as earthquakes, firebombing raids, or nuclear explosions.

Firebreaks in Tokyo failed to stop the spread of fire there, and the fires set by the raid in one-third of the city spread to engulf another third of Tokyo-Yokohama.

In addition, by 1945 the U.S. Air Force had acquired the much bigger B-29 bombers that could carry heavier bomb loads than the aircraft used in Europe. They were also able to fly relatively low-altitude bombing runs, allowing crews to concentrate firebombs in the most susceptible areas.

Some 65 Japanese cities were firebombed in those months of 1945, including Tokyo (the first hit and worst damaged), Osaka, Kobe, Kyoto, Nagoya, and Kunugaya (the last attacked). Figure 6 is an aerial view of a portion of the city of Nagoya, showing in the foreground some of the effects of fire. Along the canal, the firebreak under construction can be seen; in the background, the dense construction of Japanese cities is evident.

In the last weeks of the war, the atomic bombs dropped on Hiroshima and Nagasaki started fires in nearly every structure within a mile of the burst. Most of the buildings within that distance from ground zero in the city of Hiroshima were totally destroyed by the resulting firestorm. Fires in Nagasaki were also of firestorm intensity, but not as large in area coverage because of variations in the density of structures and the greater importance of topographical features. The Tokyo fire resulting from the first of the 1945 firebomb raids on Japan caused more casualties than resulted from either the Hiroshima or Nagasaki attacks, and a much larger area was destroyed in Tokyo (41 km^2 compared with 11 km^2 at Hiroshima). But these latter were small cities attacked with what may now be considered low-yield nuclear weapons. Larger cities have more to burn, and larger yield weapons expose more to ignition.

FIRES FROM NUCLEAR WARFARE

Today the greatest military threat comes from nuclear weapons--in general, weapons of a thousand times larger yield than those used in Hiroshima (14 kT) and Nagasaki (23 kT). Although radiation and the initial blast would cause great damage, fires represent the most serious threat to life and property in a nuclear attack. Fires are

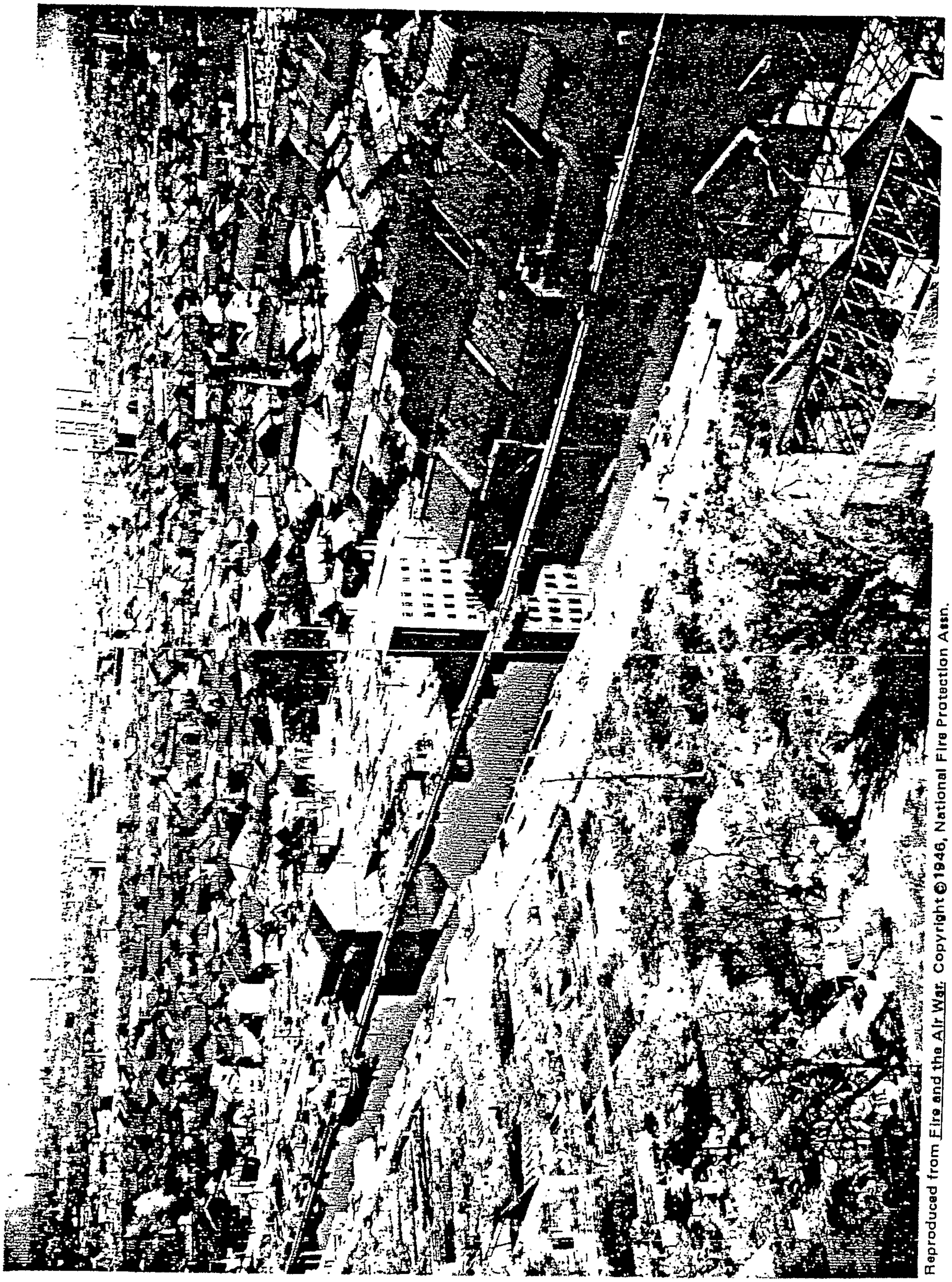

Figure 6. Aerial view of burned-out section of Nagoya.

created both by the initial thermal radiation--that is, the bright light and intense heat of the radiating fireball; and by the physical disruptions caused by the nuclear blast wave--that is, the scattering of existing fires as well as the overturning, bursting, and spilling of fuel containers or combustibles. With so many ignitions expected throughout large areas, the individual fires will almost certainly grow, then amalgamate into one great conflagration. That fire may in turn be driven before the wind, or become a firestorm that burns in super-bonfire fashion at high intensity--generating hurricane-force surface winds and an enormous rising column of smoke and hot gases.

Primary Fires

In primary fires ignited by a nuclear burst--i.e., those started by the intense thermal radiation--many factors determine whether exposed fuels will ignite or not. Table 4 enumerates the principal factors characterizing the source, the transmission, and the exposed materials that control ignition. In addition, other factors can be important, such as air temperature, blast-flame interactions, dust obscurations, or reflections from surrounding materials.

Table 4. Factors influencing primary fires.

Source Factors	Transmission Factors	Material Factors
Weapon yield	Distance from burst	Color
Burst height	Visibility (transmissivity)	Reflectivity
Fireball contaminants	Clouds/fog/mist	Conductivity
Fireball shape	Smoke/haze/smog/dust	Density
	Humidity/water vapor/rain	Thickness
	Altitude (air density)	Moisture content
	Fireball shadowing	Flammability
		Surface roughness
		Exposure angle

Atmospheric bursts--in the air above the target--demonstrate a complex time history of thermal radiation, with a double peak and a pulse that lasts (for megaton weapons) for several seconds. If bursts occur at very high altitudes where the air is so rarefied that the fireball dissipates rapidly, then the thermal pulse may be more intense but last for mere milliseconds. The pulse of light from a burst outside the earth's atmosphere may last even shorter times, being measured in microseconds. Yet each is capable of igniting fires. Sketches of such bursts are shown in Fig. 7, together with corresponding graphs of the thermal flux as a function of time.

Secondary Fires

Secondary fires are those ignited as a result of mechanical disruption by the blast wave, by ground motion, or by debris impact from a nuclear detonation. Much of the damage from conventional high-explosive bombing in World War II was due to disruption fires. However, there is little record of such fires playing a significant role in the firebomb raids. In the atomic bombings of Hiroshima and Nagasaki, the relative importance of secondary fires has never been satisfactorily resolved. Certainly there were many opportunities for charcoal cooking fires (hibachis) to be overturned and brought into contact with flammables. Nevertheless, very few specific fire starts, either primary or secondary, have been documented for either city.

Experience with disruptive events, such as explosions, earthquakes, hurricanes, and bombing raids, suggests a long list of potential fire sources in elements common to modern urban areas:

Open flames
Arc or spark ignitions
Short circuits
Hypergolic or exothermic chemical spills
Broken furnaces or boilers
Scattered cooking fires
Ruptured fuel tanks
Spilled volatiles
Broken pipelines
Vehicle impacts (railroads, trucks, autos)
Burnable/detonatable dust raised
Friction/spark fires started
Overturned space/water heaters, with gas ignited by pilot lights

Because of its intensity, a nuclear blast would greatly exacerbate these same sources. Multiple nuclear bursts would even further increase the probability of secondary fires. If the first burst was followed by additional bursts, then fuels exposed by the first might be ignited by the subsequent thermal pulses. In addition, the fires

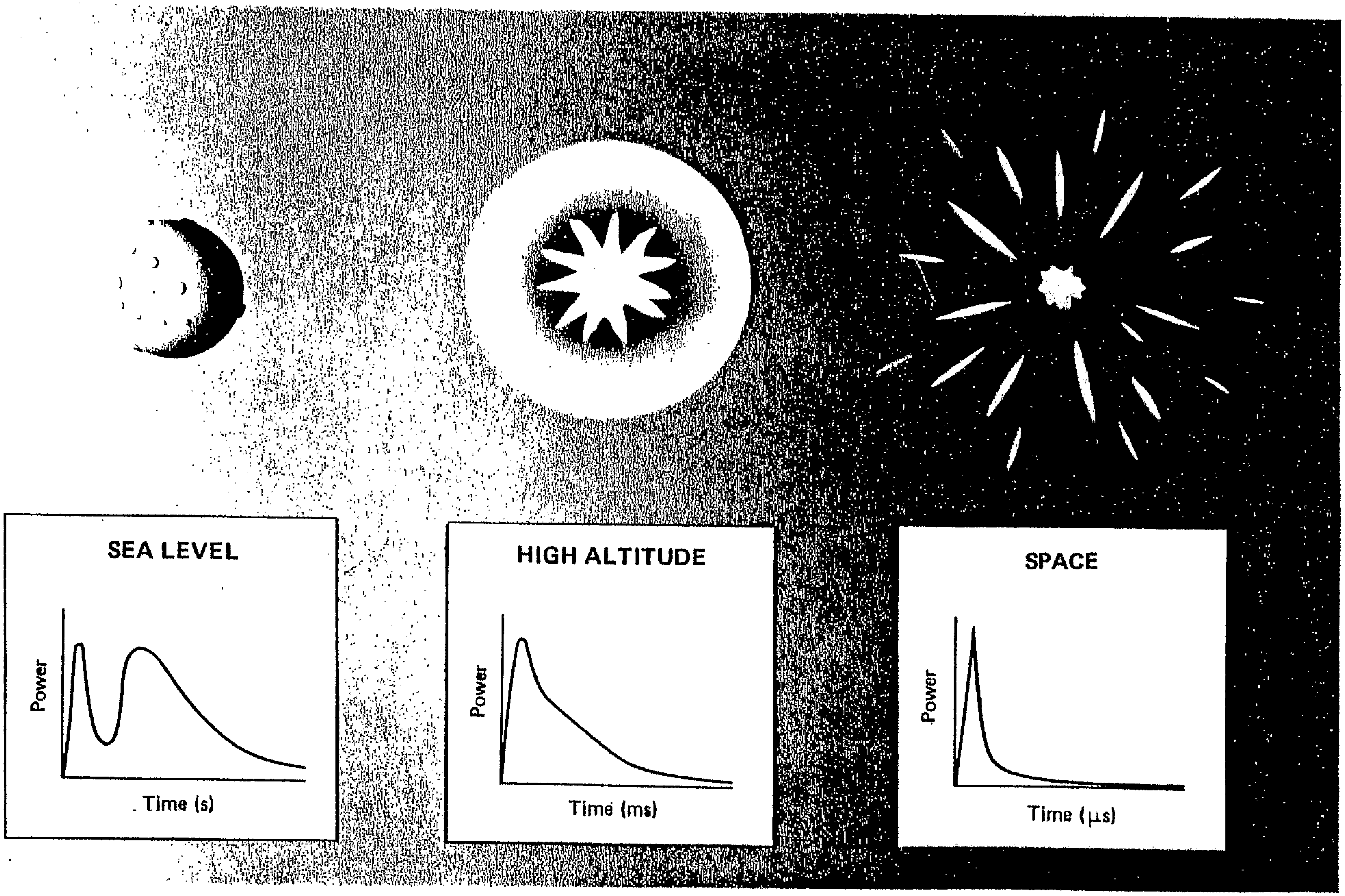

Figure 7. Sketches of high-altitude bursts and effects of altitude on thermal pulse.

initiated by the first bomb might be spread by blast winds from subsequent bursts.

POSSIBLE MITIGATING MEASURES

In light of the enormous carnage and confusion accompanying a nuclear attack, and the unprecedented potential for casualties and damage from the subsequent fires, it is often said that few meaningful preventive or mitigating safety measures can be taken, and that our greatest hope is to avoid entirely the use of nuclear weapons. The more I learn about nuclear weapon effects, the more convinced I am that their use should be avoided. But since we are not free to dictate to the world what weapons may be used, it may be important to question the notion that nothing much can be done to minimize loss of life and damage. Reasonable and modest civil defense preparations have been very effective in reducing the harmful effects of both natural and man-made disasters.

For example, the occasional mass rescues of persons caught in firestorms in Germany in World War II required considerable prior planning and preparation. The fires were fought for days by thousands of trained firefighters. Some rescues were accomplished by creating a water spray tunnel leading to shelters within the burning region. Some massive shelters were constructed and made safe by deep burial or by heat-resistant construction; but they seldom had adequate sources of fresh air for firestorm survival.

Successful rescues during large-scale fires are possible only with training, discipline, organization, experience, timely acquisition of accurate information, and maintenance of good communications. Such a capability was developed gradually as the war progressed; and the need became more acute as bombing raids increased in frequency and intensity. When it comes to preparations, the hard questions are usually not what *can* be done but what *should* be done in the context of limited budgets, rising objections to inconvenience and regulation, and no obvious or immediate need for such expenditure and effort.

Before advocating an extensive and sophisticated shelter program, acquisition of techniques appropriate for massive fires, or promoting a particular plan for community recovery or repair in the aftermath of a superfire, we must understand what actions are possible before, during, or after a nuclear attack. *Before an attack,* many measures are both possible and prudent--construction of fire- and blast-resistant shelters, planning for mass evacuations, training of personnel for fighting large-scale fires, providing extraordinary water storage, protecting firefighting equipment and personnel from blast and fire, creating storage and availability for essential emergency materials, providing protection for particularly sensitive communication and command elements--all properly the responsibilities of professional firefighters, urban planners and administrators, and emergency management authorities. Plans and budgets must be worked out for dealing realistically with the extraordinary problems and expenses, and convincing arguments put forward to convince legislators and funding agencies of the need for support.

While a massive fire is raging, conventional firefighting organizations become overwhelmed, and coordinated actions are extremely difficult; such was often the case in World War II, even with well-trained and organized rescue and fire-suppression crews. Although some rescue and evacuation may be possible, as well as limited peripheral fire suppression, the inner portions of a firestorm defy any prolonged or concerted effort. And the ever-present threat of more nuclear bursts is likely to preclude meaningful action. *Postattack* activities are primarily related to relief and relocation of displaced and homeless persons, and to reconstruction or rehabilitation of facilities. Here again, thoughtful planning and stockpiling of crucial items can greatly speed recovery.

Table 5 lists the most obvious measures for preventing or mitigating the consequences of superfires. Although most of the measures listed may be self-evident, the details of how to accomplish each are far from clear, and may depend a good deal on local conditions as well as on our appreciation of the forces that govern a superfire. Relocation may be the ideal solution, but both residential and industrial locations are determined by a great many factors, and the hazards of a large-scale fire may be thought too unlikely to influence a decision.

Table 5. Civil defense actions related to superfires.

Preparatory Actions	Firefighting Actions	Postfire Actions
Relocate industries or residential complexes	Suppress flames	Provide relief
Construct fire-resistant structures	Rescue and evacuate	Reconstruct essential facilities
Plan for evacuation	Limit damage	Relocate industries and residences
Aid local water storage	Maintain access	Rehabilitate damaged structures
Provide thermal protection	Establish communications	Revise regulations
Train and educate professionals	Provide emergency fresh air/oxygen	
Build fire- and gas-proof shelters		

For example, consider the many residences in Southern California that are built on the sites of burned-out homes in the highly flammable mountains. Location in areas of low-density fuel and population would reduce the fire hazard, but might not meet the overriding economic needs of an industry or the life-style criteria of a household.

In addition to nonflammable exteriors (walls, roofs, window frames) and removal of combustibles from around or in key structures, wind resistance and structural dynamics under high external heat loads may be important. Underground or below-grade construction is particularly suited to resisting massive fires and nuclear effects (blast, debris impacts, thermal and nuclear radiation). Partially buried buildings are often advocated as energy conserving as well.

Mass evacuations seldom go smoothly without considerable planning and some rehearsal. Evacuation within an urban area already engulfed by fire requires heroic effort, high-performance equipment, good communication and cooperation between well-trained and experienced crews, and considerable planning. Such a rescue was accomplished in a 1944 incendiary attack on Brunswick, Germany, where the fire burned for six days. Large firefighting crews (4500 men) created a water spray screen or tunnel leading to shelters within the burning area, then evacuated 23,000 people through the heart of the raging firestorm. However, many died inside shelters before the rescuers could reach them. Most shelters provided little protection from the total devastation of a firestorm. In one basement shelter, for example, only 9 out of 104 persons were revived; the others had been killed by carbon monoxide and heat.

Moreover, simple evacuation to open spaces, such as parks, river banks, and railroad yards, often proved inadequate in the firestorms of World War II. Since then, urban areas have expanded, and the likelihood of simultaneous ignitions over larger areas has increased, so evacuation problems are likewise seriously exacerbated. However, with training, organization, and practice, very impressive evacuations become practical. Witness the evacuation each evening by more than one million people from Manhattan Island.

Local water storage and mobile emergency pumping capacity are much-needed assets during major fires or disasters, since sudden demand combined with damaged distribution systems make for unreliable conventional sources in times of emergency. Where possible, below-grade storage and auxiliary power pumps with both blast and thermal protection would be more reliable. Such protection could be important in the event of earthquake, hurricane, or flood, as well as nuclear attack. Water requirements vary for control of local fires, but demand may grow considerably during a massive fire, when water may be used to provide long-term cooling and spray screens to protect against heat and flames from surrounding areas.

Thermal protection in the form of reflective outer coverings for structures and equipment or window protection with nonflammable and reflective closures (e.g., aluminum foil) may be helpful in reducing ignitions from nuclear bursts, as well as in combating the radiation from surrounding fires. In great firestorms, however, high winds may strip coverings, break windows, and transport heat convectively, making radiation shielding of minimal value without further protective measures. Covering machines and critical pieces of equipment with masses of earth (after encasing them in grease or plastic) could provide good thermal protection as well as blast and debris-impact resistance.

Of particular importance--because of the accompanying physical damage from blast and other effects--is the maintenance of access and communication. In many cases in burning German cities, effective coordination of firefighters ceased with loss of communications. The fires raced out of control, and rescue operations were much inhibited. Ready access and communications are essential to effective damage limitation and mitigation, and require thorough planning and proven equipment as well as protected radios and telephone systems.

Training and experience under emergency conditions or in simulated exercises are equally vital. Few emergency crews function efficiently without some prior exposure to similar conditions, or to simulated emergency action. The problem is to know what to simulate, since the mass fire is unfamiliar; and how to simulate it, since the environment is likely to be of extreme winds, temperatures, and durations. Even experienced firefighters may not comprehend how very limited will be the opportunities to operate, withdraw, move about, communicate, or seek shelter within a mass fire; they may need special indoctrination and training to successfully confront the unusually life-threatening environment of a superfire.

Recovery can be much accelerated through advance planning and stocking of key equipment and supplies. Since local sources of such items are likely to be unavailable, it is of relatively greater importance to provide and protect the most crucial materials. Before making and implementing such plans, however, we must construct a model of the postfire circumstances, using it to analyze the constraints imposed on postfire operations. What will be the damage? What should the postfire objectives be? What are the priorities? What manpower will be available? What skills will be most needed?

THE MESSAGE TO REMEMBER

To be effective, advance planning and preparations should take into account the unique dynamics and consequences of a superfire, which derive from very large areas burning simultaneously. Unlike most urban fires, which involve a single or a few buildings, superfires resulting from nuclear attack will develop from many tens of thousands of ignitions over a vast area, and will converge into a single enormous fire. Very little effective firefighting is possible at the peak of such a massive fire; and even extraordinary lifesaving or survival techniques would be of limited usefulness. The violent environment created by such fierce firestorms is difficult to appreciate, since we have never experienced fires of such large dimensions. Some indications from history and from our approximate calculations suggest that large-scale fires would be accompanied by hurricane-force winds that would fill the air in the fire area with hot gas and flames. Even outside the burning area, the winds themselves could cause considerable damage and prohibit effective evacuation, rescue, or firefighting. Entire buildings could be blown down and streets blocked at considerable distances from the burning area.

In such a holocaust, the utility and adequacy of prior preparations and plans will depend on the extent to which planners have comprehended the need for efforts well beyond the normal measures for fire protection and suppression. There is a great potential for saving lives and limiting damage from such large-scale fires, but special planning and coordinated actions are necessary. Special construction or even relocation would be necessary to ensure survival of any industry and its employees. Partially buried or below-grade designs and isolated sites may become more acceptable when the true nature of massive fires is better understood, and nuclear attack perhaps more immediately probable. Unfortunately, such relocation and construction require years, and strategic warning or changes in threat perception can occur in much shorter times.

What to expect? Plan for very high winds, very high temperatures, and often poisonous gases in or near a superfire. Plan on little effective firefighting, rescue, or evacuation during such a fire. Plan on superfires accompanying a nuclear attack, and being a likely consequence of several other large-scale disasters such as earthquakes, hurricanes, explosions, or large spills of combustibles--any of which could overwhelm conventional means of fire suppression and spread fire over large urban areas.

IMPORTANT RESEARCH STILL NEEDED

It is clear that we know very little about either the dynamics or the consequences of superfires--especially those resulting from nuclear attack. Indeed, we have scarcely formulated the questions that must be answered. For example, what is the probability that a superfire would result from a nuclear attack on an urban area? That is, would a superfire result from every attack, most, some, few? What is the rationale for the decision? Is it calculable? Is it highly dependent on weather, on the structure of the attacked city, on the nature of the nuclear attack? What are the important variables? What damage would be exclusively due to fire, rather than blast? How is fire damage different from blast damage? More severe? More permanent? What is the relationship of fire damage to postattack recovery relative to that for blast damage? Are blasted structures more easily rehabilitated?

Other questions relate to casualties or hazards to life. Most deaths in Hiroshima resulted from fire--but directly or indirectly? That is, were the victims initially trapped by blast and only subsequently killed by fire? During the major raids in Germany and Japan, many died because fire filled the streets and cut off escape routes, whereas relatively few died in the localized fires ignited by scattered and less intense raids.

Will fire spread be important? What are typical fire spread ranges? That is, what percentage of the total fire area is beyond the initial ignition area? Obviously, if the fire is started by an isolated source--as in Chicago in 1871--the spread area comprises the total area engulfed by flames. A large fire raid or nuclear attack, however, causes multiple primary and secondary ignitions over a large area, which then merge and spread over an even greater area. Therefore, we must calculate the threat of fire spreading into undamaged or only partially damaged regions, as well as the dependence of fire size on variables such as nuclear yield, height of burst, and atmospheric transmission.

What sort of winds can be expected to accompany such fires? How fast? How long might they blow? How high might they reach into the atmosphere? What would be the scaling for these winds versus yield, fire size, density of fuel, intensity of burning? What effect would atmospheric conditions have? Is topography important? What local environments would be produced by a superfire? That is, what concentrations of carbon dioxide, carbon monoxide, smoke, hot air, and so on? At what velocity would fire-generated winds themselves destroy buildings, independent of the fire itself? What size of fire generates such winds, and what type of construction resists wind damage? What is the decay pattern for winds outside the fire? That is, how rapidly do wind velocities fall as a function of range beyond the fire?

How can the effects of fire be included in targeting? That is, how can the targeteers or damage assessment methodologies take into account the additional damage due to fire? How can civil defenders prepare for the consequences of phenomena unique to large-scale fires? What will constitute adequate shelter and rescue? Must shelters provide a fresh air supply other than that drawn in from outside on the streets? Must they have stored compressed or liquid air or bottled oxygen? Will it be possible to create rescue avenues in such fires or will the burn products--such as carbon monoxide--poison the firefighters and rescue personnel, thus crippling civil defense operations? Will the winds themselves hamper or prevent rescue efforts?

Presuming surface winds are a major problem, how effectively would nonflammable areas such as rivers, very wide streets, or firebreaks block large-scale fires and thus reduce the attendant surface winds? Might analytic models of superfires provide useful quantitative descriptions of the holocaust environment? That is, will we be able to easily predict the fire environment as a function of the more obvious variables--yield, height of burst, nature of the city, type and density of construction, available fuel?

Using current analytic models, how much can we predict about the scaling of winds or circulation, burning rate and influence of fire circulation on burning rate, or other behavior of superfires?

Research could help delineate the damage expected from a superfire, and could aid both those planning or assessing nuclear weapon attacks and those planning defense against such attacks. As long as the consequences are so poorly understood, little effort is justified in including fire damage in targeting considerations--meaning not only that much damage is not counted, but also that much larger attacks than necessary may be planned. On the defense side, efforts at sheltering or evacuation might be drastically affected by the consequences of large-scale fires. Some areas where research on large-scale fires would be of help are as follows:

Spread by fire-induced winds: role of high winds in flame dynamics.
Spread by radiation: radiation environments in large area fires.
Spread by brands: possible enhanced firespread by brands in high winds.
Life threats in shelters: added hazards in a superfire.
Death and destruction due to fire winds: hurricane forces outside the fire.
Effectiveness of firebreaks: value in the context of large-scale fires.
Effectiveness of thermal shielding: can fire ignitions be reduced and superfires avoided?
Possibilities for rescue: what kinds of organizations and equipment would be effective in a superfire?
Possibilities for effective fire suppression: planning and preparations in the face of large area fires.
Appropriate overall planning and organization to deal with superfires.
Multiple bursts: the increased hazards of fire starts from more than one burst.
Blast-fire interactions: blast waves can blow out or spread fires, and thus add or subtract from the hazard.
Secondary fires: the role disruption fires play in large area fires.

Agencies such as the Defense Nuclear Agency or the Federal Emergency Management Agency currently sponsor research on nuclear effects, and in particular, work toward a better understanding of the damage and life-hazards possible from nuclear-induced fires. Some of their fire research efforts are aimed at the above problem areas, but a coordinated program has been slow to materialize. Greater program emphasis and corresponding budgetary attention to the subject would help bring the importance of understanding large area fires into focus.

REFERENCES

1. Small, R. D., and H. L. Brode, *Physics of Large Urban Fires*, Pacific-Sierra Research Corporation, Report 1010, March 1980.

2. Bond, H. (ed.), *Fire and the Air War*, National Fire Protection Association, Boston, 1946.

3. Taylor, D. H., *Methodology for Estimating Casualties from High Intensity Attacks*, SAI, February 1978.

4. Irving, D., *The Destruction of Dresden*, Wm. Kimber and Co., London, 1963.

CHAPTER 3

METHODOLOGY FOR PREDICTING URBAN FIRE DAMAGE FROM NUCLEAR BURSTS

Richard D. Small
Harold L. Brode

The work reported in this chapter is an initial effort to develop a capability for predicting damage from nuclear-weapon-induced fires. The result will be an algorithm that assists the user in evaluating nuclear-induced fire effects in any urban-industrial area. There already exist fire-damage or fire-spread prediction codes such as the Stanford Research Institute program as modified by Science Applications, Inc.* Our objective is to provide a more flexible program that can accommodate a detailed analysis of fire damage in specific cities as well as very general predictions of the extent of fires in unspecified urban areas. More important, the program's results should be compatible with targeting procedures, and its predictions should be as reliable as those for blast damage. If the latter can be accomplished, then a distinct improvement is possible in targeting and in the effective application of nuclear weapons. Further, such a reliable prediction technique may allow more realistic evaluation of collateral damage hazards and defensive actions.

This section details the organization of a master computer code. Our goal is a code that computes fire damage, but we include blast effects because of the interdependence of blast and thermal processes. The current vulnerability number (VN) system for treating blast effects can be incorporated--possibly with minor modifications--into the suggested format.

In addition to providing an outline for a final user code, the flowcharts (Figs. 1 through 8) provide a framework into which future research results should fit. The relationships between the various fire-related physical processes are clarified, and areas in which our current understanding or predictive capabilities are deficient can be evaluated. Thus, monitoring the development and progress of relevant fire research will be assisted, and useful guidance for remaining work may result.

---

*Drake, M. K., M. P. Fricks, D. Groce, C. J. Rindfleisch, Jr., J. B. Swenson, and W. A. Woolson, *An Interim Report on Collateral Damage*, DNA Report 4734Z, Science Applications, Inc., October 1978.

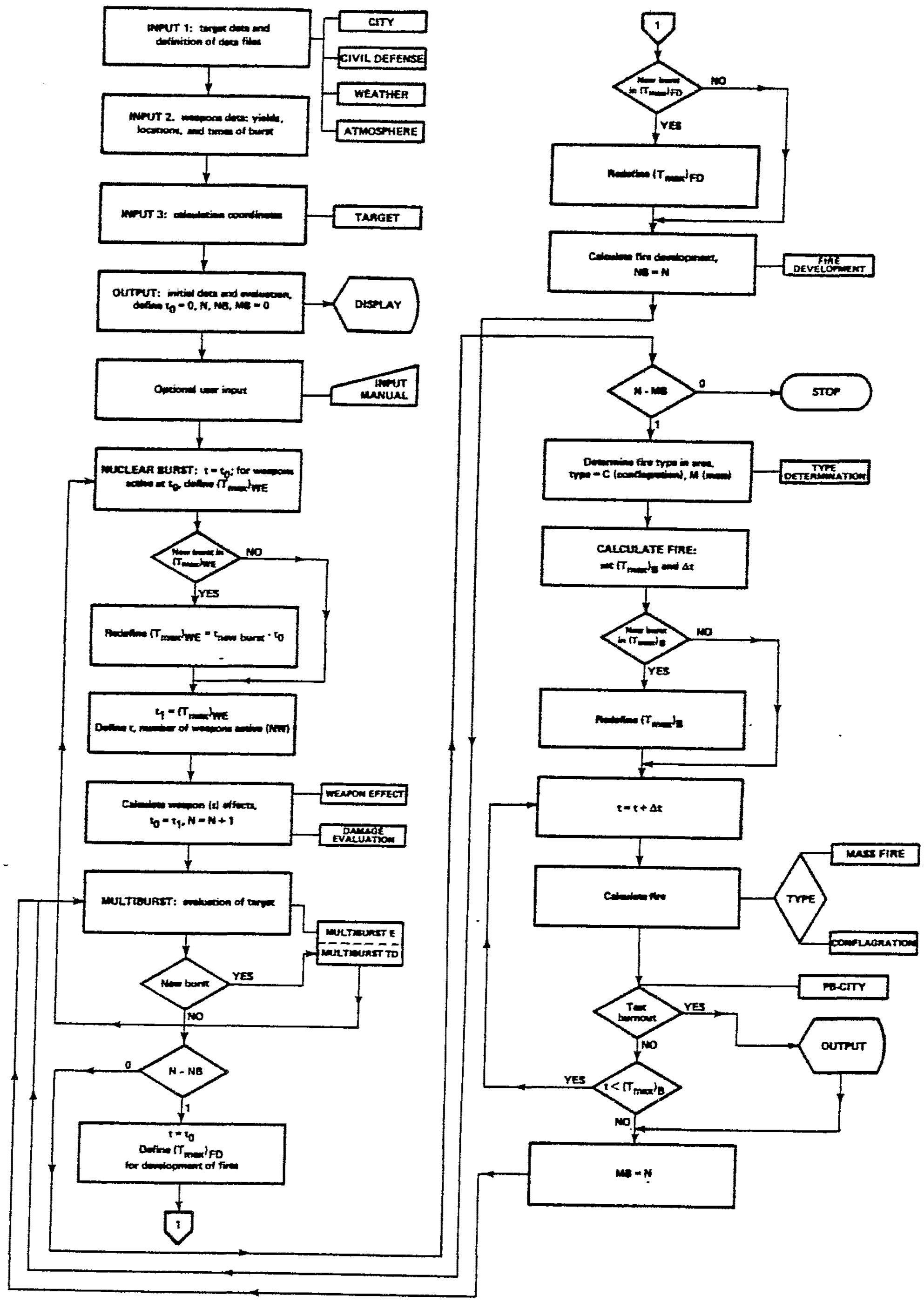

Figure 1. MAIN program.

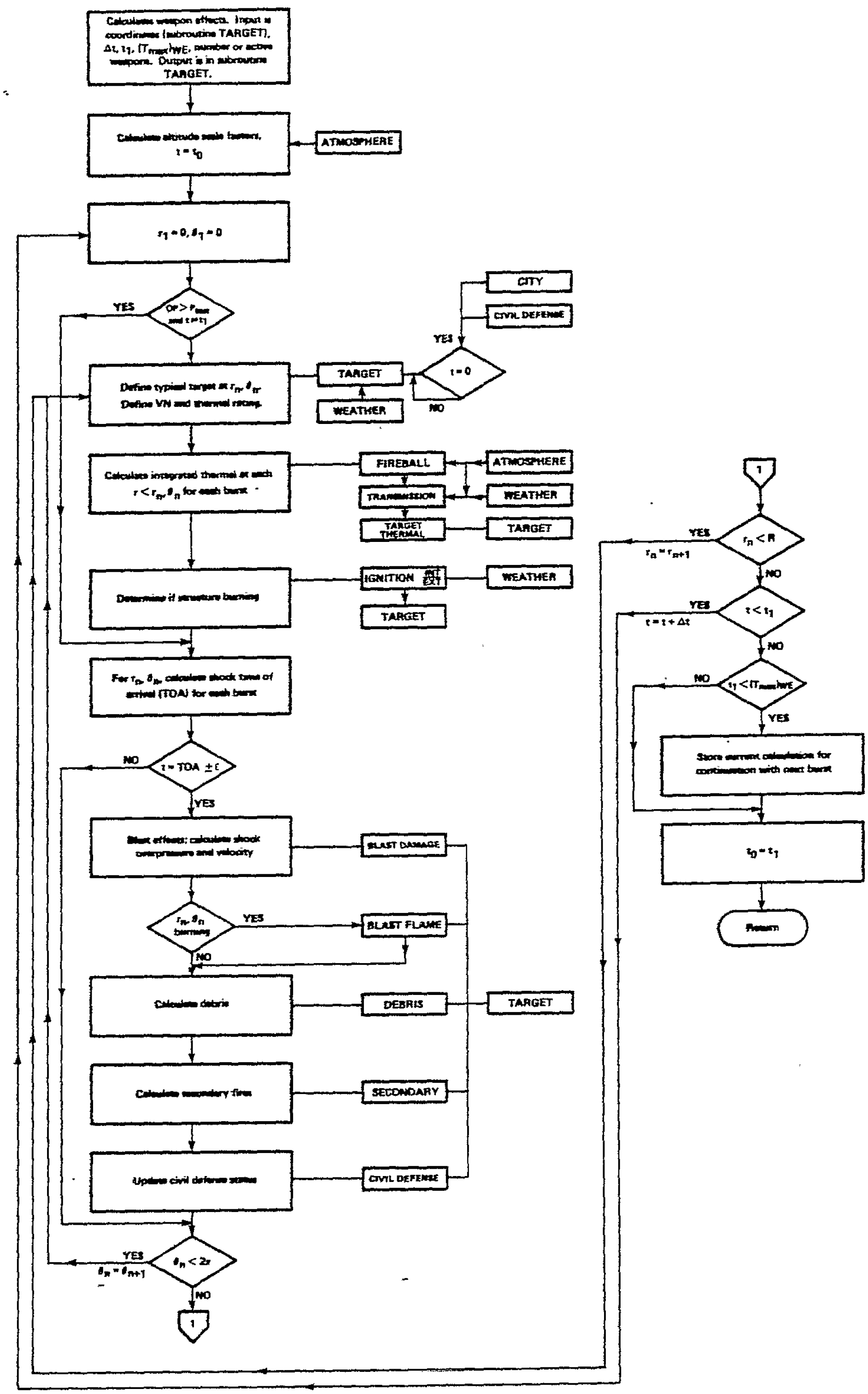

Figure 2. WEAPON EFFECT subprogram.

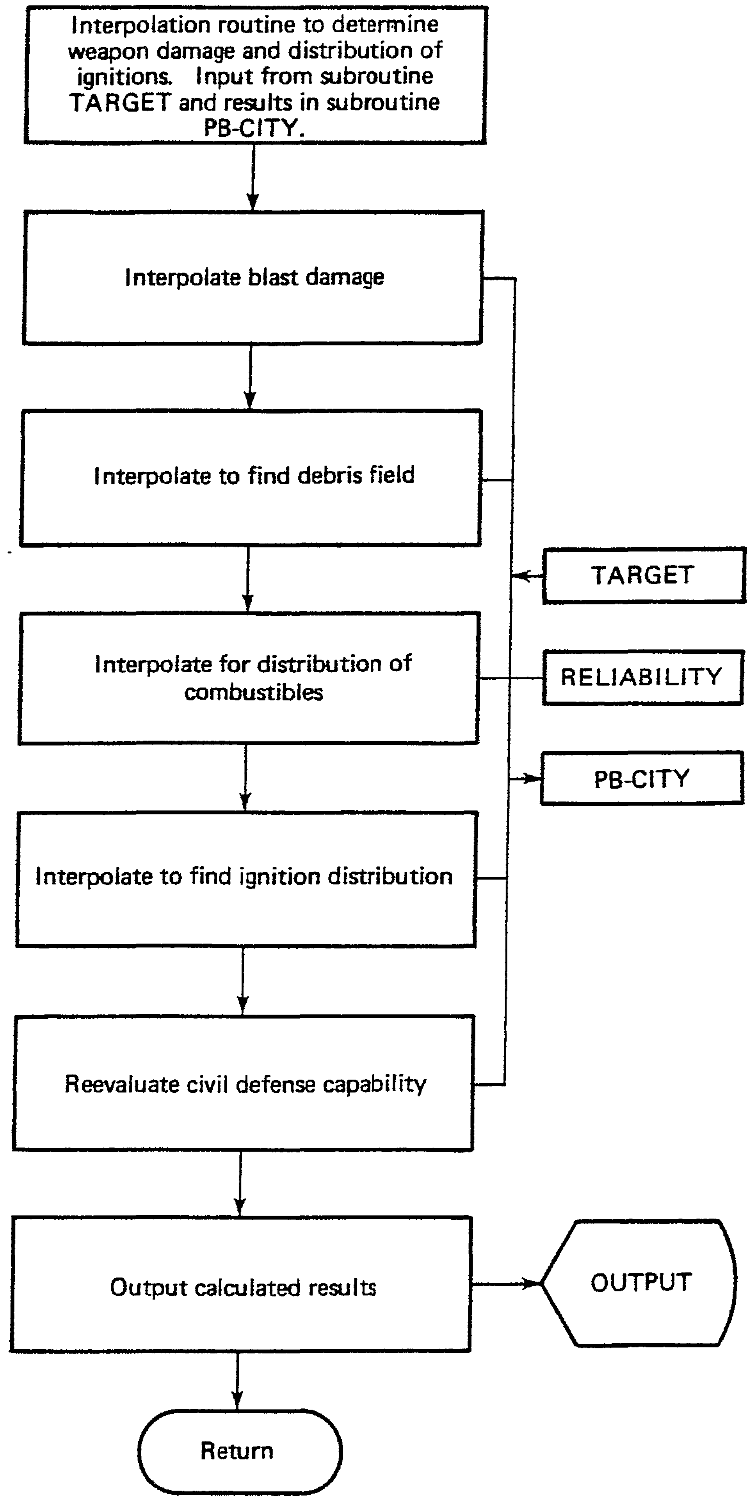

Figure 3. DAMAGE EVALUATION subprogram.

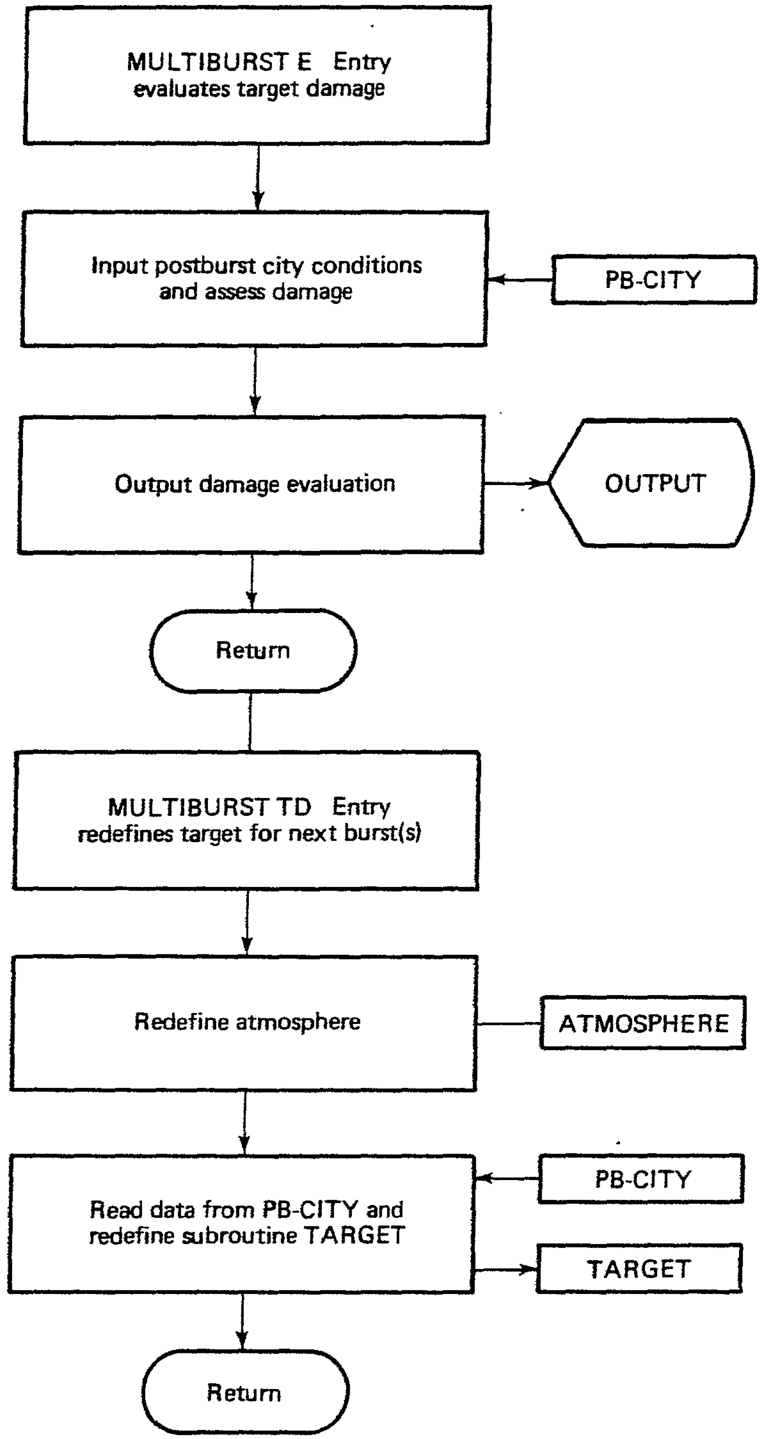

Figure 4. MULTIBURST subprogram.

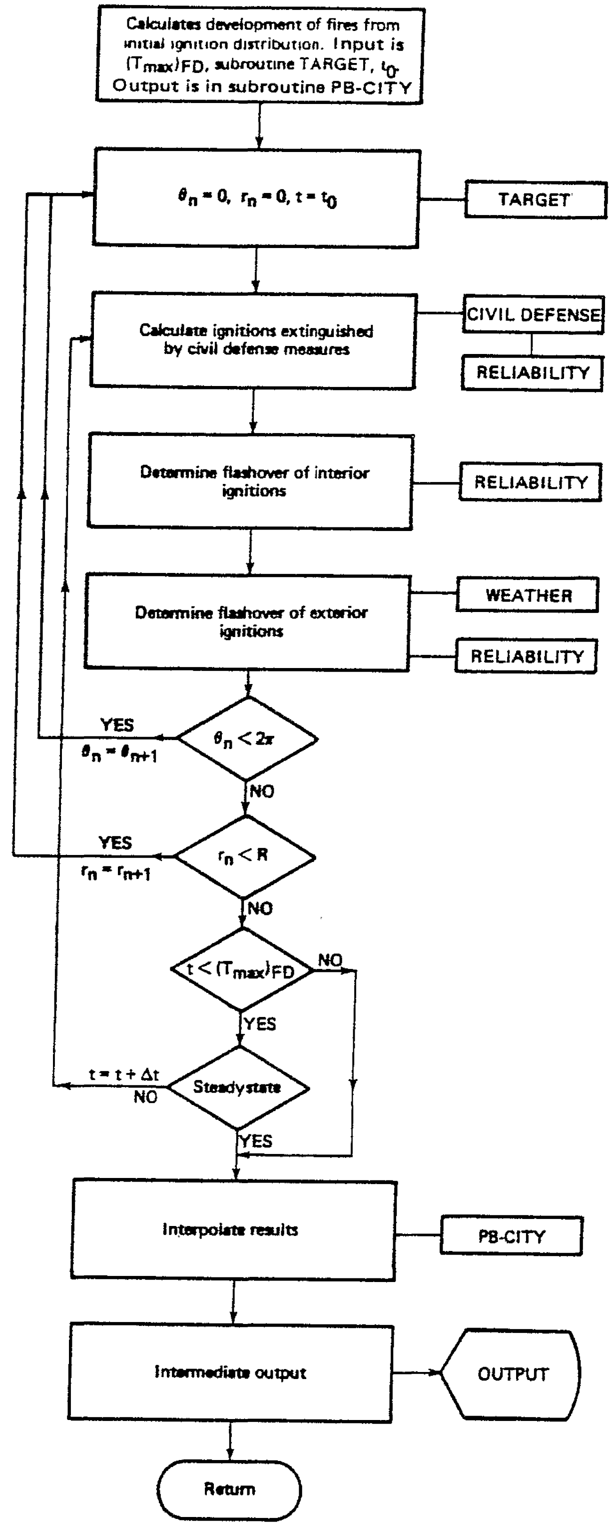

Figure 5. FIRE DEVELOPMENT subprogram.

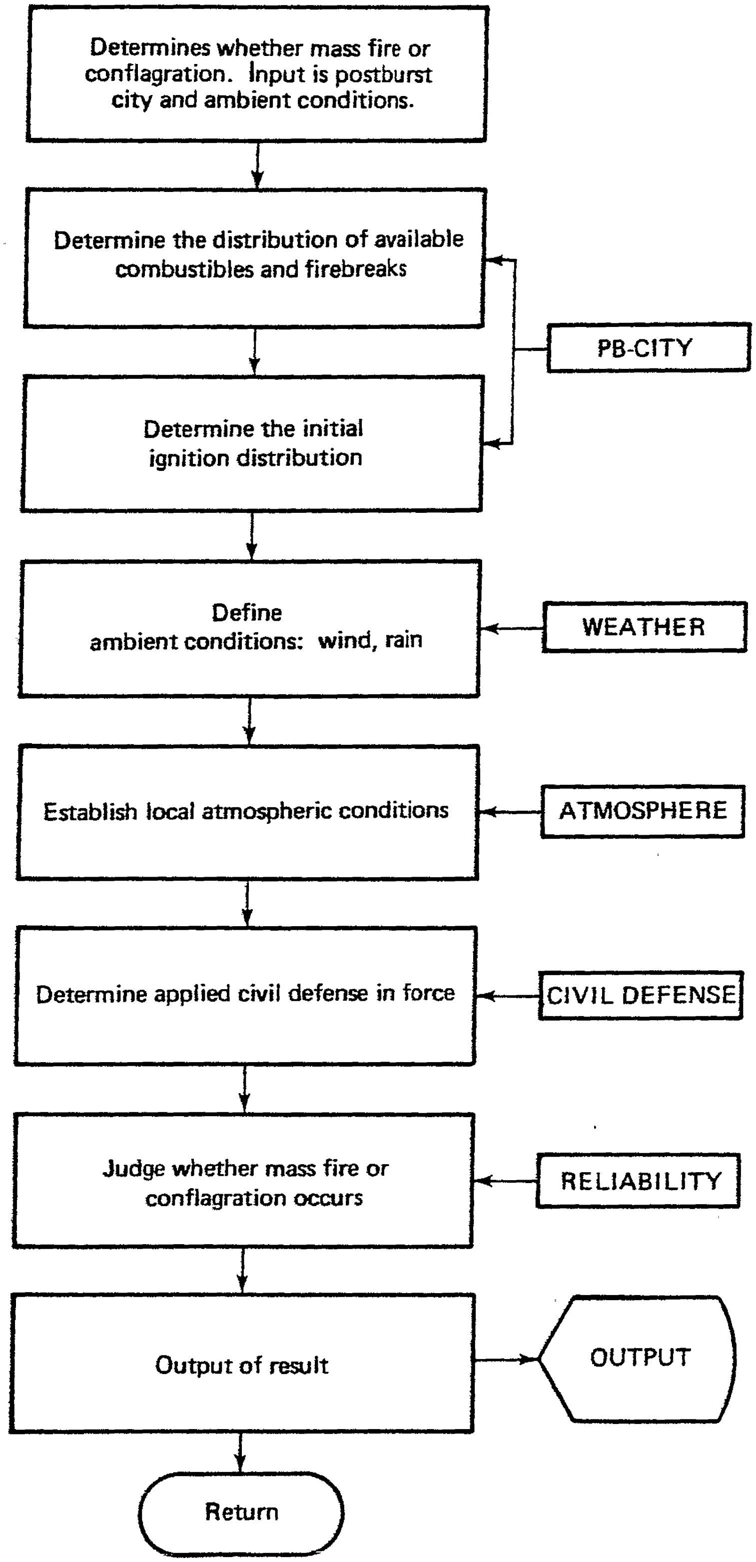

Figure 6. TYPE DETERMINATION subprogram.

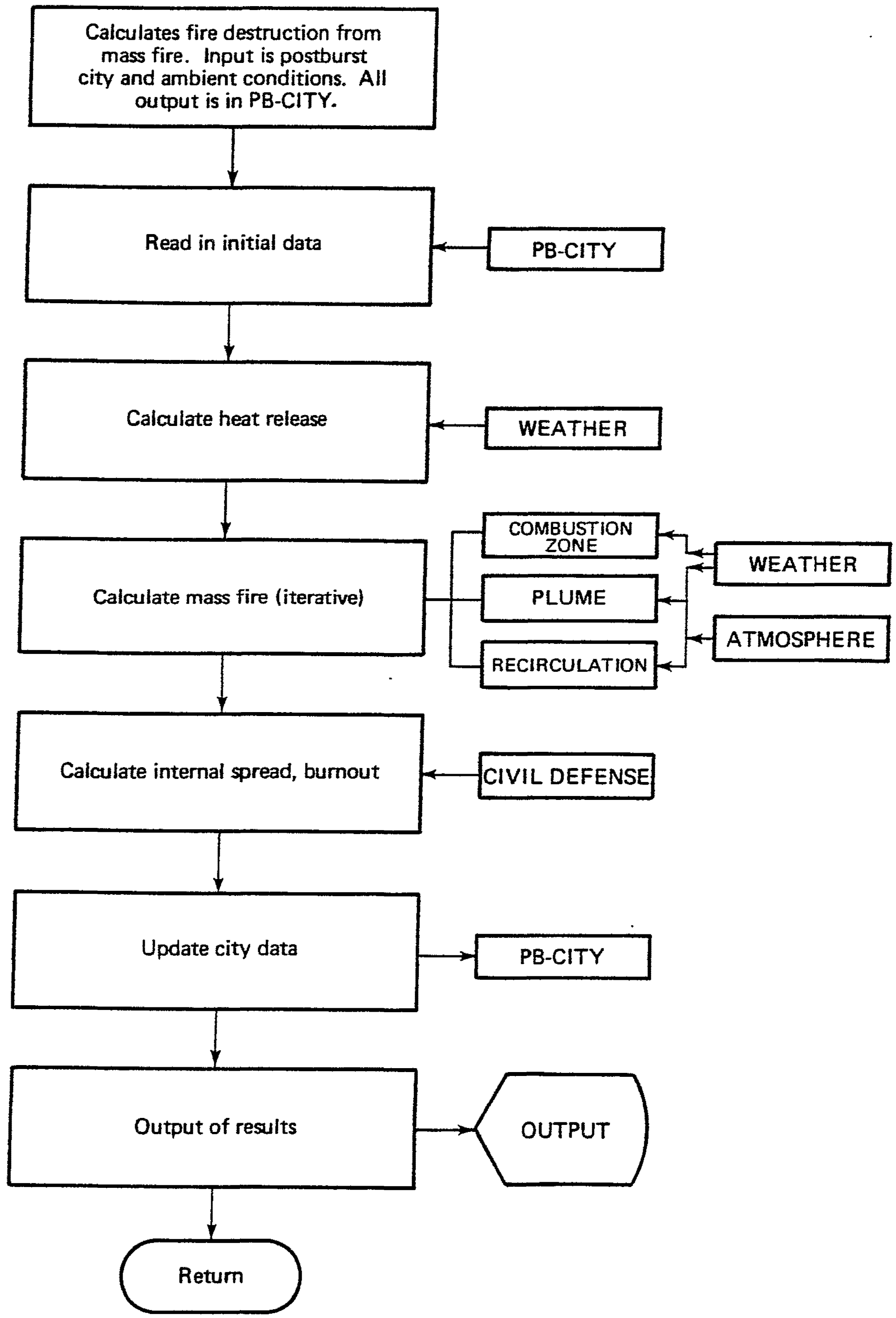

Figure 7. MASS FIRE subprogram.

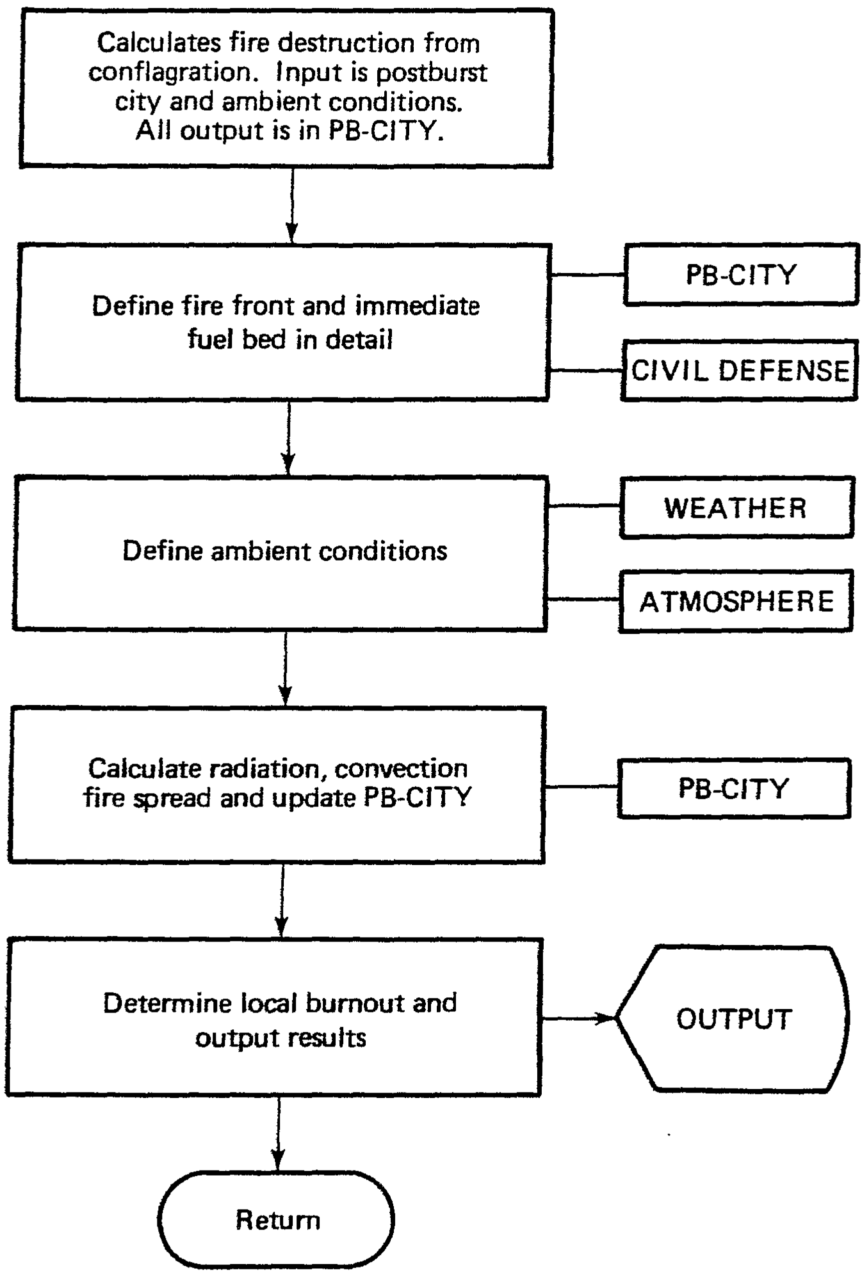

Figure 8. CONFLAGRATION subprogram.

One of our objectives in designing this code is to allow immediate development of a program utilizing existing theories and correlations. Initially, large uncertainties may be inherent in the resulting code (it is hoped they will be clearly indicated). As research results become available and are incorporated in the program, some uncertainties will be reduced and the confidence level increased. This procedure should aid in directing program improvements while providing a state-of-the-art method for predicting fire damage.

The design of the fire damage algorithm includes a main program (MAIN) and 27 subprograms. MAIN directs the calculation of all relevant physical processes from the instant of the nuclear burst until final burnout. Additionally, MAIN manages the data flow to the subprograms, as well as input and output to internal and external files and devices. It is designed to operate using multiple time scales. A short-time clock is used to compute blast and thermal effects, and a long-time clock to calculate fire effects. The program logic admits multiburst (nonsimultaneous) situations and different large-scale fire situations (firestorms or more general conflagrations). MAIN manages both data and program flow; it does not involve new technology and can be set up at the outset. The program is intended to provide predictions even when very little input data can be provided--the accuracy or reliability of results presumably improving with more detailed inputs.

Initial target-specific data are input in the first segment of MAIN through such subroutines as CITY, CIVIL DEFENSE, and WEATHER. (Display and evaluation of the subject data are provided.) Complete specification of the target and weapon data may (but need not) include

- Urban "map" detailing physical characteristics of the target by location. Level of detail may range from simple area definition to very specific identification of structure types and building density and distribution, including firebreaks.
- Active and passive civil defense measures applicable to immediate (preburst) and long-term (hours) target vulnerability.

- Weather conditions that may affect target vulnerability and fire development.
- Local atmospheric conditions (thermodynamic state of the atmosphere, particulate content and visibility).
- Weapon(s) data, including yields, locations, and burst times.
- Target (computation) coordinates.

If any of these descriptors are missing, the subroutines provide average or typical values so that the prediction can proceed.

The MAIN program computes the blast and thermal effects on the chosen targets (INPUT 3) for each time step, defined such that the thermal input before and after damage due to the blast can be calculated separately, and estimates made for the various burst (INPUT 2) interactions at each target. The time increments depend both on the target coordinates and on the weapon(s) yields and locations.

At each node, the interaction of the weapon effect with a specific building may be considered. While the calculation can be performed several ways, a thermal effects target-rating system similar to the VN blast-rating system might provide a practical and efficient computational method. The calculation basically requires a definition of the target in sufficient detail to assign both a thermal and a blast rating. An optimum data base would include a complete description of each building in the target area; however, identification of a limited number of buildings or types of buildings can be used as a basis for interpolation or extrapolation over an entire urban area. The preattack target definition is input through the subroutine CITY, and the data necessary for computation transferred to TARGET.

Active and passive civil defense measures may considerably influence both near- and long-term effects. If effective civil defense measures are anticipated, accounting must be made for them in calculating the density of initial ignitions, as well as in calculating fire development and control of spread.

Meteorological data are input to subroutines WEATHER and ATMOSPHERE. Weather data include past and present moisture levels, extent of cloud cover, and wind velocities. Some exterior ignitions may be affected by rain or other moisture (possibly increasing the long-time clock and allowing for effective civil defense measures), and fire development will depend on ambient wind velocities. Atmospheric conditions affect fireball dynamics and transmission of thermal radiation, as well as influence the plume characteristics of the subsequent large area fire. Furthermore, the atmosphere around any urban area will be drastically modified by a nuclear weapon burst. Modification of the atmospheric conditions may include dust, smoke, and particulates as relevant to calculations of transmission from subsequent bursts and to fire spread by radiation.

MAIN accepts the initial data and sets up data files and subroutines for each class of data (see Fig. 1). Separate data subroutines are used for flexibility and efficiency during the course of the computation and as an aid to parameter and sensitivity studies. While a calculation procedure that allows consideration of specific targets at prescribed (INPUT 3) coordinates is used, an interpolation routine (subroutine DAMAGE EVALUATION) is also included to provide a continuous analysis of the damage and a distribution of ignitions. If specific target structures are not called out, the interpolation routine will still provide a damage distribution.

After the input of initial data, an output segment is specified so as to allow evaluation and display of the given data base. Manual (interactive) user input can be entered at this point to either supplement the data base or override previous input.

With the initial conditions specified, computation begins in the program segment NUCLEAR BURST. Weapon effect and damage calculations are performed in called subroutines. The NUCLEAR BURST segment of MAIN defines the short-time clock used in calculating immediate burst effects. As the characteristic time for all (99 percent) thermal radiation to reach the target is longer than the time required for the shock wave to sweep an entire city,* a maximum time $(T_{max})_{WE}$ is

*Collateral-damage-type geometries may require modification of this criterion.

defined as the calculation time interval. Should another burst occur (INPUT 2) within that interval, the calculation interval is redefined as $[(T_{max})_{WE} = t_{new\ burst} - t_0]$. The time steps ($\Delta t$) are chosen so that the shock wave(s) will be allowed to interact with the targets at the predefined coordinates. Subprogram WEAPON EFFECT is called to perform detailed computations of the blast and thermal effects at each node. At the end of the calculation interval, subroutine DAMAGE EVALUATION is called to interpolate the results between coordinates and thereby provide a continuous map of the damaged urban area.

The program segment MULTIBURST deals with multiburst situations. Initially, the damaged target is evaluated (subroutine MULTIBURST E) to allow the user to assess the value of an additional burst. If another burst is programmed, MULTIBURST TD is used, and the target redefined to account for the previous burst. Control is then returned to the previous segment, NUCLEAR BURST, and the weapon effect calculations performed for the new burst. If there are no additional bursts, control transfers to the following segment, DEVELOPMENT (of ignitions).

At this stage, the calculation time interval must be redefined. While weapon effects are manifested in seconds, the growth of interior (and exterior) ignitions into complete building fires may require an interval $(T_{max})_{FD}$ of several minutes to an hour. Therefore, an intermediate time clock is defined, and the fire development calculated in subroutine FIRE DEVELOPMENT. If an additional burst is programmed within this calculation interval, $(T_{max})_{FD}$ is redefined and control returns to MULTIBURST for evaluating and redefining the target, then to NUCLEAR BURST for calculating the new burst effects.

At the conclusion of the intermediate time clock, a subprogram is provided (FIRE TYPE) to determine whether a mass fire or conflagration is developing. It is conceivable that a mass fire will occur in the primary target area, while a lesser conflagration will develop in the surrounding or adjacent areas. FIRE TYPE examines the distribution of combustibles and ignitions, considers weather and civil defense factors, and determines the type of fire. Control is then passed to the final segment of MAIN, in which the characteristics of the fire are calculated.

At this point, the time scale is redefined to reflect the interval required for the fire to act, be it a mass fire or conflagration. The calculation of fire damage (burnout) requires an interval $(T_{max})_B$ of tens of hours. As before, the computation is incremental, and an appropriate duration and time step (long-term time clock) are defined. Should an additional burst be planned in this interval, $(T_{max})_B$ is redefined; at that time, control is passed first to MULTI-BURST and then to NUCLEAR BURST. At each time step in CALCULATE FIRE, either the MASS FIRE or CONFLAGRATION subprogram is called and the result tested for burnout. The calculation proceeds until either the prescribed time interval is reached or complete burnout is achieved.

MAIN directs the computation in time and does not involve new technology. The relevant physical processes and interactions are computed entirely in the called subprograms. While some aspects of the calculation can now be performed with sufficient accuracy, others can only be approximated, and several of the subroutines cannot be constructed without further research. The following paragraphs briefly discuss the subprogram logic; we end by evaluating the research development needed for constructing all requisite subroutines.

Detailed calculation of the major physical processes is performed in the subprograms WEAPON EFFECT, MASS FIRE, and CONFLAGRATION, each of which calls subroutines that compartmentalize the physical events. This compartmentalization allows constructing and operating the basic program at an early date, with subprograms and subroutines developing and changing as information becomes available or as research dictates. The breakdown allows a clear definition of the unknowns.

The input (from MAIN) into the subprogram WEAPON EFFECT consists of the number of yields, burst locations and heights, and other specifications for the "active" (at time t_0) weapons; a set of computation coordinates; appropriate time intervals; and the target description. For the first entry into WEAPON EFFECT, the target data are defined from the preburst data base (CITY). In subsequent entries, the target is described by an updated TARGET. In either event, at each coordinate a specific (representative) building is defined and a blast and thermal rating applied to it. A thermal rating system will need to be developed to account for building contents and surroundings, position with respect to adjacent structures, susceptibility to interior and exterior primary ignitions or secondary ignitions, and susceptibility to ignition from adjacent burning buildings.

At each time increment, the computation is stepped in space radially and circumferentially. The integrated thermal radiation received at each target from each burst is computed through subroutines FIREBALL, TRANSMISSION, and TARGET THERMAL, which in turn use data from ATMOSPHERE, WEATHER, and TARGET. The target at (r_n, θ_n) is then checked to see whether ignition has occurred. If the shock wave's time of arrival is within a prescribed error limit $t = TOA \pm \varepsilon$, blast-effect computations are performed at (r_n, θ_n). Subroutines are included for calculating BLAST DAMAGE, BLAST FLAME interactions, DEBRIS distribution, SECONDARY fire starts, and modification of the CIVIL DEFENSE posture. All calculations are used to update the target status in TARGET. The computation is serially incremented in angle, radius, and time. Should another burst be activated before (T_{max}) is reached, the current computation is stored so it can be continued on the next entry.

After control is returned to NUCLEAR BURST, subprogram DAMAGE EVALUATION is called. Its purpose is to interpolate the computations at specific coordinates, and present a continuous damage spectrum. The results are stored in PB-CITY, then called in later subprograms specific to the long-term fire calculation. The interpolation procedure includes provisions for estimating the reliability of the result of the weapon-caused damage and its output. Control is returned to MAIN, which then calls MULTIBURST.

The first entry is to MULTIBURST E, which evaluates the efficacy of additional bursts on the target area. The evaluation is based on data passed from the interpolation routine in PB-CITY. If an additional burst is programmed, reentry into the MULTIBURST subprogram is effected at MULTIBURST TD. In this segment, the target is redefined for initiating an additional burst calculation; ATMOSPHERE is similarly redefined to include the effects of smoke and dust raised by the previous burst(s).

The characteristic time for immediate weapon effects to occur is several seconds. Development of building fires from ignited points can require 5 to 60 min. The FIRE DEVELOPMENT subprogram calculates the number of structure fires developing from the initial ignitions. Input to this subroutine is the state of the city as determined in PB-CITY. Modifications to the initial distribution of ignitions by civil defense actions are allowed for in CIVIL DEFENSE. Finally, the FIRE DEVELOPMENT subprogram calculates whether a building fire develops from an ignition, interpolates the resulting fire distribution (makes an entry in subprogram DAMAGE EVALUATION), updates PB-CITY, and provides output information.

Subprogram TYPE DETERMINATION reads in all postburst information, and on the basis of the distribution of developed (and developing) initial ignitions, weather, and atmosphere, judges whether a mass fire or conflagration will develop. The subroutine RELIABILITY assigns a confidence level to the judgment, depending on the detail provided on input, and on the uncertainties and variabilities inherent in each step in the computation of fire growth and development.

Evaluating long-term urban fire damage is performed in either MASS FIRE or CONFLAGRATION. The required input is passed to these subprograms through subroutines PB-CITY, WEATHER, ATMOSPHERE, and CIVIL DEFENSE. Output is contained in an updated PB-CITY. Subprogram MASS FIRE computes fire damage using an iterative procedure involving the combustion zone (flaming urban area), column (subroutine PLUME), and meso-scale recirculation. The subprogram computation is quasi-steady, with time incremented in MAIN. Burnout is tested in the subprogram for its effects on the amount of heat released in the combustion zone. After damage levels are measured in the CALCULATE FIRE segment of MAIN, the computation is either continued or stopped. If the predefined burnout criteria are attained, external device output is called, and the calculation repeated for additional bursts.

Computation of a conflagration (fire spread on a front) uses a marching procedure in which the computation advances with the fire's propagation. Because the computation is performed in a zone around the fire front, some description of local structure is necessary

(PB-CITY). Burnout is tested in CONFLAGRATION to determine the location and speed of the fire front. As with MASS FIRE, the extent of damage is tested in MAIN, and the calculation accordingly continued or interrupted.

In designing the program flow, subroutines describing relevant physical processes were included irrespective of whether sufficient knowledge currently exists to describe the physics. This is especially true for the segments used in computing the fire physics, and to some extent in computing burst-related effects. Inclusion of all relevant physical processes provides a framework for augmenting or improving the code without major recoding of the program as research results become available. The urban fire damage algorithm can represent the changing state of the art, with minimal updating effort.

The 27 subprograms can be divided into four groups: input data, data management, burst-related physics, and fire-related physics. The first group (CITY, CIVIL DEFENSE, WEATHER, ATMOSPHERE) does not involve development of new technology; however, it must be flexible enough to allow either unspecified inputs or a completely specified data base describing the target in detail. Similarly, the data management group (MANUAL INPUT, OUTPUT, TARGET, and PB-CITY) does not require any new development in technology, but should be able to accommodate both detailed input and very general cases.

Many burst-related phenomena are well understood, and existing codes or methods that describe them can be modified for inclusion in this urban fire damage algorithm. Subprogram WEAPON EFFECT directs the near-time burst calculations, and requires virtually no new technology. The suggested calculation procedure is based on the VN system for computing blast damage and calls for a similar rating system to measure thermal vulnerabilities and damage. Development of a thermal rating system that leads to a practical, efficient calculation procedure seems possible. Research will be required, although the technology base appears at hand. An important complication to developing a thermal rating system, however, will be the need to include the effects of blast on thermal vulnerability (broken windows, exposed contents, removed roofing, etc., can drastically lower a structure's ignition-resistance). Weapon effects as needed in FIREBALL, DAMAGE EVALUATION, TARGET THERMAL, and BLAST DAMAGE can be modeled using currently available methods and codes. Certain criteria (as in DAMAGE EVALUATION) may need reexamination as regards fire destruction or damage due to heat and smoke.

Additional weapon effects are computed in subroutines TRANSMISSION, BLAST FLAME, DEBRIS, SECONDARY, and RELIABILITY. In all these subroutines, further research would be useful in describing the phenomenon or its interactions with structural characteristics. A more complete understanding of the transmission of thermal radiation would help, as would better estimates of secondary ignitions. Additionally, criteria for determining the confidence level of the fire damage predictions will need development at the outset. Initially, the subroutines calculating blast-flame interactions, debris distribution, and secondary fires can be based on only crude theories or estimates. Future research could significantly improve the initial estimates. It should be noted that including these routines from the outset permits parametric studies that can provide insight into the relative importance of each effect.

The final burst-related subprogram is MULTIBURST, which evaluates the damage of previous bursts and redefines the target in the event of an additional burst. Subroutine ATMOSPHERE is modified by MULTIBURST TD to account for dust and smoke, as these will greatly affect the transmission of thermal radiation to the target from subsequent bursts. Methods for estimating the amount of dust and smoke need to be developed, as well as procedures for computing the reduction in transmission of the ensuing thermal radiation.

A further group of eight subprograms is related exclusively to thermal effects. As part of the WEAPON EFFECT subprogram, subroutine IGNITION is called to determine whether combustion is initiated by the fireball radiation. Although a substantial data base (both laboratory and weapon-test data) exists upon which to determine if primary ignitions do occur, the data are subject to critical reexamination. Further, ignition limits need to be determined for many modern materials not previously exposed to thermal radiation. A currently well-developed aspect of predicting fire growth is in calculating FIRE DEVELOPMENT (flashover). Codes to rigorously compute flashover can be appended to the urban fire damage algorithm, although development of correlations to predict flashover (based on the thermal rating system) would be more practical in most targeting or civil defense exercises.

The type of fire (large area or conflagration) that will develop after a weapon bursts depends on the state of the damaged city, the density and distribution of ignitions (primary and secondary), and ambient weather. Subroutine TYPE DETERMINATION defines the type of fire from the state of the postblast city. Judgments can currently be made as to the type of fire, although as our understanding of large area fires and conflagrations improves, the criteria can be made more rigorous.

The characteristics of a long-term city fire are calculated by the subprograms MASS FIRE (which includes subroutines PLUME, COMBUSTION ZONE, and RECIRCULATION) and CONFLAGRATION. The calculation must now rely on stochastic methods that cannot, however, account for many basic physical interactions. Current and projected research will significantly improve our predictive capability and should be incorporated in the algorithm as early as possible.

NOMENCLATURE

n = index.

N, NB, MB = counters--used in MAIN.

NW = number of weapons active at time t.

R = outer radius of target area.

r, θ = axisymmetric coordinates.

t = time.

t_0 = initial time at start of weapon effect calculation.

t_1 = maximum time allotted for calculating short-time weapon effects.

$(T_{max})_{WE}$ = maximum process time (~2 min) for 99 percent of thermal radiation to hit target.

$(T_{max})_{FD}$ = maximum process time (~30 min) for development of initial ignitions to building fires.

$(T_{max})_B$ = maximum process time (~10 to 24 hr) for calculation of urban fires.

TOA = shock-wave time of arrival.

ε = error limit for determining if shock at r_n, θ_n at time t.

OP = shock wave overpressure.

P_{test} = overpressure at which desired damage level achieved.

LIST OF SUBPROGRAMS

ATMOSPHERE
BLAST DAMAGE
BLAST FLAME
CITY
CIVIL DEFENSE
COMBUSTION ZONE
CONFLAGRATION
DAMAGE EVALUATION
DEBRIS
FIREBALL
FIRE DEVELOPMENT
IGNITION
MANUAL INPUT
MASS FIRE
MULTIBURST
OUTPUT
PB-CITY
PLUME
RECIRCULATION
RELIABILITY
SECONDARY
TARGET
TARGET THERMAL
TRANSMISSION
TYPE DETERMINATION
WEAPON EFFECT
WEATHER

CHAPTER 4

LARGE AREA FIRE--AN ANALYTIC MODEL

Dale A. Larson
Richard D. Small

SECTION 1

OVERVIEW

Large-scale fires have devastated urban areas in both wartime and peacetime. During World War II, firebombing raids sometimes led to firestorms that destroyed entire urban areas. While concentrated bombing raids were necessary to initiate and ensure firestorm development in target cities, the two atomic weapon bursts over Hiroshima and Nagasaki caused immense fire destruction. The fires that resulted from these low-yield nuclear bomb bursts and those from the firebombing (using many thousands of 2 kg thermite bombs) caused extensive damage and destruction. The damage due to fire was much greater and more complete than that due to blast from the nuclear bombs or from equal tonnages of high-explosive bombs.

History tells of city after city destroyed or severely damaged by fires--many times set as acts of war--but the simultaneous burning of large urban areas is a modern phenomenon that began in World War II and is projected as a consequence of any future nuclear attack on cities. Moreover, modern nuclear weapons have the potential for causing even larger area fires than those of World War II.

The World War II firestorms involved relatively extensive areas (Hiroshima, 12 km^2; Dresden, 21 to 28 km^2; Hamburg, 21 km^2), and survivor reports describe fires much more violent than is common with burning front (line) fires or individual building fires. Hurricane-force fire winds were reported, and high street-level temperatures indicated. All combustibles in the firestorm areas burned, with tremendous loss of life--even in shelters. It is hence clear that large area fires (simultaneous burning over a whole area) give rise to phenomena not present in small fires.*

---

*For the present, we define a small fire as one in which flame height is comparable to or greater than the typical horizontal dimension of the fuel bed, and all dimensions are much smaller than the scale height of the atmosphere. Large area fires are those in which

Megaton-yield nuclear weapons are expected to light fires (primary and secondary) over even greater areas than in the past. For example, a 1 megaton burst (height-of-burst, 700 m) can irradiate an area 7 km from ground zero with 30 cal/cm^2 of thermal radiation--more than sufficient to ignite lightweight household goods and many typical exterior materials. In a few tens of minutes, urban areas of more than 180 km^2 could be on fire, leading to firestorms at least ten times as great as those of World War II. It is reasonable to expect that phenomena observed in the earlier large-scale fires will be dwarfed in comparison with the effects of these nuclear-induced superfires that could engulf whole urban areas.

Despite the fact that numerous significant large-scale fires have occurred, the documentation of these events [e.g., Irving, 1963; Miller, 1968a, 1968b; Miller and Kerr, 1965] is fragmentary, anecdotal, and imprecise, and contains few quantitative observations. Accordingly, current understanding of the physics of firestorms (and hence predictive capability) is fairly limited. Past analyses have relied either on stochastic formulations [Miller, Jenkins, and Keller, 1970] for treating urban fires resulting from a given weapon burst, or on extrapolation from small-fire theory [Lommasson, 1965, 1967; Lommasson et al., 1968]. Neither approach has described the special features anticipated for large-scale firestorms. Experimental work has not to date provided much insight into the nature and characteristics of firestorms. One difficulty is that even large experiments such as Operation Flambeau [Countryman, 1964] are only small-scale compared with what we can expect from actual, large urban fires.

A consistent physical model based on scalings of the full conservation equations has recently been developed [Small and Brode, 1980]. The aspect ratio (mean flame height divided by typical burning area width) of the burning urban area is of major importance; it has been found that the characteristic velocities (induced fire winds) are proportional to the heat release, and inversely proportional to the aspect ratio. Small and Brode proposed a complete flow

---

the typical urban (burning) dimension is the same order as the scale height of the atmosphere, and the ratio of flame height to fire width is low.

pattern that identifies the major physics of large area fires. A principal feature of their model is that a simultaneously burning large urban area significantly perturbs the local atmosphere, and hence drives an external vortex (recirculation) flow that "pumps" ambient air to the combustion zone.

The following describes a first effort at theoretically modeling the hydrodynamics and thermodynamics of superfires. Since the work is still in progress, the results presented are interim. The thrust of the work is to analytically ascertain the special features of large area fires and to construct a model that will predict the velocity, temperature, pressure, and density distributions throughout a burning area and its surroundings. While conclusions are still tentative, it is apparent that higher velocities than previously experienced will occur in superfires due simply to the large scale of the event. Further, high velocities extend past the outer edge of the fire into relatively undamaged areas. The resulting wind and drag forces may exceed natural winds and structural resistances for appreciable distances beyond the fire, and cause additional damage not previously acknowledged as probable.

MODEL OVERVIEW

The basic features of a large area fire are illustrated in Fig. 1. The principal elements are a strongly buoyant, high-velocity flow through and about the combustion region (the burning urban area); a natural convection column above the combustion zone; and meso-scale atmospheric recirculation.

Characteristic dimensions of the combustion zone are mean flame height L and horizontal extent of the burning region D. The ratio L/D defines a small parameter ($\varepsilon = L/D$) that represents the aspect ratio of the burning urban area. For the present analysis, L and D are taken to be of the order 10^2 m and 10^4 m, respectively. Above the burning region, the convection column is expected to rise through much of the atmosphere, and accordingly have a height-to-width ratio $D/H \sim O(1)$--that is, the column should have similar horizontal and vertical extent above the burning city. Plume heights comparable in

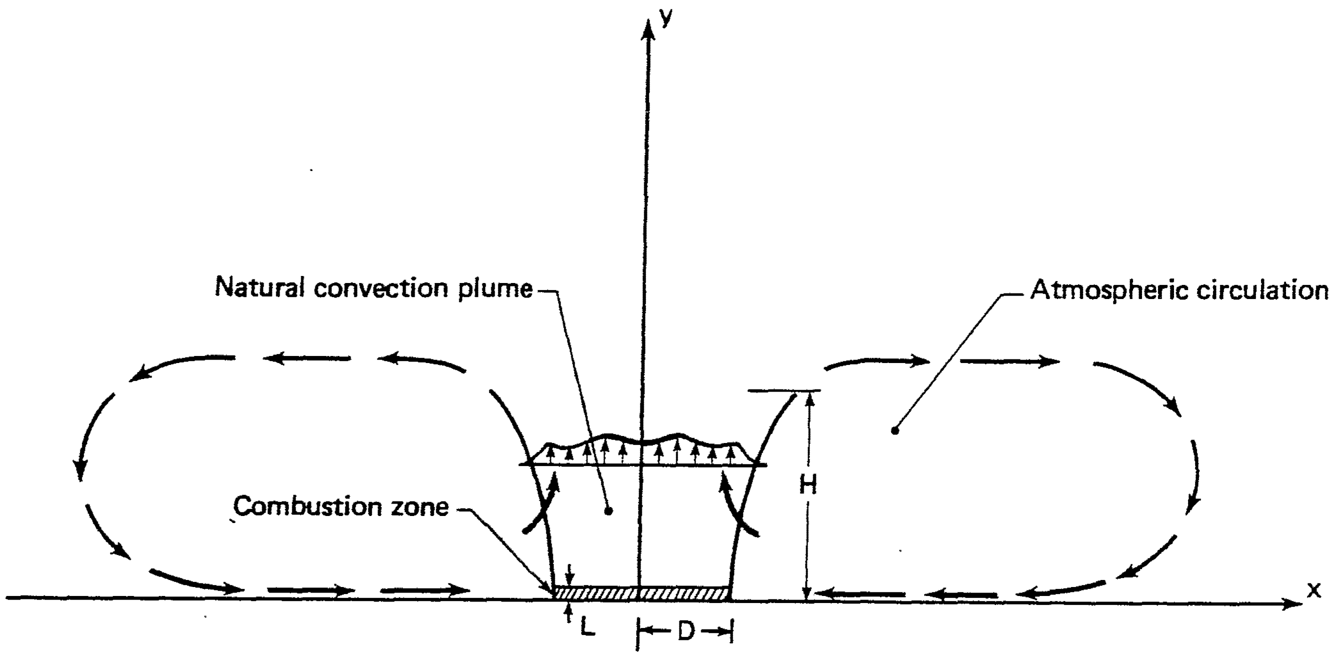

Figure 1. Schematic of large area fire.

magnitude to the atmosphere scale height H were observed in Dresden [Irving, 1963] and Hiroshima [Thomas and Witts, 1978]. We anticipate that the plumes or columns above large area fires can be characterized by $D/H \sim O(1)$. Small fires (building fires, bonfires) in the open have long, narrow plumes characterized by $D/H \ll 1$. The difference, though important, has not been considered in previous work.

The entire flow is driven by the interactions occurring in the combustion zone. The basic results of interest (wind velocities, temperature, density, pressure levels, and combustion rates) all need to be found in this region. Thus, while the combustion zone is considerably smaller than either the free convection column or the recirculation region, it assumes primary importance in our analytic modeling and must be considered in detail as a separate component. For the present, we focus on the basic flow pattern in the combustion zone, rather than on details of the combustion process. The effect of the combustion process is therefore simply modeled by a volume source of heat addition in the combustion zone.

The convection column is driven by the buoyancy generated by the combustion processes. The massive heat addition in the combustion zone significantly perturbs the atmosphere and causes a meso-scale recirculation--a phenomenon similar to that observed on still nights for an urban heat island [Delage and Taylor, 1970].

The analytic model for large area fires is thus a multicomponent one. In each region, different physical phenomena govern the hydrodynamics and thermodynamics of the flow. Appropriately scaled equations of mass, momentum, and energy conservation, plus an equation of state, are introduced for each component. An overall description of the airflow can be provided by suitably matching the solutions to those various equation sets. The basic results of interest concern the solutions in and around the combustion zone. However, to obtain these solutions, it is necessary to determine the solutions in the other regions as well, because the appropriate boundary conditions are interdependent. Solutions for the combustion zone and convection column determine the characteristics of the recirculating flow, which in turn provides the inflow velocity distribution in the combustion zone.

As depicted in Fig. 2, more than three simple regions must actually be considered. Analysis shows that the convection plume is not of the standard long, thin type, but rather more like the "potential core" of a plume, with temperature and vertical velocity profiles of basically "top-hat" shape.

The plume region of Fig. 1 must therefore be subdivided into regions II and III, as in Fig. 2. Equations describing the physics over most of the plume region are not appropriate at the side of the top hat, where there are very large shears and thermal gradients. A new region (V) must also be introduced in the upper part of the atmosphere. Equations other than those appropriate for regions II, III, and IV are required for describing the relatively large horizontal velocities that develop there, as convection column air is ultimately spread laterally. Finally, since the high-velocity winds characteristic of large area fires occur in regions around as well as in the burning zone, we redefine the first major component of the overall

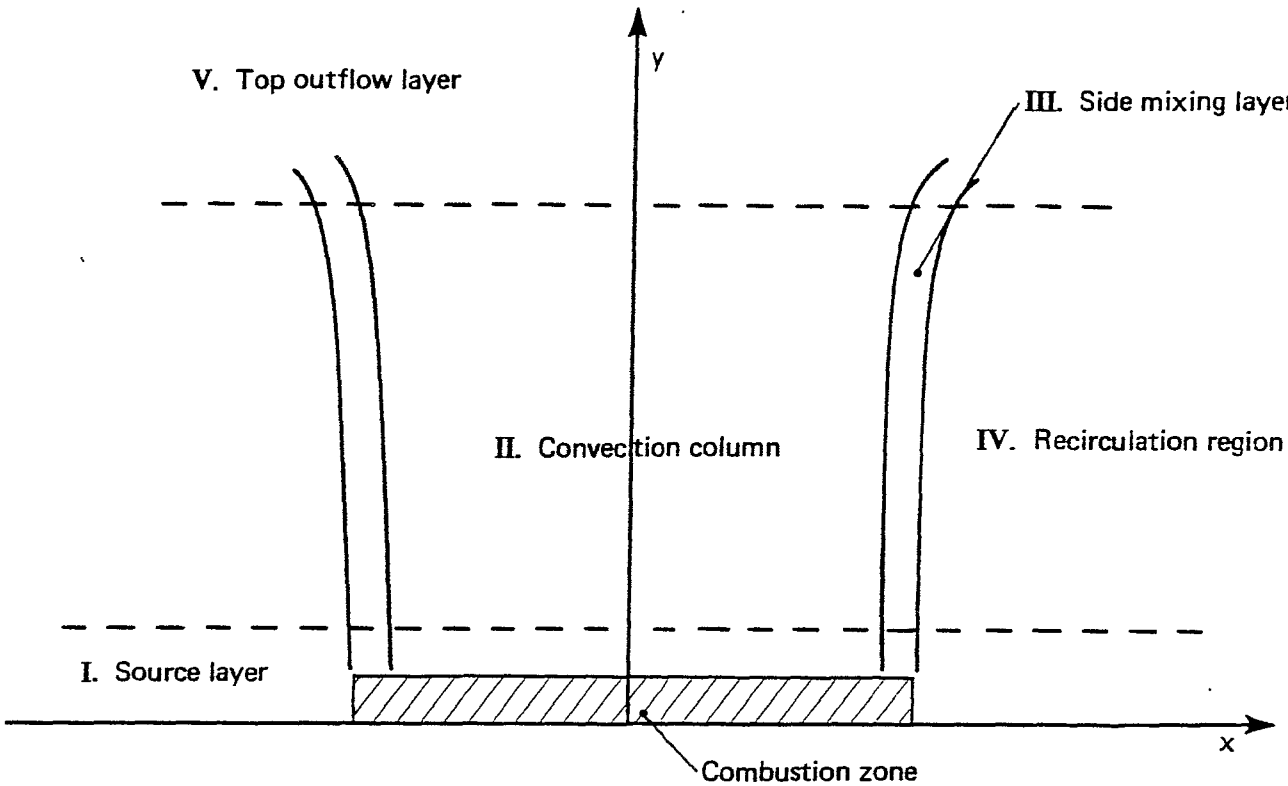

Figure 2. Components of large area fire.

airflow as the high-speed flow through a layer some hundreds of meters thick, which contains, but is somewhat larger than, the actual combustion zone. Piecemeal analysis is facilitated by this enlargement of the burning zone.

ANALYSIS SUMMARY

A unified quantitative description of the physics of large area fires has been developed for most of the component regions defined in Fig. 2--including complete coordinated analyses of the mean airflow in the source layer, convection column, and mixing layers on the sides of the convection column (i.e., regions I, II, and III). The nature of the pressure, density, and temperature fields in the recirculation region (IV) has also been ascertained. The essential features of the overall recirculating airflow are then completely described once the velocity fields in this region are calculated. This determination requires a study of the airflow in region V (the top outflow region), and also of the sink-like flow at the bottom of the recirculation region. These studies are being pursued in an extension of the work reported here.

The coordinated analyses of the airflow in regions I, II, III, and IV are described in Sec. 3 and Appendixes A and B. The approach [Small and Brode, 1980] is to use the combustion-zone aspect ratio $\varepsilon = L/D$ as a small parameter, construct suitable asymptotic expansions for the model solutions in each region, then match the expansions in a unified manner. Analysis shows that the characteristic horizontal velocity scale in and around the combustion zone is approximately 240 km/hr (150 mph) for $D \sim 10^4$ m, and appears to increase linearly with QD. The average airflow in the combustion zone itself (hatched part of region I in Fig. 2) must be found by numerical computation, but the equation set to be solved is considerably simpler than that posed by the full set of state and conservation laws. Furthermore, this equation set can be solved analytically in region I above the combustion zone.

An explicit analytic solution that suitably matches the overall solutions for region I can also be found for the airflow equations that are appropriate to region II. That solution represents a vertical flow with temperature, density, and pressure having top-hat profiles (independent of the horizontal coordinate at all heights). Similarly, a partial analysis of the flow equations appropriate for region IV shows that temperature, density, and pressure are functions of height alone in this region as well.

Differences in temperature, density, and pressure (as well as velocity) between regions II and IV are smoothed out in region III (which straddles the side of the top hat). Since the flow equations appropriate for this intermediate region contain diffusional (smoothing) terms, these equations are less amenable to explicit analysis than those used in other regions, and must also be solved by numerical computation. It is anticipated that numerical computation will also be necessary in determining the region IV velocity fields. As described further below, the region IV airflow is expected to be generally vortex-like, but to exhibit a strong sink-flow behavior near the entrance of the combustion zone. The properties of the recirculation flow should depend functionally on the magnitude of heat release in the combustion zone and, to a lesser degree, on dissipative forces.

SECTION 2

MODEL

PHYSICS

The dominant physical effect in the combustion zone is the heat addition resulting from the fires. In and around this zone, the flow is treated as that of an ideal, compressible gas being heated by ongoing combustion processes, then rising under buoyant forces to expand further as it rises in the atmosphere. For the present, the combustion mechanisms are not considered in detail; the overall combustion effect is simply taken to be a volumetric heat addition in the combustion zone. Details of the combustion process, particulate concentrations, gas generation, etc., are avoided, but may subsequently be considered as model refinements.

Shear forces are considered small compared with the large buoyant forces present in the combustion zone. Diffusion of heat (in the burning region) is a weak effect compared with heat addition due to combustion, and can be accounted for by modifying the heat addition rate. The principal departure from previous fire research [Morton, Taylor, and Turner, 1956; Murgai and Emmons, 1960; Murgai, 1962; Smith, Morton, and Leslie, 1975] is that the combustion zone is treated as a separate, distinct region, and heat is supplied volumetrically rather than at the boundary. Further, due to the large changes in temperature but small changes in pressure [McCaffrey, 1979], the Boussinesq approximation is not employed in the combustion region.

The flow is also taken to be that of an ideal compressible gas in the column and recirculation regions; however, there are no volume sources of heat, and dissipative transport mechanisms for both heat and momentum are no longer negligible. Hot, light air from the combustion zone rises in the column, mixing and spreading slightly, then expanding significantly in the upper atmosphere ($H \sim D \sim 10^4$ m).*
The air is then recirculated to the combustion zone in a vortex-like

*See Appendix C for list of symbols.

pattern. Since the column is so wide (aspect ratio $D/H \sim 1$, compared with $D/H << 1$ for standard plumes), entrainment and mixing of non-heated and heated air occurs principally very near the sides of the column; the temperature and velocity profiles in the column are therefore of top-hat shape.

Some mixing takes place in the free convection column (region II), but the largest shears and thermal gradients occur in region III (a "side-mixing layer"). The main vortical recirculation takes place in region IV, fed to some extent by flow from region V, where horizontal velocities become large as the convection column air spills out on top of the atmosphere--just as warm fluid from an artesian spring spreads on a pond. Since the vortex recirculation occurs over a height of order H, and the combustion zone has a height $L << H$, the final recirculation stage is sink-like. Constriction of a relatively thick layer of recirculating air away from the combustion zone into the thin layer entering the zone necessarily leads to a considerable increase in velocities within this zone.

SCALINGS

The conservation equations for mass, momentum, and energy and an equation of state appropriate to the steady-state description of a (two-dimensional) large area fire are as follows:

$$\frac{\partial}{\partial x}(\rho u) + \frac{\partial}{\partial y}(\rho v) = 0 ;$$

$$\rho\left(u\frac{\partial u}{\partial x} + v\frac{\partial u}{\partial y}\right) = -\frac{\partial P}{\partial x} + \mathcal{E}_{11}\frac{\partial^2 u}{\partial x^2} + \mathcal{E}_{12}\frac{\partial^2 u}{\partial y^2} ;$$

$$\rho\left(u\frac{\partial v}{\partial x} + v\frac{\partial v}{\partial y}\right) = -\left(\frac{\partial P}{\partial y} + g\rho\right) + \mathcal{E}_{21}\frac{\partial^2 v}{\partial x^2} + \mathcal{E}_{22}\frac{\partial^2 v}{\partial y^2} ;$$

$$\rho C_P\left(u\frac{\partial T}{\partial x} + v\frac{\partial T}{\partial y}\right) = \left(u\frac{\partial P}{\partial x} + v\frac{\partial P}{\partial y}\right) + Q \cdot q(x, y) + k_1\frac{\partial^2 T}{\partial x^2} + k_2\frac{\partial^2 T}{\partial y^2} ;$$

$$P = \rho RT . \qquad (2.1)$$

Here, the various $\mathcal{E}_{ij}$ and k_i are diffusion coefficients representing all dissipative processes (molecular and turbulent) for momentum and heat. It is assumed that the Reynolds stresses may be approximated as proportional to appropriate second-derivative terms. $Q \cdot q(x, y)$ is the volumetric heat addition rate due to combustion with Q the mean rate and q(x, y) a specified spatial distribution; all other variables have their usual meanings [Small and Brode, 1980].

Pressure, density, and temperature are expected to be of the same order of magnitude in all regions of interest as they are in the far-field atmosphere; ground-level atmospheric values hence serve as nominal scales for these variables. Since the driving force for a firestorm's entire airflow lies in the combustion zone, the model uses the characteristic dimension and flow speeds of that zone as nominal scales (denoted by "{ }") for spatial coordinates and velocities:

$$\{x\} = D,\ \{y\} = L\ ; \qquad \{P\} = P_a,\ \{\rho\} = \rho_a,\ \{T\} = T_a\ ;$$

$$\{u\} = U,\ \{v\} = \varepsilon U,\ U \text{ yet to be chosen}\ . \qquad (2.2)$$

Here, subscript a refers to ground-level atmospheric values,

$$\varepsilon = \left(\frac{L}{D}\right) \sim 10^{-2} << 1 \quad \text{for } L \sim 10^2 \text{ m},\ D \sim 10^4 \text{ m}\ , \qquad (2.3)$$

and U is chosen such that the terms for convective transport and heat addition rate in the fourth expression in Eq. (2.1) balance (that is, so the equation represents a flow driven by combustion heating). As we show below, $U \sim 240$ km/hr is the indicated scale for $L \sim 10^2$ m and $D \sim 10^4$ m. The scaling between u and v is chosen to preserve the continuity equation [Eq. (2.1)] subject to the x and y scalings.

The nominal scalings in Eq. (2.2) are appropriate for the study of firestorm airflow in region I (see Fig. 2). Other regions require rescalings. For example, for $H \sim D$ and ε as in Eq. (2.3), the appropriate scaling for y in regions II, III, and IV is $\{y\} = H$, in contrast to Eq. (2.2). All rescalings are discussed as needed in Sec. 3.

MATHEMATICAL MODEL

The nondimensional version of Eq. (2.1), obtained by scaling Eq. (2.1) as in Eq. (2.2), is

$$\frac{\partial}{\partial x}(\rho u) + \frac{\partial}{\partial y}(\rho v) = 0 \;;$$

$$\rho\left(u\frac{\partial u}{\partial x} + v\frac{\partial u}{\partial y}\right) = -\left(\frac{1}{\delta_1}\right)\frac{\partial P}{\partial x} + \varepsilon M_{11}\frac{\partial^2 u}{\partial x^2} + \frac{1}{\varepsilon}M_{12}\frac{\partial^2 u}{\partial y^2} \;;$$

$$\rho\left(u\frac{\partial v}{\partial x} + v\frac{\partial v}{\partial y}\right) = -\left(\frac{1}{\varepsilon^2\delta_1}\right)\frac{\partial P}{\partial y} - \left(\frac{1}{\varepsilon\delta_1}\right)\rho + \varepsilon M_{21}\frac{\partial^2 v}{\partial x^2} + \frac{1}{\varepsilon}M_{22}\frac{\partial^2 v}{\partial y^2} \;;$$

$$\rho\left(u\frac{\partial T}{\partial x} + v\frac{\partial T}{\partial y}\right) = \left(\frac{\gamma - 1}{\gamma}\right)\left(u\frac{\partial P}{\partial x} + v\frac{\partial P}{\partial y}\right) + \beta q(x, y) + \varepsilon K_1\frac{\partial^2 T}{\partial x^2} + \frac{K_2}{\varepsilon}\frac{\partial^2 T}{\partial y^2} \;;$$

$$P = \rho T \;, \qquad (2.4)$$

where

$$\delta_1 = \left[\frac{U^2}{(P_a/\rho_a)}\right], \quad \left(\frac{P_a}{\rho_a}\right) \approx (1010 \text{ km} \cdot \text{hr}^{-1})^2 \;;$$

$$\delta_2 = \left(\frac{U^2}{gD}\right), \quad gD \approx (1080 \text{ km} \cdot \text{hr}^{-1})^2 \quad \text{for } D = 10^4 \text{ m} \;;$$

$$M_{ij} = \left(\frac{\mathcal{E}_{ij}}{P_a UL}\right), \quad K_i = \left(\frac{k_i}{\rho_a UL}\right) \quad \text{for } 1 \le i, j \le 2 \;;$$

$$\beta = \left(\frac{\gamma - 1}{\gamma}\right)\left(\frac{QD}{\rho_a U}\right), \quad \gamma = 1.4 \;; \qquad (2.5)$$

and

$$q \equiv 0 \quad \text{for } y > 1 \quad \text{and/or } |x| > 1 \;. \qquad (2.6)$$

Setting $\beta = 1$, so that the heat released by combustion is the dominant term, we determine the nominal velocity scale U from the last expression in Eq. (2.5) as

$$U = \left(\frac{\gamma - 1}{\gamma}\right)\left(\frac{Q}{P_a}\right)\left(\frac{L}{\varepsilon}\right) . \tag{2.7}$$

For $L \sim 10^2$ m, $D \sim 10^4$ m, and $QL \sim 58 \times 10^{-3}$ cal/m^2 - sec [DCPA, 1973], we therefore have

$$U \sim 240 \text{ km/hr} . \tag{2.8}$$

From Eq. (2.5), we also then have δ_1, $\delta_2 = 0(\varepsilon)$, and Eq. (2.4) can be rewritten in final form as

$$\frac{\partial}{\partial x}(\rho u) + \frac{\partial}{\partial y}(\rho v) = 0 ;$$

$$\rho\left(u\frac{\partial u}{\partial x} + v\frac{\partial u}{\partial y}\right) = -\frac{B}{\varepsilon}\frac{\partial P}{\partial x} + \varepsilon M_{11}\frac{\partial^2 u}{\partial x^2} + \frac{1}{\varepsilon}M_{12}\frac{\partial^2 u}{\partial y^2} ;$$

$$\rho\left(u\frac{\partial v}{\partial x} + v\frac{\partial v}{\partial y}\right) = -\frac{B}{\varepsilon^3}\left(\frac{\partial P}{\partial y} + \varepsilon A\rho\right) + \varepsilon M_{21}\frac{\partial^2 v}{\partial x^2} + \frac{1}{\varepsilon}M_{22}\frac{\partial^2 v}{\partial y^2} ;$$

$$\rho\left(u\frac{\partial T}{\partial x} + v\frac{\partial T}{\partial y}\right) = \frac{\gamma - 1}{\gamma}\left(u\frac{\partial P}{\partial x} + v\frac{\partial P}{\partial y}\right) + q(x, y) + \varepsilon K_1\frac{\partial^2 T}{\partial x^2} + \frac{1}{\varepsilon}K_2\frac{\partial^2 T}{\partial y^2} ;$$

$$P = \rho T , \tag{2.9}$$

where

$$A = \frac{\delta_1}{\delta_2} \approx 1 , \qquad B = \frac{\varepsilon}{\delta_1} = 0(1) . \tag{2.10}$$

The various M_{ij} and K_i are phenomenological coefficients that describe the extent of the turbulent forces. At present, it is only possible to estimate the magnitudes of these coefficients in each region, relying on physical understanding of the balance of forces and crude calculations to approximate the $\mathcal{E}_{ij}$ and k_i. While phenomenological theories such as mixing-length theory can provide useful approximations for the turbulent forces in most of the regions (II, III, IV, V) of this component model, they are not applicable to the turbulence generated by the fire in region I. In view of the scalings applied to region I, and in consideration of the limit $\varepsilon \to 0$, we assume that the pressure and buoyancy forces are large compared with the diffusive forces (i.e., for $\varepsilon \to 0$, M_{ij}, $k_i \to 0$). The effect of turbulence in region I provides only a correction to the basic flow.

SECTION 3
MODEL ANALYSIS

Here, we present a unified description of the overall airflow generated by a large area fire, using asymptotic analysis in the limit where the combustion zone aspect ratio ε (= L/D) tends towards zero. The analysis involves constructing asymptotic expansions for the solution to the mathematical model equations [Eq. (2.9)] in each component region defined in Fig. 2, and suitably matching the various expansions. The matching proceeds as diagrammed in Fig. 3. Expansions in the two parts of region I (the combustion zone and the area above it), are carried out separately, then matched. An expansion in region II is then developed and matched to the expansion in the upper part of region I. Finally, a partial expansion in region IV is developed and matched with the region II expansion by means of yet another expansion in the intermediate region III. The last step in the basic overall flow description is the completion of the region IV expansion and its matching with the inflow in region I. Iterative steps may involve further intermediate analysis in one or both of regions IA and IB. (For the moment, $\hat{\alpha}$ in Fig. 3 is left arbitrary; it is defined later in this section.)

The solution expansions for region I are based directly on the model equations [Eq. (2.9)]. In other regions, expansions are derived from rescaled versions of those equations. In all regions, however, the expansions have the same general form, namely

$$u = u_0 + \varepsilon u_1 + \varepsilon^2 u_2 + \varepsilon^3 u_3 + \cdots ;$$

$$v = v_0 + \varepsilon v_1 + \varepsilon^2 v_2 + \varepsilon^3 v_3 + \cdots ;$$

$$P = P_0 + \varepsilon P_1 + \varepsilon^2 P_2 + \varepsilon^3 P_3 + \cdots ;$$

$$\rho = \rho_0 + \varepsilon \rho_1 + \varepsilon^2 \rho_2 + \varepsilon^3 \rho_3 + \cdots ;$$

$$T = T_0 + \varepsilon T_1 + \varepsilon^2 T_2 + \varepsilon^3 T_3 + \cdots . \qquad (3.1)$$

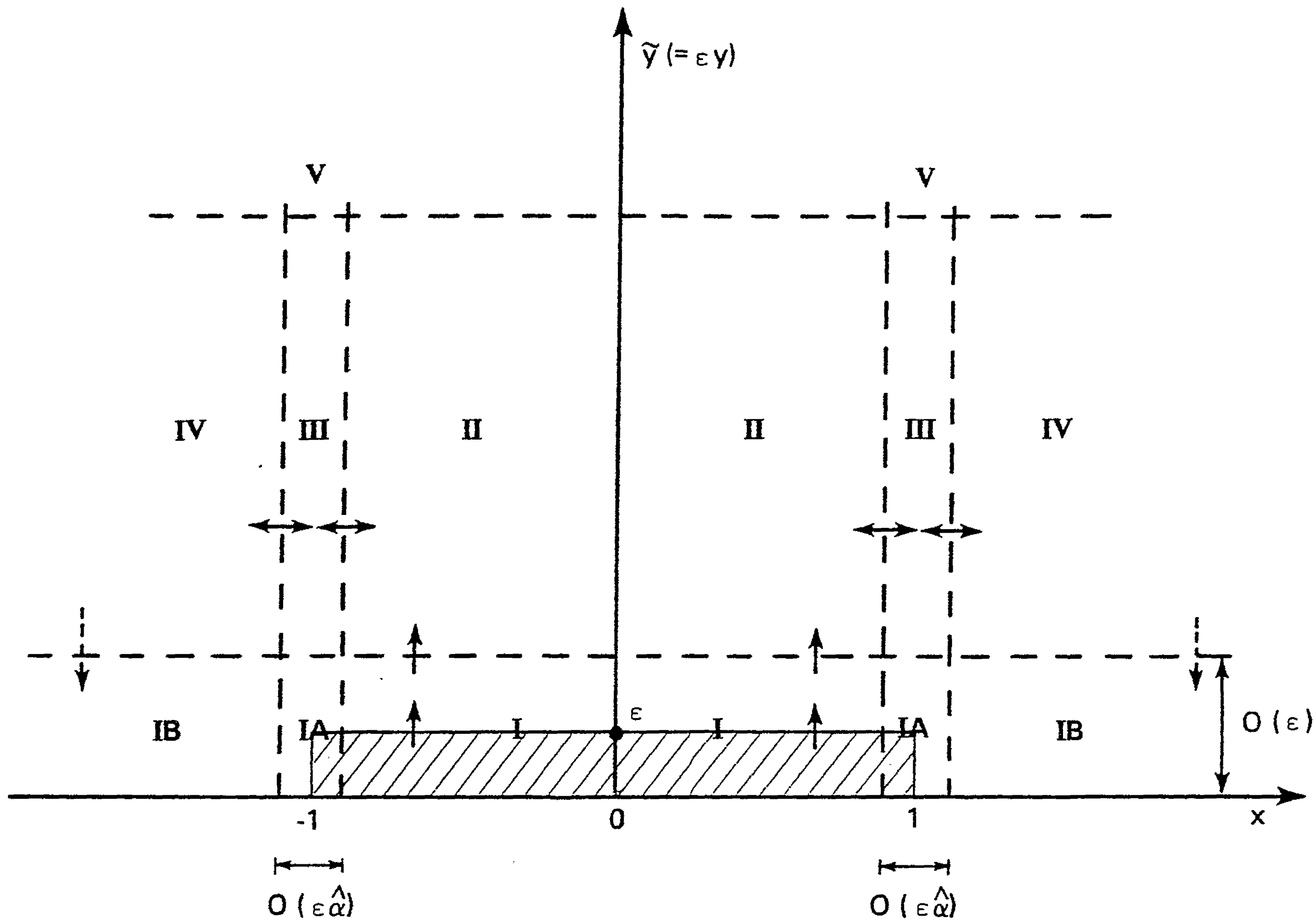

Figure 3. Matching diagram for asymptotic solution of mathematical model equations.

Below, we focus on determining the leading-order terms in the expansions. The leading-order equations (which describe the basic flow structure for a large area fire) are introduced and solutions discussed. Derivations and further discussion are given in Appendixes A and B.

SOURCE LAYER

Substituting Eq. (3.1) into Eq. (2.9) and assuming all M_{ij}, $K_i \ll 1$ gives the leading-order equation set in region I:

$$\frac{\partial}{\partial x}(\rho_0 u_0) + \frac{\partial}{\partial y}(\rho_0 v_0) = 0 \ ;$$

$$\rho_0 \left(u_0 \frac{\partial u_0}{\partial x} + v_0 \frac{\partial u_0}{\partial y} \right) = - B \frac{\partial P_1}{\partial x} \ ;$$

$$\frac{\partial P_1}{\partial y} + A\rho_0 = 0 \ ;$$

$$\rho_0 \left(u_0 \frac{\partial T_0}{\partial x} + v_0 \frac{\partial T_0}{\partial y} \right) = q(x, y) \ ;$$

$$\rho_0 T_0 = P_0 = \text{constant} \ . \qquad (3.2)$$

The momentum equations here are actually first-order correction ones. The leading-order equations $\partial P_0/\partial x = 0$ and $\partial P_0/\partial y = 0$ imply that P_0 = constant and changes in pressure are at most $O(\varepsilon)$, which is consistent with experimental evidence on small (unenclosed) fires [McCaffrey, 1979].

The equation set in Eq. (3.2) is to be solved subject to the natural boundary conditions

(a) along $y = 0$: $v_0 = 0$;

(b) along $x = 0$: $u_0 = 0$; $\frac{\partial v_0}{\partial x} = \frac{\partial P_1}{\partial x} = \frac{\partial \rho_0}{\partial x} = \frac{\partial T_0}{\partial x} = 0 \qquad (3.3)$

(i.e., there can be no flow into the ground, and the flow is symmetric about the x = 0 line). Since the diffusion terms are small with respect to the pressure and buoyancy terms, second derivatives do not appear in the leading-order equations, and the no-slip condition at y = 0 cannot be specified as a boundary condition. This implies the need for an additional rescaling (e.g., $y^* \sim \varepsilon y$), in which a thin region near y = 0 is defined and turbulent forces balance pressure and inertia forces to leading order. Since the addition of a thin region near y = 0 does not affect the basic flow structure in region I, we proceed with the model development as defined; we will treat the thin subregion in future research.

The solution of Eq. (3.2) divides into two parts. In the combustion zone itself (i.e., where $0 \leq y \leq 1$), q(x, y) is in general nonzero; it seems the solution must be determined by numerical computation. Outside the combustion zone, though, q(x, y) is zero, and the solution may be found by analytical methods.

Before discussing the analytic solution, we note that whereas q(x, y) is by definition zero outside the combustion zone, radiation is an important factor in the energy balance in that area and must ultimately be included in the model. Studies of plume behavior [Murgai, 1962] show that including radiation effects causes the thermodynamic variables to rapidly approach the local outside atmospheric values. This finding is consistent with McCaffrey [1979], whose measurements showed temperature rapidly approaching atmospheric values in the region near the fire. Radiation effects have been modeled [Murgai, 1962] by assuming either a flux term of the form

$$q_{rad} = c(T^4 - T_\infty) \; , \qquad (3.4)$$

or a diffusion term of the form

$$q_{rad} = c\nabla^2(T^4) \; , \qquad (3.5)$$

where c is a constant and T_∞ the local ambient temperature. To elucidate the general form of the solution, we ignore the effect of radiation for the sake of analytic simplicity, and determine the basic flow structure. Future work will include the effect of radiation, with $q(x, y)$ replaced by $q(x, y) - q_{rad}$, with q_{rad} as given in Eq. (3.4) or (3.5).

As shown in Appendix A, a stream (or pseudostream) function $\psi(x, y)$ can be defined for Eq. (3.2) by

$$\frac{\partial\psi}{\partial x} = - v_0 \ , \qquad \frac{\partial\psi}{\partial y} = u_0 \tag{3.6}$$

in the region outside the combustion zone. The general solution of Eq. (3.2) is then given by

$$u_0 = \frac{\partial\psi}{\partial y} \ , \qquad v_0 = -\frac{\partial\psi}{\partial x} \ ;$$

$$T_0 = T_0(\psi) \ , \qquad \rho_0 = \frac{P_0}{T_0} = \rho_0(\psi) \ ;$$

$$P_1 = P_1(x, 1) - A\int_1^y \rho_0 \, dy \ , \tag{3.7}$$

with ψ required to satisfy

$$\frac{\partial^2\psi}{\partial y^2} + \left[\left(\frac{1}{\rho_0}\right)\left(\frac{d\rho_0}{d\psi}\right)\right]\left[\frac{1}{2}\left(\frac{\partial\psi}{\partial y}\right)^2 + ABy\right] = E(\psi) \ , \tag{3.8}$$

and the forms of the functions $P_1(x, 1)$, $\rho_0(\psi)$, and $E(\psi)$ being arbitrary. In general, the behavior along the y = 1 line of the solution to Eq. (3.2) inside the combustion zone determines the forms of the three functions (for example, ρ_0 must be continuous across the line); the complete solution outside the combustion zone is then found by a simple numerical integration of the (ordinary) differential equation in Eq. (3.8). As further shown in Appendix A, however, suitably matching the outside solution to a solution inside region II (the convection column) actually restricts the former to the following form:

$$u_0 \equiv 0 \ , \qquad v_0 = v_\infty(x) \ ;$$

$$\rho_0 \equiv \rho_\infty \ , \qquad T_0 \equiv \frac{P_0}{\rho_\infty} \ ;$$

$$P_1 = P_{10} - A\rho_\infty(y - 1) \ , \tag{3.9}$$

where ρ_∞ and P_{10} are constants to be determined and $v_\infty(x)$ is a function of x alone, also to be determined (ψ is a function of x alone as well).

The solution of Eq. (3.2) inside the combustion zone must satisfy the boundary conditions in Eq. (3.3). If the solution is to match with that for Eq. (3.9), the inside solution must satisfy the further boundary conditions that P_1, ρ_0, and T_0 are each constant and that $u_0 = 0$ along the y = 1 line. Analytic solutions to this boundary value problem have been sought in various ways (for example, by similarity solution methods, by means of coordinate changes), but no approach has succeeded, and it appears that the problem must be solved numerically.

A significant reduction in the problem's complexity is effected, however, by introducing the stream function $\tilde{\psi}(x, y)$, defined by

$$\frac{\partial\tilde{\psi}}{\partial x} = - \rho_0 v_0 \ , \qquad \frac{\partial\tilde{\psi}}{\partial y} = \rho_0 u_0 \tag{3.10}$$

[compare Eq. (3.6)]. As Appendix A shows, the five equations in Eq. (3.2), the boundary conditions in Eq. (3.3), and the additional y = 1 boundary conditions just mentioned can be simplified to

$$\frac{\partial}{\partial y}\left[\left(\frac{\partial\tilde{\psi}}{\partial y}\right)\frac{\partial}{\partial x}\left(\frac{\frac{\partial\tilde{\psi}}{\partial y}}{\rho_0}\right) - \left(\frac{\partial\tilde{\psi}}{\partial x}\right)\frac{\partial}{\partial y}\left(\frac{\frac{\partial\tilde{\psi}}{\partial y}}{\rho_0}\right)\right] = AB\left(\frac{\partial\rho_0}{\partial x}\right) \;;$$

$$\left[\left(\frac{\partial\tilde{\psi}}{\partial y}\right)\left(\frac{\partial\rho_0}{\partial x}\right) - \left(\frac{\partial\tilde{\psi}}{\partial x}\right)\left(\frac{\partial\rho_0}{\partial y}\right)\right] = -\left[\frac{q(x,\, y)}{P_0}\right]\rho_0^2 \;, \tag{3.11}$$

subject to the following conditions:

(a) along $y = 0$: $\tilde{\psi} = 0$;

(b) along $x = 0$: $\tilde{\psi} = 0$;

(c) along $y = 1$: $\frac{\partial\tilde{\psi}}{\partial y} = \frac{\partial^2\tilde{\psi}}{\partial y^2} = 0$, $\rho_0 = \rho_\infty$.

The boundary value problem is actually an eigenvalue problem: P_0 and ρ_∞ may be chosen as required to find an appropriate solution. Such freedom is presumably necessary to adjust the solution to match with solutions in regions II and IV (Fig. 3), and hence complete the unified description of the overall flow for a large area fire.

Once an appropriate (numerical) solution of Eq. (3.11) is constructed, including choices of P_0 and ρ_∞, the complete solution of Eq. (3.2) inside the combustion zone is given by

$$u_0 = \left(\frac{1}{\rho_0}\right)\left(\frac{\partial\tilde{\psi}}{\partial y}\right), \quad v_0 = -\left(\frac{1}{\rho_0}\right)\left(\frac{\partial\tilde{\psi}}{\partial x}\right),$$

$$T_0 = \frac{P_0}{\rho_0} ,$$

and

$$P_1 = P_{10} + A\int_y^1 \rho_0 \, dy \;, \tag{3.12}$$

with P_{10} now arbitrary (and subject to eventual determination by matching requirements). The continuation of the solution above the combustion zone is then given by Eq. (3.9), with

$$v_\infty(x) = -\left(\frac{1}{\rho_0}\right)\left[\frac{\partial\tilde{\psi}}{\partial x}(x, 1)\right] . \qquad (3.13)$$

Since $u_0 \equiv 0$ in Eq. (3.9), the flow in the upper part of the source layer is nearly vertical (deviations from the vertical coming only from correction terms in the expansion for the solution to the model equations). As we show below, such is also the case for the flow in the convection column above the source layer.

CONVECTION COLUMN

Since the characteristic height H of the convection column is on the order of D ($\sim 10^4$ m) and not L ($\sim 10^2$ m, Fig. 1), the vertical spatial coordinate must be rescaled as

$$\tilde{y} = \varepsilon y . \qquad (3.14)$$

To preserve continuity in rescaling Eq. (2.9), we nominally assume $u = O(\varepsilon)$ in the column and introduce the further rescaling

$$\tilde{u} = \frac{u}{\varepsilon} , \qquad (3.15)$$

where $\tilde{u}$ is of order 1. Subject to Eqs. (3.14) and (3.15), the nominal rescaling of Eq. (2.9) is then

$$\frac{\partial}{\partial x}(\rho\tilde{u}) + \frac{\partial}{\partial\tilde{y}}(\rho v) = 0 ;$$

$$\rho\left(\tilde{u}\frac{\partial\tilde{u}}{\partial x} + v\frac{\partial\tilde{u}}{\partial\tilde{y}}\right) = -\frac{B}{\varepsilon^3}\frac{\partial P}{\partial x} + M_{11}\frac{\partial^2\tilde{u}}{\partial x^2} + M_{12}\frac{\partial^2\tilde{u}}{\partial\tilde{y}^2} ;$$

$$\rho\left(\tilde{u}\frac{\partial v}{\partial x} + v\frac{\partial v}{\partial\tilde{y}}\right) = -\frac{B}{\varepsilon^3}\left(\frac{\partial P}{\partial\tilde{y}} + A\rho\right) + M_{21}\frac{\partial^2 v}{\partial x^2} + M_{22}\frac{\partial^2 v}{\partial\tilde{y}^2} ;$$

$$\rho\left(\tilde{u}\frac{\partial T}{\partial x} + v\frac{\partial T}{\partial \tilde{y}}\right) = \left(\frac{\gamma - 1}{\gamma}\right)\left(\tilde{u}\frac{\partial P}{\partial x} + v\frac{\partial P}{\partial \tilde{y}}\right) + K_1\frac{\partial^2 T}{\partial x^2} + K_2\frac{\partial^2 T}{\partial \tilde{y}^2} ;$$

$$P = \rho T , \tag{3.16}$$

where q(x, y) is dropped because it is identically zero everywhere above the combustion zone. We will show that this version of Eq. (2.9) is appropriate for the study of both the convection column and the recirculation zone (regions II and IV, Fig. 2), but that it must be further rescaled for the side mixing layer (region III), where large shears and thermal gradients give large horizontal derivatives.

The leading-order equations to be obtained from Eq. (3.16) in the limit $\varepsilon \to 0$ clearly depend on the magnitude of the various M_{ij} and K_i. Considering first the convection column, we note that it is basically a vertical flow, with the dominant shear represented by $\partial v/\partial x$. We apply mixing-length theory to estimate $\mathcal{E}_{ij}$. Modeling turbulent diffusion in this manner is implicitly an approximation, in that it infers knowledge of the structure of the turbulence. However, in the absence of a definitive understanding of the local turbulence, and in the interest of obtaining a leading-order approximation, we use conventional mixing-length theory and estimate the turbulent diffusion coefficients for the convection column as follows:

$$M_{ij},\ K_i \sim \left(\frac{1}{U\varepsilon D}\right)\left[\ell^2\left(\frac{\varepsilon U}{D}\right)\frac{\partial v}{\partial x}\right] , \tag{3.17}$$

where ℓ is the mixing length and v and x are the scaled order one variables in Eq. (3.16). Assuming $\ell \sim \alpha D$ where $\alpha < 1$, then

$$M_{ij},\ K_i \sim \alpha^2\frac{\partial v}{\partial x} . \tag{3.18}$$

Recalling that $D \sim 10^4$ m and assuming a mixing length $\ell \sim 10^3$ m yields $\alpha \sim 10^{-1}$, and hence

$$M_{ij},\ K_i \sim 0(\varepsilon) \tag{3.19}$$

in the convection column. That expression is consistent with the mixing coefficients used by Smith, Morton, and Leslie [1975] and by Delage and Taylor [1970]. In the side mixing layers, x is rescaled, and we expect the M_{ij} and K_i to be at least one order of magnitude larger.

From Eq. (3.1), Eq. (3.15), and the assumption that $u = O(\varepsilon)$ in the convection column, the appropriate expansion for $\tilde{u}$ in region II is

$$\tilde{u} = u_1 + \varepsilon u_2 + \varepsilon^2 u_3 + \cdots \quad . \tag{3.20}$$

Substituting into Eq. (3.16) the expansions for v, P, ρ, and T in Eq. (3.1), Eq. (3.19), and Eq. (3.20), the leading-order equation set in region II is

$$\frac{\partial}{\partial x}(\rho_0 u_1) + \frac{\partial}{\partial \tilde{y}}(\rho_0 v_0) = 0 \ ;$$

$$\frac{\partial P_0}{\partial x} = 0 \ ;$$

$$\frac{\partial P_0}{\partial \tilde{y}} + A\rho_0 = 0 \ ;$$

$$\rho_0\left(u_1 \frac{\partial T_0}{\partial x} + v_0 \frac{\partial T_0}{\partial \tilde{y}}\right) = \left(\frac{\gamma - 1}{\gamma}\right)\left(u_1 \frac{\partial P_0}{\partial x} + v_0 \frac{\partial P_0}{\partial \tilde{y}}\right) ;$$

$$P_0 = \rho_0 T_0 \ . \tag{3.21}$$

In what follows, we show that a unified description of a large area fire can be constructed with the convection column flow governed by Eq. (3.21) if we set

$$u_1 \equiv 0 \ . \tag{3.22}$$

Moreover, further analysis suggests that a unified description is not possible if Eq. (3.22) does not hold. We therefore postulate Eq. (3.22) and use it in Eq. (3.21) to derive the final leading-order equation set for region II:

$$\frac{\partial}{\partial \tilde{y}} (\rho_0 v_0) = 0 , \quad u_1 \equiv 0 ;$$

$$\frac{\partial P_0}{\partial x} = 0 ;$$

$$\frac{\partial P_0}{\partial \tilde{y}} + A\rho_0 = 0 ;$$

$$\rho_0 \left(\frac{\partial T_0}{\partial \tilde{y}}\right) = \left(\frac{\gamma - 1}{\gamma}\right)\left(\frac{\partial P_0}{\partial \tilde{y}}\right) ;$$

$$P_0 = \rho_0 T_0 . \tag{3.23}$$

Appendix A shows that the unique solution of Eq. (3.23) that matches (as $\tilde{y} \to 0$) with the region I solution in Eq. (3.9) (as $y \to \infty$) is

$$u_1 \equiv 0 , \quad v_0 = \left(\frac{\rho_\infty}{\rho_0(\tilde{y})}\right) v_\infty(x) ;$$

$$\rho_0 = \rho_0(\tilde{y}) = \rho_\infty \left[1 - A\left(\frac{\rho_\infty}{P_\infty}\right)\left(\frac{\gamma - 1}{\gamma}\right) \tilde{y}\right]^{\left(\frac{1}{\gamma-1}\right)} ;$$

$$T_0 = \left(\frac{P_\infty}{\rho_\infty}\right)\left[1 - A\left(\frac{\rho_\infty}{P_\infty}\right)\left(\frac{\gamma - 1}{\gamma}\right) \tilde{y}\right] ;$$

$$P_0 = P_\infty \left[1 - A\left(\frac{\rho_\infty}{P_\infty}\right)\left(\frac{\gamma - 1}{\gamma}\right) \tilde{y}\right]^{\left(\frac{\gamma}{\gamma-1}\right)} , \tag{3.24}$$

where P_∞ is the constant value of P_0 in region I. With P_0, ρ_0, and T_0 as in Eq. (3.24), the thermodynamic state in the convection column is that of a specific adiabatic atmosphere. Furthermore, in view of the velocity scalings in Eq. (2.2), the rescaling in Eq. (3.15), the expansion in Eq. (3.20), and the forms of u_1 and v_0 in Eq. (3.24), the flow in the column is basically vertical: the dimensional vertical velocity is much larger than the dimensional horizontal velocity.

RECIRCULATION REGION

As pointed out earlier, Eq. (3.16) is the appropriately scaled version of Eq. (2.9) for studying the flow in the recirculation region (IV), and as with the convection column, the leading-order equations to be obtained from Eq. (3.16) in the $\varepsilon \to 0$ limit depend on the magnitudes of the M_{ij} and K_i. From mixing-length theory, we expect values for the M_{ij} and K_i in the recirculation region to be similar to those in the convection column. We note, however, that the recirculation flow is basically two-dimensional, with comparable shear in both x and y directions. For the present analysis, we therefore rely on published estimates for the turbulent coefficients.

Owing to the uncertainty of the levels of turbulence, a considerable spread of values has been used in past studies. Delage and Taylor [1970] use M_{ij} and $K_i \sim O(\varepsilon)$ ($\mathcal{E}_{ij}/\rho_a \sim 50$ m^2/sec); Smith, Morton, and Leslie [1975] use $O(\varepsilon^{3/2}) \le M_{ij}$, $K_i \le O(\varepsilon^{1/2})$, which corresponds to 5 m^2/sec $\le \mathcal{E}_{ij}/\rho_a \le$ 500 m^2/sec. It is interesting that despite the spread of values, the numerical results are all similar. Relative to the above studies, fairly large values of the diffusion coefficients, $M_{ij} \sim O(1)$ ($\mathcal{E}_{ij}/\rho_a$ = 2000 m^2/sec), were used by Estoque and Bhumralkar [1969]. Consistent with the ordering performed in the convection column, we adopt M_{ij}, $K_i \sim O(\varepsilon)$ for the recirculation region. We recognize that this choice warrants critical reexamination in the future; however, the basic flow structure should remain qualitatively the same.

Substituting Eq. (3.20) and the expansions for v, P, ρ, and T defined in Eq. (3.1) into Eq. (3.16), we show the leading-order equation set in region IV to be the basic one initially developed for region II--i.e., Eq. (3.21). In the convection column (region II), a nearly vertical flow is reasonable, and the corresponding solution of Eq. (3.21) [Eq. (3.24)] has $u_1 \equiv 0$. This clearly cannot be the case in region IV, where the vortical recirculation requires that dimensional horizontal and vertical velocities (and hence u_1 and v_0) be the same order of magnitude. The region IV solution therefore cannot be found by the reduction used in the analysis of Eq. (3.21) for region II; in fact, the solution cannot be completely found at all without recourse to further, lower order perturbation analysis. That is, as shown in Appendix A, the last four equations in Eq. (3.21) are useful only in determining the thermodynamic state, leaving just the first equation,

$$\frac{\partial}{\partial x} (\rho_0 u_1) + \frac{\partial}{\partial \tilde{y}} (\rho_0 v_0) = 0 \ , \tag{3.25}$$

to relate the remaining two unknowns, u_1 and v_0. Another relationship between u_1 and v_0, which is provided by lower order analysis, involves still further relationships with new (lower order) variables. All the relationships are easily derived from analysis of lower order equation sets.

As shown in Appendix A, P_0, ρ_0, and T_0 must all be functions of $\tilde{y}$ alone and satisfy

$$\frac{dP_0}{d\tilde{y}} + A\rho_0 = 0 \ ;$$

$$\rho_0 \frac{dT_0}{d\tilde{y}} = \left(\frac{\gamma - 1}{\gamma}\right) \frac{dP_0}{d\tilde{y}} \ ;$$

$$P_0 = \rho_0 T_0 \ . \tag{3.26}$$

The solution of Eq. (3.26) that appropriately gives pressure, density, and temperature at atmospheric values along the ground (y = 0) is

$$T_0 = \left[1 - A\left(\frac{\gamma - 1}{\gamma}\right)\tilde{y}\right] ;$$

$$\rho_0 = \left[1 - A\left(\frac{\gamma - 1}{\gamma}\right)\tilde{y}\right]^{\left(\frac{1}{\gamma-1}\right)} ;$$

$$P_0 = \left[1 - A\left(\frac{\gamma - 1}{\gamma}\right)\tilde{y}\right]^{\left(\frac{\gamma}{\gamma-1}\right)} . \qquad (3.27)$$

This solution also represents an adiabatic atmosphere, though not the same atmosphere as in region II [compare Eq. (3.24)]--ρ_∞, the density just above the combustion zone, must be less than 1, for example. The leading-order flow field (u_1, v_0) in region IV remains to be found.

SIDE MIXING LAYER

Differences in temperature, density, pressure, and velocity between the convection column and the atmospheric recirculation region are smoothed out in a thin mixing layer (region III) along the side of the column. Since the smoothing involves (horizontal) diffusion of heat and momentum, the leading-order equations for the flow in this layer must retain horizontal diffusion terms from the rescaled version of the basic model equations [Eq. (2.9)]. For that flow, the coordinate rescaling

$$\tilde{x} = \left(\frac{x - 1}{\varepsilon}\right) \qquad (3.28)$$

proves appropriate: continuity is preserved subject to $\tilde{u} = O(\varepsilon)$, which is required in order for the mixing-layer flow to match the convection column flow (where $u_1 \equiv 0$). A characteristic mixing-layer thickness of $O(\varepsilon)$ is implied by Eq. (3.28) ($\hat{\alpha} = 1$ in Fig. 3).

Appendix A shows that, subject to Eq. (3.28) and the requirement that horizontal diffusion be a dominant effect in the side mixing layer, the leading-order equation set for the flow in that layer is given by

$$\frac{\partial}{\partial \tilde{x}} (\rho_0 u_2) + \frac{\partial}{\partial \tilde{y}} (\rho_0 v_0) = 0 , \quad u_1 \equiv 0 ;$$

$$-B \frac{\partial P_0}{\partial \tilde{x}} + \tilde{M}_{11} \left(\frac{\partial^2 u_2}{\partial \tilde{x}^2} \right) = 0 ;$$

$$-B \left(\frac{\partial P_0}{\partial \tilde{y}} + A\rho_0 \right) + \tilde{M}_{21} \left(\frac{\partial^2 v_0}{\partial \tilde{x}^2} \right) = 0 ;$$

$$\rho_0 \left(u_2 \frac{\partial T_0}{\partial \tilde{x}} + v_0 \frac{\partial T_0}{\partial \tilde{y}} \right) = \left(\frac{\gamma - 1}{\gamma} \right) \left(u_2 \frac{\partial P_0}{\partial \tilde{x}} + v_0 \frac{\partial P_0}{\partial \tilde{y}} \right) + \tilde{K}_1 \left(\frac{\partial^2 T_0}{\partial \tilde{x}^2} \right) ;$$

$$P_0 = \rho_0 T_0 . \tag{3.29}$$

Here, all variables with single subscripts are as in Eq. (3.1), and $\tilde{M}_{11}$, $\tilde{M}_{21}$, and $\tilde{K}_1$ are the rescalings of M_{11}, M_{21}, and K_1. Formally, the mixing-layer flow is nearly vertical: both u_1 and u_0 are taken to be identically zero. The flow actually represents a transition between the vertical flow in the convection column and the vortex-like flow in the atmospheric recirculation region, however: from the final boundary condition introduced in Eq. (3.30b), u_2 must grow toward infinity as $\tilde{x} \to \infty$.

The leading-order set in Eq. (3.29) is to be solved subject to the boundary conditions

$$\text{(a)} \quad \tilde{x} \to -\infty: \quad T_0 \to \left(\frac{P_\infty}{\rho_\infty} \right) \left[1 - A \left(\frac{\rho_\infty}{P_\infty} \right) \left(\frac{\gamma - 1}{\gamma} \right) \tilde{y} \right] ,$$

$$\rho_0 \to \rho_\infty \left[1 - A \left(\frac{\rho_\infty}{P_\infty} \right) \left(\frac{\gamma - 1}{\gamma} \right) \tilde{y} \right]^{\left(\frac{1}{\gamma - 1}\right)} ,$$

$$v_0 \to \left[1 - A \left(\frac{\rho_\infty}{P_\infty} \right) \left(\frac{\gamma - 1}{\gamma} \right) \tilde{y} \right]^{-\left(\frac{1}{\gamma - 1}\right)} \left[\lim_{x \to 1} v_\infty(x) \right] ;$$

and

$$\text{(b)} \quad \tilde{x} \to +\infty: \quad T_0 \to \left[1 - A\left(\frac{\gamma - 1}{\gamma}\right)\tilde{y}\right] ,$$

$$\rho_0 \to \left[1 - A\left(\frac{\gamma - 1}{\gamma}\right)\tilde{y}\right]^{\left(\frac{1}{\gamma-1}\right)} ,$$

$$v_0 \to \left[\lim_{x\to1} v_{IV}(x, \tilde{y})\right] ,$$

$$\frac{\partial u_2}{\partial \tilde{x}} \to \left[\lim_{x\to1}\left(\frac{\partial u_{IV}}{\partial x}\right)(x, \tilde{y})\right] , \tag{3.30}$$

where ρ_∞ and $v_\infty(x)$ are as in Eq. (3.9), P_∞ is as in Eq. (3.24), and v_{IV} and u_{IV} are the v_0 and u_1 velocity fields (yet to be found) in region IV. These conditions are prescribed to ensure that the model equation solutions developed thus far for regions II, III, and IV are smoothly matched and thus provide the basis for a unified description of the hydrodynamics and thermodynamics of a large area fire. The solution of Eq. (3.29), which is subject to Eq. (3.30), must seemingly be numerically computed.

DISCUSSION

The model equations may admit a second overall solution, which could describe some large area fires. The solution represents a flow with the same basic components as depicted in Fig. 1, but the convection plume is somewhat thinner. A schematic illustration of the components of this flow is given in Fig. 4 (to be compared with Fig. 3).

The second analytic possibility results from inspecting the behavior of the region I flow in the limit $y \to \infty$. Previously, streamlines rose vertically from the combustion zone, which implied the development of a thick column. Alternatively, all streamlines from the combustion zone could asymptotically approach the ($x = 0$) centerline as $y \to \infty$. This converging flow is to be matched as $y \to \infty$ with a plume solution in region II (Fig. 4), however, and is spread somewhat

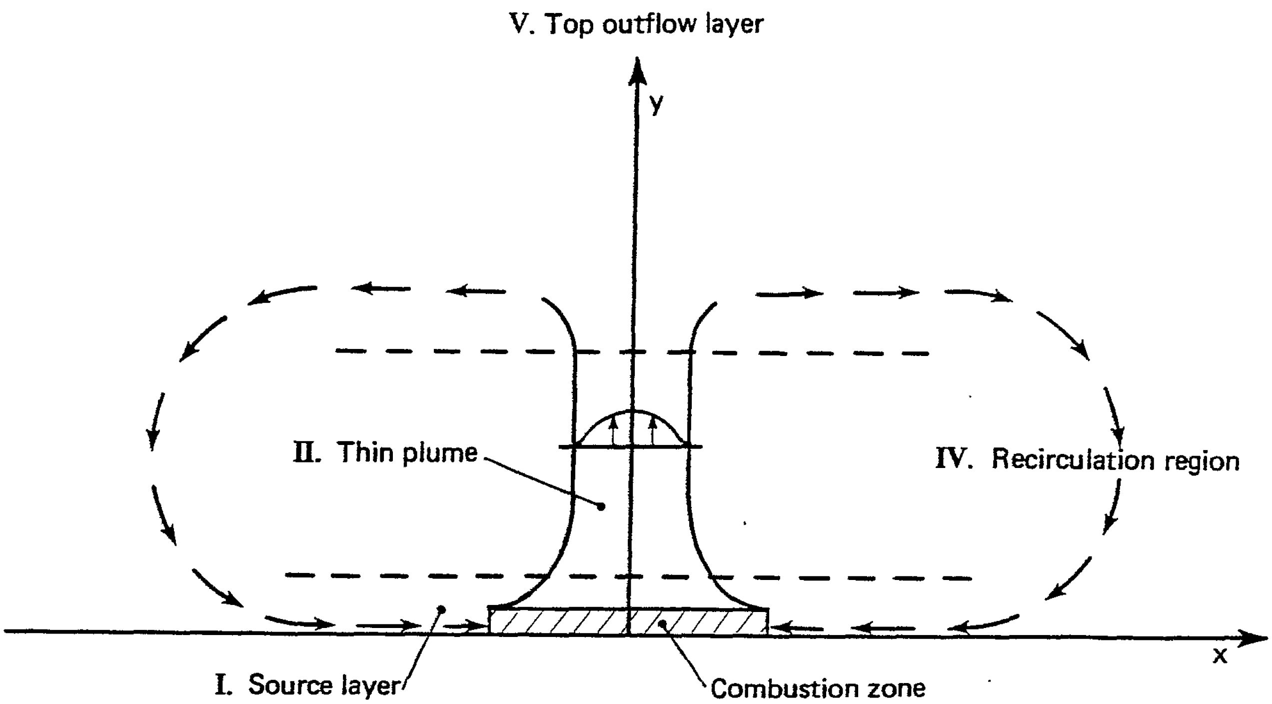

Figure 4. Schematic flow for alternative model solution.

by diffusion of heat and momentum. Therefore, convergence to a point is mathematical only, the physical import being that the flow forms a thin plume. In this type of flow behavior, the side mixing layer--necessary in the earlier treatment--is not required, as the thinner column can adjust to its surrounding atmospheric state through diffusion (because the plume aspect ratio is no longer unity). While the thick column solution seems appropriate for most physical cases, the thin plume structure may occur as the result of certain burning rates in an urban cross section. This issue requires further study.

Construction of this second type of solution is outlined below, with a more complete derivation presented in Appendix B. Constructing a solution also involves the use and matching of asymptotic expansions; the matching proceeds as diagrammed in Fig. 5 (compare Figs. 2, 3, and 4). Expansions for the solution in the source layer and the thin

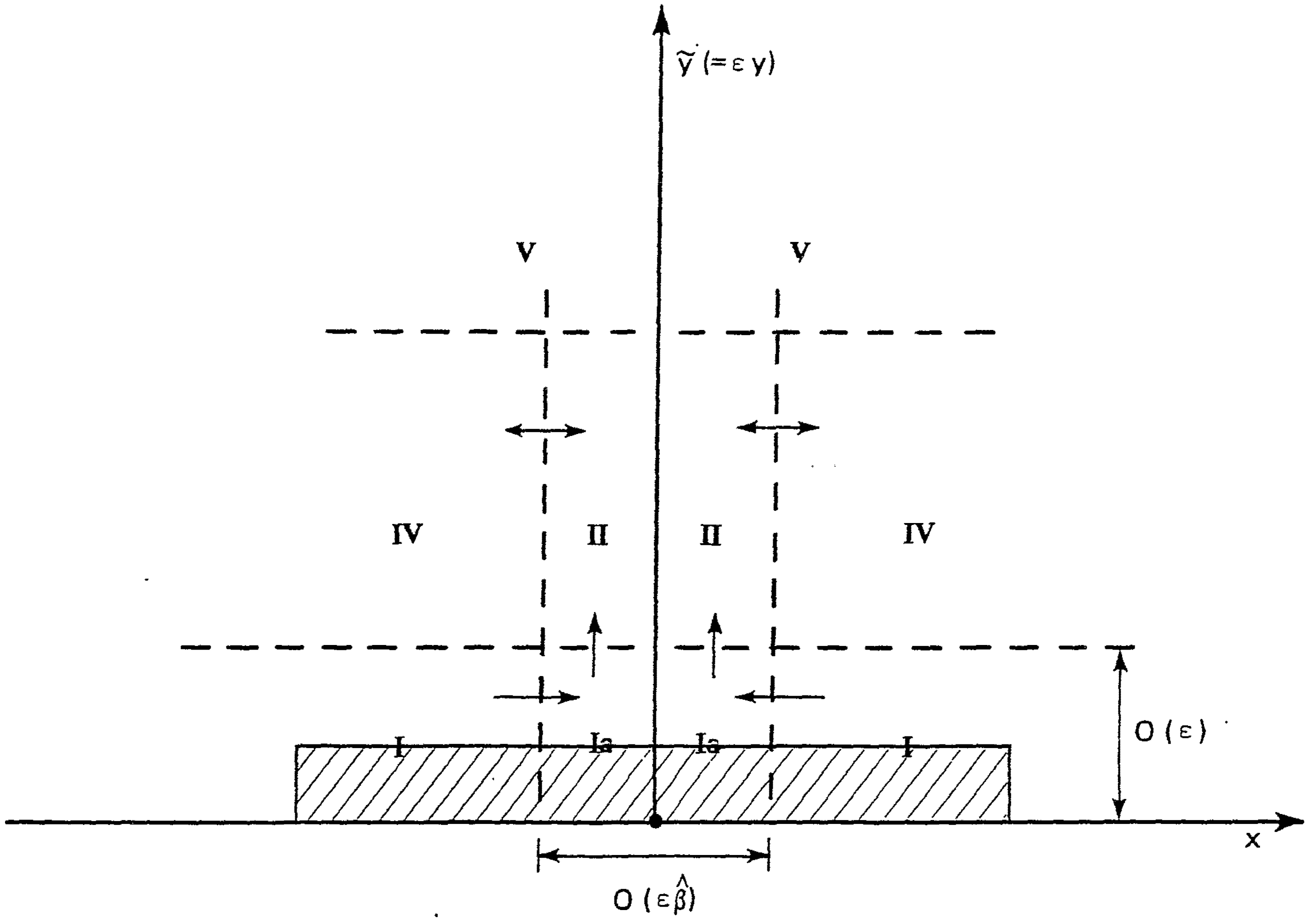

Figure 5. Matching diagram for second asymptotic solution.

plume region (regions I and II, respectively) are joined by means of an intermediate expansion in corner zone Ia. The characteristic thickness of the thin plume--and hence $\hat{\beta}$ (refer to Fig. 5)--depends on the magnitudes of the diffusion coefficients M_{ij} and K_i in the basic model equations [Eq. (2.9)]. For concreteness, we consider the sample case where

$$M_{11} = \left(\frac{\hat{M}_{11}}{\varepsilon^{1/2}}\right), \quad M_{21} = \left(\frac{\tilde{M}_{21}}{\varepsilon^{1/2}}\right), \quad K_1 = \left(\frac{\hat{K}_1}{\varepsilon^{1/2}}\right),$$

and

$$M_{12} = \hat{M}_{12}\varepsilon^{3/2}, \quad M_{22} = \hat{M}_{22}\varepsilon^{3/2}, \quad K_2 = \hat{K}_2\varepsilon^{3/2}, \qquad (3.31)$$

where all $\hat{M}_{ij}$ and $\hat{K}_i$ are $O(1)$. As we discuss shortly, choosing $\hat{\beta} = 1/2$ [that is, defining a characteristic plume thickness $O(\varepsilon^{1/2}D)$, which is on the order of several kilometers] is appropriate for this particular case. Other selections for the M_{ij} and K_i lead to other choices for $\hat{\beta}$.

Subject to Eq. (3.31), the following expansions prove appropriate for the unified description of the solution to Eq. (2.9) over regions I, Ia, and II (Fig. 5):

$$u = u_0 + \varepsilon^{3/2}u_{1/2} + \varepsilon u_1 + \varepsilon^{3/2}u_{3/2} + \varepsilon^2 u_2 + \cdots ;$$

$$v = \left(\frac{1}{\varepsilon^{1/2}}\right) v_{-1/2} + v_0 + \varepsilon^{1/2}v_{1/2} + \varepsilon v_1 + \varepsilon^{3/2}v_{3/2} + \varepsilon^2 v_2 + \cdots ;$$

$$P = P_0 + \varepsilon^{1/2}P_{1/2} + \varepsilon P_1 + \varepsilon^{3/2}P_{3/2} + \varepsilon^2 P_2 + \cdots ;$$

$$\rho = \rho_0 + \varepsilon^{1/2}\rho_{1/2} + \varepsilon\rho_1 + \varepsilon^{3/2}\rho_{3/2} + \varepsilon^2 \rho_2 + \cdots ;$$

$$T = T_0 + \varepsilon^{1/2}T_{1/2} + \varepsilon T_1 + \varepsilon^{3/2}T_{3/2} + \varepsilon^2 T_2 + \cdots . \quad (3.32)$$

The leading-order term in the expansion for v must be $O[(1/\varepsilon^{1/2})]$ for mass to be conserved while the air in region I--which has order one (scaled) width--is funneled into regions Ia and II--which have $O(\varepsilon^{1/2})$ width for $\hat{\beta} = 1/2$.

In region I, however, $v = O(\varepsilon)$ and $v_{-1/2} \equiv 0$, and the leading-order equations derived after substituting Eqs. (3.31) and (3.32) into Eq. (2.9) are exactly those of Eq. (3.2):

$$\frac{\partial}{\partial x}(\rho_0 u_0) + \frac{\partial}{\partial y}(\rho_0 v_0) = 0 ;$$

$$\rho_0 \left(u_0 \frac{\partial u_0}{\partial x} + v_0 \frac{\partial u_0}{\partial y}\right) = -B \frac{\partial P_1}{\partial x} ;$$

$$\frac{\partial P_1}{\partial y} + A\rho_0 = 0 \ ;$$

$$\rho_0 \left(u_0 \frac{\partial T_0}{\partial x} + v_0 \frac{\partial T_0}{\partial y} \right) = q(x, y) \ ;$$

$$\rho_0 T_0 = P_0 = \text{constant} \ . \tag{3.33}$$

These equations must be solved subject to the first boundary condition in Eq. (3.3), namely,

$$\text{along } y = 0: \quad v_0 = 0 \ , \tag{3.34}$$

but the solution need not satisfy the boundary conditions along $x = 0$ in Eq. (3.3) (which now serve as restrictions on the solution in region Ia). Great flexibility is therefore afforded in the selection of a solution to Eq. (3.33). Presumably, this flexibility is necessary for an eventual final matching of solutions in regions I and IV (and, by continuation, elsewhere as well). In any case, solutions to Eq. (3.33) are to be constructed as previously specified: by numerical computation for $0 \leq y \leq 1$ (where $q \not\equiv 0$), and from the solution of Eq. (3.8) (numerically, if necessary) and using Eq. (3.7) for $y > 1$ (where $q \equiv 0$). The solution for $y > 1$ is now not of the special type in Eq. (3.9): solution "streamlines" [i.e., lines of constant ψ or $\tilde{\psi}$, ψ and $\tilde{\psi}$ as defined in Eqs. (3.6) and (3.10)] are to sweep in toward the $x = 0$ symmetry line, and not go straight upwards.

In region Ia, the region I flow that converges towards the $x = 0$ symmetry axis is turned upwards by pressure and strong shear forces. A rescaling of the x coordinate that gives a leading-order model equation set appropriate for the description of this turning flow is

$$\hat{x} = \left(\frac{x}{\varepsilon^{1/2}} \right) . \tag{3.35}$$

As shown in Appendix B, the resultant leading-order equation set is

$$\frac{\partial}{\partial \hat{x}} (\rho_0 u_0) + \frac{\partial}{\partial y} (\rho_0 v_{-1/2}) = 0 ;$$

$$\rho_0 \left(u_0 \frac{\partial u_0}{\partial \hat{x}} + v_{-1/2} \frac{\partial u_0}{\partial y} \right) = -B \frac{\partial P_1}{\partial \hat{x}} + \hat{M}_{11} \frac{\partial^2 u_0}{\partial \hat{x}^2} ;$$

$$\frac{\partial P_1}{\partial y} + A\rho_0 = 0 ;$$

$$\rho_0 \left(u_0 \frac{\partial T_0}{\partial \hat{x}} + v_{-1/2} \frac{\partial T_0}{\partial y} \right) = \hat{K}_1 \frac{\partial^2 T_0}{\partial \hat{x}^2} ;$$

$$\rho_0 T_0 = P_0 = \text{constant} , \qquad (3.36)$$

which takes into account the diffusion of both horizontal momentum and heat. With x rescaled as in Eq. (3.35), the characteristic thickness of region Ia is $O(\varepsilon^{1/2})$ ($\hat{\beta} = 1/2$, Fig. 5).

Equation (3.36) is to be solved subject to the following boundary conditions:

(a) along $y = 0$: $v_{-1/2} = 0$;

(b) along $\hat{x} = 0$: $u_0 = 0$, $\frac{\partial v_{-1/2}}{\partial \hat{x}} = \frac{\partial P_1}{\partial \hat{x}} = \frac{\partial \rho_0}{\partial \hat{x}} = \frac{\partial T_0}{\partial \hat{x}} = 0$;

(c) as $\hat{x} \to \infty$:

$$v_{-1/2} \to 0 ,$$

$$u_0 \to \left[\lim_{x \to 0} u_I(x, y) \right] ,$$

$$P_1 \to \left[\lim_{x \to 0} P_I(x, y) \right] ,$$

$$\rho_0 \to \left[\lim_{x \to 0} \rho_I(x, y) \right] ,$$

$$T_0 \to \left[\lim_{x \to 0} T_I(x, y) \right] , \qquad (3.37)$$

where u_I, P_I, ρ_I, and T_I are the (region I) solutions of Eq. (3.33). In Eq. (3.36), P_0 is also to have the same constant value it has in region I. It and Eq. (3.37c) are prescribed so that the region I and region Ia solutions match smoothly. The solution of Eq. (3.36) subject to the boundary conditions in Eq. (3.37) must presumably be found by numerical computation. As we discuss shortly, the behavior of this solution as $y \to \infty$ is then to be used in the model description of the airflow in the thin plume (region II).

In region II, the flow that is turned in region Ia rises almost vertically in something of a standard plume, vertical momentum finally being diffused. The x rescaling in Eq. (3.35) is also appropriate for region II [so the scaled plume thickness is $O(\varepsilon^{1/2})$], as is the y rescaling in Eq. (3.14) as well (since $H \sim D = L/\varepsilon$). As shown in Appendix B, the equation set that must be solved to provide the leading-order velocity fields in region II is then

$$\frac{\partial}{\partial \hat{x}} (\rho_0 u_1) + \frac{\partial}{\partial \tilde{y}} (\rho_0 v_{-1/2}) = 0 ;$$

$$-B \frac{\partial P_2}{\partial \hat{x}} + \hat{M}_{11} \frac{\partial^2 u_1}{\partial \hat{x}^2} = 0 ;$$

$$-B \left(\frac{\partial P_2}{\partial \tilde{y}} + A\rho_2 \right) + \hat{M}_{21} \frac{\partial^2 v_{-1/2}}{\partial \hat{x}^2} = 0 ;$$

$$\frac{\partial^2 T_2}{\partial \hat{x}^2} = 0 ;$$

$$P_2 = \rho_0 T_2 + \rho_{1/2} T_{3/2} + \rho_1 T_1 + \rho_{3/2} T_{1/2} + \rho_2 T_0 , \qquad (3.38)$$

where ρ_0, $\rho_{1/2}$, ρ_1, $\rho_{3/2}$, T_0, $T_{1/2}$, T_1, $T_{3/2}$, and P_1 (as well as P_0, $P_{1/2}$, and $P_{3/2}$) are all functions of $\tilde{y}$ alone that are to be determined from a matching of the solution expansions in regions II and IV. These functions are found to satisfy the following equation sets:

$$\frac{dP_0}{d\tilde{y}} + A\rho_0 = 0 \ ,$$

$$\rho_0 \frac{dT_0}{d\tilde{y}} = \left(\frac{\gamma - 1}{\gamma}\right) \frac{dP_0}{d\tilde{y}} \ ,$$

$$P_0 = \rho_0 T_0 \ ; \tag{3.39}$$

$$\frac{dP_{1/2}}{d\tilde{y}} + A\rho_{1/2} = 0 \ ,$$

$$\rho_0 \frac{dT_{1/2}}{d\tilde{y}} + \rho_{1/2} \frac{dT_0}{d\tilde{y}} = \left(\frac{\gamma - 1}{\gamma}\right) \frac{dP_{1/2}}{d\tilde{y}} \ ,$$

$$P_{1/2} = \rho_0 T_{1/2} + \rho_{1/2} T_0 \ ; \tag{3.40}$$

$$\frac{dP_1}{d\tilde{y}} + A\rho_1 = 0 \ ,$$

$$\rho_0 \frac{dT_1}{d\tilde{y}} + \rho_{1/2} \frac{dT_{1/2}}{d\tilde{y}} + \rho_1 \frac{dT_0}{d\tilde{y}} = \left(\frac{\gamma - 1}{\gamma}\right) \frac{dP_1}{d\tilde{y}} \ ,$$

$$P_1 = \rho_0 T_1 + \rho_{1/2} T_{1/2} + \rho_1 T_0 \ ; \tag{3.41}$$

$$\frac{dP_{3/2}}{d\tilde{y}} + A\rho_{3/2} = 0 \ ,$$

$$\rho_0 \frac{dT_{3/2}}{d\tilde{y}} + \rho_{1/2} \frac{dT_1}{d\tilde{y}} + \rho_1 \frac{dT_{1/2}}{d\tilde{y}} + \rho_{3/2} \frac{dT_0}{d\tilde{y}} = \left(\frac{\gamma - 1}{\gamma}\right) \frac{dP_{3/2}}{d\tilde{y}} \ ,$$

$$P_{3/2} = \rho_0 T_{3/2} + \rho_{1/2} T_1 + \rho_1 T_{1/2} + \rho_{3/2} T_0 \ . \tag{3.42}$$

The general solutions of these sets are easily found: Eqs. (3.40), (3.41), and (3.42) are linear systems, and Eq. (3.39) is exactly Eq. (3.26), its solutions all having $dT_0/d\tilde{y}$ as a constant and thus representing an adiabatic atmosphere. Any one choice of solutions can be made to match the prescribed conditions of the far-field atmosphere [as x $(= \varepsilon\hat{x}) \to \infty$]. A simple nominal choice is to take P_0, ρ_0, and T_0 as in Eq. (3.27) and then set $P_{1/2} = \rho_{1/2} = T_{1/2} = P_1 = \rho_1 = T_1 = P_{3/2} = \rho_{3/2} = T_{3/2} = 0$.

The basic equation set in Eq. (3.38) is to be solved subject to the following boundary conditions:

(a) as $\tilde{y} \to 0$: $v_{-1/2}$, P_2, ρ_2, and T_2 profiles in $\hat{x}$ tend towards corresponding $y \to \infty$ profiles from the region Ia solution; the u_1 profile $\hat{x}$ similarly matches with the $\{[(1/\varepsilon)\ u_0 + u_1]\}$ solution from region Ia;

(b) along $\hat{x} = 0$: $u_1 = 0\ ,\quad \dfrac{\partial v_{-1/2}}{\partial \hat{x}} = \dfrac{\partial P_2}{\partial \hat{x}} = \dfrac{\partial \rho_2}{\partial \hat{x}} = \dfrac{\partial T_2}{\partial \hat{x}} = 0\ ;$

(c) as $\hat{x} \to \infty$: u_1, P_2, ρ_2, and T_2 profiles in $\tilde{y}$ tend towards corresponding $x \to 0$ profiles from the region IV solution; $v_{-1/2} \to 0$. (3.43)

Conditions (a) and (c) are required for the solution expansions in regions Ia, II, and IV to match smoothly, and condition (b) is the natural analog of (b) in Eq. (3.37) [and in Eq. (3.3)]. The solution of Eq. (3.38) subject to Eq. (3.43) must presumably also be found by numerical computation. However, as shown in Appendix B, Eq. (3.38) may preliminarily be reduced to the following single equation for $v_{-1/2}$ alone:

$$\frac{\partial^2 v_{-1/2}}{\partial \hat{x}^2} + \left(\frac{\hat{M}_1}{\hat{M}_2}\right)\frac{\partial}{\partial \tilde{y}}\left[\left(\frac{1}{\rho_0}\right)\frac{\partial}{\partial \tilde{y}}\ (\rho_0 v_{-1/2})\right] + \left(\frac{A}{B}\right)\left(\frac{\hat{M}_1}{\hat{M}_2}\right)\left(\frac{1}{\rho_0 T_0}\right)\frac{\partial}{\partial \tilde{y}}\ (\rho_0 v_{-1/2})$$

$$= \left(\frac{1}{\hat{M}_2}\right)\left\{\frac{dP_{2\infty}}{d\tilde{y}} + \left(\frac{A}{T_0}\right)\left[P_{2\infty}(\tilde{y}) - \rho_0 T_{2\infty}(\tilde{y}) - \rho_{1/2}T_{3/2} - \rho_1 T_1 - \rho_{3/2}T_{1/2}\right]\right\}. \tag{3.44}$$

Here, $P_{2\infty}(\tilde{y})$ and $T_{2\infty}(\tilde{y})$ are to be the far-field ($\hat{x}$, $x \to \infty$) atmospheric pressure and temperature profiles [at second order in the Eq. (3.1) expansion]. Further discussion of the model equations appropriate for the description of the flow in region IV is presented in Appendix B.

REFERENCES

Countryman, C. M., *Mass Fires and Fire Behavior*, U.S. Department of Agriculture, U.S. Forest Service, Research Paper PSW-19, 1964.

DCPA Attack Environment Manual, Chap. 3, "What the Planner Needs to Know about Fire Ignition and Spread," U.S. Defense Civil Preparedness Agency and U.S. Department of Defense, June 1973.

Delage, Y., and P. A. Taylor, "Numerical Studies of Heat Island Circulations," *Boundary-Layer Meteorology*, Vol. 1, 1970, pp. 201-226.

Estoque, M. A., and C. M. Bhumralkar, "Flow over a Localized Heat Source," *Monthly Weather Review*, Vol. 97, No. 12, 1969, pp. 850-859.

Irving, D., *Destruction of Dresden*, Wm. Kimber and Co., London, 1963.

Lee, S., and H. W. Emmons, "A Study of Natural Convection above a Line Fire," *J. Fluid Mech.*, Vol. 11, 1961, pp. 353-368.

Lommasson, T. E., *Firestorm Analysis*, The Dikewood Corporation, Report DC-TN-2046-1, 1967.

-----, *Preliminary Investigation of Firestorm Start-Criteria*, The Dikewood Corporation, Report DC-TN-1050-1, 1965.

-----, et al., *A "Firestorm" Existence and Buildup Hypothesis*, The Dikewood Corporation, Report DC-FR-1058.0, September 1968 (DASA Report 2174).

McCaffrey, B. J., *Purely Buoyant Diffusion Flames: Some Experimental Results*, National Bureau of Standards, Washington, D.C., Report NBSIR79-1910, October 1979.

Miller, C. F., *Appendixes 1 through 19 to the Hamburg Police President's Report on the Large Scale Air Attacks on Hamburg, Germany in WWII*, prepared for OCD by Stanford Research Institute, December 1968a.

-----, *Summary of Damage Inflicted by Air Raids on the City of Hamburg in the Period July 25 to August 3, 1943*, Stanford Research Institute, Report NRDL-TRC-68-30, July 1968b.

-----, and J. W. Kerr, *Field Notes on World War II German Fire Experience*, Stanford Research Institute, SRI Project MU-5070, October 1965.

Miller, R. K., M. E. Jenkins, and J. A. Keller, *Analysis of Four Models of Nuclear-Caused Ignitions and Early Fires in Urban Areas*, The Dikewood Corporation, Report DC-FR-1210, August 1970.

Morton, B. R., "Forced Plumes," *J. Fluid Mech.*, Vol. 5, 1959, pp. 151-163.

-----, C. Taylor, and J. S. Turner, "Turbulent Gravitational Convection from Maintained and Instantaneous Sources," *Proc. Roy. Soc. A*, Vol. 24, 1956, pp. 1-23.

Murgai, M. P., "Radiative Transfer Effects in Natural Convections above Fires, *Fluid Mech.*, Vol. 12, 1962, pp. 441-448.

-----, and H. W. Emmons, "Natural Convection above Fires," *J. Fluid Mech.*, Vol. 8, 1960, pp. 622-624.

Small, R. D., and H. L. Brode, *Physics of Large Urban Fires*, Pacific-Sierra Research Corporation, Report 1010, March 1980.

Smith, R. K., B. R. Morton, and L. M. Leslie, "The Role of Dynamic Pressure in Generating Fire Wind," *J. Fluid Mech.*, Vol. 68, 1975, pp. 1-19.

Thomas, G., and M. M. Witts, *Enola Gay*, Pocket Books, New York, June 1978.

APPENDIX A

ANALYTIC DEVELOPMENT 1

This appendix completes the derivation of the model described in Sec. 3. The discussion is based on the (matching) diagram in Fig. 3 of the text; analyses of the flow in regions I, II, IV, and III are completed in turn.

SOURCE LAYER

The general solution in Eqs. (3.7) and (3.8) for Eq. (3.2) with $q(x, y) \equiv 0$ is derived as follows. For $q(x, y) \equiv 0$, the energy equation in Eq. (3.2) can be rewritten as

$$u_0 \frac{\partial T_0}{\partial x} + v_0 \frac{\partial T_0}{\partial y} = 0 \; ; \qquad \text{(A.1)}$$

this and the equation of state can then be used to rewrite the first equation as the incompressible continuity equation

$$\frac{\partial u_0}{\partial x} + \frac{\partial v_0}{\partial y} = 0 \; . \qquad \text{(A.2)}$$

The stream function defined by Eq. (3.6) can then be introduced, with Eq. (A.1) integrated to yield

$$T_0 = T_0(\psi) \; , \qquad \rho_0 = \frac{P_0}{T_0(\psi)} \equiv \rho_0(\psi) \; , \qquad \text{(A.3)}$$

and P_1 eliminated from the second and third expressions in Eq. (3.2) to provide the following single equation for $\psi(x, y)$ alone:

$$\frac{\partial}{\partial y} \left\{ \rho_0(\psi) \left[\left(\frac{\partial \psi}{\partial y}\right) \frac{\partial}{\partial x} \left(\frac{\partial \psi}{\partial y}\right) - \left(\frac{\partial \psi}{\partial x}\right) \frac{\partial}{\partial y} \left(\frac{\partial \psi}{\partial y}\right) \right] \right\} = AB \frac{\partial}{\partial x} [\rho_0(\psi)] \; . \qquad \text{(A.4)}$$

This equation can be rewritten as

$$\left(\frac{\partial\psi}{\partial y}\right)\frac{\partial}{\partial x}\left\{\left(\frac{\partial^2\psi}{\partial y^2}\right)+\left[\left(\frac{1}{\rho_0}\right)\left(\frac{d\rho_0}{d\psi}\right)\right]\left[\frac{\left(\frac{\partial\psi}{\partial y}\right)^2}{2}+ABy\right]\right\}-\left(\frac{\partial\psi}{\partial x}\right)\frac{\partial}{\partial y}\left\{\left(\frac{\partial^2\psi}{\partial y^2}\right)\right.$$

$$\left.+\left[\left(\frac{1}{\rho_0}\right)\left(\frac{d\rho_0}{d\psi}\right)\right]\left[\frac{\left(\frac{\partial\psi}{\partial y}\right)^2}{2}+ABy\right]\right\}=0\ , \qquad \text{(A.5)}$$

which has the general solution of Eq. (3.8) [with $E(\psi)$ an arbitrary function of ψ]. The solutions in Eq. (3.7) then follow from Eqs. (3.6) and (A.3) and an elementary integration of the third equation in Eq. (3.2). The reduction of Eq. (A.4) to Eq. (A.5) begins by rewriting Eq. (A.4) as

$$0=\rho_0(\psi)\left[\left(\frac{\partial\psi}{\partial y}\right)\frac{\partial}{\partial x}\left(\frac{\partial^2\psi}{\partial y^2}\right)+\left(\frac{\partial^2\psi}{\partial y^2}\right)\left(\frac{\partial^2\psi}{\partial x\partial y}\right)-\left(\frac{\partial^2\psi}{\partial x\partial y}\right)\left(\frac{\partial^2\psi}{\partial y^2}\right)-\left(\frac{\partial\psi}{\partial x}\right)\frac{\partial}{\partial y}\left(\frac{\partial^2\psi}{\partial y^2}\right)\right]$$

$$+\left[\left(\frac{d\rho_0}{d\psi}\right)\left(\frac{\partial\psi}{\partial y}\right)\right]\left[\left(\frac{\partial\psi}{\partial y}\right)\frac{\partial}{\partial x}\left(\frac{\partial\psi}{\partial y}\right)-\left(\frac{\partial\psi}{\partial x}\right)\frac{\partial}{\partial y}\left(\frac{\partial\psi}{\partial y}\right)\right]-AB\left[\left(\frac{d\rho_0}{d\psi}\right)\left(\frac{\partial\psi}{\partial x}\right)\right]$$

$$=\rho_0(\psi)\left[\left\{\left[\left(\frac{\partial\psi}{\partial y}\right)\frac{\partial}{\partial x}\left(\frac{\partial^2\psi}{\partial y^2}\right)-\left(\frac{\partial\psi}{\partial x}\right)\frac{\partial}{\partial y}\left(\frac{\partial^2\psi}{\partial y^2}\right)\right]+\left[\frac{\left(\frac{d\rho_0}{d\psi}\right)}{\rho_0(\psi)}\right]\right\}\right.$$

$$\left.\times\left\{\left(\frac{\partial\psi}{\partial y}\right)\frac{\partial}{\partial x}\left[\frac{\left(\frac{\partial\psi}{\partial y}\right)^2}{2}+ABy\right]-\left(\frac{\partial\psi}{\partial x}\right)\frac{\partial}{\partial y}\left[\frac{\left(\frac{\partial\psi}{\partial y}\right)}{2}+ABy\right]\right\}\right]\ . \qquad \text{(A.6)}$$

As can easily be checked,

$$\left[\frac{\left(\frac{d\rho_0}{d\psi}\right)}{\rho_0(\psi)}\right]\left\{\left(\frac{\partial\psi}{\partial y}\right)\frac{\partial}{\partial x}\left[\frac{\left(\frac{\partial\psi}{\partial y}\right)^2}{2} + ABy\right] - \left(\frac{\partial\psi}{\partial x}\right)\frac{\partial}{\partial y}\left[\frac{\left(\frac{\partial\psi}{\partial y}\right)}{2} + ABy\right]\right\}$$

$$= \left[\left(\frac{\partial\psi}{\partial y}\right)\frac{\partial}{\partial x}\left\{\left[\frac{\left(\frac{d\rho_0}{d\psi}\right)}{\rho_0(\psi)}\right]\left[\frac{\left(\frac{\partial\psi}{\partial y}\right)^2}{2} + ABy\right]\right\} - \left(\frac{\partial\psi}{\partial x}\right)\frac{\partial}{\partial y}\right.$$

$$\left. \times \left\{\left[\frac{\left(\frac{d\rho_0}{d\psi}\right)}{\rho_0(\psi)}\right]\left[\frac{\left(\frac{\partial\psi}{\partial y}\right)^2}{2} + ABy\right]\right\}\right], \qquad (A.7)$$

which can be used in Eq. (A.6) to complete the reduction.

We now show that the solution in Eqs. (3.7) and (3.8) must actually be of the specific form of Eq. (3.9) to represent a flow of the type sketched in Fig. 2. Streamlines [lines of constant ψ or $\tilde{\psi}$--compare Eq. (3.10)] passing through the combustion zone must be bent sharply upwards; they tend toward lines of constant and order one x as $y \to \infty$ (so the heated air is not simply swept into a thin plume of the type sketched in Fig. 4). That is, $\partial\psi/\partial y$ (= u_0) and all its derivatives must tend toward zero as $y \to \infty$, so that from Eq. (A.4), $\partial\rho_0/\partial x \to 0$ and hence $\rho_0 \to$ a constant--say, ρ_∞--in that limit. Therefore, from Eq. (3.7), for all $y \geq 1$,

$$\rho_0 = \rho_0(\psi) \equiv \rho_\infty , \quad P_1 = P_1(x, 1) - A\rho_\infty(y - 1) . \qquad (A.8)$$

Similarly, if the second equation in Eq. (3.2) is satisfied as $y \to \infty$ (with $u_0 \to 0$), $P_1(x, 1)$ must be identically constant--say, P_{10}--and this second equation can be simplified to

$$u_0 \frac{\partial u_0}{\partial x} + v_0 \frac{\partial u_0}{\partial y} = 0 . \qquad (A.9)$$

Subject to the conditions that $u_0 \to 0$ as $y \to \infty$, the solution of this equation is $u_0 = u_0(\psi) \equiv 0$, and the solution in Eq. (3.7) is as in Eq. (3.9), the choice of $v_\infty(x)$ being arbitrary.

The boundary value problem posed for $|x| \leq 1$ and $0 \leq y \leq 1$ by Eqs. (3.2), (3.3), and (3.9) is reduced to Eq. (3.11) in the following way. Subject to the first expression in Eq. (3.2), the stream function defined by Eq. (3.10) can be introduced, and the first equation in Eq. (3.11) derived by eliminating P_1 from the second and third equations in Eq. (3.2). The second equation in Eq. (3.11) is then obtained by combining the fourth and fifth equations in Eq. (3.2). The first two boundary conditions in Eq. (3.11) are derived from the first two [condition (a) and $u_0 = 0$ in condition (b)] in Eq. (3.3). Equation (3.10), $v_0 = 0$ along $y = 0$, and $u_0 = 0$ along $x = 0$ imply that $\tilde{\psi}$ is a constant, which we arbitrarily take to be zero, along $y = 0$ and $x = 0$. No further conditions need be prescribed along $x = 0$. $\partial\rho_0/\partial x = 0$ (and so forth) are automatically satisfied along this line, as long as $\tilde{\psi} = 0$ and the first expression in Eq. (2.5) is satisfied. The other boundary conditions in Eq. (3.11) represent the required solution match with Eq. (3.9) along $y = 1$. $\rho_0 = \rho_\infty$ and $\partial\tilde{\psi}/\partial y$ ($= u_0$) $= 0$ are clearly necessary, and $\partial^2\tilde{\psi}/\partial\tilde{y}^2 = 0$ must also hold if the first equation in Eq. (3.11) is to be satisfied along that line.

CONVECTION COLUMN

The general solution of Eq. (3.23) is derived as follows. From the second equation, P_0 must be a function of $\tilde{y}$ alone. From the third and fifth equations, the same must be true for ρ_0 and T_0, and these three functions must satisfy Eq. (3.26)—that is,

$$\frac{dP_0}{d\tilde{y}} + A\rho_0 = 0 \ ;$$

$$\rho_0 \frac{dT_0}{d\tilde{y}} = \left(\frac{\gamma - 1}{\gamma}\right)\frac{dP_0}{d\tilde{y}} \ ;$$

$$P_0 = \rho_0 T_0 \ , \qquad \text{(A.10)}$$

the second equation coming from the fourth in Eq. (3.23). Substituting the first equation into the second shows that $dT_0/d\tilde{y} = -A[(\gamma - 1)/\gamma]$;

from that, the system is easily integrated to yield the general solution

$$T_0(\tilde{y}) = T_{00}\left[1 - \left(\frac{A}{T_{00}}\right)\left(\frac{\gamma - 1}{\gamma}\right)\tilde{y}\right] ;$$

$$\rho_0(\tilde{y}) = \rho_{00}\left[1 - \left(\frac{A}{T_{00}}\right)\left(\frac{\gamma - 1}{\gamma}\right)\tilde{y}\right]^{\left(\frac{1}{\gamma-1}\right)} ;$$

$$P_0(\tilde{y}) = (\rho_{00}T_{00})\left[1 - \left(\frac{A}{T_{00}}\right)\left(\frac{\gamma - 1}{\gamma}\right)\tilde{y}\right]^{\left(\frac{\gamma}{\gamma-1}\right)} , \qquad \text{(A.11)}$$

T_{00} and ρ_{00} being arbitrary. Finally, the first equation in Eq. (3.23) is integrated as

$$v_0(x, \tilde{y}) = \frac{f(x)}{\rho_0(\tilde{y})} , \qquad \text{(A.12)}$$

f(x) being an arbitrary function of x alone.

If T_0, ρ_0, and v_0 in Eqs. (A.11) and (A.12) are to match the region I values in Eq. (3.9) as $\tilde{y} \to 0$, T_{00}, ρ_{00}, and f(x) must clearly be chosen as follows:

$$T_{00} = \frac{P_\infty}{\rho_\infty} , \qquad \rho_{00} = \rho_\infty , \qquad f(x) = \rho_\infty v_\infty(x) , \qquad \text{(A.13)}$$

where P_∞ is the constant value of P_0 in region I. Substituting Eq. (A.13) into Eqs. (A.11) and (A.12) gives Eq. (3.24).

As discussed in Sec. 3, the leading-order region II equations in Eq. (3.23) are derived under the assumptions governing the M_{ij} and K_i in Eq. (3.19). We now consider the changes in Eq. (3.23), and hence in Eq. (3.24), that follow if the assumption for the K_i in Eq. (3.19) does not hold. For the basically vertical convection column flow, we assume $K_1 > K_2$, and hence do not consider changes in K_2. If $K_1 = 0(1)$, a rederivation of the leading-order region II equations [following that used to obtain Eq. (3.23)] results in exactly the same formulas as in Eq. (3.23), except that the fourth equation is modified to

$$\rho_0\left(\frac{\partial T_0}{\partial \tilde{y}}\right) = \left(\frac{\gamma - 1}{\gamma}\right)\left(\frac{\partial P_0}{\partial \tilde{y}}\right) + K_1\left(\frac{\partial^2 T_0}{\partial x^2}\right) . \tag{A.14}$$

But as discussed above, the second, third, and fifth equations in Eq. (3.23) imply that P_0, ρ_0--and hence T_0--are functions of $\tilde{y}$ alone. The $K_1[\partial^2 T_0/\partial x^2]$ term in Eq. (A.14) is thus identically zero, and the leading-order equations subject to K_1 being $0(1)$ are completely the same as those in Eq. (3.23). Similarly, if $K_1 >> 1$, a rederivation of the leading-order region II equations results in Eq. (3.23), except that the fourth equation is modified to

$$\frac{\partial^2 T_0}{\partial x^2} = 0 . \tag{A.15}$$

P_0, ρ_0, and T_0 are again required to be functions of $\tilde{y}$ alone, so that this equation is identically satisfied; these functions must also satisfy

$$\frac{dP_0}{d\tilde{y}} + A\rho_0 = 0 ; \qquad P_0 = \rho_0 T_0 . \tag{A.16}$$

A further equation is required for determining these functions [compare Eq. (A.10)], which must come from a study of lower order terms in the Eq. (3.1) expansions. However, such a study is unimportant: the point is that P_0, ρ_0, and T_0 are functions of $\tilde{y}$ alone (that is, "tops" in top-hat profiles) no matter what K_1 is, and the leading-order region II solution for $K_1 >> \varepsilon$ is qualitatively the same as in Eq. (3.24) for $K_1 = 0(\varepsilon)$.

RECIRCULATION REGION

In Eq. (3.21) as well as Eq. (3.23), the second, third, and fifth equations imply that P_0, ρ_0, and T_0 are all functions of $\tilde{y}$ alone, the third, fourth, and fifth equations then reducing to Eq. (3.26). The second through fifth equations thus serve to determine P_0, ρ_0, and T_0 [as a solution set for Eq. (3.26)], but provide no information about the velocity fields u_1 and v_0, which must be found by future analysis of lower order equation sets.

The general solution of Eq. (3.26) is as in Eq. (A.11), T_{00} and ρ_{00} being arbitrary. Since temperature, density, and pressure are scaled with ground-level atmospheric values [compare Eq. (2.2)], these values are represented nondimensionally by $T_0 = \rho_0 = P_0 = 1$. If Eq. (A.11) is to reduce to this for $\tilde{y} = 0$ (i.e., at ground level), it must be that

$$\rho_{00} = T_{00} = 1 \; , \tag{A.17}$$

in which case Eq. (A.11) becomes Eq. (3.27).

SIDE MIXING LAYER

The leading-order region III equations in Eq. (3.29) are derived as follows. Subject to the coordinate rescaling in Eq. (3.28), the basic model equations in Eq. (3.16) become

$$\frac{\partial}{\partial \tilde{x}} (\rho \tilde{u}) + \varepsilon \frac{\partial}{\partial \tilde{y}} (\rho v) = 0 \; ;$$

$$\rho \left(\tilde{u} \frac{\partial \tilde{u}}{\partial \tilde{x}} + \varepsilon v \frac{\partial \tilde{u}}{\partial \tilde{y}} \right) = -\left(\frac{B}{\varepsilon^3} \right) \frac{\partial P}{\partial \tilde{x}} + \left(\frac{M_{11}}{\varepsilon} \right) \frac{\partial^2 \tilde{u}}{\partial \tilde{x}^2} + \varepsilon M_{12} \frac{\partial^2 \tilde{u}}{\partial \tilde{y}^2} \; ;$$

$$\rho \left(\tilde{u} \frac{\partial v}{\partial \tilde{x}} + \varepsilon v \frac{\partial v}{\partial \tilde{y}} \right) = -\left(\frac{B}{\varepsilon^2} \right) \left(\frac{\partial P}{\partial \tilde{y}} + A\rho \right) + \left(\frac{M_{21}}{\varepsilon} \right) \frac{\partial^2 v}{\partial \tilde{x}^2} + \varepsilon M_{22} \frac{\partial^2 v}{\partial \tilde{y}^2} \; ;$$

$$\rho \left(\tilde{u} \frac{\partial T}{\partial \tilde{x}} + \varepsilon v \frac{\partial T}{\partial \tilde{y}} \right) = \left(\frac{\gamma - 1}{\gamma} \right) \left(\tilde{u} \frac{\partial P}{\partial \tilde{x}} + \varepsilon \frac{\partial P}{\partial \tilde{y}} \right) + \left(\frac{K_1}{\varepsilon} \right) \frac{\partial^2 T}{\partial \tilde{x}^2} + \varepsilon K_2 \frac{\partial^2 T}{\partial \tilde{y}^2} \; ;$$

$$P = \rho T \; . \tag{A.18}$$

Substituting the expansions in Eq. (3.1) for v, P, ρ, and T and the expansion in Eq. (3.20) for $\tilde{u}$ into Eq. (A.18) gives leading-order equations as in Eq. (3.29), as long as $u_1 \equiv 0$ and M_{11}, M_{21}, and K_1 are chosen such that the $\partial^2\tilde{u}/\partial\tilde{x}^2$, $\partial^2 v/\partial\tilde{x}^2$, and $\partial^2 T/\partial\tilde{x}^2$ terms appear. As discussed in Sec. 3, these choices [represented by order one values for $\tilde{M}_{11}$, $\tilde{M}_{12}$, and $\tilde{K}_1$ in Eq. (3.29)] reflect the physical fact that horizontal diffusion smoothing is a principal effect in the side mixing layer. Second derivatives of $\tilde{y}$ are seen from Eq. (A.18) to be of lower order than those in $\tilde{x}$; accordingly, they do not appear in Eq. (3.29). This omission is consistent with previous shear layer analyses [Morton, 1959; Lee and Emmons, 1961]. The choice for u_1 is made so that solution expansions for regions II and III can be suitably matched.

APPENDIX B

ANALYTIC DEVELOPMENT 2

This appendix completes the derivation of the model description in Sec. 3 of the firestorm airflow sketched in Fig. 4. The discussion is based on the matching diagram in Fig. 5, and follows the order of analysis in Sec. 3.

The analysis in Sec. 3 of the region I flow is self-contained. The leading-order equations in Eq. (3.36) for the region Ia solution are derived as follows. Subject to the coordinate rescaling in Eq. (3.35) and the (sample) diffusion coefficient choices in Eq. (3.31), the basic model equations in Eq. (2.9) become

$$\frac{\partial}{\partial \hat{x}} (\rho u) + \varepsilon^{1/2} \frac{\partial}{\partial y} (\rho v) = 0 \; ;$$

$$\rho \left(u \frac{\partial u}{\partial \hat{x}} + \varepsilon^{1/2} v \frac{\partial u}{\partial y} \right) = - \left(\frac{B}{\varepsilon}\right) \frac{\partial P}{\partial \hat{x}} + \hat{M}_{11} \left(\frac{\partial^2 u}{\partial \hat{x}^2} \right) + \varepsilon^{1/2} \hat{M}_{12} \left(\frac{\partial^2 u}{\partial y^2} \right) \; ;$$

$$\rho \left(u \frac{\partial v}{\partial \hat{x}} + \varepsilon^{1/2} v \frac{\partial v}{\partial y} \right) = - \left(\frac{B}{\varepsilon^{5/2}} \right) \left(\frac{\partial P}{\partial y} + \varepsilon A \rho \right) + \varepsilon \hat{M}_{21} \left(\frac{\partial^2 v}{\partial \hat{x}^2} \right) + \varepsilon^{3/2} \hat{M}_{22} \left(\frac{\partial^2 v}{\partial y^2} \right) \; ;$$

$$\rho \left(u \frac{\partial T}{\partial \hat{x}} + \varepsilon^{1/2} v \frac{\partial T}{\partial y} \right) = \left(\frac{\gamma - 1}{\gamma} \right) \left(u \frac{\partial P}{\partial \hat{x}} + \varepsilon^{1/2} v \frac{\partial P}{\partial y} \right)$$

$$+ \varepsilon^{1/2} q \left(\varepsilon^{1/2} \hat{x}, y \right) + \hat{K}_1 \left(\frac{\partial^2 T}{\partial \hat{x}^2} \right) + \varepsilon^{1/2} \hat{K}_2 \left(\frac{\partial^2 T}{\partial y^2} \right) \; ;$$

$$P = \rho T \; . \qquad \text{(B.1)}$$

Straightforward substitution of the expansions in Eq. (3.32) into Eq. (B.1) results in the leading-order region Ia equations as in Eq. (3.36), with $\partial P_{1/2}/\partial \tilde{x} = \partial P_{-1/2}/\partial y = 0$ (so $P_{1/2}$ as well as P_0 must be constant).

Subject to the further coordinate rescaling in Eq. (3.14) and the associated velocity rescaling in Eq. (3.15), Eq. (B.1) becomes

$$\frac{\partial}{\partial \hat{x}} (\rho\tilde{u}) + \varepsilon^{1/2} \frac{\partial}{\partial \tilde{y}} (\rho v) = 0 \ ;$$

$$\rho \left(\tilde{u} \frac{\partial \tilde{u}}{\partial \hat{x}} + \varepsilon^{1/2} v \frac{\partial \tilde{u}}{\partial \tilde{y}} \right) = - \left(\frac{B}{\varepsilon^3} \right) \frac{\partial P}{\partial \hat{x}} + \left(\frac{\hat{M}_{11}}{\varepsilon} \right) \left(\frac{\partial^2 \tilde{u}}{\partial \tilde{x}^2} \right) + \varepsilon^{3/2} \hat{M}_{12} \left(\frac{\partial^2 \tilde{u}}{\partial \tilde{y}^2} \right) \ ;$$

$$\rho \left(\tilde{u} \frac{\partial v}{\partial \hat{x}} + \varepsilon^{1/2} v \frac{\partial v}{\partial \tilde{y}} \right) = - \left(\frac{B}{\varepsilon^{5/2}} \right) \left(\frac{\partial P}{\partial \tilde{y}} + A\rho \right) + \hat{M}_{21} \left(\frac{\partial^2 v}{\partial \hat{x}^2} \right) + \varepsilon^{5/2} \hat{M}_{22} \left(\frac{\partial^2 v}{\partial \tilde{y}^2} \right) \ ;$$

$$\rho \left(\tilde{u} \frac{\partial T}{\partial \hat{x}} + \varepsilon^{1/2} v \frac{\partial T}{\partial \tilde{y}} \right) = \left(\frac{\gamma - 1}{\gamma} \right) \left(\tilde{u} \frac{\partial P}{\partial \hat{x}} + \varepsilon^{1/2} v \frac{\partial P}{\partial \tilde{y}} \right)$$

$$+ \left(\frac{\hat{K}_1}{\varepsilon} \right) \left(\frac{\partial^2 T}{\partial \hat{x}^2} \right) + \varepsilon^{3/2} \hat{K}_2 \left(\frac{\partial^2 T}{\partial \tilde{y}^2} \right) \ ;$$

$$P = \rho T \tag{B.2}$$

[with $q \equiv 0$ for $\tilde{y} = 0(1)$]. Under the velocity rescaling in Eq. (3.15), $\tilde{u}$ should be 0(1) [to preserve continuity under the rescaling in Eq. (3.14)]. From Eq. (3.32), the appropriate expansion for $\tilde{u}$ ($= u/\varepsilon$) is therefore

$$\tilde{u} = u_1 + \varepsilon^{1/2} u_{3/2} + \varepsilon u_2 + \cdots \ . \tag{B.3}$$

Substituting this expression for $\tilde{u}$ and the expansions for v, P, ρ, and T in Eq. (3.32) into Eq. (B.2), we develop the following hierarchy of perturbation equations:

$$0\left(\frac{1}{\varepsilon^3}\right): \qquad \frac{\partial P_0}{\partial \hat{x}} = 0 \ . \tag{B.4}$$

$$0\left(\frac{1}{\varepsilon^{5/2}}\right): \qquad \frac{\partial P_{1/2}}{\partial \tilde{x}} = 0 \ ;$$

$$\frac{\partial P_0}{\partial \tilde{y}} + A\rho_0 = 0 \ . \tag{B.5}$$

$$0\left(\frac{1}{\varepsilon^2}\right): \qquad \frac{\partial P_1}{\partial \hat{x}} = 0 \ ;$$

$$\frac{\partial P_{1/2}}{\partial \tilde{y}} + A\rho_{1/2} = 0 \ . \tag{B.6}$$

$$0\left(\frac{1}{\varepsilon^{3/2}}\right): \qquad \frac{\partial P_{3/2}}{\partial \hat{x}} = 0 \ ;$$

$$\frac{\partial P_1}{\partial \tilde{y}} + A\rho_1 = 0 \ . \tag{B.7}$$

$$0\left(\frac{1}{\varepsilon}\right): \qquad -B\,\frac{\partial P_2}{\partial \hat{x}} + \hat{M}_{11}\left(\frac{\partial^2 u_1}{\partial \hat{x}^2}\right) = 0 \ ;$$

$$\frac{\partial P_{3/2}}{\partial \tilde{y}} + A\rho_{3/2} = 0 \ ;$$

$$\frac{\partial^2 T_0}{\partial \hat{x}^2} = 0 \ . \tag{B.8}$$

$$0\left(\frac{1}{\varepsilon^{1/2}}\right): \qquad -B\,\frac{\partial P_{5/2}}{\partial \hat{x}} + \hat{M}_{11}\left(\frac{\partial^2 u_{3/2}}{\partial \hat{x}^2}\right) = 0 \ ;$$

$$-B\left(\frac{\partial P_2}{\partial \tilde{y}} + A\rho_2\right) + \hat{M}_{21}\left(\frac{\partial^2 v_{-1/2}}{\partial \hat{x}^2}\right) = 0 \ ;$$

$$\frac{\partial^2 T_{1/2}}{\partial \hat{x}^2} = 0 \ . \tag{B.9}$$

$$0(1): \qquad \frac{\partial}{\partial \hat{x}}\,(\rho_0 u_1) + \frac{\partial}{\partial \tilde{y}}\,(\rho_0 v_{-1/2}) = 0 \ ;$$

$$\hat{K}_1\left(\frac{\partial^2 T_1}{\partial \hat{x}^2}\right) = \rho_0\left(u_1\,\frac{\partial T_0}{\partial \hat{x}} + v_{-1/2}\,\frac{\partial T_0}{\partial \tilde{y}}\right) - \left(\frac{\gamma - 1}{\gamma}\right)\left(u_1\,\frac{\partial P_0}{\partial \hat{x}} + v_{-1/2}\,\frac{\partial P_0}{\partial \tilde{y}}\right) \ ;$$

$$P_0 = \rho_0 T_0 \ ; \tag{B.10}$$

(plus unneeded equations involving $\hat{M}_{11}$ and $\hat{M}_{21}$)

$$0\left(\varepsilon^{1/2}\right): \quad \hat{K}_1\left(\frac{\partial^2 T_{3/2}}{\partial\hat{x}^2}\right) = \rho_0\left(u_1 \frac{\partial T_{1/2}}{\partial\hat{x}} + u_{3/2}\frac{\partial T_0}{\partial\hat{x}} + v_{-1/2}\frac{\partial T_{1/2}}{\partial\tilde{y}} + v_0\frac{\partial T_0}{\partial\tilde{y}}\right)$$

$$+ \rho_{1/2}\left(u_1\frac{\partial T_0}{\partial\hat{x}} + v_{-1/2}\frac{\partial T_0}{\partial\tilde{y}}\right) - \left(\frac{\gamma - 1}{\gamma}\right)$$

$$\times\left(u_1\frac{\partial P_{1/2}}{\partial\hat{x}} + u_{3/2}\frac{\partial P_0}{\partial\hat{x}} + v_{-1/2}\frac{\partial P_{1/2}}{\partial\tilde{y}} + v_0\frac{\partial P_0}{\partial\tilde{y}}\right);$$

$$P_{1/2} = \rho_0 T_{1/2} + \rho_{1/2}T_0 ; \qquad \text{(B.11)}$$

(plus unneeded equations)

$$0(\varepsilon): \quad \hat{K}_1\left(\frac{\partial^2 T_2}{\partial\hat{x}^2}\right) = \rho_0\left(u_1\frac{\partial T_1}{\partial\hat{x}} + u_{3/2}\frac{\partial T_{1/2}}{\partial\hat{x}} + u_2\frac{\partial T_0}{\partial\hat{x}} + v_{-1/2}\frac{\partial T_1}{\partial\tilde{y}}\right.$$

$$\left. + v_0\frac{\partial T_{1/2}}{\partial\tilde{y}} + v_{1/2}\frac{\partial T_0}{\partial\tilde{y}}\right) + \rho_{1/2}\left(u_1\frac{\partial T_{1/2}}{\partial\hat{x}} + u_{3/2}\frac{\partial T_0}{\partial\hat{x}}\right.$$

$$\left. + v_{-1/2}\frac{\partial T_{1/2}}{\partial\tilde{y}} + v_0\frac{\partial T_0}{\partial\tilde{y}}\right) + \rho_1\left(u_1\frac{\partial T_0}{\partial\hat{x}} + v_{-1/2}\frac{\partial T_0}{\partial\tilde{y}}\right)$$

$$-\left(\frac{\gamma - 1}{\gamma}\right)\left(u_1\frac{\partial P_1}{\partial\hat{x}} + u_{3/2}\frac{\partial P_{1/2}}{\partial\hat{x}} + u_2\frac{\partial P_0}{\partial\hat{x}}\right.$$

$$\left. + v_{-1/2}\frac{\partial P_1}{\partial\tilde{y}} + v_0\frac{\partial P_{1/2}}{\partial\tilde{y}} + v_{1/2}\frac{\partial P_0}{\partial\tilde{y}}\right) ;$$

$$P_1 = \rho_0 T_1 + \rho_{1/2}T_{1/2} + \rho_1 T_0 ; \qquad \text{(B.12)}$$

(plus unneeded equations)

$$0\left(\varepsilon^{3/2}\right): \quad P_{3/2} = \rho_0 T_{3/2} + \rho_{1/2}T_1 + \rho_1 T_{1/2} + \rho_{3/2}T_0 ; \qquad \text{(B.13)}$$

(plus unneeded equations)

$$0\left(\varepsilon^2\right): \qquad P_2 = \rho_0 T_2 + \rho_{1/2} T_{3/2} + \rho_1 T_1 + \rho_{3/2} T_{1/2} + \rho_2 T_0 \; ; \qquad \text{(B.14)}$$

(plus unneeded equations).

The first three equations in Eq. (3.38) are derived from the first equation in Eq. (B.10), the first equation in Eq. (B.8), and the second equation in Eq. (B.9), respectively. The fifth equation in Eq. (3.38) follows from Eq. (B.14), and the fourth equation comes from the first equation in Eq. (B.12), once the righthand side is shown to be zero. Proof involves the derivation of Eqs. (3.39) through (3.42), as follows.

From the first equations of Eqs. (B.4), (B.5), (B.6), and (B.7), P_0, $P_{1/2}$, P_1, and $P_{3/2}$ must be functions of $\tilde{y}$ alone. From the second equations in Eqs. (B.5), (B.6), (B.7), and (B.8), the same must be true for ρ_0, $\rho_{1/2}$, ρ_1, and $\rho_{3/2}$; and the first equations in Eqs. (3.39) through (3.42) must hold. From the final equations in Eqs. (B.10), (B.11), (B.12), and (B.13), T_0, $T_{1/2}$, T_1, and $T_{3/2}$ must also be functions of $\tilde{y}$ alone; and the final equations in Eqs. (3.39) through (3.42) must hold. The final equations in Eqs. (B.8) and (B.9) are therefore automatically satisfied, and the second equation in Eq. (B.10) and first equation in Eq. (B.11) reduce to

$$\rho_0 \frac{\partial T_0}{\partial \tilde{y}} - \left(\frac{\gamma - 1}{\gamma}\right) \frac{\partial P_0}{\partial \tilde{y}} = 0 \qquad \text{(B.15)}$$

and

$$\rho_0 \left(v_{-1/2} \frac{\partial T_{1/2}}{\partial \tilde{y}} + v_0 \frac{\partial T_0}{\partial \tilde{y}}\right) + \rho_{1/2} \left(v_{1/2} \frac{\partial T_0}{\partial \tilde{y}}\right) - \left(\frac{\gamma - 1}{\gamma}\right) \times \left(v_{-1/2} \frac{\partial P_{1/2}}{\partial \tilde{y}} + v_0 \frac{\partial P_0}{\partial \tilde{y}}\right) = 0 \; , \qquad \text{(B.16)}$$

respectively. The second equation in Eq. (3.39) follows from Eq. (B.15); using Eq. (B.15) in Eq. (B.16) gives

$$\rho_0 \frac{\partial T_{1/2}}{\partial \tilde{y}} + \rho_{1/2} \frac{\partial T_0}{\partial \tilde{y}} - \left(\frac{\gamma - 1}{\gamma}\right) \frac{\partial P_{1/2}}{\partial \tilde{y}} = 0 , \qquad \text{(B.17)}$$

from which the second equation in Eq. (3.40) follows. We show shortly that the second equations in Eqs. (3.41) and (3.42) must be satisfied as well if solution expansions in regions II and IV are to be smoothly matched. This completes the derivation of the equation sets in Eqs. (3.39) through (3.42). The fourth equation in Eq. (3.38) is then derived by using those equations. With $\hat{x}$ derivatives set equal to zero in the righthand side of the first equation in Eq. (B.12), that side is made identically zero by using the second equations in Eqs. (3.40), (3.41), and (3.42).

The second expressions in Eqs. (3.41) and (3.42) are derived by considering the region IV solution expansion. In the (atmospheric recirculation) region, the x coordinate must be rescaled back from $\hat{x}$ to x [compare Eq. (3.35)] by

$$x = \varepsilon^{1/2} \hat{x} . \qquad \text{(B.18)}$$

Subject to this rescaling, the basic model equations in Eq. (B.2) become

$$\frac{\partial}{\partial x} (\rho\tilde{u}) + \frac{\partial}{\partial \tilde{y}} (\rho v) = 0 ;$$

$$\rho \left(\tilde{u} \frac{\partial \tilde{u}}{\partial x} + v \frac{\partial \tilde{u}}{\partial \tilde{y}} \right) = - \left(\frac{B}{\varepsilon^3} \right) \frac{\partial P}{\partial x} + \left(\frac{\hat{M}_1}{\varepsilon^{1/2}} \right) \left(\frac{\partial^2 \tilde{u}}{\partial x^2} \right) + \left(\varepsilon \hat{M}_{12} \right) \left(\frac{\partial^2 \tilde{u}}{\partial \tilde{y}^2} \right) ;$$

$$\rho \left(\tilde{u} \frac{\partial v}{\partial x} + v \frac{\partial v}{\partial \tilde{y}} \right) = - \left(\frac{B}{\varepsilon^3} \right) \left(\frac{\partial P}{\partial \tilde{y}} + A\rho \right) + \left(\varepsilon^{1/2} \hat{M}_2 \right) \left(\frac{\partial^2 v}{\partial x^2} \right) + \left(\varepsilon^2 \hat{M}_{22} \right) \left(\frac{\partial^2 v}{\partial \tilde{y}^2} \right) ;$$

$$\rho \left(\tilde{u} \frac{\partial T}{\partial x} + v \frac{\partial T}{\partial \tilde{y}} \right) = \left(\frac{\gamma - 1}{\gamma} \right) \left(\tilde{u} \frac{\partial P}{\partial x} + v \frac{\partial P}{\partial \tilde{y}} \right) + \left(\frac{\hat{K}_1}{\varepsilon^{1/2}} \right) \left(\frac{\partial^2 T}{\partial x^2} \right) + \left(\varepsilon \hat{K}_2 \right) \left(\frac{\partial^2 T}{\partial \tilde{y}^2} \right) ;$$

$$P = \rho T . \qquad \text{(B.19)}$$

In the vortex-like recirculating flow of region IV, horizontal and vertical velocities must have the same magnitude order (discussed in Sec. 3 for recirculation as sketched in Fig. 2). Keeping $\tilde{u}$ in the region as in Eq. (B.3), we must require

$$v_{-1/2} = 0 \tag{B.20}$$

in the Eq. (3.32) expansion for v. Subject to this rescaling, substituting the expansion in Eq. (B.3) for $\tilde{u}$ and the expansions for v, P, ρ, and T in Eq. (3.32) into Eq. (B.19) results in a hierarchy of perturbation equations very similar to those in Eqs. (B.4) through (B.14). In particular, from the second, third, and fifth equations in Eq. (B.19), it is found that

$$\frac{\partial P_0}{\partial x} = \frac{\partial P_{1/2}}{\partial x} = \frac{\partial P_1}{\partial x} = \frac{\partial P_{3/2}}{\partial x} = \frac{\partial P_2}{\partial x} = 0 \ ; \tag{B.21}$$

$$\frac{\partial P_0}{\partial \tilde{y}} + A\rho_0 = 0 \ , \qquad \frac{\partial P_{1/2}}{\partial \tilde{y}} + A\rho_{1/2} = 0 \ , \qquad \frac{\partial P_1}{\partial \tilde{y}} + A\rho_1 = 0 \ ,$$

$$\frac{\partial P_{3/2}}{\partial \tilde{y}} + A\rho_{3/2} = 0 \ , \qquad \frac{\partial P_2}{\partial \tilde{y}} + A\rho_2 = 0 \ ; \tag{B.22}$$

and

$$P_0 = \rho_0 T_0 \ , \qquad P_{1/2} = \rho_0 T_{1/2} + \rho_{1/2} T_0 \ ;$$

$$P_1 = \rho_0 T_1 + \rho_{1/2} T_{1/2} + \rho_1 T_0 \ ;$$

$$P_{3/2} = \rho_0 T_{3/2} + \rho_{1/2} T_1 + \rho_1 T_{1/2} + \rho_{3/2} T_0 \ ;$$

$$P_2 = \rho_0 T_2 + \rho_{1/2} T_{3/2} + \rho_1 T_1 + \rho_{3/2} T_{1/2} + \rho_2 T_0 \ , \tag{B.23}$$

so that P_2, ρ_2, and T_2 as well as P_0, ρ_0, T_0, $P_{1/2}$, $\rho_{1/2}$, $T_{1/2}$, P_1, ρ_1, T_1, $P_{3/2}$, $\rho_{3/2}$, and $T_{3/2}$ are all functions of $\tilde{y}$ alone, the first and third equations in Eqs. (3.39) through (3.42) being satisfied by the last twelve of these, as in region II. Additionally, it is found from the fourth equation in Eq. (B.19) that the last twelve functions must satisfy the second equations in Eqs. (3.39) through (3.42) [in the same way the second equations in Eqs. (3.39) and (3.40) were explicitly derived in the region II analysis]. Thus, since P_1, ρ_1, T_1, $P_{3/2}$, $\rho_{3/2}$, and $T_{3/2}$ are all functions of $\tilde{y}$ alone in both region II and region IV, a smooth matching of the region II and region IV solution expansions requires that these functions satisfy the same equations in both regions. In particular, these functions must satisfy the second equations in Eqs. (3.41) and (3.42) in region II.

Finally, Eq. (3.38) is reduced to Eq. (3.44). The first equation in Eq. (3.38) can be rewritten as

$$\frac{\partial u_1}{\partial \hat{x}} = -\left(\frac{1}{\rho_0}\right)\frac{\partial}{\partial \tilde{y}}\left(\rho_0 v_{-1/2}\right) \quad , \tag{B.24}$$

and the second integrated (in x) to yield

$$P_2 = P_{2\infty}(\tilde{y}) + \left(\frac{\hat{M}_1}{B}\right)\left(\frac{\partial u_1}{\partial x}\right) \quad . \tag{B.25}$$

Here, $P_{2\infty}(\tilde{y})$ is the region IV $P_2(\tilde{y})$ profile (that is, the $x \to \infty$ far-field atmosphere), so that the region II and region IV solution expansions match smoothly. From the fourth equation in Eq. (3.38), T_2 must be a linear function of $\hat{x}$, with coefficients depending on $\tilde{y}$. The only such function that matches smoothly (as $\hat{x} \to \infty$) with the region IV $T_2(\tilde{y})$ profile--say, $T_{2\infty}(\tilde{y})$--is the profile itself. Thus,

$$T_2 = T_{2\infty}(\tilde{y}) \quad , \tag{B.26}$$

and from the fifth equation in Eq. (3.38),

$$\rho_2 = \left(\frac{1}{T_0}\right)\left[P_2 - G(\tilde{y})\right]$$

and

$$G(\tilde{y}) = \rho_0 T_{2\infty} + \rho_{1/2} T_{3/2} + \rho_1 T_1 + \rho_{3/2} T_{1/2} \ . \qquad \text{(B.27)}$$

Substituting the forms for ρ_2 and P_2 in Eqs. (B.27) and (B.25) into the third equation of Eq. (3.38), and using Eq. (B.24), we have

$$\hat{M}_2 \frac{\partial^2 v_{-1/2}}{\partial \hat{x}^2} = B \left\{ \frac{\partial}{\partial \tilde{y}} \left[P_{2\infty}(\tilde{y}) - \left(\frac{\hat{M}_1}{B}\right)\left(\frac{1}{\rho_0}\right) \frac{\partial}{\partial \tilde{y}} \left(\rho_0 v_{-1/2}\right) \right] \right.$$
$$\left. + \left(\frac{A}{T_0}\right) \left[P_{2\infty}(\tilde{y}) - \left(\frac{\hat{M}_1}{B}\right)\left(\frac{1}{\rho_0}\right) \frac{\partial}{\partial \tilde{y}} \left(\rho_0 v_{-1/2}\right) - G(\tilde{y}) \right] \right\} ,$$

(B.28)

from which Eq. (3.44) follows.

APPENDIX C

SYMBOLS

A, B = dimensionless constants

c = constant of proportionality

c_p = specific heat capacity at constant pressure

D = half-width of combustion zone

E, f = arbitrary constants of integration

g = gravitational acceleration

H = scale height of atmosphere

k_1, k_2 = effective thermal conductivities (including turbulence effects)

K_1, K_2 = dimensionless heat-diffusion coefficients

$\tilde{K}_1$ = rescaling of K_1

$\hat{K}_1, \hat{K}_2$ = rescalings of K_1 and K_2

ℓ = mixing length

L = mean height of combustion zone

$M_{11}, M_{12}, M_{21}, M_{22}$ = dimensionless momentum diffusion coefficients

$\tilde{M}_{11}, \tilde{M}_{21}$ = rescalings of M_{11} and M_{21}

$\hat{M}_{11}, \hat{M}_{12}, \hat{M}_{21}, \hat{M}_{22}$ = rescalings of M_{11}, M_{12}, M_{21}, M_{22}

P = pressure

P_a = ground-level atmospheric pressure in far field

P_0 = leading-order pressure in $\varepsilon \to 0$ limit

P_1, P_2, P_3 = correction pressures in $\varepsilon \to 0$ limit

P_{10} = constant value of P_1 at top of combustion zone

P_∞ = constant value of P_0 at top of combustion zone

$P_{1/2}$, $P_{3/2}$ = correction pressure in $\varepsilon \to 0$ limit

P_I = solution of Eq. (3.33) for region I

$P_{2\infty}$ = far-field P_2

q = dimensionless volumetric heat addition rate distribution in combustion zone

Q = volume heat source

q_{rad} = volumetric heat flux due to radiation

R = universal gas constant

T = temperature

T_a = ground-level atmospheric temperature in far field

T_0 = leading-order temperature in $\varepsilon \to 0$ limit

T_1, T_2, T_3 = correction temperatures in $\varepsilon \to 0$ limit

T_{00} = constant value of T_0 at top of combustion zone

$T_{1/2}$, $T_{3/2}$ = correction temperatures in $\varepsilon \to 0$ limit

T_∞ = far-field ambient temperature in radiation law

T_I = T_0 solution of Eq. (3.33) for region I

$T_{2\infty}$ = far-field T_2

u = horizontal velocity

$\tilde{u}$ = rescaled horizontal velocity

u_0 = leading-order horizontal velocity in $\varepsilon \to 0$ limit

u_1, u_2, u_3 = correction horizontal velocities in $\varepsilon \to 0$ limit

u_{IV} = u_1 solution for region IV

$u_{1/2}$, $u_{3/2}$ = correction horizontal velocities in $\varepsilon \to 0$ limit

u_I = u_0 solution of Eq. (3.33) for region I

U = horizontal velocity scale

v = vertical velocity

v_0 = leading-order vertical velocity in $\varepsilon \to 0$ limit and correction term

v_1, v_2, v_3 = correction vertical velocities in $\varepsilon \to 0$ limit

v_∞ = vertical velocity versus x profile at top of combustion zone

v_{IV} = v_0 solution for region IV

$v_{-1/2}$ = leading-order vertical velocity in $\varepsilon \to 0$ limit

$v_{1/2}, v_{3/2}$ = correction vertical velocities in $\varepsilon \to 0$ limit

x = horizontal position coordinate

$\tilde{x}$ = rescaled horizontal coordinate

$\hat{x}$ = rescaled horizontal coordinate

y = vertical position coordinate

$\tilde{y}$ = rescaled vertical coordinate

y^* = rescaled vertical coordinate

α = dimensionless constant

$\hat{\alpha}$ = exponent such that side mixing layer thickness is $\varepsilon^{\hat{\alpha}}$

β = dimensionless constant

$\hat{\beta}$ = exponent such that thin plume thickness is $\varepsilon^{\hat{\beta}}$

γ = ratio of specific heats

δ_1, δ_2 = dimensionless constants

ε = combustion zone aspect ratio

$\mathcal{E}_{11}, \mathcal{E}_{12}, \mathcal{E}_{21}, \mathcal{E}_{22}$ = effective kinematic viscosities (including turbulence effects)

ρ = density

ρ_a = ground-level atmospheric density in far field

ρ_0 = leading-order density in $\varepsilon \to 0$ limit

ρ_1, ρ_2, ρ_3 = correction densities in $\varepsilon \to 0$ limit

ρ_∞ = constant value of ρ_0 at top of combustion zone

$\rho_{00} = \rho_\infty$, defined by Eqs. (A.11) and (A.13)

$\rho_{1/2}, \rho_{3/2}$ = correction densities in $\varepsilon \to 0$ limit

$\rho_I = \rho_0$ solution of Eq. (3.33) for region I

ψ = incompressible stream function

$\tilde{\psi}$ = compressible stream function

CHAPTER 5

ANALYTIC APPROXIMATION FOR PEAK OVERPRESSURE VERSUS BURST HEIGHT AND GROUND RANGE OVER AN IDEAL SURFACE

Stephen J. Speicher
Harold L. Brode

One analytic approximation to the revised EM-1 HOB peak overpressure curves is reported in Chap. 7. The procedure uses an interpolation scheme between similarities in the HOB curves; the curves are illustrated in Figs. 1 through 3 below.

Another procedure was reported at an Airblast Working Group meeting at DNA on 12 December 1979. It did not provide as good a fit to the new EM-1 curves, but was somewhat simpler and more direct. Subsequent refinement of the earlier form has resulted in a better fit. It is suggested that this modified procedure be used in calculations of peak overpressure, since it is simpler and more accurate. We intend to use it in our analytic approximations to pressure-time histories, now being derived.

To proceed, given x, the scaled ground range, and y, the scaled height of burst, an overpressure is calculated as follows:*

$$r = \sqrt{x^2 + y^2} \quad kft/kT^{1/3} ,$$

$$z = y/x .^{\dagger}$$

The peak overpressure (in psi and $kft/kT^{1/3}$) is then given as

$$\Delta P(r,\ z) = \frac{10.47}{r^{a(z)}} + \frac{b(z)}{r^{c(z)}} + \frac{d(z) \cdot e(z)}{1.0 + f(z) r^{g(z)}} + h(z,\ r,\ y) \quad psi ,$$

where

$$a(z) = 1.22 - \frac{3.908 z^2}{1 + 810.2 z^5} ,$$

*The range of pressures for which the procedure is intended is from 1 to 10,000 psi (7 kPa to 70 MPa); all distances are in scaled kilofeet ($kft/kT^{1/3}$) or kilometers ($km/kT^{1/3}$).

†To avoid the singularity in z as $x \to 0$, it is suggested that a small number limit be placed on x, and the magnitude of z be limited so as not to overflow when z is raised to the 18*th* power. These values are machine-dependent.

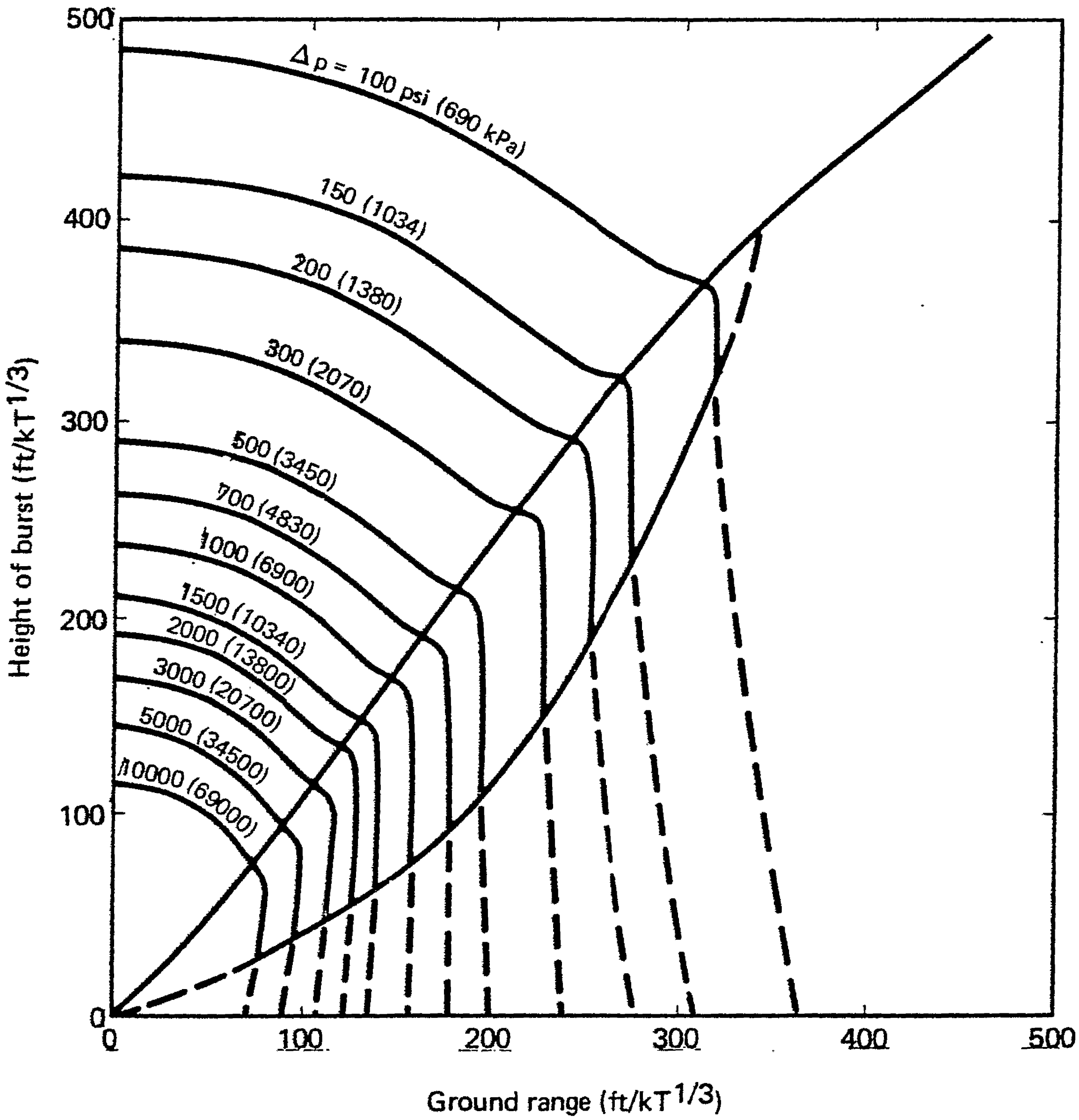

Figure 1. Near-ideal peak overpressure HOB vs. ground range curves.

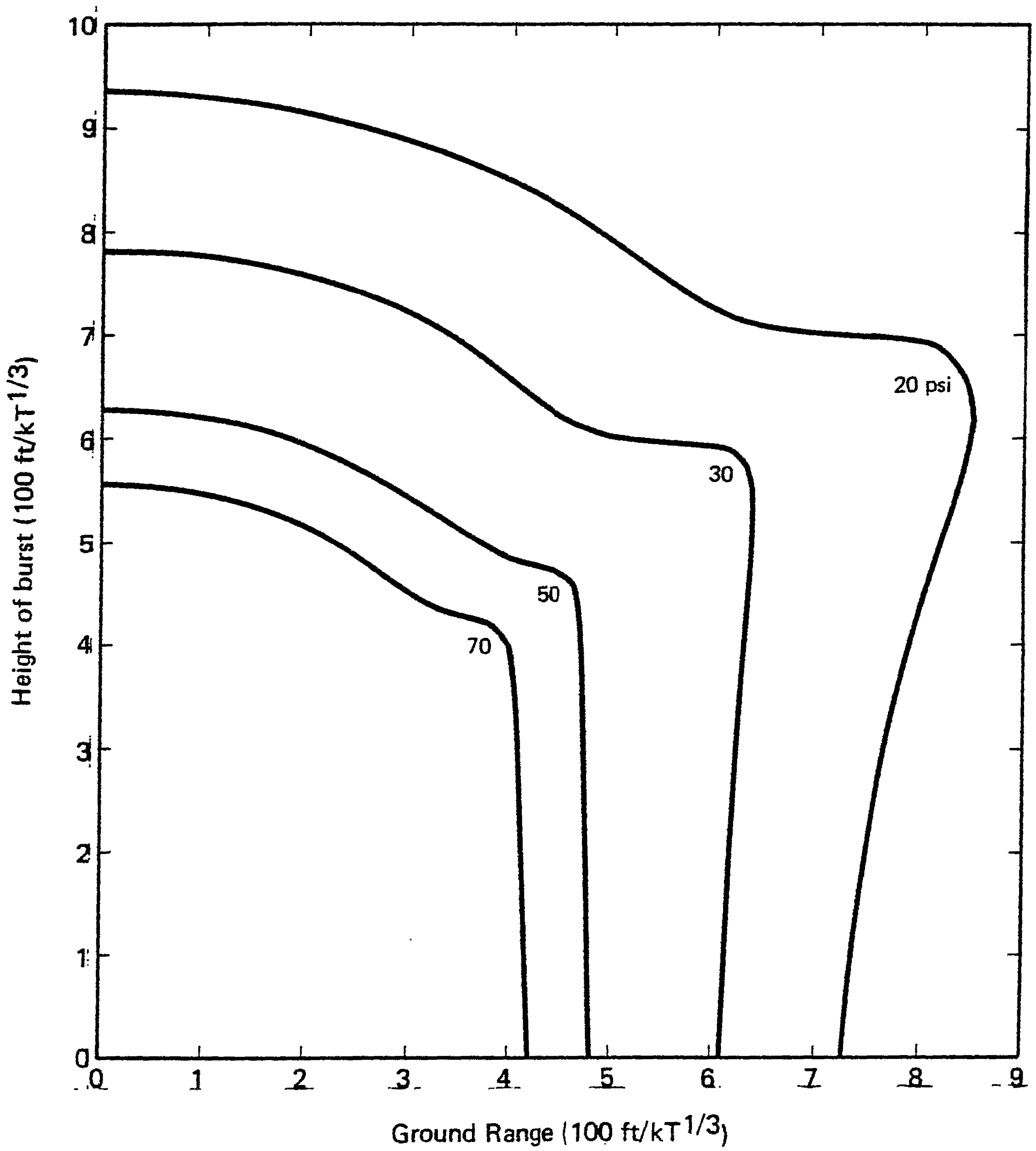

Figure 2. Peak overpressure HOB curves for ideal surface (20-70 psi).

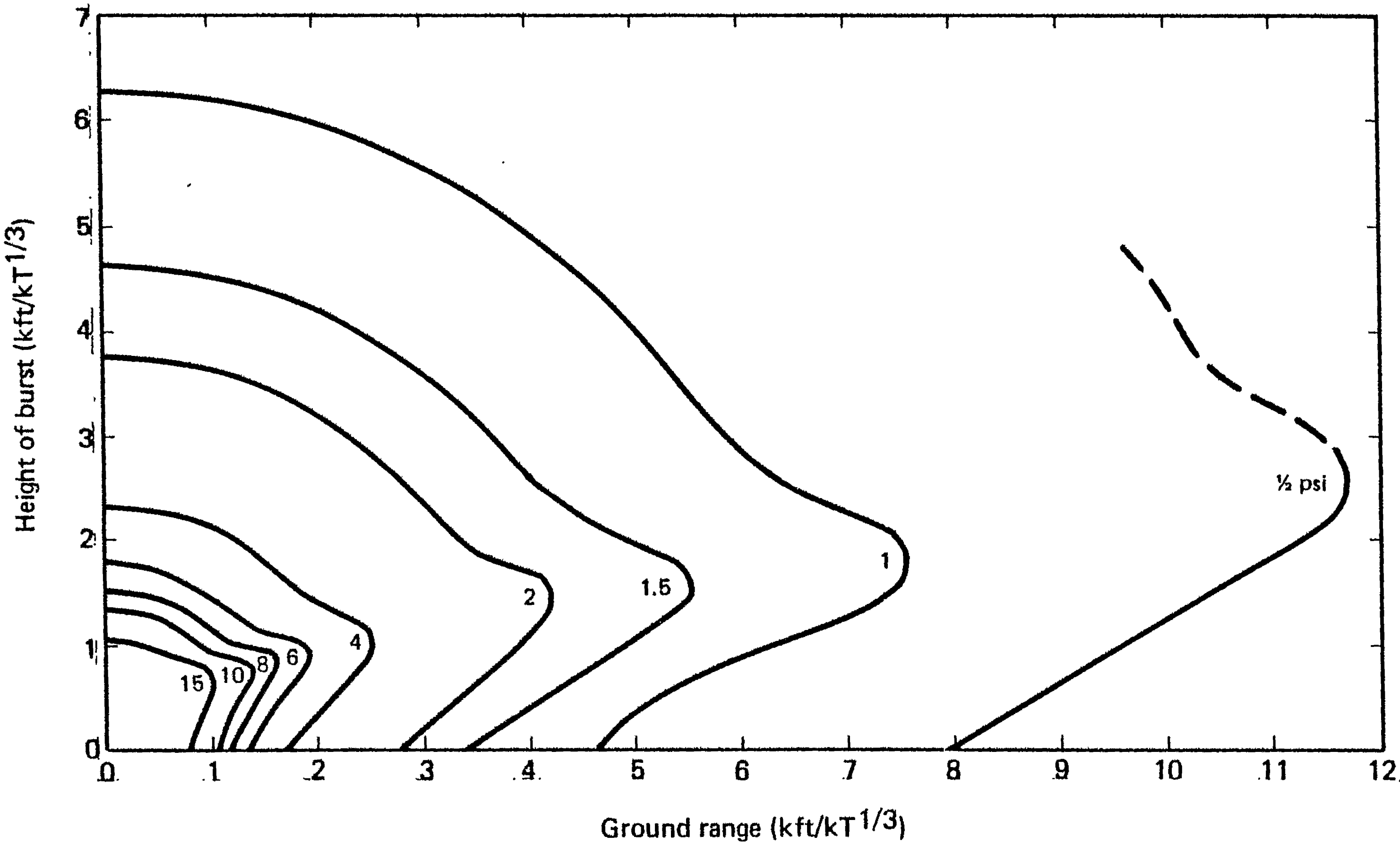

Figure 3. Peak overpressure HOB curves for near-ideal/ideal surfaces.

$$b(z) = 2.321 + \frac{6.195z^{18}}{1 + 1.113z^{18}} - \frac{0.03831z^{17}}{1 + 0.02415z^{17}} + \frac{0.6692}{1 + 4164z^{8}} ,$$

$$c(z) = 4.153 - \frac{1.149z^{18}}{1 + 1.641z^{18}} - \frac{1.1}{1 + 2.771z^{2.5}} ,$$

$$d(z) = -4.166 + \frac{25.76z^{1.75}}{1 + 1.382z^{18}} + \frac{8.257z}{1 + 3.219z} ,$$

$$e(z) = 1 - \frac{0.004642z^{18}}{1 + 0.003886z^{18}} ,$$

$$f(z) = 0.6096 + \frac{2.879z^{9.25}}{1 + 2.359z^{14.5}} - \frac{17.15z^{2}}{1 + 71.66z^{3}} ,$$

$$g(z) = 1.83 + \frac{5.361z^{2}}{1 + 0.3139z^{6}} ,$$

and

$$h(z, r, y) = \frac{-(64.67z^{5} + 0.2905)}{1 + 441.5z^{5}} - \frac{1.389z}{1 + 49.03z^{5}} + \frac{8.808z^{1.5}}{1 + 154.5z^{3.5}}$$

$$+ \frac{0.0014(\alpha r)^{2}}{[1 - 0.158(\alpha r) + 0.0486(\alpha r)^{1.5} + 0.00128(\alpha r)^{2}](1 + 2y)} .$$

The peak overpressure in kPa and km is

$$r = \sqrt{x^2 + y^2} , \quad \left(x, y, r \text{ in } \frac{\text{km}}{\text{kT}^{1/3}}\right) ,$$

$$z = y/x ,$$

and

$$\Delta P(r, z) = \beta \left[\frac{10.47}{(\alpha r)^{a(z)}} + \frac{b(z)}{(\alpha r)^{c(z)}} + \frac{d(z) \cdot e(z)}{1 + f(z)(\alpha r)^{g(z)}} + h(z, r, y) \right] ,$$

where

$$h(z, r, y) = \frac{-(64.67z^5 + 0.2905)}{1 + 441.5z^5} - \frac{1.389z}{1 + 49.03z^5} + \frac{8.808z^{1.5}}{1 + 154.5z^{3.5}}$$

$$+ \frac{0.0014(\alpha r)^2}{[1 - 0.158(\alpha r) + 0.0486(\alpha r)^{1.5} + 0.00128(\alpha r)^2](1 + 2y)} ,$$

$$\alpha = (0.3048)^{-1} \quad \text{kft/km} ,$$

$$\beta = \left(\frac{100}{14.504}\right) \quad \text{kPa/psi} .$$

Figures 4 through 8 show pressure contour plots generated using the above formulas for ranges of 1500 to 10,000 psi (Fig. 4), 200 to 1500 psi (Fig. 5), 30 to 200 psi (Fig. 6), 6 to 30 psi (Fig. 7), and 1 to 6 psi (Fig. 8). The Appendix provides a series of test cases that may be used to verify application of the analytic approximation formulas.

Comparisons with the EM-1 revised curves are provided for 5000, 1000, 200, 50, 10, and 1 psi in Figs. 9 through 14. Since the disparity is much less than the accuracy of the original curves, and very much less than the scatter in supporting data, we suggest that the fit-generated curves could be substituted without loss of validity. There would then be no difference between displayed curves and analytic approximations to confuse the novice user.

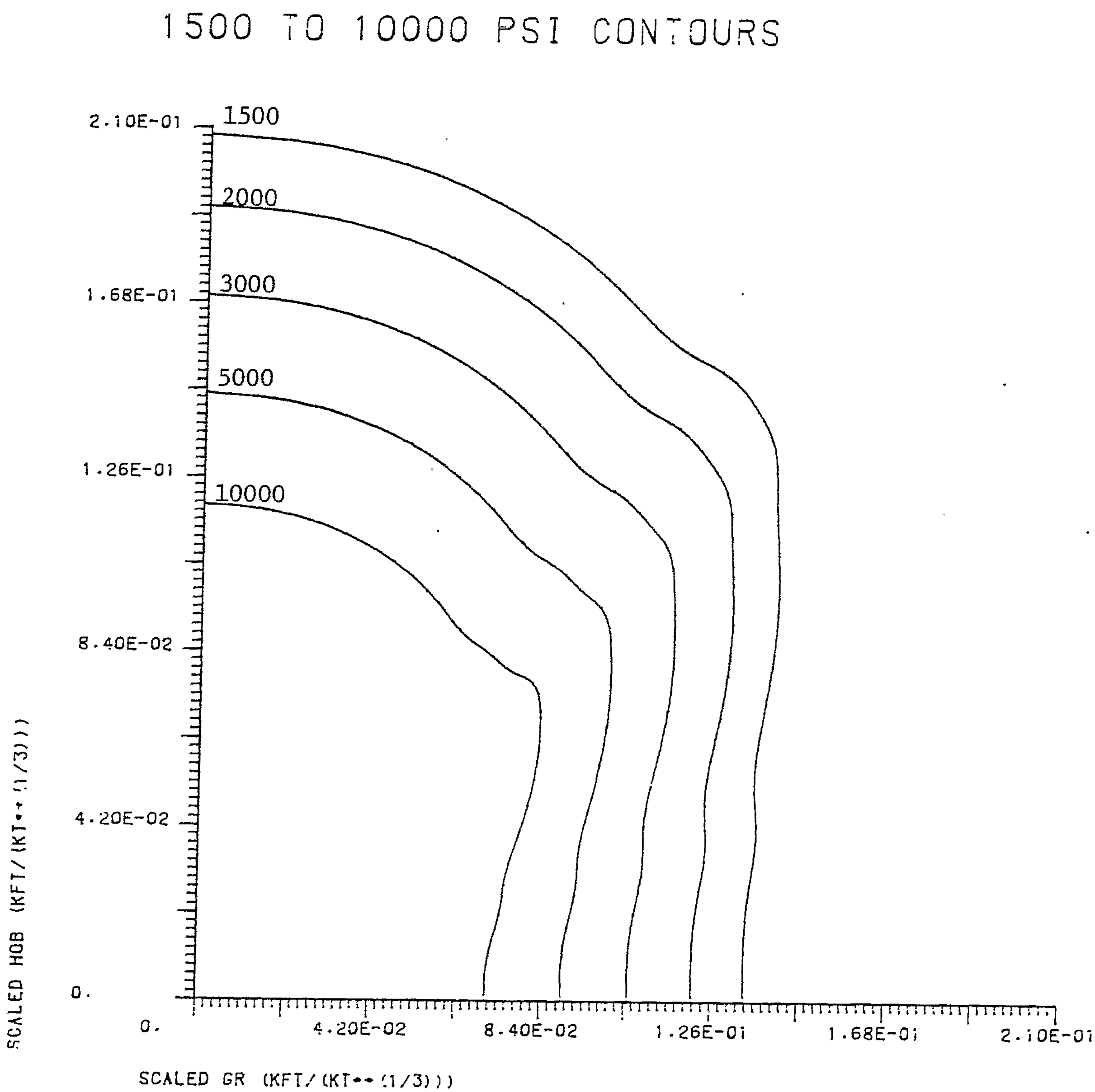
1500 TO 10000 PSI CONTOURS
1500
2000
3000
5000
10000
2.10E-01
1.68E-01
1.26E-01
8.40E-02
4.20E-02
0.
0.
4.20E-02
8.40E-02
1.26E-01
1.68E-01
2.10E-01
SCALED HOB (KFT/(KT** (1/3)))
SCALED GR (KFT/(KT** (1/3)))

Figure 4

200 TO 1500 PSI CONTOURS

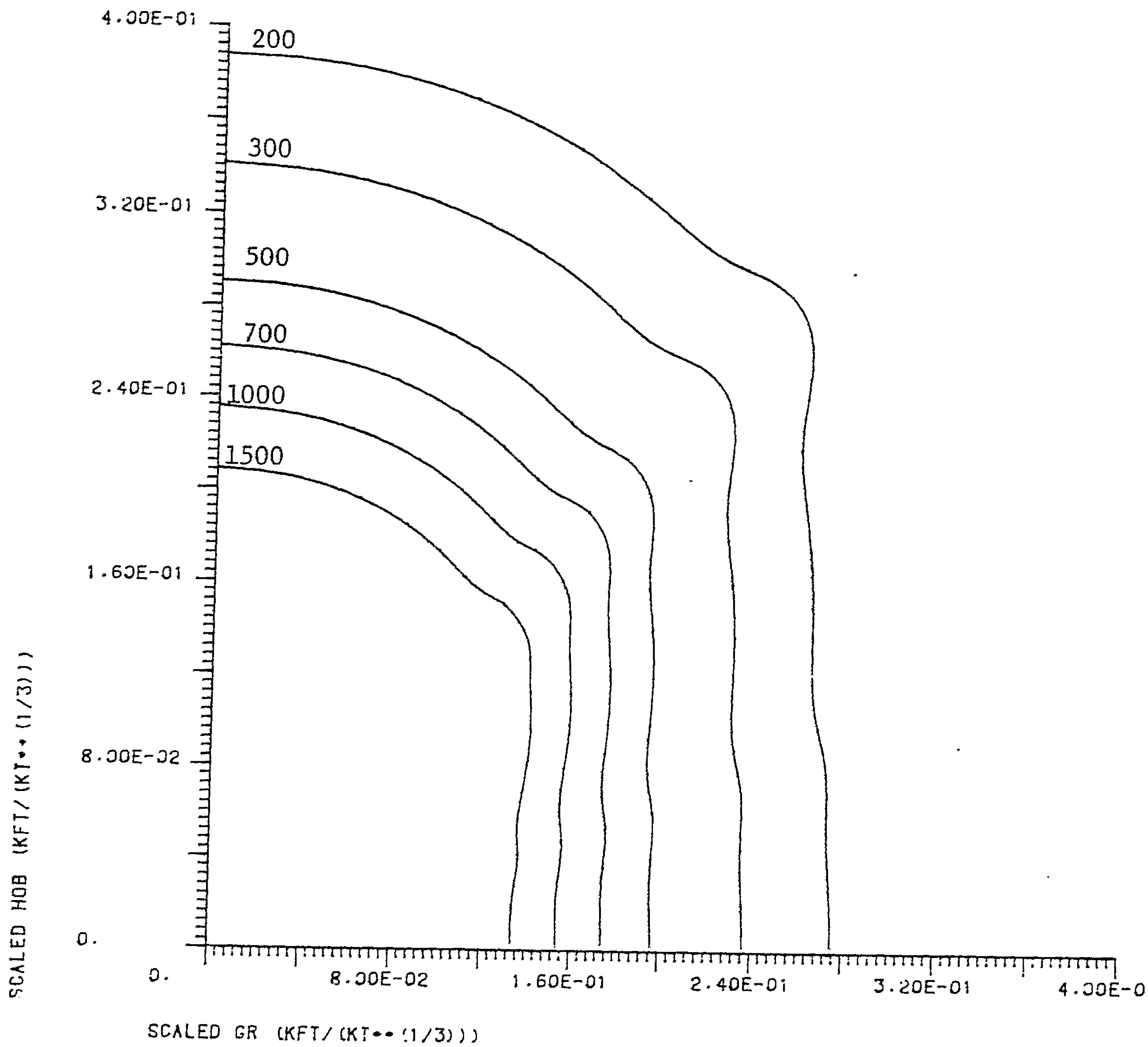

Figure 5

30 TO 200 PSI CONTOURS

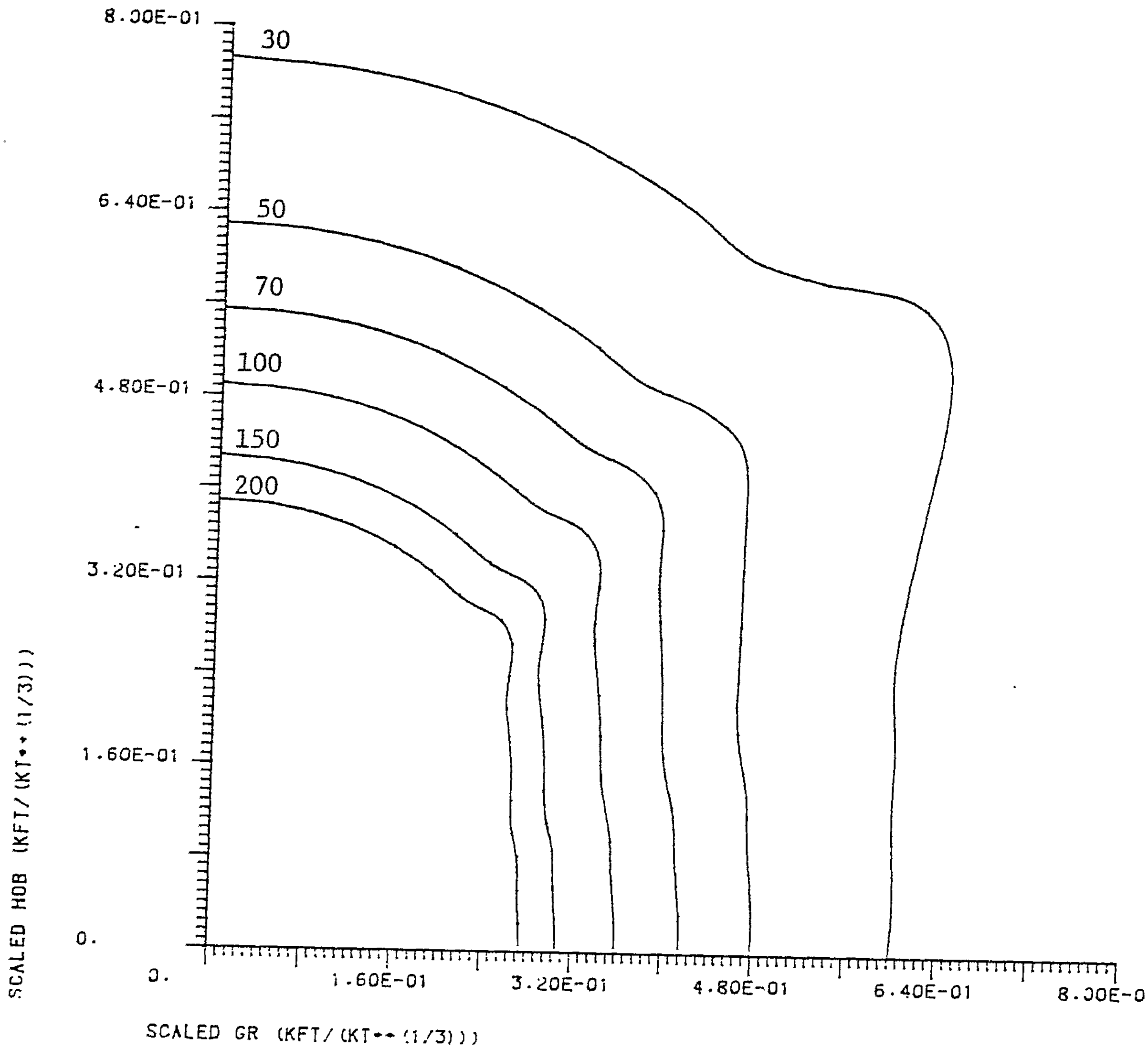

Figure 6

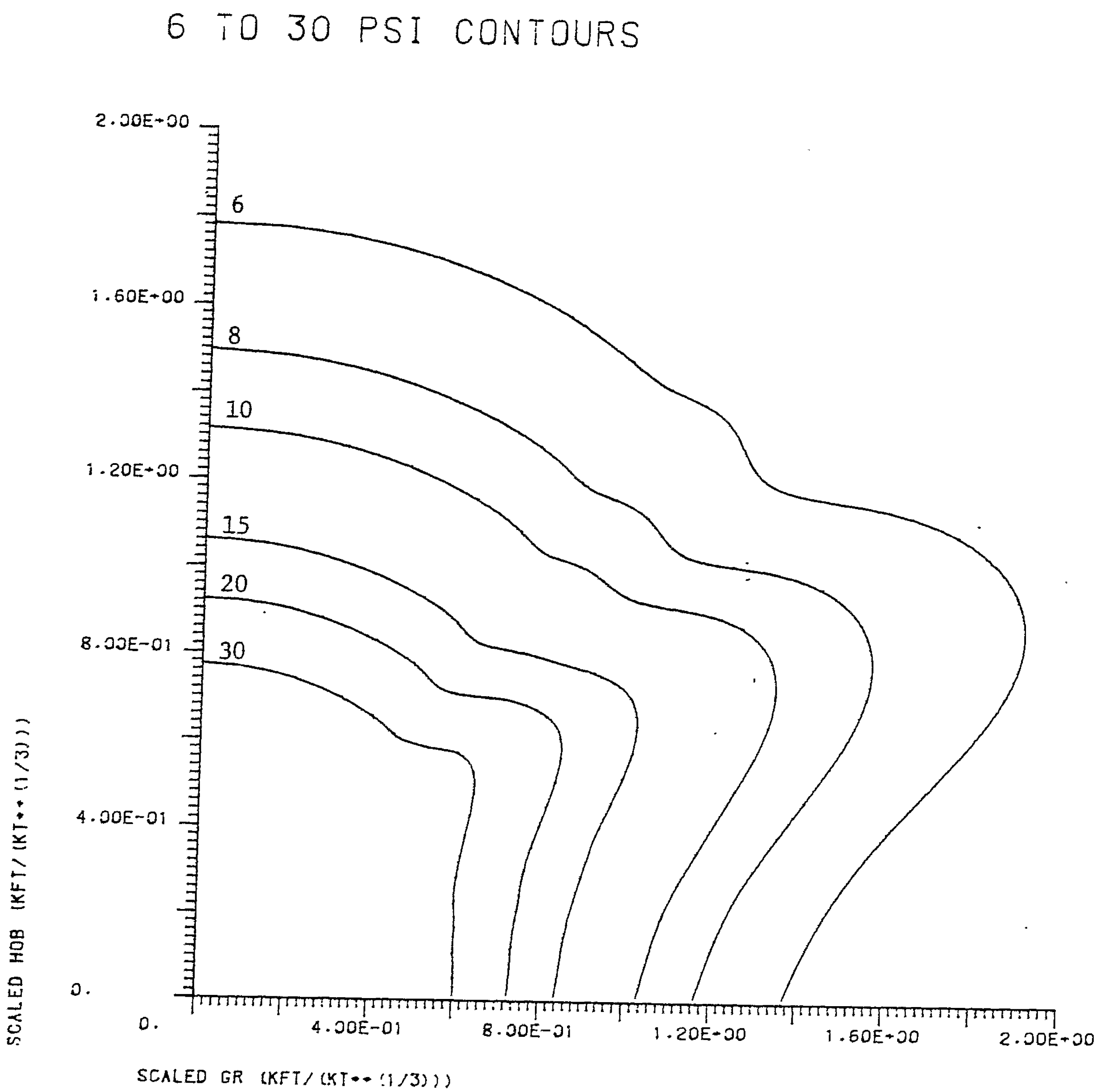
6 TO 30 PSI CONTOURS
2.00E+00
1.60E+00
1.20E+00
8.00E-01
4.00E-01
0.
6
8
10
15
20
30
SCALED HOB (KFT/(KT** (1/3)))
0.
4.00E-01
8.00E-01
1.20E+00
1.60E+00
2.00E+00
SCALED GR (KFT/(KT** (1/3)))

Figure 7

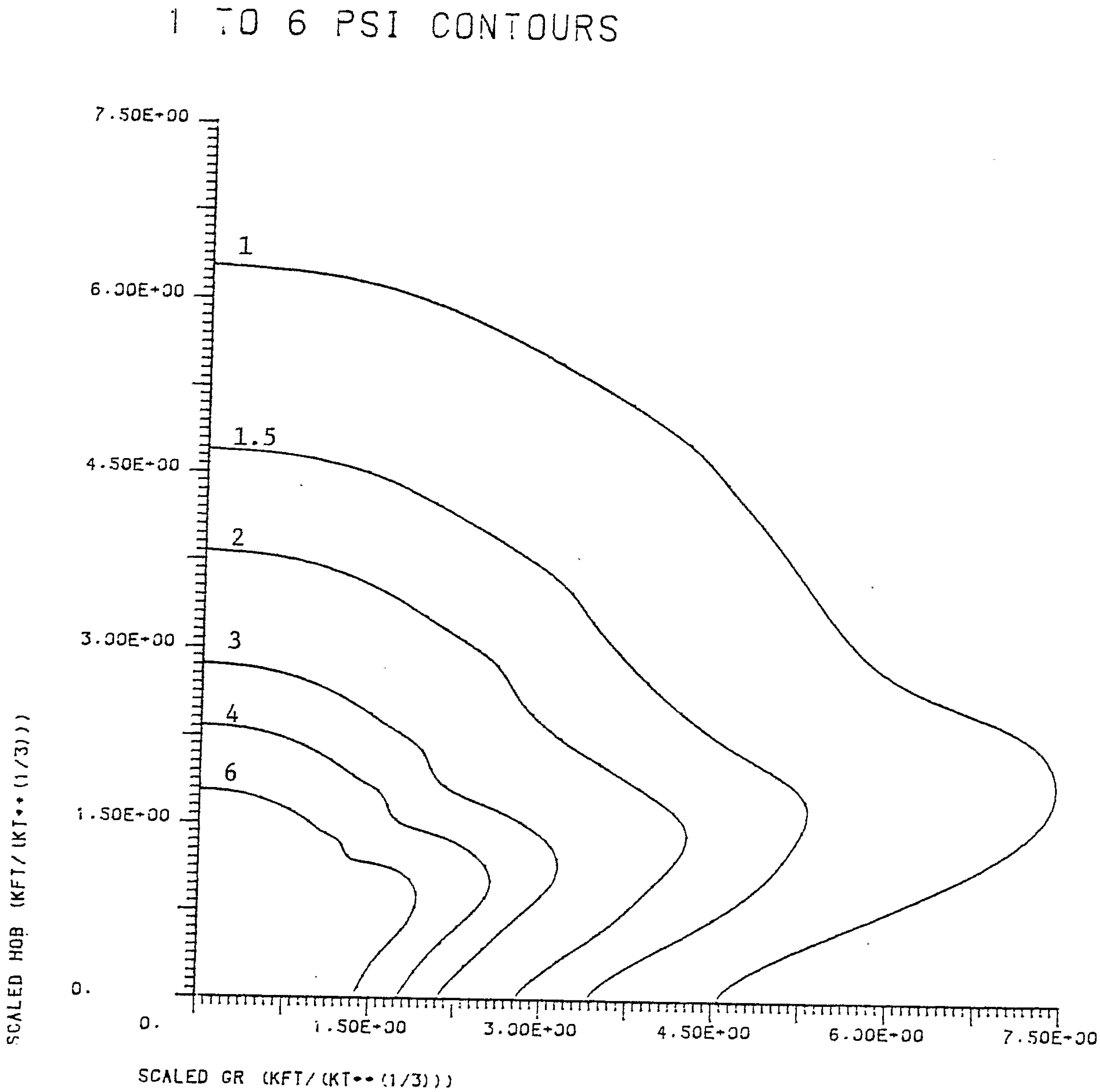
1 TO 6 PSI CONTOURS
7.50E+00
6.00E+00
4.50E+00
3.00E+00
1.50E+00
0.
1
1.5
2
3
4
6
0.
1.50E+00
3.00E+00
4.50E+00
6.00E+00
7.50E+00
SCALED GR (KFT/(KT**(1/3)))
SCALED HOB (KFT/(KT**(1/3)))

Figure 8

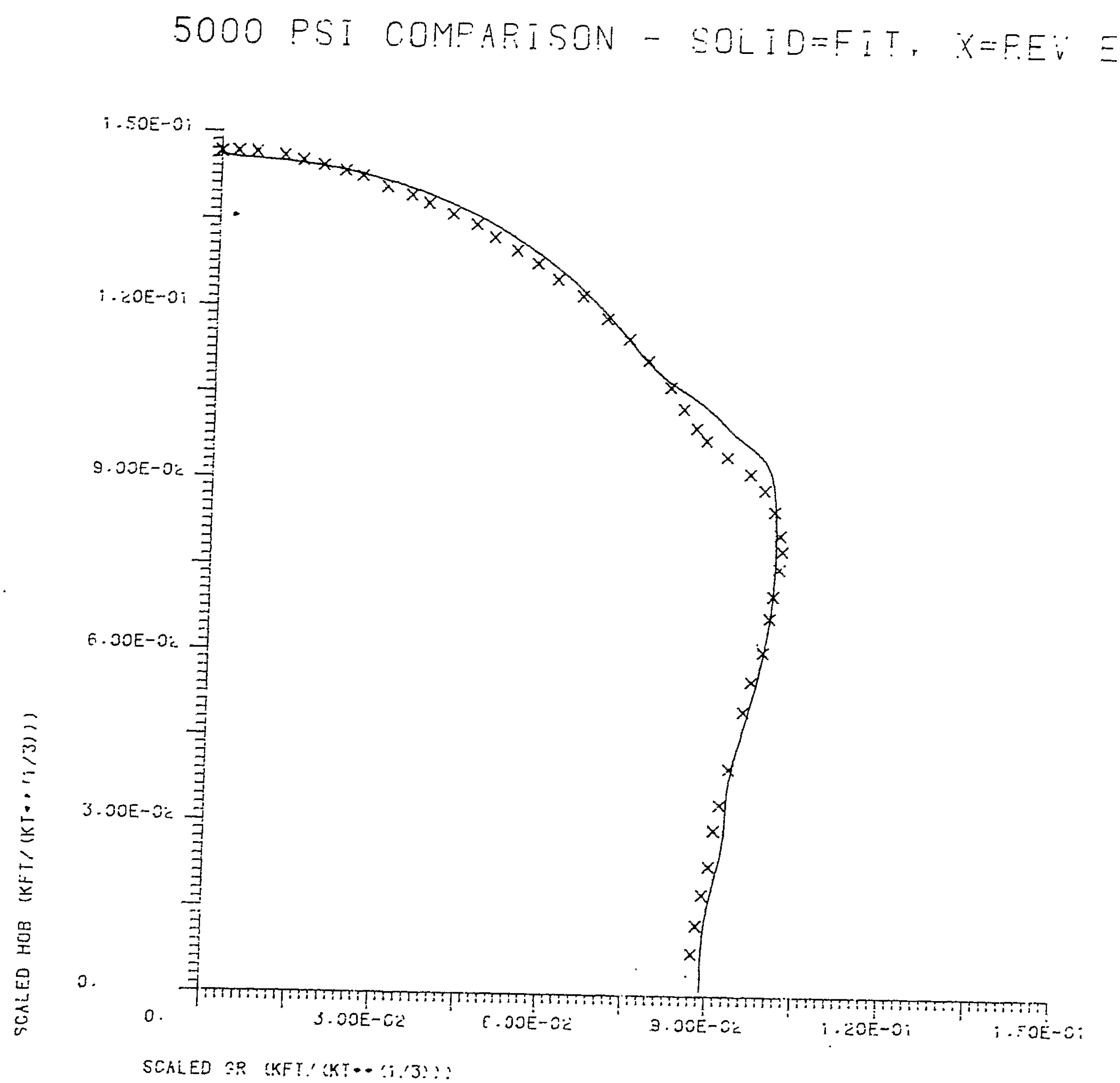
5000 PSI COMPARISON - SOLID=FIT, X=REV E
1.50E-01
1.20E-01
9.00E-02
6.00E-02
3.00E-02
0.
0.
3.00E-02
6.00E-02
9.00E-02
1.20E-01
1.50E-01
SCALED HOB (KFT/(KT**(1/3)))
SCALED GR (KFT/(KT**(1/3)))

Figure 9

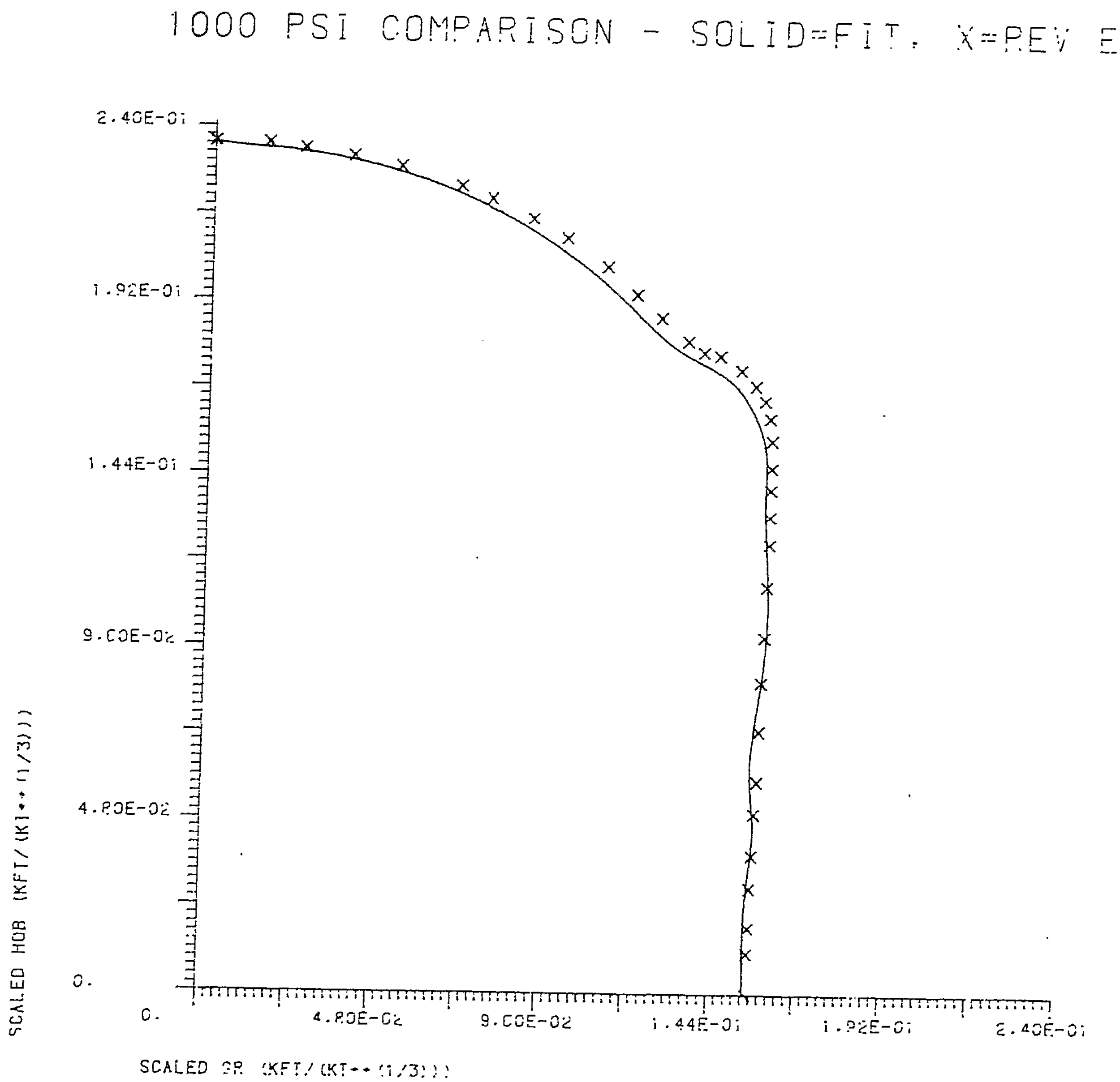
1000 PSI COMPARISON - SOLID=FIT, X=REV E
2.40E-01
1.92E-01
1.44E-01
9.00E-02
4.80E-02
0.
SCALED HOB (KFT/(KT**(1/3)))
0.
4.80E-02
9.00E-02
1.44E-01
1.92E-01
2.40E-01
SCALED GR (KFT/(KT**(1/3)))

Figure 10

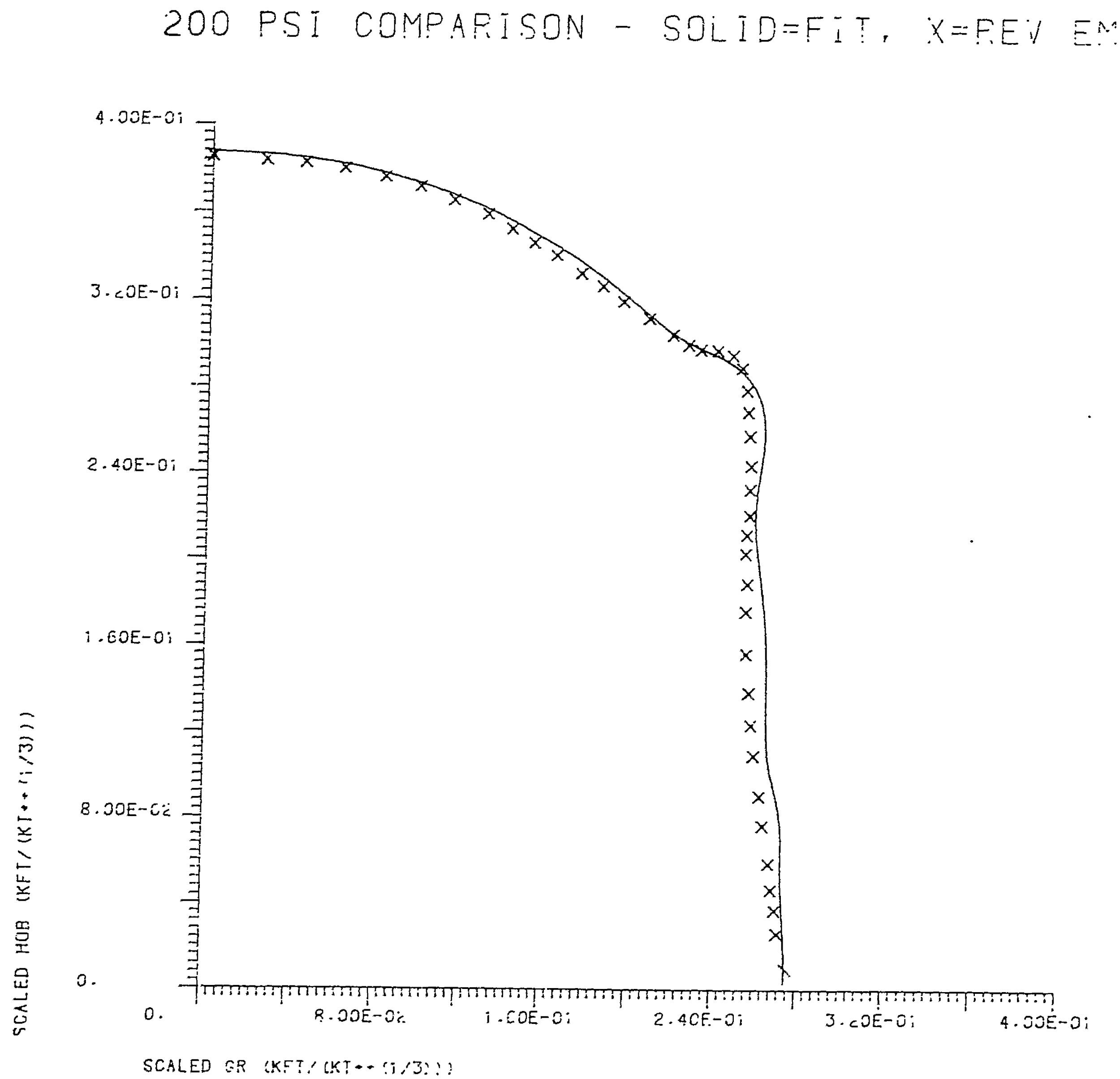
200 PSI COMPARISON - SOLID=FIT, X=REV EM
4.00E-01
3.20E-01
2.40E-01
1.60E-01
8.00E-02
0.
SCALED HOB (KFT/(KT**(1/3)))
0.
8.00E-02
1.60E-01
2.40E-01
3.20E-01
4.00E-01
SCALED GR (KFT/(KT**(1/3)))

Figure 11

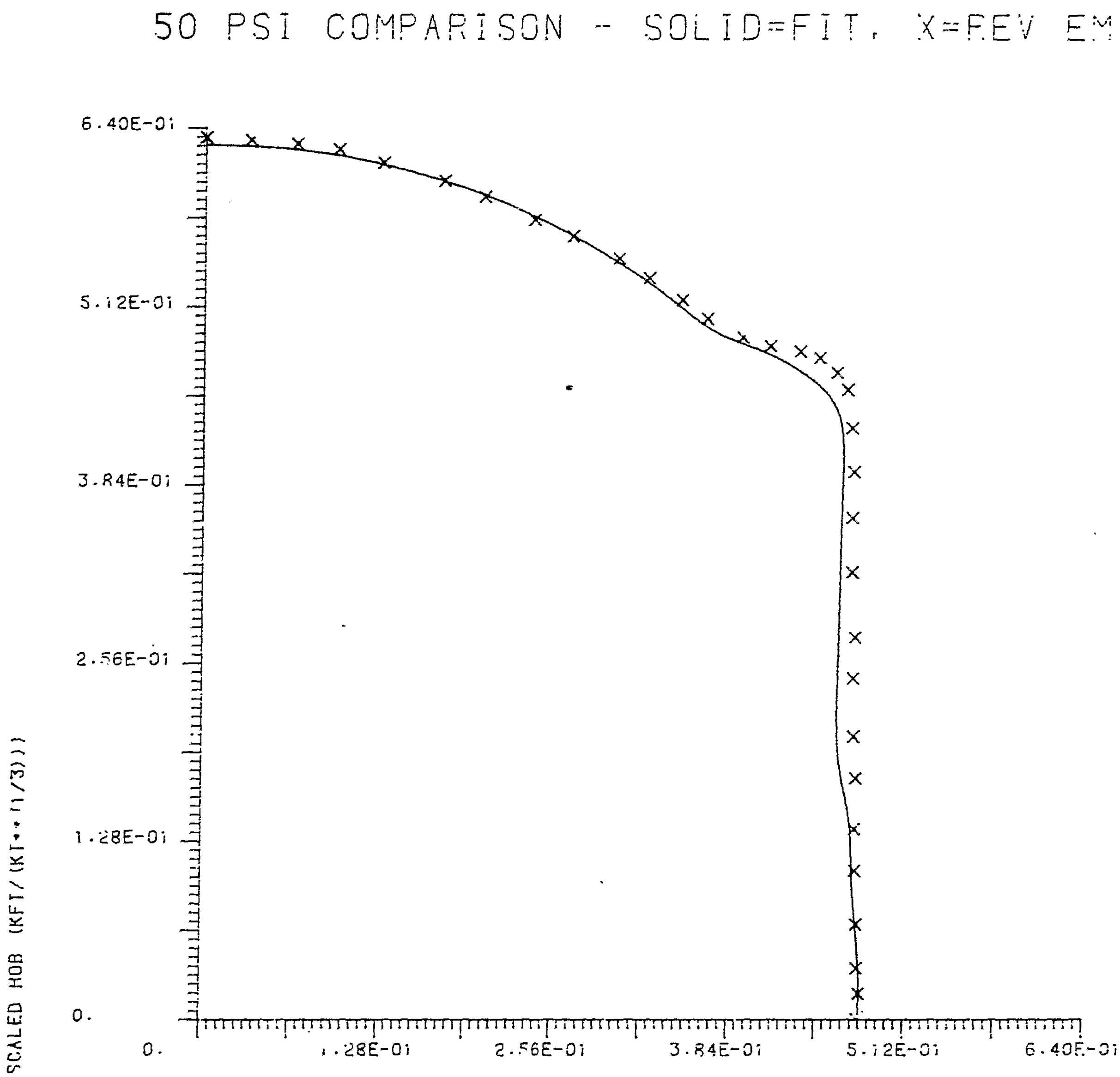

50 PSI COMPARISON - SOLID=FIT, X=REV EM1
6.40E-01
5.12E-01
3.84E-01
2.56E-01
1.28E-01
0.
0.
1.28E-01
2.56E-01
3.84E-01
5.12E-01
6.40E-01
SCALED HOB (KFT/(KT**(1/3)))
SCALED GR (KFT/(KT**(1/3)))

Figure 12

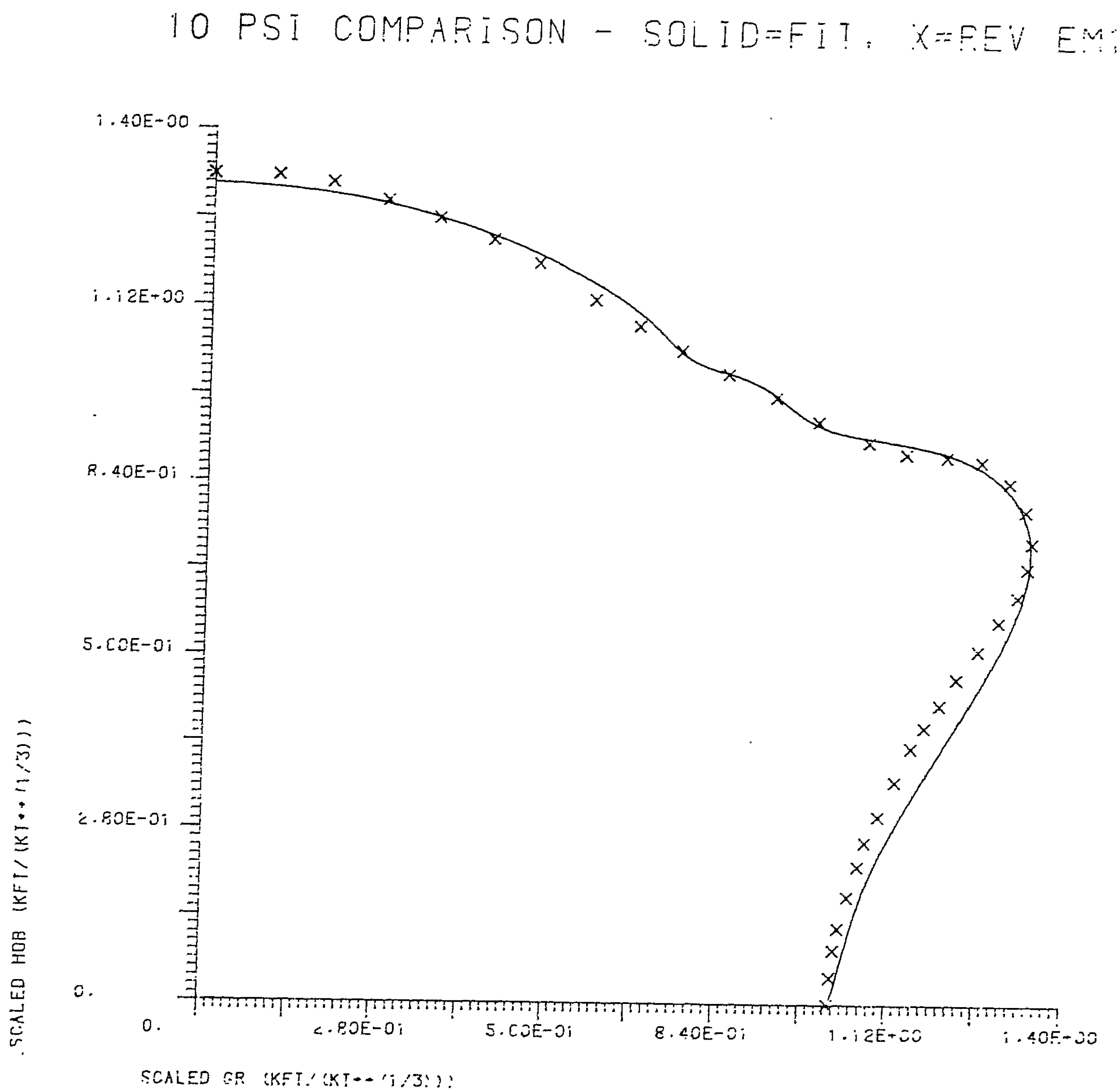
10 PSI COMPARISON - SOLID=FIT, X=REV EM1
1.40E+00
1.12E+00
8.40E-01
5.60E-01
2.80E-01
0.
SCALED HOB (KFT/(KT** (1/3)))
0.
2.80E-01
5.60E-01
8.40E-01
1.12E+00
1.40E+00
SCALED GR (KFT/(KT** (1/3)))

Figure 13

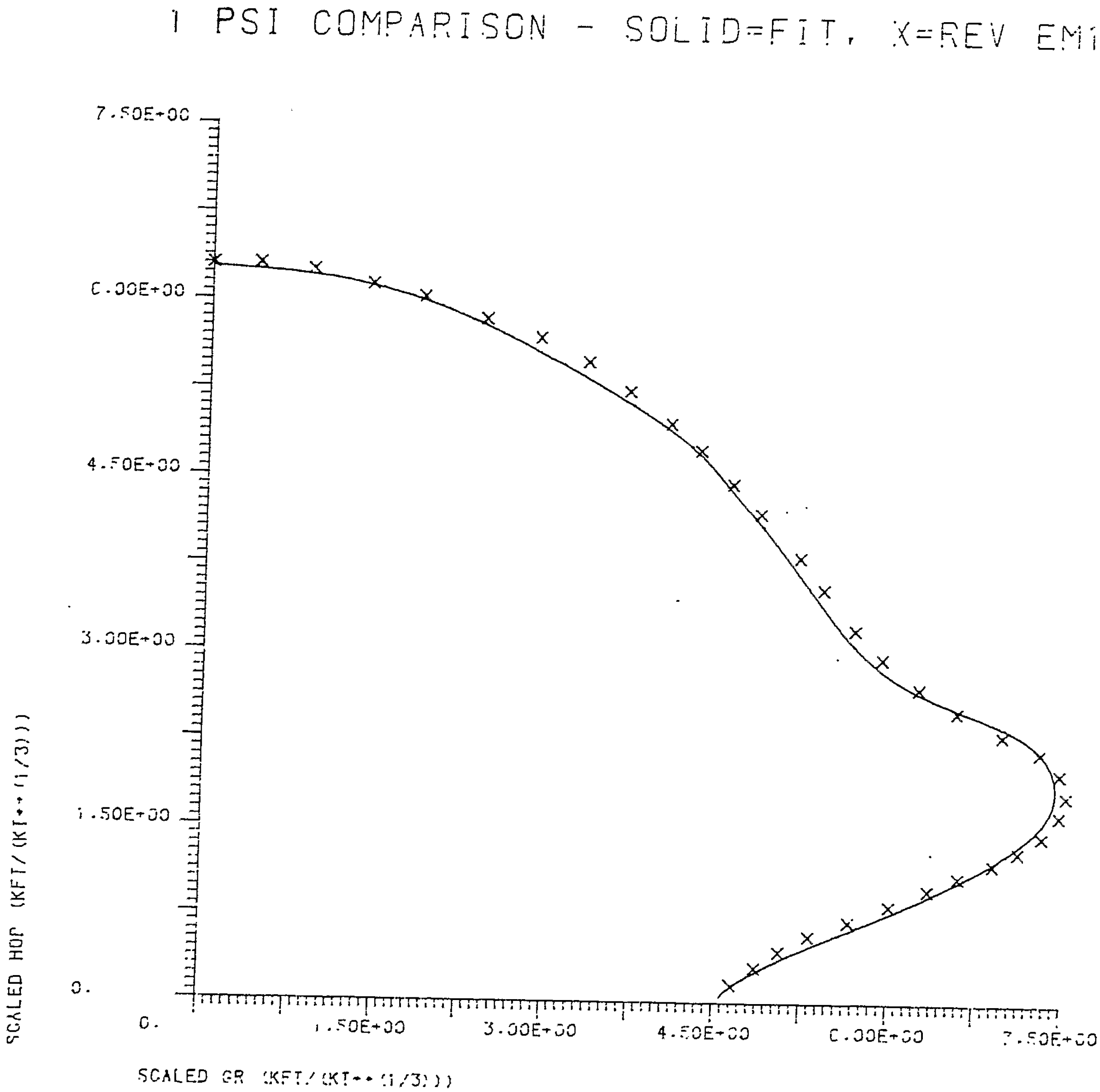
1 PSI COMPARISON - SOLID=FIT, X=REV EM1
7.50E+00
6.00E+00
4.50E+00
3.00E+00
1.50E+00
0.
0.
1.50E+00
3.00E+00
4.50E+00
6.00E+00
7.50E+00
SCALED HOP (KFT/(KT** (1/3)))
SCALED GR (KFT/(KT** (1/3)))

Figure 14

APPENDIX

TEST CASES

X=SCALED GROUND RANGE (KFT/KT**(1/3))
Y=SCALED HOB (KFT/KT**(1/3))
P=PRESSURE (PSI) -ROUNDED TO 4 DECIMAL PLACES

X	Y	P
.08	.08	9273.9215
.08	.11	4842.7312
.08	.14	3013.3145
.08	.17	1921.5384
.08	.2	1258.7035
.08	.23	854.3914
.08	.26	600.9706
.08	.29	436.7590
.11	.08	3605.3036
.11	.11	3171.0038
.11	.14	2050.6448
.11	.17	1374.3730
.11	.2	979.7990
.11	.23	706.6103
.11	.26	518.6033
.11	.29	388.6285
.14	.08	1486.0246
.14	.11	1525.3549
.14	.14	1423.5866
.14	.17	1059.9104
.14	.2	743.9925
.14	.23	563.2797
.14	.26	432.9844
.14	.29	336.1554
.17	.08	755.4464
.17	.11	793.1934
.17	.14	769.8760
.17	.17	756.7070
.17	.2	616.8401
.17	.23	454.6880
.17	.26	355.1937
.17	.29	284.9511
.2	.08	456.4937
.2	.11	463.8922
.2	.14	461.9013
.2	.17	444.7910
.2	.2	451.8764
.2	.23	390.5615
.2	.26	302.3742
.2	.29	240.7564

.23	.08	310.5259
.23	.11	300.2334
.23	.14	301.7340
.23	.17	292.4009
.23	.2	284.8834
.23	.23	294.0338
.23	.26	263.8051
.23	.29	213.2791
.26	.08	224.5847
.26	.11	211.6172
.26	.14	210.3212
.26	.17	207.3167
.26	.2	199.4590
.26	.23	197.5318
.26	.26	204.4450
.26	.29	187.6294
.29	.08	168.3002
.29	.11	159.4008
.29	.14	155.1115
.29	.17	153.8709
.29	.2	150.1906
.29	.23	145.1146
.29	.26	145.6736
.29	.29	149.8596
.35	.4	78.7224
.35	.6	37.9459
.35	.8	22.4828
.35	1	15.0125
.55	.4	37.5970
.55	.6	28.1263
.55	.8	17.6802
.55	1	13.0221
.75	.4	21.9922
.75	.6	23.2702
.75	.8	15.1194
.75	1	10.7456
.95	.4	14.6927
.95	.6	16.6934
.95	.8	13.4738
.95	1	9.5912
2.5	1.1	4.0595
2.5	1.4	3.5345
2.5	1.7	2.9317
2.5	2	2.5338
4.5	1.1	1.7258
4.5	1.4	1.8466
4.5	1.7	1.7932
4.5	2	1.6286
6.5	1.1	1.0435
6.5	1.4	1.1345
6.5	1.7	1.1633
6.5	2	1.1515

CHAPTER 6

ANALYTIC APPROXIMATION FOR DYNAMIC PRESSURE VERSUS TIME

Harold L. Brode
Stephen J. Speicher

The procedure reported here was contrived to satisfy a limited request: for dynamic pressure as a function of burst height for 5, 15, and 25 psi at scaled burst heights of 0, 200, and 700 ft, for 40 kT. The procedure, which may be extended to broader applications at a later date, is designed to use the approximations given in Brode [1970], but can readily be adapted to the new fit to peak overpressure, which corresponds to the recently recommended correction curves for EM-1.* The steps in the approximation are as follows:

Given

1. Height of burst (HOB) "y" (kft).
2. Ground range "x" (kft).
3. Yield "W" (kT).

Step 1. Solve for $t_a(w, r)$ *[free-air burst]*

We can derive the free-air-burst time-of-arrival from Eq. (5) of Brode [1970]:

$$t_a = \frac{(0.5429m^3 - 21.185rm^2 + 361.8r^2m + 2383r^3)}{(m^2 + 2.048rm + 2.6872r^2)} \quad \text{msec} , \qquad (1)$$

where $m = W^{1/3}$,

$r = (x^2 + y^2)^{1/2}$.

Step 2. Solve for $\Delta P_s(t_a, W)$ *[free-air burst]*

Next, we can solve for free-air-burst peak overpressure at this range, HOB, and yield, using Eq. (13) of Brode [1970], with $t = t_a$. (For overpressures above 1000 psi, Brode's Eq. (13) has been modified to give faster decay from the peak; but the correction is irrelevant for the dynamic pressure application here, which

*The new fit was reported at the 31 March 1980 meeting (at RDA, Marina del Rey, California) of the DNA Airblast Working Group, and in PSR's progress report for December 1979 through February 1980 on Contract DNA001-80-C-0065.

uses only peak overpressure.) For peak overpressure, with $t = t_a$, Brode's Eq. (13) becomes

$$\Delta P_s(t_a, W) = \frac{(14{,}843m)}{(0.0135m + t_a)} \frac{\left(m^2 + 0.6715mt_a + 0.00481t_a^2\right)}{\left(m^2 + 1.8836mt_a + 0.02161t_a^2\right)} \quad \text{psi} . \qquad (2)$$

A simpler form appropriate for peak overpressures is

$$\Delta P_s(t_a, W) = \frac{1.05 \times 10^6}{1 + 130t^{1.14}} \quad \text{psi} , \qquad (3)$$

where $t = t_a/m$. This expression is reasonable from 2 psi to 1 million psi, and is accurate to within 10 percent in the range 2 to 10,000 psi. Figure 1 compares the approximation with several calculated results.

Both Eqs. (2) and (3) represent the peak overpressure for a free-air burst as a function of arrival time (and yield). A surface burst is approximated by the same form, with 2W in place of W ($2^{1/3}$ m in place of m).

Step 3. Solve for $t_a(x, y, W)$ *[HOB]*

For bursts near but not on the ground surface, arrival time is approximated by Eq. (16) of Brode [1970]:

$$t_a(x, y, W) = t_a(r, W) , \qquad \text{for } x \le y$$

$$= t_a(r, W)\frac{y}{x} + t_a(r, 2W)\left(\frac{1 - y}{x}\right) , \qquad \text{for } x \ge y . \qquad (4)$$

Step 4. Solve for $\Delta P_s(t_a, x, y, W)$ *[HOB]*

Peak overpressure as approximated by Eq. (20) of Brode [1970] is

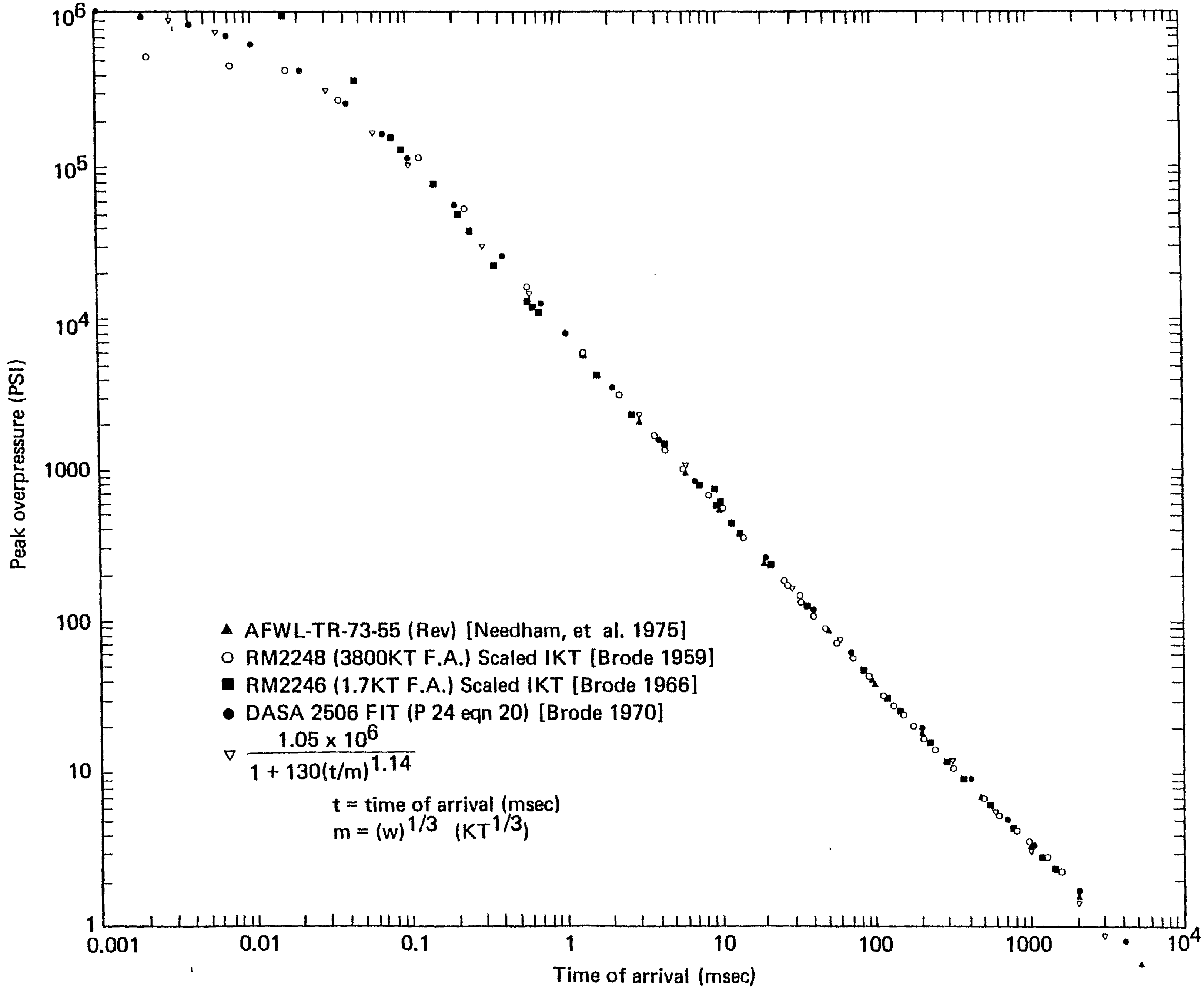

Figure 1 Comparison of peak overpressure versus time of arrival [illegible]

$$\Delta P_s(P,\ z) = H(P,\ z)\left[1 + \frac{E(P)}{1 + (0.4/z^4)}\right]$$

$$\times\left[a\ \Delta P_s(t_a,\ W) + (1 - a)\ \Delta P_s(t_a,\ 2W)\right] , \qquad (5)$$

where $\Delta P_s(t_a,\ W)$ and $\Delta P_s(t_a,\ 2W)$ are defined by Eq. (2) or (3) above, and

$$z \equiv \frac{y}{x(t_a)} ,$$

$$P \equiv \frac{1.58W}{r^3} + \frac{5.3\ \sqrt{W/r}}{r} + 0.0215 \qquad \text{(Eq. (1) of Brode [1970])} ,$$

$$H(P,\ z) = 1 + A + \frac{BP^{3/2}}{C + P^3} + \frac{FP}{I + P^2} ,$$

$$A = \frac{0.743(1.136 - z)z^2}{1.544 + z^6} - \frac{0.0257z^6}{0.004435 + z^{12}} ,$$

$$B = \frac{z(20.42 + 35.5z)}{3.57 + z^2} + \frac{2500z^4}{29.3 + z^{14}} ,$$

$$C = \left[1 + \frac{z(2.23z - 0.225)}{(0.148 + z^2)} + \frac{28.4z^7}{0.905 + z^7}\right]^3 ,$$

$$E(P) = 1 + \frac{0.002655P}{1 + 0.0001728P + 1.921 \times 10^{-9}P^2}$$

$$+ \frac{0.004218 + 0.04824P + 6.856 \times 10^{-6}P^2}{1 + 0.008P + 3.844 \quad 10^{-6}P^2} ,$$

$$F = \frac{2.07z^2}{0.00125 + 0.0146z^2 + z^8} + \frac{221.25z^8}{1 + z^{20}} ,$$

$$I = 40,000 - \frac{17,650z^2}{0.235 + z^6} ,$$

and

$$a = \frac{z^2(1 + 2z^4)}{1 + 2z^6} .$$

Any other definition of the peak-overpressure/HOB/range relationship can, of course, be used at this step. One example is the new fit for the revised EM-1 curves, which take advantage of the similarities in the family of HOB curves from 1.0 to 10,000 psi. The behavior along the x-axis (zero HOB) is that of a surface burst, for which overpressure can be expressed as a simple function of ground range:

$$PD \simeq \frac{6.5}{x^{4/3}} + \frac{4}{x^3} \quad \text{psi} . \tag{6}$$

Along the vertical axis (zero ground range), the behavior is approximated by

$$PK \simeq \frac{11}{y^{1.3}} + \frac{6}{y^{3.5}} \quad \text{psi} , \tag{7}$$

where x and y are in kft.

Along a curve through the maximum horizontal range for each isobar (y = RA in Fig. 2), pressure is expressed by

$$PE \simeq \frac{1.8}{x^{3.4}} + \frac{4.4 \times 10^5 x^9}{1 + 2.8 \times 10^4 x^{10}} - \frac{5(RA)^{2.3}}{1 + (RA)^{4.8}} - 0.22(RA) , \tag{8}$$

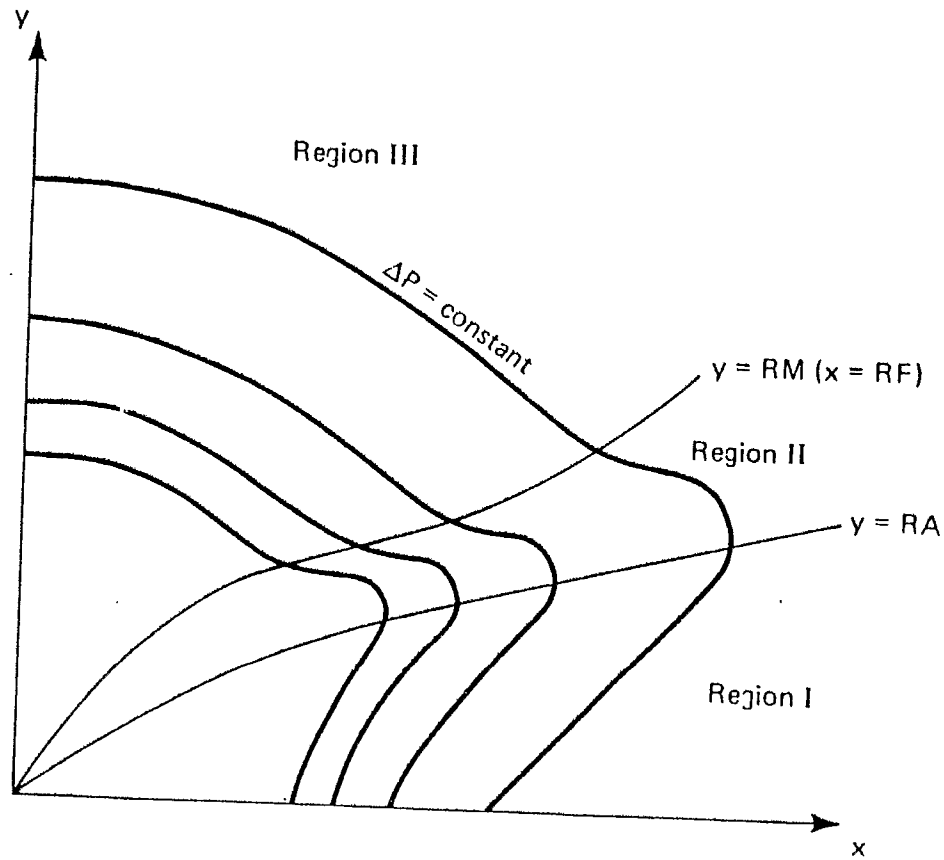

Figure 2. Typical isobars and fit regions.

where the curve

$$y = RA = 1 \times 10^{-4}x^2 + 0.7x^{1/2} - \frac{0.12x^{0.02}}{1 + 297x^{4.0}} - 0.23 \ . \qquad (9)$$

Along a curve through the relative minimum above the knees ($y = RM$ in Fig. 2), pressure is approximated as

$$PJ \simeq \frac{14.35}{(RI)^{1.45}} + 0.056 + \frac{4}{(RI)^{3.71}} - \frac{0.171}{(RI)^{4.716}} \ , \qquad (10)$$

where $RI = (RF^2 + y^2)^{1/2}$, with

$$RF \simeq 4.1y^{0.76} - 2.3y^{0.31} + \frac{10.3y^{1.8}}{1 + 231y^{2.1}} - \frac{2.29y^{1.3}}{1 + y^{2.2}} + 0.56 \ . \qquad (11)$$

Interpolating between the pressures along the four curves $y = 0$, $x = 0$, $y = RA(x)$, and $x = RF(y)$ defines peak overpressure for any height of burst (y) and range (x).

The interpolation is not linear and differs in each region. In region I, between $y = 0$ and $y = RA$,

$$\Delta P_s \simeq (1 - FC)PD + FC \cdot PE \ , \qquad (12)$$

where

$$FC \simeq FB \frac{(0.433 + 1.011FB)}{1 + 0.444(FB)^5}$$

and

$$FB = \frac{y}{RA} \ .$$

In region II, between $y = RA(x)$ and $x = RF(y)$,

$$\Delta P_s \simeq FO \cdot PL + (1 - FP) \cdot FC \cdot PE \, , \qquad (13)$$

where

$$FO \simeq 0.77(FN)^{2.74} + 0.23(FN)^{0.70} \, ,$$

$$FN \simeq \frac{y(y - RA)}{RM(RM - RA)} \, ,$$

$$FP \simeq FO^{[1+0.00594(x^2+y^2)^{1.28}]} \, ,$$

$$PL \simeq (1 - FH)PK + FH \cdot PJ \, ,$$

$$FH \simeq 0.093(FG)^{1.03} + \frac{7.7(FG)^{2.51}}{1 + 7.49(FG)^{2.15}} \, ,$$

$$FG = \frac{x}{RF} \, ,$$

and

$$RM \simeq 0.0036 - \frac{0.092x^{-0.39}}{1 + 31x^{3.11}} + \frac{0.69x^{0.46}}{1 - 0.2x^{0.47}} + \frac{0.006}{x^{1.11}} \, .$$

In region III,

$$\Delta P_s \simeq PL \, . \qquad (14)$$

This fit provides a continuous analytic approximation to the new (and improved) peak-overpressure curves recommended for EM-1.

Step 5. Solve for $Q_s(\Delta P_s)$ *[HOB]*

Peak dynamic pressure in an adiabatic shock is directly related to peak overpressure by the expression

$$Q_s = \frac{\Delta P_s^2}{2\gamma P_0 + (\gamma - 1)P_s} , \tag{15}$$

where P_0 is the ambient air (preshock) pressure and γ is the effective specific heat ratio for air. For overpressures less than 300 psi, γ may be approximated as 1.4. For all overpressures at sea level ($P_0 \approx 14.7$ psi or 10^5 P_a), $1.16 < \gamma < 1.67$ [Brode, 1968].

For the revised peak overpressure fit [Eqs. (6) through (14)], peak values do not in all cases correspond to shock front values: in part of the Mach reflection region, the second peak exceeds the shock value, so that the Hugoniot (shock) expression for dynamic pressure is not rigorously valid in that region. However, since both peak overpressure and dynamic pressure increase in the double Mach region, we assume the same relation applies.

In the regular reflection region, effective dynamic pressure does not equal total dynamic pressure, since at the surface the flow is constrained to horizontal velocities only. An approximate correction for that effect is to express horizontal dynamic pressure as

$$Q_H(x, y) = Q_s(r_s)\left(\frac{x}{y}\right) , \qquad \text{for } x < y . \tag{16a}$$

In the Mach reflection region, the flow has presumably been turned parallel to the surface, and the horizontal component is the total dynamic pressure:

$$Q_H(x, y) = Q_s(r_s) , \qquad \text{for } x \geq y . \tag{16b}$$

Although the transition between regular and Mach reflection does not occur exactly at $x = y$, the approximation brings the horizontal dynamic pressure to zero at the point on the surface directly beneath the burst ($x = 0$), and allows full dynamic forces as the shock passes into the Mach region.

Step 6. Solve for Q(t)

The following approximation for dynamic pressure as a function of HOB, range, time, and yield is based on the observation that dynamic pressure behind the shock front at any time is a rapidly decreasing function of distance behind the front. A reasonable approximation is

$$Q(r) = Q(r_s)\left(\frac{r_0}{r_s}\right)^9 , \qquad (17)$$

where $r_0 = (x_0^2 + y^2)^{1/2}$, with x_0 the original ground range of interest; and $r_s = (x^2 + y^2)^{1/2}$, with x the subsequent shock position ground range. Thus, if t_0 represents the shock arrival time at the position of interest (x_0, y) and t represents the shock arrival time at further positions (x, y),

$$Q(t) = Q_H(x, y)\left(\frac{r_0}{r}\right)^9 , \qquad (18)$$

and x, r, and t are related by $r = (x^2 + y^2)^{1/2}$, $t = t_a(r, W)$ [Eq. (1)].

The ninth-power decay is only an approximation to the dynamic pressure behavior behind the shock front at low overpressures (5 to 30 psi). The best fit power in this range varies between 8.8 and 10.2 [Brode, 1966, Figs. 37 and 38]; the fit is illustrated in Fig. 3.

Using the above procedure, we approximated both overpressure versus time and dynamic pressure versus time for three scaled burst heights, three peak overpressures, and one yield of 40 kT (as requested by George Ullrich of DNA, 31 March 1980). The peak overpressures are 5, 15, and 25 psi (34, 103, and 172 P_a); the scaled burst heights are 0, 200, and 700 ft (0, 61, and 312 m). Also approximated are the overpressures and dynamic pressures at the same ground range at which 15 psi occurs for a surface burst, but at a burst height of 200 ft.

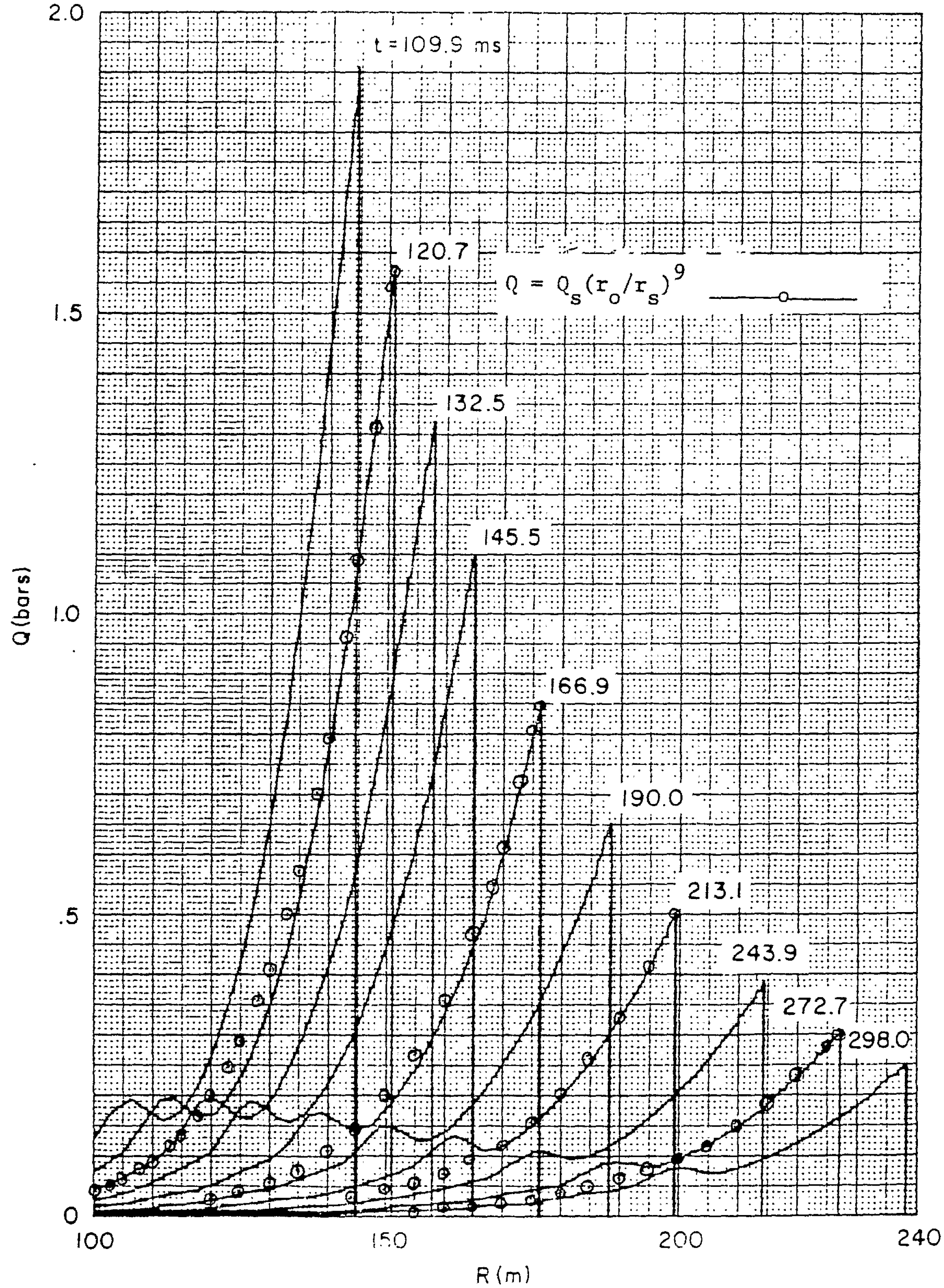

Figure 3. Comparison of dynamic pressures at indicated times from numerical calculation [Brode, 1966] and current fit (1.7 kT free-air burst).

In Tables 1 through 10, each time-of-arrival [Eq. (4)] is listed with its corresponding dynamic impulse (horizontal component), time after time-of-arrival (TIME - TOA), dynamic pressure [horizontal component as defined in Eq. (16)], and shock ground range (G/R). The impulse is the partial integral

$$I(t) = \int_{t_0}^{t} Q(t)\ dt \ . \qquad (19)$$

Listed above each table are the relevant yield (kT), burst height (kft), initial ground range (kft), free-air peak overpressure (psi) at the given initial range, time (msec), peak overpressure (OP), peak dynamic pressure, and horizontal component of the peak dynamic pressure [Eq. (16)]. Note that the integration is not carried to the time of velocity reversal, which is appreciably longer than the overpressure positive phase.

Tables 11 through 20 provide similar listings of overpressure, overpressure impulse, and shock ground range as functions of time or time after initial shock arrival. Again yield, burst height, and initial ground range are given above each table, along with free-air overpressure at the given distance, time of arrival, peak overpressure expected at the given range for a surface burst, and peak overpressure for the given HOB. The overpressure records are terminated at the end of the positive phase.

The approximation outlined above makes use of the rapid decay of dynamic pressure behind the shock front from a free-air burst, but even that decay may not be rapid enough in the early Mach reflection region. Preliminary study of the results of the 200-ft-HOB HULL calculation [McNamara, Jordano, and Lewis, 1977] suggests that the dynamic impulse in the Mach region where the second peak is the larger is not as strongly influenced by HOB as are peak overpressure and corresponding peak dynamic pressure. This is not likely to be the case unless the early dynamic pressure fades more rapidly behind the shock than does the free-air dynamic pressure. Thus, dynamic pressure impulse HOB curves should have less pronounced knees.

This conjecture is a preliminary one, based solely on unverified observations from a numerical calculation; a physical explanation does not yet exist. However, if true, the fit suggested here would need further modification in the Mach reflection region.

Table 1

YIELD = 40 KT
HEIGHT OF BURST = 0 KFT
GROUND RANGE = 5.591 KFT
PEAK OVERPRESSURE = 2.9665 PSI
TIME OF ARRIVAL = 3038.3332 MSEC
PEAK OP (T=TA) = 4.9996 PSI
PEAK DYNAMIC PRES.= .5791 PSI
PEAK HORIZ. COMPT.= .5791 PSI

TIME (MSEC)	DYN. IMPULSE(HORIZ) (PSI-MSEC)	TIME-TOA (MSEC)	DYN. HORIZ. COMPT. (PSI)	SHOCK G/R (KFT)
3043.8141	3.1509	5.4808	.5706	5.5975
3049.2962	6.2566	10.9630	.5623	5.6046
3054.7797	9.3177	16.4464	.5541	5.6115
3060.2645	12.3350	21.9312	.5460	5.6183
3071.2379	18.2404	32.9046	.5303	5.6320
3082.2165	23.9785	43.8832	.5150	5.6457
3093.2002	29.5542	54.8669	.5003	5.6593
3104.1890	34.9727	65.8557	.4859	5.6730
3115.1829	40.2387	76.8496	.4721	5.6867
3126.1818	45.3570	87.8485	.4586	5.7004
3148.1946	55.1668	109.8613	.4330	5.7277
3170.2272	64.4376	131.8939	.4089	5.7551
3192.2794	73.2015	153.9461	.3862	5.7825
3214.3508	81.4886	176.0176	.3649	5.8098
3236.4414	89.3269	198.1081	.3449	5.8372
3258.5508	96.7427	220.2175	.3261	5.8645
3280.6788	103.7608	242.3456	.3084	5.8919
3302.8253	110.4043	264.4920	.2917	5.9193
3324.9899	116.6947	286.6567	.2760	5.9466
3347.1726	122.6526	308.8393	.2613	5.9740
3391.5910	133.6410	353.2577	.2342	6.0287
3436.0788	143.5133	397.7455	.2102	6.0834
3480.6345	152.3918	442.3012	.1889	6.1381
3525.2565	160.3844	486.9232	.1698	6.1929
3569.9432	167.5866	531.6100	.1529	6.2476
3614.6933	174.0827	576.3600	.1378	6.3023
3659.5052	179.9474	621.1720	.1243	6.3570
3704.3777	185.2471	666.0444	.1122	6.4117
3749.3092	190.0404	710.9760	.1014	6.4665
3794.2986	194.3797	755.9654	.0917	6.5212
3878.8052	201.4420	840.4719	.0761	6.6238
3963.5025	207.3294	925.1692	.0634	6.7264

HORIZONTAL DYNAMIC IMPULSE (PSI-SEC) = .2073

Table 2

YIELD = 40 KT
HEIGHT OF BURST = 0 KFT
GROUND RANGE = 2.977 KFT
PEAK OVERPRESSURE = 9.0659 PSI
TIME OF ARRIVAL = 1096.8521 MSEC
PEAK OP (T=TA) = 14.9996 PSI
PEAK DYNAMIC PRES.= 4.7707 PSI
PEAK HORIZ. COMPT.= 4.7707 PSI

TIME (MSEC)	DYN. IMPULSE(HORIZ) (PSI-MSEC)	TIME-TOA (MSEC)	DYN. HORIZ. COMPT. (PSI)	SHOCK G/R (KFT)
1101.3123	20.9714	4.4601	4.6342	2.9838
1105.7773	41.3662	8.9251	4.5020	2.9906
1110.2473	61.2016	13.3951	4.3738	2.9975
1114.7222	80.4940	17.8700	4.2496	3.0043
1123.6866	117.5101	26.8345	4.0125	3.0180
1132.6705	152.5412	35.8183	3.7896	3.0317
1141.6735	185.7022	44.8213	3.5801	3.0453
1150.6957	217.1009	53.8435	3.3831	3.0590
1159.7368	246.8384	62.8846	3.1979	3.0727
1168.7967	275.0096	71.9446	3.0235	3.0864
1186.9724	326.9836	90.1202	2.7050	3.1137
1205.2216	373.6951	108.3694	2.4226	3.1411
1223.5432	415.7171	126.6910	2.1719	3.1685
1241.9361	453.5562	145.0839	1.9491	3.1958
1260.3992	487.6600	163.5470	1.7509	3.2232
1278.9314	518.4255	182.0792	1.5743	3.2505
1297.5317	546.2041	200.6795	1.4170	3.2779
1316.1991	571.3080	219.3470	1.2765	3.3053
1334.9326	594.0143	238.0804	1.1511	3.3326
1353.7312	614.5696	256.8790	1.0389	3.3600
1391.5196	650.0343	294.6674	.8485	3.4147
1429.5568	679.2420	332.7046	.6954	3.4694
1467.8354	703.3731	370.9832	.5719	3.5241
1506.3484	723.3714	409.4962	.4718	3.5789
1545.0888	739.9941	448.2366	.3905	3.6336
1584.0501	753.8511	487.1979	.3241	3.6883
1623.2258	765.4350	526.3736	.2699	3.7430
1662.6096	775.1452	565.7574	.2253	3.7977
1702.1957	783.3062	605.3435	.1887	3.8525

HORIZONTAL DYNAMIC IMPULSE (PSI-SEC) = .7833

Table 3

```
YIELD                = 40 KT
HEIGHT OF BURST      = 0 KFT
GROUND RANGE         = 2.316 KFT
PEAK OVERPRESSURE    = 14.7987 PSI
TIME OF ARRIVAL      = 692.4409 MSEC
PEAK OP (T=TA)       = 24.9944 PSI
PEAK DYNAMIC PRES.   = 12.2116 PSI
PEAK HORIZ. COMPT.   = 12.2116 PSI
```

TIME (MSEC)	DYN. IMPULSE(HORIZ) (PSI-MSEC)	TIME-TOA (MSEC)	DYN. HORIZ. COMPT. (PSI)	SHOCK G/R (KFT)
696.3199	46.4806	3.8789	11.7585	2.3228
700.2060	91.3224	7.7651	11.3235	2.3296
704.0994	134.5876	11.6584	10.9059	2.3365
707.9998	176.3361	15.5589	10.5049	2.3433
715.8222	255.4960	23.3812	9.7498	2.3570
723.6728	329.2483	31.2318	9.0530	2.3707
731.5514	397.9901	39.1104	8.4098	2.3843
739.4579	462.0876	47.0169	7.8158	2.3980
747.3920	521.8783	54.9510	7.2668	2.4117
755.3535	577.6735	62.9125	6.7593	2.4254
771.3578	678.3402	78.9168	5.8556	2.4527
787.4692	766.2049	95.0282	5.0812	2.4801
803.6860	843.0108	111.2450	4.4163	2.5075
820.0066	910.2485	127.5656	3.8446	2.5348
836.4293	969.1949	143.9883	3.3522	2.5622
852.9526	1020.9454	160.5116	2.9273	2.5895
869.5748	1066.4414	177.1339	2.5601	2.6169
886.2946	1106.4931	193.8536	2.2422	2.6443
903.1102	1141.7990	210.6692	1.9666	2.6716
920.0203	1172.9622	227.5794	1.7274	2.6990
954.1181	1224.7701	261.6771	1.3382	2.7537
988.5764	1265.4383	296.1354	1.0422	2.8084
1023.3842	1297.5155	330.9432	.8158	2.8631
1058.5307	1322.9338	366.0898	.6418	2.9179
1094.0057	1343.1654	401.5647	.5073	2.9726
1129.7990	1359.3380	437.3580	.4028	3.0273
1165.9010	1372.3198	473.4601	.3213	3.0820

HORIZONTAL DYNAMIC IMPULSE (PSI-SEC) = 1.3723

Table 4

YIELD = 40 KT
HEIGHT OF BURST = .684 KFT
GROUND RANGE = 6.171 KFT
PEAK OVERPRESSURE = 2.4931 PSI
TIME OF ARRIVAL = 3575.2327 MSEC
PEAK OP (T=TA) = 5.0002 PSI
PEAK DYNAMIC PRES.= .5792 PSI
PEAK HORIZ. COMPT.= .5792 PSI

TIME (MSEC)	DYN. IMPULSE(HORIZ) (PSI-MSEC)	TIME-TOA (MSEC)	DYN. HORIZ. COMPT. (PSI)	SHOCK G/R (KFT)
3580.7616	3.1826	5.5289	.5719	6.1778
3586.2916	6.3256	11.0589	.5647	6.1846
3591.8228	9.4295	16.5900	.5576	6.1915
3597.3549	12.4950	22.1222	.5506	6.1983
3608.4225	18.5123	33.1898	.5368	6.2120
3619.4943	24.3817	44.2616	.5234	6.2257
3630.5703	30.1071	55.3376	.5104	6.2393
3641.6505	35.6923	66.4178	.4977	6.2530
3652.7349	41.1411	77.5022	.4854	6.2667
3663.8235	46.4572	88.5908	.4734	6.2804
3686.0130	56.7040	110.7803	.4504	6.3077
3708.2189	66.4607	132.9862	.4286	6.3351
3730.441	75.7525	155.2082	.4079	6.3625
3752.6790	84.6036	177.4463	.3883	6.3898
3774.9329	93.0366	199.7002	.3697	6.4172
3797.2025	101.0730	221.9697	.3521	6.4445
3819.4875	108.7328	244.2548	.3354	6.4719
3841.7879	116.0354	266.5551	.3196	6.4993
3864.1034	122.9986	288.8707	.3046	6.5266
3886.4339	129.6397	311.2012	.2903	6.5540
3931.1393	142.0154	355.9066	.2639	6.6087
3975.9028	153.2856	400.6701	.2401	6.6634
4020.7232	163.5570	445.4905	.2187	6.7181
4065.5992	172.9250	490.3665	.1992	6.7729
4110.5298	181.4755	535.2971	.1817	6.8276
4155.5138	189.2854	580.2811	.1658	6.8823
4200.5501	196.4240	625.3174	.1514	6.9370
4245.6376	202.9535	670.4049	.1384	6.9917
4290.7754	208.9300	715.5426	.1266	7.0465
4335.9622	214.4041	760.7295	.1159	7.1012
4420.8167	223.4611	845.5840	.0983	7.2038
4505.8342	231.1701	930.6015	.0836	7.3064
4591.0088	237.7461	1015.7760	.0713	7.4090

HORIZONTAL DYNAMIC IMPULSE (PSI-SEC) = .2377

Table 5

YIELD = 40 KT
HEIGHT OF BURST = .684 KFT
GROUND RANGE = 3.001 KFT
PEAK OVERPRESSURE = 8.5133 PSI
TIME OF ARRIVAL = 1209.3571 MSEC
PEAK OP (T=TA) = 14.9964 PSI
PEAK DYNAMIC PRES.= 4.7688 PSI
PEAK HORIZ. COMPT.= 4.7688 PSI

TIME (MSEC)	DYN. IMPULSE(HORIZ) (PSI-MSEC)	TIME-TOA (MSEC)	DYN. HORIZ. COMPT. (PSI)	SHOCK G/R (KFT)
1213.7684	20.7547	4.4112	4.6419	3.0078
1218.1844	40.9796	8.8273	4.5186	3.0146
1222.6053	60.6892	13.2481	4.3989	3.0215
1227.0308	79.8978	17.6737	4.2826	3.0283
1235.8962	116.8632	26.5390	4.0599	3.0420
1244.7803	151.9849	35.4232	3.8497	3.0557
1253.6832	185.3622	44.3260	3.6512	3.0693
1262.6045	217.0890	53.2474	3.4639	3.0830
1271.5443	247.2533	62.1872	3.2869	3.0967
1280.5024	275.9383	71.1452	3.1197	3.1104
1298.4728	329.1619	89.1156	2.8123	3.1377
1316.5147	377.3552	107.1575	2.5376	3.1651
1334.6271	421.0304	125.2700	2.2918	3.1925
1352.8091	460.6437	143.4519	2.0716	3.2198
1371.0595	496.6021	161.7023	1.8742	3.2472
1389.3775	529.2691	180.0203	1.6971	3.2745
1407.7620	558.9693	198.4049	1.5380	3.3019
1426.2122	585.9931	216.8550	1.3950	3.3293
1444.7271	610.6006	235.3699	1.2664	3.3566
1463.3057	633.0247	253.9486	1.1505	3.3840
1500.6508	672.0924	291.2936	.9519	3.4387
1538.2404	704.6775	328.8832	.7900	3.4934
1576.0676	731.9325	366.7105	.6576	3.5481
1614.1260	754.7917	404.7688	.5489	3.6029
1652.4090	774.0154	443.0518	.4596	3.6576
1690.9105	790.2236	481.5533	.3858	3.7123
1729.6245	803.9237	520.2673	.3247	3.7670
1768.5452	815.5323	559.1880	.2740	3.8217
1807.6669	825.3922	598.3097	.2318	3.8765
1846.9842	833.7861	637.6270	.1966	3.9312

HORIZONTAL DYNAMIC IMPULSE (PSI-SEC) = .8337

Table 6

YIELD = 40 KT
HEIGHT OF BURST = .684 KFT
GROUND RANGE = 2.977 KFT
PEAK OVERPRESSURE = 8.6363 PSI
TIME OF ARRIVAL = 1193.9169 MSEC
PEAK OP (T=TA) = 15.2102 PSI
PEAK DYNAMIC PRES.= 4.8969 PSI
PEAK HORIZ. COMPT.= 4.8969 PSI

TIME (MSEC)	DYN. IMPULSE(HORIZ) (PSI-MSEC)	TIME-TOA (MSEC)	DYN. HORIZ. COMPT. (PSI)	SHOCK G/R (KFT)
1198.3112	21.2278	4.3943	4.7655	2.9838
1202.7104	41.9095	8.7934	4.6379	2.9906
1207.1144	62.0603	13.1975	4.5140	2.9975
1211.5232	81.6948	17.6063	4.3937	3.0043
1220.3552	119.4687	26.4383	4.1634	3.0180
1229.2063	155.3444	35.2894	3.9462	3.0317
1238.0763	189.4250	44.1593	3.7412	3.0453
1246.9651	221.8075	53.0481	3.5477	3.0590
1255.8724	252.5834	61.9555	3.3650	3.0727
1264.7983	281.8389	70.8814	3.1925	3.0864
1282.7051	336.0901	88.7882	2.8756	3.1137
1300.6844	385.1771	106.7674	2.5926	3.1411
1318.7350	429.6295	124.8181	2.3396	3.1685
1336.8560	469.9186	142.9391	2.1132	3.1958
1355.0464	506.4643	161.1295	1.9104	3.2232
1373.3052	539.6415	179.3883	1.7286	3.2505
1391.6314	569.7848	197.7145	1.5654	3.2779
1410.0241	597.1931	216.1071	1.4188	3.3053
1428.4823	622.134	234.5653	1.2870	3.3326
1447.0050	644.8468	253.0881	1.1684	3.3600
1484.2406	684.3791	290.3237	.9654	3.4147
1521.7238	717.3101	327.8069	.8001	3.4694
1559.4477	744.8206	365.5307	.6651	3.5241
1597.4055	767.8667	403.4885	.5545	3.5789
1635.5907	787.2250	441.6737	.4637	3.6336
1673.9971	803.5284	480.0802	.3888	3.6883
1712.6187	817.2939	518.7017	.3269	3.7430
1751.4494	828.9454	557.5324	.2755	3.7977
1790.4836	838.8314	596.5667	.2329	3.8525

HORIZONTAL DYNAMIC IMPULSE (PSI-SEC) = .8388

Table 7

YIELD = 40 KT
HEIGHT OF BURST = .684 KFT
GROUND RANGE = 2.282 KFT
PEAK OVERPRESSURE = 13.9840 PSI
TIME OF ARRIVAL = 776.1969 MSEC
PEAK OP (T=TA) = 24.9958 PSI
PEAK DYNAMIC PRES.= 12.2128 PSI
PEAK HORIZ. COMPT.= 12.2128 PSI

TIME (MSEC)	DYN. IMPULSE(HORIZ) (PSI-MSEC)	TIME-TOA (MSEC)	DYN. HORIZ. COMPT. (PSI)	SHOCK G/R (KFT)
779.9936	45.5547	3.7967	11.7880	2.2888
783.7974	89.6087	7.6004	11.3792	2.2956
787.6081	132.2150	11.4112	10.9856	2.3025
791.4259	173.4253	15.2289	10.6067	2.3093
799.0822	251.8412	22.8852	9.8907	2.3230
806.7661	325.2419	30.5691	9.2268	2.3367
814.4773	393.9730	38.2804	8.6107	2.3503
822.2158	458.3542	46.0189	8.0390	2.3640
829.9813	518.6821	53.7844	7.5081	2.3777
837.7736	575.2314	61.5767	7.0150	2.3914
853.4379	677.9387	77.2409	6.1307	2.4187
869.2071	768.3679	93.0101	5.3659	2.4461
885.0796	848.0927	108.8826	4.7033	2.4735
901.0540	918.4722	124.8571	4.1284	2.5008
917.1289	980.6813	140.9319	3.6289	2.5282
933.3027	1035.7375	157.1057	3.1941	2.5555
949.5740	1084.5235	173.3770	2.8153	2.5829
965.9414	1127.8055	189.7444	2.4846	2.6103
982.4034	1166.2502	206.2065	2.1956	2.6376
998.9589	1200.4380	222.7619	1.9427	2.6650
1032.3442	1257.8994	256.1473	1.5266	2.7197
1066.0869	1303.6473	289.8899	1.2054	2.7744
1100.1765	1340.2264	323.9796	.9562	2.8291
1134.6032	1369.5957	358.4062	.7619	2.8839
1169.3572	1393.2712	393.1602	.6097	2.9386
1204.4291	1412.4308	428.2321	.4899	2.9933
1239.8098	1427.9940	463.6129	.3953	3.0480
1275.4906	1440.6819	499.2936	.3201	3.1027

HORIZONTAL DYNAMIC IMPULSE (PSI-SEC) = 1.4406

Table 8

YIELD = 40 KT
HEIGHT OF BURST = 2.394 KFT
GROUND RANGE = 8.065 KFT
PEAK OVERPRESSURE = 1.5272 PSI
TIME OF ARRIVAL = 5489.1631 MSEC
PEAK OP (T=TA) = 4.9991 PSI
PEAK DYNAMIC PRES.= .5790 PSI
PEAK HORIZ. COMPT.= .5790 PSI

TIME (MSEC)	DYN. IMPULSE(HORIZ) (PSI-MSEC)	TIME-TOA (MSEC)	DYN. HORIZ. COMPT. (PSI)	SHOCK G/R (KFT)
5494.6581	3.1662	5.4949	.5733	8.0718
5500.154	6.3021	10.9908	.5677	8.0786
5505.6507	9.4078	16.4875	.5622	8.0855
5511.1482	12.4838	21.9851	.5567	8.0923
5522.1459	18.5476	32.9827	.5460	8.1060
5533.1469	24.4960	43.9837	.5354	8.1197
5544.1512	30.3312	54.9881	.5251	8.1333
5555.1590	36.0557	65.9958	.5150	8.1470
5566.1700	41.6716	77.0069	.5050	8.1607
5577.1844	47.1812	88.0212	.4953	8.1744
5599.2230	57.8895	110.0599	.4765	8.2017
5621.2748	68.1979	132.1116	.4585	8.2291
5643.3395	78.1224	154.1763	.4412	8.2565
5665.4171	87.6785	176.2540	.4246	8.2838
5687.5075	96.8807	198.3444	.4086	8.3112
5709.6106	105.7432	220.4474	.3933	8.3385
5731.7262	114.2794	242.5631	.3787	8.3659
5753.8543	122.5022	264.6912	.3646	8.3933
5775.9948	130.4240	286.8316	.3511	8.4206
5798.1475	138.0565	308.9843	.3381	8.4480
5842.4893	152.4961	353.3261	.3136	8.5027
5886.8789	165.9091	397.7158	.2911	8.5574
5931.3156	178.3735	442.1525	.2702	8.6121
5975.7986	189.9612	486.6355	.2510	8.6669
6020.3272	200.7382	531.1640	.2333	8.7216
6064.9006	210.7652	575.7374	.2169	8.7763
6109.5180	220.0980	620.3549	.2017	8.8310
6154.1789	228.7881	665.0157	.1876	8.8857
6198.8825	236.8829	709.7193	.1747	8.9405
6243.6281	244.4260	754.4650	.1626	8.9952
6327.6372	257.2130	838.4741	.1424	9.0978
6411.7876	268.4374	922.6244	.1249	9.2004
6496.0751	278.3025	1006.912	.1096	9.3030
6580.4959	286.9839	1091.3328	.0964	9.4056

HORIZONTAL DYNAMIC IMPULSE (PSI-SEC) = .2869

Table 9

YIELD = 40 KT
HEIGHT OF BURST = 2.394 KFT
GROUND RANGE = 4.346 KFT
PEAK OVERPRESSURE = 3.6289 PSI
TIME OF ARRIVAL = 2703.1845 MSEC
PEAK OP (T=TA) = 14.9972 PSI
PEAK DYNAMIC PRES.= 4.7693 PSI
PEAK HORIZ. COMPT.= 4.7693 PSI

TIME (MSEC)	DYN. IMPULSE(HORIZ) (PSI-MSEC)	TIME-TOA (MSEC)	DYN. HORIZ. COMPT. (PSI)	SHOCK G/R (KFT)
2707.7280	21.4968	4.5435	4.6936	4.3528
2712.2748	42.6679	9.0903	4.6191	4.3596
2716.8249	63.5184	13.6404	4.5459	4.3665
2721.3783	84.0532	18.1938	4.4739	4.3733
2730.4949	124.1946	27.3104	4.3334	4.3870
2739.6246	163.1320	36.4401	4.1975	4.4007
2748.7672	200.9030	45.5827	4.0661	4.4143
2757.9227	237.5437	54.7382	3.9390	4.4280
2767.0910	273.0894	63.9065	3.8160	4.4417
2776.2721	307.5739	73.0875	3.6970	4.4554
2794.6720	373.4826	91.4875	3.4706	4.4827
2813.1221	435.5293	109.9375	3.2587	4.5101
2831.6216	493.9492	128.4371	3.0603	4.5375
2850.1700	548.9631	146.9855	2.8746	4.5648
2868.7668	600.7779	165.5823	2.7006	4.5922
2887.4114	649.5875	184.2269	2.5377	4.6195
2906.1032	695.5740	202.9187	2.3851	4.6469
2924.8418	738.9079	221.6573	2.2422	4.6743
2943.6266	779.7493	240.4421	2.1082	4.7016
2962.4570	818.2481	259.2725	1.9827	4.7290
3000.2529	888.7404	297.0684	1.7547	4.7837
3038.2254	951.4453	335.0409	1.5543	4.8384
3076.3706	1007.2643	373.1861	1.3779	4.8931
3114.6848	1056.9908	411.5003	1.2226	4.9479
3153.1641	1101.3235	449.9796	1.0858	5.0026
3191.8051	1140.8781	488.6205	.9652	5.0573
3230.6041	1176.1973	527.4196	.8587	5.1120
3269.5578	1207.7596	566.3732	.7646	5.1667
3308.6628	1235.9870	605.4783	.6815	5.2215
3347.9159	1261.2522	644.7313	.6079	5.2762
3421.9036	1301.7022	718.7191	.4919	5.3788
3496.381	1334.7030	793.1964	.3993	5.4814
3571.3287	1361.7027	868.1442	.3252	5.5840

HORIZONTAL DYNAMIC IMPULSE (PSI-SEC) = 1.3617

Table 10

YIELD = 40 KT
HEIGHT OF BURST = 2.394 KFT
GROUND RANGE = 1.521 KFT
PEAK OVERPRESSURE = 9.9411 PSI
TIME OF ARRIVAL = 1192.6267 MSEC
PEAK OP (T=TA) = 25.0019 PSI
PEAK DYNAMIC PRES.= 12.2183 PSI
PEAK HORIZ. COMPT.= 7.7627 PSI

TIME (MSEC)	DYN. IMPULSE(HORIZ) (PSI-MSEC)	TIME-TOA (MSEC)	DYN. HORIZ. COMPT. (PSI)	SHOCK G/R (KFT)
1195.2194	20.0090	2.5926	7.6726	1.5278
1197.8216	39.8590	5.1948	7.5838	1.5346
1200.4334	59.5516	7.8066	7.4963	1.5415
1203.0547	79.0883	10.4279	7.4101	1.5483
1208.3257	117.6999	15.6989	7.2416	1.5620
1213.6344	155.7069	21.0076	7.0781	1.5757
1218.9808	193.1224	26.3540	6.9196	1.5893
1224.3646	229.9594	31.7378	6.7660	1.6030
1229.7856	266.2311	37.1588	6.6170	1.6167
1235.2436	301.9505	42.6168	6.4727	1.6304
1246.2700	371.7791	53.6432	6.1971	1.6577
1257.4424	439.5457	64.8156	5.9377	1.6851
1268.7592	505.3370	76.1324	5.6928	1.7125
1280.2190	569.2270	87.5922	5.4603	1.7398
1291.8202	631.2738	99.1934	5.2385	1.7672
1303.5615	691.5186	110.9347	5.0254	1.7945
1315.4413	749.9856	122.8145	4.8192	1.8219
1327.4582	806.6842	134.8314	4.6185	1.8493
1339.6107	861.6120	146.9839	4.4222	1.8766
1351.8973	914.7597	159.2705	4.2299	1.9040
1376.8672	1015.6715	184.2404	3.8566	1.9587
1402.3561	1109.3785	209.7293	3.5010	2.0134
1428.3527	1195.9857	235.7259	3.1681	2.0681
1454.8455	1275.7723	262.2187	2.8622	2.1229
1481.8232	1349.1593	289.1964	2.5856	2.1776
1509.2748	1416.6471	316.6480	2.3382	2.2323
1537.1892	1478.7535	344.5624	2.1179	2.2870
1565.5556	1535.9685	372.9288	1.9217	2.3417
1594.1312	1588.3113	401.5044	1.7454	2.3965
1618.3710	1628.3431	425.7442	1.5635	2.4512
1665.2592	1694.6261	472.6324	1.2818	2.5538
1713.9298	1751.3907	521.3030	1.0651	2.6564
1764.2804	1800.5445	571.6536	.8976	2.7590

HORIZONTAL DYNAMIC IMPULSE (PSI-SEC) = 1.8005

Table 11

YIELD = 40 KT
HEIGHT OF BURST = 0 KFT
GROUND RANGE = 5.591 KFT
PEAK OVERPRESSURE = 2.9665 PSI
TIME OF ARRIVAL = 3038.3332 MSEC
PEAK OP (T=TA) = 4.9996 PSI

TIME (MSEC)	IMPULSE (PSI-MSEC)	TIME-TOA (MSEC)	OVERPRESSURE (PSI)	SHOCK G/R (KFT)
3043.8141	27.2060	5.4808	4.9283	5.5978
3049.2962	54.0305	10.9630	4.8580	5.6046
3054.7797	80.4789	16.4464	4.7887	5.6115
3060.2645	106.5564	21.9312	4.7205	5.6183
3071.2379	157.6182	32.9046	4.5868	5.6320
3082.2165	207.2575	43.8832	4.4569	5.6457
3093.2002	255.5134	54.8669	4.3307	5.6593
3104.1890	302.4236	65.8557	4.2079	5.6730
3115.1829	348.0245	76.8496	4.0885	5.6867
3126.1818	392.3514	87.8485	3.9724	5.7004
3148.1946	477.3100	109.8613	3.7496	5.7277
3170.2272	557.5670	131.8939	3.5385	5.7551
3192.2794	633.3646	153.9461	3.3385	5.7825
3214.3508	704.9291	176.0176	3.1487	5.8098
3236.4414	772.4724	198.1081	2.9686	5.8372
3258.5508	836.1929	220.2175	2.7976	5.8645
3280.6788	896.2763	242.3456	2.6349	5.8919
3302.8253	952.8963	264.4920	2.4801	5.9193
3324.9899	1006.2162	286.6567	2.3328	5.9466
3347.1726	1056.3887	308.8393	2.1924	5.9740
3391.5910	1147.8234	353.2577	1.9306	6.0287
3436.0788	1228.2811	397.7455	1.6917	6.0834
3480.6345	1298.6821	442.3012	1.4730	6.1381
3525.2565	1359.8394	486.9232	1.2722	6.1929
3569.9432	1412.4725	531.6100	1.0871	6.2476
3614.6933	1457.2190	576.3600	.9160	6.3023
3659.5052	1494.6454	621.1720	.7572	6.3570
3704.3777	1525.2556	666.0444	.6096	6.4117
3749.3092	1549.4989	710.9760	.4718	6.4665
3794.2986	1567.7766	755.9654	.3427	6.5212
3878.8052	1587.1296	840.4719	.1214	6.6238
3963.5025	1588.7901	925.1692	-.0771	6.7264

IMPULSE (PSI-SEC) = 1.5953

Table 12

YIELD = 40 KT
HEIGHT OF BURST = 0 KFT
GROUND RANGE = 2.977 KFT
PEAK OVERPRESSURE = 9.0659 PSI
TIME OF ARRIVAL = 1096.8521 MSEC
PEAK OP (T=TA) = 14.9996 PSI

TIME (MSEC)	IMPULSE (PSI-MSEC)	TIME-TOA (MSEC)	OVERPRESSURE (PSI)	SHOCK G/R (KFT)
1101.3123	66.0213	4.4601	14.6085	2.9838
1105.7773	130.3967	8.9251	14.2295	2.9906
1110.2473	193.1752	13.3951	13.8621	2.9975
1114.7222	254.4036	17.8700	13.5059	3.0043
1123.6866	372.3794	26.8345	12.8253	3.0180
1132.6705	484.6793	35.8183	12.1847	3.0317
1141.6735	591.6237	44.8213	11.5814	3.0453
1150.6957	693.5105	53.8435	11.0127	3.0590
1159.7368	790.6175	62.8846	10.4762	3.0727
1168.7967	883.2037	71.9446	9.9696	3.0864
1186.9724	1055.7083	90.1202	9.0382	3.1137
1205.2216	1212.8299	108.3694	8.2038	3.1411
1223.5432	1356.0877	126.6910	7.4539	3.1685
1241.9361	1486.8082	145.0839	6.7774	3.1958
1260.3992	1606.1517	163.5470	6.1652	3.2232
1278.9314	1715.1346	182.0792	5.6092	3.2505
1297.5317	1814.6494	200.6795	5.1025	3.2779
1316.1991	1905.4807	219.3470	4.6391	3.3053
1334.9326	1988.3197	238.0804	4.2137	3.3326
1353.7312	2063.7766	256.8790	3.8220	3.3600
1391.5196	2194.528	294.6674	3.1244	3.4147
1429.5568	2301.4980	332.7046	2.5208	3.4694
1467.8354	2387.5525	370.9832	1.9919	3.5241
1506.3484	2454.9811	409.4962	1.5230	3.5789
1545.0888	2505.6307	448.2366	1.1027	3.6336
1584.0501	2541.0062	487.1979	.7222	3.6883
1623.2258	2562.3466	526.3736	.3747	3.7430
1662.6096	2570.6833	565.7574	.0549	3.7977
1702.1957	2566.8846	605.3435	-.2414	3.8525

IMPULSE (PSI-SEC) = 2.5764

Table 13

YIELD = 40 KT
HEIGHT OF BURST = 0 KFT
GROUND RANGE = 2.316 KFT
PEAK OVERPRESSURE = 14.7987 PSI
TIME OF ARRIVAL = 692.4409 MSEC
PEAK OP (T=TA) = 24.9944 PSI

TIME (MSEC)	IMPULSE (PSI-MSEC)	TIME-TOA (MSEC)	OVERPRESSURE (PSI)	SHOCK G/R (KFT)
696.3199	95.3047	3.8789	24.1539	2.3228
700.2060	187.5888	7.7651	23.3483	2.3296
704.0994	276.9722	11.6584	22.5758	2.3365
707.9998	363.5689	15.5589	21.8348	2.3433
715.8222	528.8067	23.3812	20.4414	2.3570
723.6728	684.1402	31.2318	19.1568	2.3707
731.5514	830.3059	39.1104	17.9708	2.3843
739.4579	967.9737	47.0169	16.8744	2.3980
747.3920	1097.7535	54.9510	15.8593	2.4117
755.3535	1220.2009	62.9125	14.9181	2.4254
771.3578	1444.9694	78.9168	13.2315	2.4527
787.4692	1645.9532	95.0282	11.7686	2.4801
803.6860	1826.1078	111.2450	10.4920	2.5075
820.0066	1987.9078	127.5656	9.3712	2.5348
836.4293	2133.4317	143.9883	8.3809	2.5622
852.9526	2264.4304	160.5116	7.5005	2.5895
869.5748	2382.3842	177.1339	6.7130	2.6169
886.2946	2488.5484	193.8536	6.0043	2.6443
903.1102	2583.9916	210.6692	5.3628	2.6716
920.0203	2669.6267	227.5794	4.7787	2.6990
954.1181	2814.3377	261.6771	3.7518	2.7537
988.5764	2927.9376	296.1354	2.8737	2.8084
1023.3842	3014.2278	330.9432	2.1091	2.8631
1058.5307	3076.1260	366.0898	1.4326	2.9179
1094.0057	3115.9154	401.5647	.8262	2.9726
1129.7990	3135.4190	437.3580	.2763	3.0273
1165.9010	3136.1222	473.4601	-.2267	3.0820

IMPULSE (PSI-SEC) = 3.1443

Table 14

YIELD = 40 KT
HEIGHT OF BURST = .684 KFT
GROUND RANGE = 6.171 KFT
PEAK OVERPRESSURE = 2.4931 PSI
TIME OF ARRIVAL = 3575.2327 MSEC
PEAK OP (T=TA) = 5.0002 PSI

TIME (MSEC)	IMPULSE (PSI-MSEC)	TIME-TOA (MSEC)	OVERPRESSURE (PSI)	SHOCK G/R (KFT)
3580.7616	27.4703	5.5289	4.9368	6.1778
3586.2916	54.5974	11.0589	4.8742	6.1846
3591.8228	81.3855	16.5900	4.8123	6.1915
3597.3549	107.8386	22.1222	4.7512	6.1983
3608.4225	159.7545	33.1898	4.6311	6.2120
3619.4943	210.3775	44.2616	4.5140	6.2257
3630.5703	259.7378	55.3376	4.3996	6.2393
3641.6505	307.8648	66.4178	4.2880	6.2530
3652.7349	354.7871	77.5022	4.1789	6.2667
3663.8235	400.5324	88.5908	4.0725	6.2804
3686.0130	488.5926	110.7803	3.8669	6.3077
3708.2189	572.2586	132.9862	3.6707	6.3351
3730.441	651.7249	155.2082	3.4833	6.3625
3752.6790	727.1756	177.4463	3.3043	6.3898
3774.9329	798.7840	199.7002	3.1331	6.4172
3797.2025	866.7139	221.9697	2.9693	6.4445
3819.4875	931.1203	244.2548	2.8125	6.4719
3841.7879	992.1494	266.5551	2.6624	6.4993
3864.1034	1049.9394	288.8707	2.5184	6.5266
3886.4339	1104.6212	311.2012	2.3804	6.5540
3931.1393	1205.1194	355.9066	2.1208	6.6087
3975.9028	1294.5871	400.6701	1.8812	6.6634
4020.7232	1373.8408	445.4905	1.6595	6.7181
4065.5992	1443.6133	490.3665	1.4538	6.7729
4110.5298	1504.5627	535.2971	1.2626	6.8276
4155.5138	1557.2810	580.2811	1.0843	6.8823
4200.5501	1602.3013	625.3174	.9177	6.9370
4245.6376	1640.1044	670.4049	.7616	6.9917
4290.7754	1671.1246	715.5426	.6150	7.0465
4335.9622	1695.7544	760.7295	.4770	7.1012
4420.8167	1725.8628	845.5840	.2387	7.2038
4505.8342	1736.7848	930.6015	.0233	7.3064
4591.0088	1730.2298	1015.7760	-.1728	7.4090

IMPULSE (PSI-SEC) = 1.7449

Table 15

YIELD = 40 KT
HEIGHT OF BURST = .684 KFT
GROUND RANGE = 3.001 KFT
PEAK OVERPRESSURE = 8.5133 PSI
TIME OF ARRIVAL = 1209.3571 MSEC
PEAK OP (T=TA) = 14.9964 PSI

TIME (MSEC)	IMPULSE (PSI-MSEC)	TIME-TOA (MSEC)	OVERPRESSURE (PSI)	SHOCK G/R (KFT)
1213.7684	65.3603	4.4112	14.6394	3.0078
1218.1844	129.2370	8.8273	14.2923	3.0146
1222.6053	191.6695	13.2481	13.9547	3.0215
1227.0308	252.6959	17.6737	13.6264	3.0283
1235.8962	370.6686	26.5390	12.9965	3.0420
1244.7803	483.4463	35.4232	12.4001	3.0557
1253.6832	591.2935	44.3260	11.8351	3.0693
1262.6045	694.4580	53.2474	11.2995	3.0830
1271.5443	793.1725	62.1872	10.7914	3.0967
1280.5024	887.6556	71.1452	10.3093	3.1104
1298.4728	1064.6879	89.1156	9.4160	3.1377
1316.5147	1227.1031	107.1575	8.6081	3.1651
1334.6271	1376.2217	125.2700	7.8753	3.1925
1352.8091	1513.2114	143.4519	7.2089	3.2198
1371.0595	1639.1064	161.7023	6.6011	3.2472
1389.3775	1754.8236	180.0203	6.0452	3.2745
1407.7620	1861.1772	198.4049	5.5354	3.3019
1426.2122	1958.8909	216.8550	5.0663	3.3293
1444.7271	2048.6093	235.3699	4.6336	3.3566
1463.3057	2130.9068	253.9486	4.2333	3.3840
1500.6508	2275.1284	291.2936	3.5162	3.4387
1538.2404	2395.1768	328.8832	2.8918	3.4934
1576.0676	2493.8557	366.7105	2.3422	3.5481
1614.1260	2573.4353	404.7688	1.8533	3.6029
1652.4090	2635.7671	443.0518	1.4142	3.6576
1690.9105	2682.3719	481.5533	1.0160	3.7123
1729.6245	2714.5090	520.2673	.6519	3.7670
1768.5452	2733.2293	559.1880	.3165	3.8217
1807.6669	2739.4177	598.3097	5.3913E-03	3.8765
1846.9842	2733.8256	637.6270	-.2850	3.9312

IMPULSE (PSI-SEC) = 2.7450

Table 16

YIELD = 40 KT
HEIGHT OF BURST = .684 KFT
GROUND RANGE = 2.977 KFT
PEAK OVERPRESSURE = 8.6363 PSI
TIME OF ARRIVAL = 1193.9169 MSEC
PEAK OP (T=TA) = 15.2102 PSI

TIME (MSEC)	IMPULSE (PSI-MSEC)	TIME-TOA (MSEC)	OVERPRESSURE (PSI)	SHOCK G/P (KFT)
1198.3112	66.0315	4.3943	14.8454	2.9838
1202.7104	130.5539	8.7934	14.4909	2.9906
1207.1144	193.6076	13.1975	14.1462	2.9975
1211.5232	255.2318	17.6063	13.8110	3.0043
1220.3552	374.3329	26.4383	13.1681	3.0180
1229.2063	488.1557	35.2894	12.5597	3.0317
1238.0763	596.9710	44.1593	11.9836	3.0453
1246.9651	701.0327	53.0481	11.4378	3.0590
1255.8724	800.5788	61.9555	10.9203	3.0727
1264.7983	895.8328	70.8814	10.4293	3.0864
1282.7051	1074.2416	88.7882	9.5203	3.1137
1300.6844	1237.8406	106.7674	8.6988	3.1411
1318.7350	1387.9773	124.8181	7.9542	3.1685
1336.8560	1525.8420	142.9391	7.2776	3.1958
1355.0464	1652.4881	161.1295	6.6609	3.2232
1373.3052	1768.8483	179.3883	6.0972	3.2505
1391.6314	1875.7506	197.7145	5.5804	3.2779
1410.0241	1973.9300	216.1071	5.1053	3.3053
1428.4823	2064.0406	234.5653	4.6671	3.3326
1447.0050	2146.6651	253.0881	4.2619	3.3600
1484.2406	2291.3690	290.3237	3.5365	3.4147
1521.7238	2411.7072	327.8069	2.9053	3.4694
1559.4477	2510.5131	365.5307	2.3500	3.5241
1597.4055	2590.0782	403.4885	1.8561	3.5789
1635.5907	2652.2692	441.6737	1.4125	3.6336
1673.9971	2698.6179	480.0802	1.0104	3.6883
1712.6187	2730.3914	518.7017	.6428	3.7430
1751.4494	2748.6468	557.5324	.3040	3.7977
1790.4836	2754.2734	596.5667	-.0101	3.8525

IMPULSE (PSI-SEC) = 2.7546

Table 17

YIELD = 40 KT
HEIGHT OF BURST = .684 KFT
GROUND RANGE = 2.282 KFT
PEAK OVERPRESSURE = 13.9840 PSI
TIME OF ARRIVAL = 776.1969 MSEC
PEAK OP (T=TA) = 24.9958 PSI

TIME (MSEC)	IMPULSE (PSI-MSEC)	TIME-TOA (MSEC)	OVERPRESSURE (PSI)	SHOCK G/R (KFT)
779.9936	93.4463	3.7967	24.2360	2.2888
783.7974	184.2296	7.6004	23.5043	2.2956
787.6081	272.4430	11.4112	22.7993	2.3025
791.4259	358.1761	15.2289	22.1200	2.3093
799.0822	522.5197	22.8852	20.8338	2.3230
806.7661	677.9262	30.5691	19.6376	2.3367
814.4773	824.9874	38.2804	18.5239	2.3503
822.2158	964.2479	46.0189	17.4858	2.3640
829.9813	1096.2088	53.7844	16.5172	2.3777
837.7736	1221.3317	61.5767	15.6125	2.3914
853.4379	1452.6367	77.2409	13.9743	2.4187
869.2071	1661.2922	93.0101	12.5351	2.4461
885.0796	1849.8681	108.8826	11.2649	2.4735
901.0540	2020.5580	124.8571	10.1385	2.5008
917.1289	2175.2385	140.9319	9.1347	2.5282
933.3027	2315.5182	157.1057	8.2360	2.5555
949.5740	2442.7798	173.3770	7.4272	2.5829
965.9414	2558.2141	189.7444	6.6960	2.6103
982.4034	2662.8496	206.2065	6.0317	2.6376
998.9589	2757.5767	222.7619	5.4253	2.6650
1032.3442	2920.1394	256.1473	4.3570	2.7197
1066.0869	3051.1662	289.8899	3.4428	2.7744
1100.1765	3154.5323	323.9796	2.6476	2.8291
1134.6032	3233.2458	358.4062	1.9458	2.8839
1169.3572	3289.6744	393.1602	1.3180	2.9386
1204.4291	3325.7083	428.2321	.7502	2.9933
1239.8098	3342.8797	463.6129	.2315	3.0480
1275.4906	3342.4504	499.2936	-.2462	3.1027

IMPULSE (PSI-SEC) = 3.3512

Table 18

YIELD = 40 KT
HEIGHT OF BURST = 2.394 KFT
GROUND RANGE = 8.065 KFT
PEAK OVERPRESSURE = 1.5272 PSI
TIME OF ARRIVAL = 5489.1631 MSEC
PEAK OP (T=TA) = 4.9991 PSI

TIME (MSEC)	IMPULSE (PSI-MSEC)	TIME-TOA (MSEC)	OVERPRESSURE (PSI)	SHOCK G/R (KFT)
5494.6581	27.3307	5.4949	4.9484	8.0718
5500.154	54.3885	10.9908	4.8982	8.0786
5505.6507	81.1758	16.4875	4.8485	8.0855
5511.1482	107.6948	21.9851	4.7991	8.0923
5522.1459	159.9363	32.9827	4.7017	8.1060
5533.1469	211.1314	43.9837	4.6060	8.1197
5544.1512	261.2975	54.9881	4.5118	8.1333
5555.1590	310.4517	65.9958	4.4193	8.1470
5566.1700	358.6107	77.0069	4.3284	8.1607
5577.1844	405.7909	88.0212	4.2389	8.1744
5599.2230	497.2749	110.0599	4.0646	8.2017
5621.2748	585.0328	132.1116	3.8960	8.2291
5643.3395	669.1843	154.1763	3.7330	8.2565
5665.4171	749.8448	176.2540	3.5752	8.2838
5687.5075	827.1250	198.3444	3.4226	8.3112
5709.6106	901.1316	220.4474	3.2750	8.3385
5731.7262	971.9666	242.5631	3.1320	8.3659
5753.8543	1039.7288	264.6912	2.9936	8.3933
5775.9948	1104.5128	286.8316	2.8595	8.4206
5798.1475	1166.4096	308.9843	2.7296	8.4480
5842.4893	1281.8680	353.3261	2.4818	8.5027
5886.8789	1386.7881	397.7158	2.2489	8.5574
5931.3156	1481.7826	442.1525	2.0298	8.6121
5975.7986	1567.4193	486.6355	1.8235	8.6669
6020.3272	1644.2245	531.1640	1.6290	8.7216
6064.9006	1712.6867	575.7374	1.4454	8.7763
6109.5180	1773.2590	620.3549	1.2721	8.8310
6154.1789	1826.3626	665.0157	1.1082	8.8857
6198.8825	1872.3885	709.7193	.9530	8.9405
6243.6281	1911.7005	754.4650	.8060	8.9952
6327.6372	1968.4154	838.4741	.5503	9.0978
6411.7876	2004.7245	922.6244	.3180	9.2004
6496.0751	2022.3955	1006.912	.1060	9.3030
6580.4959	2022.9811	1091.3328	-.0879	9.4056

IMPULSE (PSI-SEC) = 2.0304

Table 19

YIELD = 40 KT
HEIGHT OF BURST = 2.394 KFT
GROUND RANGE = 4.346 KFT
PEAK OVERPRESSURE = 3.6289 PSI
TIME OF ARRIVAL = 2703.1845 MSEC
PEAK OP (T=TA) = 14.9972 PSI

TIME (MSEC)	IMPULSE (PSI-MSEC)	TIME-TOA (MSEC)	OVERPRESSURE (PSI)	SHOCK G/R (KFT)
2707.7280	67.6584	4.5435	14.7859	4.3528
2712.2748	134.4123	9.0903	14.5776	4.3596
2716.8249	200.2732	13.6404	14.3722	4.3665
2721.3783	265.2529	18.1938	14.1696	4.3733
2730.4949	392.6113	27.3104	13.7729	4.3870
2739.6246	516.5800	36.4401	13.3871	4.4007
2748.7672	637.2461	45.5827	13.0118	4.4143
2757.9227	754.6939	54.7382	12.6468	4.4280
2767.0910	869.0054	63.9065	12.2917	4.4417
2776.2721	980.2602	73.0875	11.9463	4.4554
2794.6720	1193.8869	91.4875	11.2830	4.4827
2813.1221	1396.1846	109.9375	10.6546	4.5101
2831.6216	1587.7095	128.4371	10.0592	4.5375
2850.1700	1768.9862	146.9855	9.4945	4.5648
2868.7668	1940.5089	165.5823	8.9589	4.5922
2887.4114	2102.7436	184.2269	8.4505	4.6195
2906.1032	2256.1294	202.9187	7.9677	4.6469
2924.8418	2401.0808	221.6573	7.5090	4.6743
2943.6266	2537.9883	240.4421	7.0729	4.7016
2962.4570	2667.2205	259.2725	6.6581	4.7290
3000.2529	2903.9500	297.0684	5.8874	4.7837
3038.2254	3113.9123	335.0409	5.1878	4.8384
3076.3706	3299.3822	373.1861	4.5513	4.8931
3114.6848	3462.3894	411.5003	3.9708	4.9479
3153.1641	3604.7457	449.9796	3.4400	5.0026
3191.8051	3728.0708	488.6205	2.9535	5.0573
3230.6041	3833.8139	527.4196	2.5065	5.1120
3269.5578	3923.2732	566.3732	2.0948	5.1667
3308.6628	3997.6132	605.4783	1.7146	5.2215
3347.9159	4057.8796	644.7313	1.3626	5.2762
3421.9036	4135.9904	718.7191	.7688	5.3788
3496.381	4173.2483	793.1964	.2481	5.4814
3571.3287	4174.0764	868.1442	-.2123	5.5840

IMPULSE (PSI-SEC) = 4.1899

Table 20

YIELD = 40 KT
HEIGHT OF BURST = 2.394 KFT
GROUND RANGE = 1.521 KFT
PEAK OVERPRESSURE = 9.9411 PSI
TIME OF ARRIVAL = 1192.6267 MSEC
PEAK OP (T=TA) = 25.0019 PSI

TIME (MSEC)	IMPULSE (PSI-MSEC)	TIME-TOA (MSEC)	OVERPRESSURE (PSI)	SHOCK G/R (KFT)
1195.2194	64.3363	2.5926	24.6290	1.5278
1197.8216	127.9477	5.1948	24.2625	1.5346
1200.4334	190.8429	7.8066	23.9020	1.5415
1203.0547	253.0304	10.4279	23.5477	1.5483
1208.3257	375.3142	15.6989	22.8568	1.5620
1213.6344	494.8689	21.0076	22.1892	1.5757
1218.9808	611.7608	26.3540	21.5438	1.5893
1224.3646	726.0549	31.7378	20.9201	1.6030
1229.7856	837.8148	37.1588	20.3172	1.6167
1235.2436	947.1025	42.6168	19.7342	1.6304
1246.2700	1158.4839	53.6432	18.6249	1.6577
1257.4424	1360.6704	64.8156	17.5857	1.6851
1268.7592	1554.0793	76.1324	16.6101	1.7125
1280.2190	1739.0867	87.5922	15.6914	1.7398
1291.8202	1916.0243	99.1934	14.8236	1.7672
1303.5615	2085.1805	110.9347	14.0008	1.7945
1315.4413	2246.8015	122.8145	13.2178	1.8219
1327.4582	2401.0975	134.8314	12.4703	1.8493
1339.6107	2548.2486	146.9839	11.7546	1.8766
1351.8973	2688.4137	159.2705	11.0682	1.9040
1376.8672	2948.3238	184.2404	9.7756	1.9587
1402.3561	3181.9959	209.7293	8.5840	2.0134
1428.3527	3390.6119	235.7259	7.4891	2.0681
1454.8455	3575.4446	262.2187	6.4867	2.1229
1481.8232	3737.8054	289.1964	5.5704	2.1776
1509.2748	3878.9595	316.6480	4.7315	2.2323
1537.1892	4000.0500	344.5624	3.9598	2.2870
1565.5556	4102.0535	372.9288	3.2450	2.3417
1594.1312	4185.0983	401.5044	2.5836	2.3965
1618.3710	4241.4240	425.7442	2.0685	2.4512
1665.2592	4316.5392	472.6324	1.1487	2.5538
1713.9298	4350.8920	521.3030	.2698	2.6564
1764.2804	4342.6967	571.6536	-.5951	2.7590

IMPULSE (PSI-SEC) = 4.3726

REFERENCES

Brode, Harold L., *Height of Burst Effects at High Overpressures,* The Rand Corporation, RM-6301-DASA, 1970 (DASA Report 2506).

-----, "Review of Nuclear Weapons Effects," *Annu. Rev. Nucl. Sci.,* 1968.

-----, *Theoretical Description of the Blast and Fireball for a Sea Level Kiloton Explosion,* The Rand Corporation, RM-2246-PR, 1966.

-----, *Theoretical Description of the Blast and Fireball for a Sea Level Megaton Explosion,* The Rand Corporation, RM-2248, 1959.

McNamara, W., R. J. Jordano (GE Tempo), and P. S. Lewis (McDonnell Douglas Astronautics), *Airblast from a One Kiloton Nuclear Burst at 60 m over an Ideal Surface,* Contract Report 353, November 1977.

Needham, Charles E., Martin L. Havens, and Carolyn S. Knauth, *Nuclear Blast Standard (1 KT),* Air Force Weapons Laboratory, Report AFWL-TR-73-55 (rev), April 1975.

CHAPTER 7

REVISED PROCEDURE FOR ANALYTIC APPROXIMATION OF DYNAMIC PRESSURE VERSUS TIME

Stephen J. Speicher
Harold L. Brode

The procedure for calculating height-of-burst dynamic pressure given in Chap. 6 was contrived to satisfy a limited request in a narrow pressure range. The procedure is here extended to the full range of pressure interests, using a new analytic fit for the duration of the dynamic pressure positive phase.

The original form used was [Chap. 6, Eq. (17)]

$$Q(r) = Q(r_s)\left(\frac{r_0}{r_s}\right)^9 ,$$

where $r_0 = (x_0^2 + y^2)^{1/2}$, with x_0 the original ground range of interest; and $r_s = (x^2 + y^2)^{1/2}$, with x the subsequent shock position ground range. Thus, if t_0 represents the shock arrival time at the position of interest (x_0, y), and t represents the shock arrival time at further positions (x, y) [Chap. 6, Eq. (18)], then

$$Q(t) = Q_H(x, y)\left(\frac{r_0}{r}\right)^9 ,$$

and x, r, and t are related by $r = (x^2 + y^2)^{1/2}$, $t = t_a(r, W)$ [Chap. 6, Eq. (4)].

The extended procedure now takes the form

$$Q(t) = Q_H(x, y)\left(\frac{r_0}{r}\right)^n \cdot \left[1 - \left(\frac{t - t_0}{D_u^+}\right)^2\right] , \qquad (1)$$

where n is a variable power such that

$$n(r, m) = 0.7917 + 11.04\left(\frac{r}{m}\right) + \frac{14.37 + 6.291\left(\frac{r}{m}\right)}{1 + 28.41\left(\frac{r}{m}\right)^3} , \qquad (2)$$

and the positive (outward) wind duration is approximated as

$$D_u^+(r_o, m') = m' \cdot \left[\frac{0.2455 - 0.0115\left(\frac{r_0}{m'}\right)}{1 + 61.43\left(\frac{r_0}{m'}\right)^6} + \frac{2.177\left(\frac{r_0}{m'}\right)^3}{1 + 0.7567\left(\frac{r_0}{m'}\right)^2 + 6.147\left(\frac{r_0}{m'}\right)^3} - 0.05546 \right] , \qquad (3)$$

where r, r_0, t, and t_0 are defined above, and

$$m = W^{1/3} , \qquad m' = (2W)^{1/3} .$$

The units for these quantities are x, y, r, r_0 (kft); W, m, m' (kT and $kT^{1/3}$); D_u^+ (sec).

The virtue of the new procedure is that the total dynamic impulse can now be calculated to the cutoff of the dynamic positive phase, and the variable power n can now track the decay rate changes in different pressure regions. More important, the correct total dynamic impulse is simulated.

Figure 1 plots n against r scaled to 1 kT; Fig. 2 plots D_u^+ against r_0, also scaled to 1 kT, and compared with the AFWL 1 kT standard [Needham, Havens, and Knauth, 1975]. The positive phase duration D_u^+ is a very close approximation (within 2 percent) to data presented in Brode [1959]. The plot of this approximation with the AFWL data reveals considerable discrepancy. This may be due to differences in interpretation of the start of the negative phase, which would change both the duration (sec) and effective range at which the velocity first reverses.

Tables 1 through 10 show the new procedure applied to the dynamic pressure cases presented in Chap. 6; Tables 11 through 20 again show

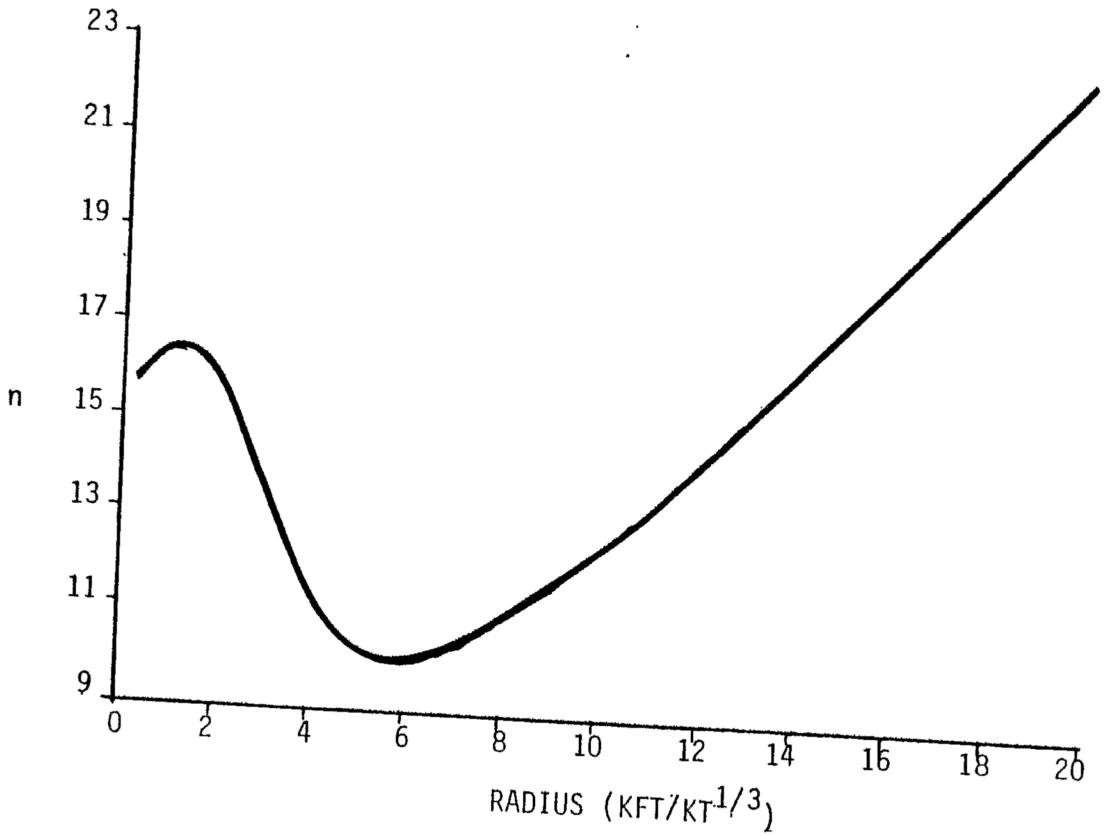

Figure 1. Plot of variable power n versus scaled radius (for 1 kT).

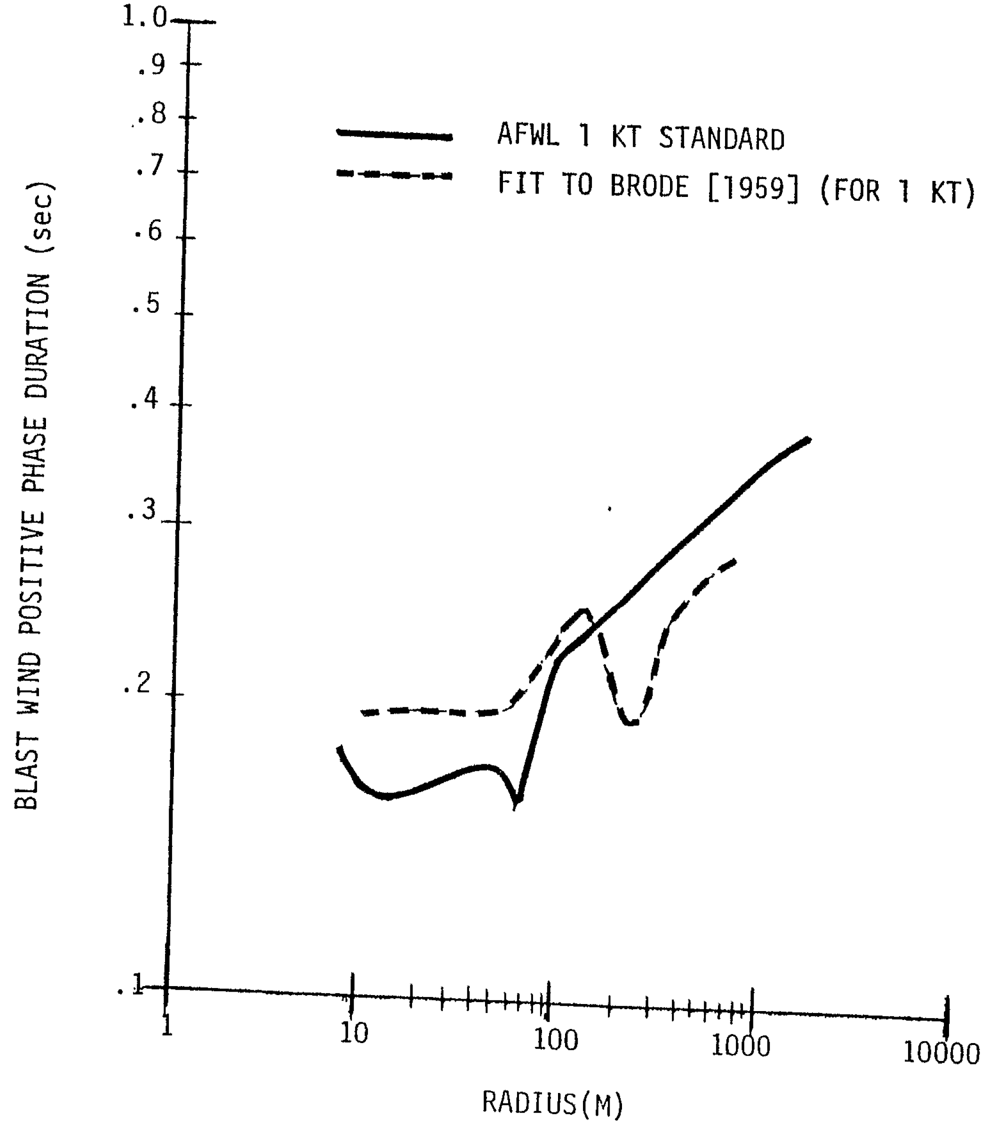

Figure 2. Comparison of positive phase duration versus range for 1 kT.

the new procedure, but use the analytic fit for the revised EM-1 curves given in Chap. 5.*

The table below is a summary comparison of total dynamic impulse (40 kT burst) given by the new procedure using the overpressure approximations in Brode [1970], and by the new procedure using the approximations to the new EM-1 curves (see the Appendix):

		Total Dynamic Impulse (psi-sec)		
HOB	Peak Overpressure (psi)	Limited Form (Chap. 6)	Improved Form (Brode [1970])	Improved Form with Revised ΔP_s (Appendix)
0	5	0.2073	0.1080	0.1043
0	15	0.7833	0.5969	0.5698
0	25	1.3723	1.1894	1.1287
0.684	5	0.2377	0.1132	0.1068
0.684	15	0.8337	0.6192	0.6059
0.684	25	1.4406	1.2297	1.2244
2.394	5	0.2869	0.1185	0.114
2.394	15	1.3617	0.7863	0.7328
2.394	25	1.8005	1.3284	1.2169

It is clear that the new procedure tends to reduce the total impulse, substantially so at the lower overpressure. This occurs because the variable power in Eq. (1) tracks a faster decay rate than the constant power used in Eq. (17) of Chap. 6. The new EM-1 approximations further reduce the total impulse.

---

*The Appendix contains a numerically more detailed presentation of the new analytic fit. The numbers presented in Chap. 6 were intended for exposition only, and so carried too few significant figures. For calculation, the numerical definition in the Appendix should be used.

Table 1

DYNAMIC PRESSURE AND IMPULSE VERSUS TIME
BASED ON PEAK OVERPRESSURES FROM BRODE [1970]

YIELD = 40 KT
HEIGHT OF BURST = 0 KFT
GROUND RANGE = 5.591 KFT
PEAK OVERPRESSURE = 2.9665 PSI (FREE AIR)
TIME OF ARRIVAL = 3038.3332 MSEC
PEAK OP (T=TA) = 4.9996 PSI
PEAK DYNAMIC PRES.= .5791 PSI
PEAK HORIZ. COMPT.= .5791 PSI
DYNAMIC POS. PHASE= 1069.4782 MSEC

TIME (MSEC)	DYN. IMPULSE(HORIZ) (PSI-MSEC)	TIME-TOA (MSEC)	DYN. HORIZ. COMPT. (PSI)	SHOCK G/R (KFT)
3043.8141	3.1316	5.4808	.5636	5.5978
3049.2962	6.1803	10.9630	.5486	5.6046
3054.7797	9.1480	16.4464	.5339	5.6115
3060.2645	12.0368	21.9312	.5195	5.6183
3071.2379	17.5843	32.9046	.4918	5.6320
3082.2165	22.8381	43.8832	.4655	5.6457
3093.2002	27.8124	54.8669	.4405	5.6593
3104.1890	32.5205	65.8557	.4166	5.6730
3115.1829	36.9756	76.8496	.3940	5.6867
3126.1818	41.1899	87.8485	.3725	5.7004
3148.1946	48.9403	109.8613	.3326	5.7277
3170.2272	55.8636	131.8939	.2967	5.7551
3192.2794	62.0406	153.9461	.2643	5.7825
3214.3508	67.5452	176.0176	.2352	5.8098
3236.4414	72.4446	198.1081	.2090	5.8372
3258.5508	76.7998	220.2175	.1855	5.8645
3280.6788	80.6666	242.3456	.1645	5.8919
3302.8253	84.0951	264.4920	.1456	5.9193
3324.9899	87.1310	286.6567	.1287	5.9466
3347.1726	89.8157	308.8393	.1137	5.9740
3391.5910	94.2689	353.2577	.0882	6.0287
3436.0788	97.7212	397.7455	.0681	6.0834
3480.6345	100.3806	442.3012	.0522	6.1381
3525.2565	102.4154	486.9232	.0397	6.1929
3569.9432	103.9605	531.6100	.0300	6.2476
3614.6933	105.1239	576.3600	.0224	6.3023
3659.5052	105.9915	621.1720	.0166	6.3570
3704.3777	106.6315	666.0444	.0121	6.4117
3749.3092	107.0973	710.9760	8.7895E-03	6.4665
3794.2986	107.4311	755.9654	6.2304E-03	6.5212
3878.8052	107.8047	840.4719	3.0557E-03	6.6238
3963.5025	107.9772	925.1692	1.2854E-03	6.7264
4048.3828	108.0400	1010.0495	3.5141E-04	6.8290
4133.4388	108.0469	1095.1055	-1.0005E-04	6.9316

HORIZONTAL DYNAMIC IMPULSE (PSI-SEC) = .1080

Table 2

DYNAMIC PRESSURE AND IMPULSE VERSUS TIME
BASED ON PEAK OVERPRESSURES FROM BRODE [1970]

YIELD = 40 KT
HEIGHT OF BURST = 0 KFT
GROUND RANGE = 2.977 KFT
PEAK OVERPRESSURE = 9.0659 PSI (FREE AIR)
TIME OF ARRIVAL = 1096.8521 MSEC
PEAK OP (T=TA) = 14.9996 PSI
PEAK DYNAMIC PRES.= 4.7707 PSI
PEAK HORIZ. COMPT.= 4.7707 PSI
DYNAMIC POS. PHASE= 807.3099 MSEC

TIME (MSEC)	DYN. IMPULSE(HORIZ) (PSI-MSEC)	TIME-TOA (MSEC)	DYN. HORIZ. COMPT. (PSI)	SHOCK G/R (KFT)
1101.3123	20.9132	4.4601	4.6084	2.9838
1105.7773	41.1367	8.9251	4.4514	2.9906
1110.2473	60.6922	13.3951	4.2995	2.9975
1114.7222	79.6005	17.8700	4.1525	3.0043
1123.6866	115.5517	26.8345	3.8729	3.0180
1132.6705	149.1508	35.8183	3.6113	3.0317
1141.6735	180.5442	44.8213	3.3666	3.0453
1150.6957	209.8693	53.8435	3.1378	3.0590
1159.7368	237.2553	62.8846	2.9238	3.0727
1168.7967	262.8239	71.9446	2.7238	3.0864
1186.9724	308.9326	90.1202	2.3620	3.1137
1205.2216	349.0587	108.3694	2.0462	3.1411
1223.5432	383.9383	126.6910	1.7706	3.1685
1241.9361	414.2211	145.0839	1.5304	3.1958
1260.3992	440.4799	163.5470	1.3212	3.2232
1278.9314	463.2196	182.0792	1.1391	3.2505
1297.5317	482.8848	200.6795	.9808	3.2779
1316.1991	499.8666	219.3470	.8433	3.3053
1334.9326	514.5090	238.0804	.7240	3.3326
1353.7312	527.1142	256.8790	.6207	3.3600
1391.5196	547.1869	294.6674	.4537	3.4147
1429.5568	561.9046	332.7046	.3292	3.4694
1467.8354	572.6071	370.9832	.2368	3.5241
1506.3484	580.3169	409.4962	.1687	3.5789
1545.0888	585.8102	448.2366	.1187	3.6336
1584.0501	589.6737	487.1979	.0824	3.6883
1623.2258	592.3485	526.3736	.0562	3.7430
1662.6096	594.1642	565.7574	.0375	3.7977
1702.1957	595.3654	605.3435	.0243	3.8525
1741.9782	596.1326	645.1260	.0151	3.9072
1817.0804	596.8170	720.2282	4.9854E-03	4.0098
1892.8184	596.9842	795.9662	3.9686E-04	4.1124
1969.1592	596.9285	872.3070	-1.3811E-03	4.2150

HORIZONTAL DYNAMIC IMPULSE (PSI-SEC) = .5969

Table 3

DYNAMIC PRESSURE AND IMPULSE VERSUS TIME
BASED ON PEAK OVERPRESSURES FROM BRODE [1970]

YIELD = 40 KT
HEIGHT OF BURST = 0 KFT
GROUND RANGE = 2.316 KFT
PEAK OVERPRESSURE = 14.7987 PSI (FREE AIR)
TIME OF ARRIVAL = 692.4409 MSEC
PEAK OP (T=TA) = 24.9944 PSI
PEAK DYNAMIC PRES.= 12.2116 PSI
PEAK HORIZ. COMPT.= 12.2116 PSI
DYNAMIC POS. PHASE= 846.9924 MSEC

TIME (MSEC)	DYN. IMPULSE(HORIZ) (PSI-MSEC)	TIME-TOA (MSEC)	DYN. HORIZ. COMPT. (PSI)	SHOCK G/R (KFT)
696.3199	46.4003	3.8789	11.7177	2.3228
700.2060	91.0073	7.7651	11.2441	2.3296
704.0994	133.8911	11.6584	10.7900	2.3365
707.9998	175.1193	15.5589	10.3545	2.3433
715.8222	252.8493	23.3812	9.5364	2.3570
723.6728	324.7003	31.2318	8.7838	2.3707
731.5514	391.1202	39.1104	8.0912	2.3843
739.4579	452.5217	47.0169	7.4538	2.3980
747.3920	509.2856	54.9510	6.8670	2.4117
755.3535	561.7626	62.9125	6.3267	2.4254
771.3578	655.0540	78.9168	5.3707	2.4527
787.4692	734.7805	95.0282	4.5593	2.4801
803.6860	802.9030	111.2450	3.8702	2.5075
820.0066	861.0955	127.5656	3.2847	2.5348
836.4293	910.7882	143.9883	2.7871	2.5622
852.9526	953.2043	160.5116	2.3641	2.5895
869.5748	989.3905	177.1339	2.0044	2.6169
886.2946	1020.2434	193.8536	1.6985	2.6443
903.1102	1046.5308	210.6692	1.4385	2.6716
920.0203	1068.9112	227.5794	1.2174	2.6990
954.1181	1104.0156	261.6771	.8698	2.7537
988.5764	1129.3160	296.1354	.6190	2.8084
1023.3842	1147.4649	330.9432	.4385	2.8631
1058.5307	1160.4122	366.0898	.3089	2.9179
1094.0057	1169.5892	401.5647	.2162	2.9726
1129.7990	1176.0450	437.3580	.1501	3.0273
1165.9010	1180.5464	473.4601	.1032	3.0820
1202.3024	1183.6522	509.8614	.0702	3.1367
1238.9941	1185.7680	546.5531	.0471	3.1915
1275.9673	1187.1869	583.5263	.0310	3.2462
1346.0217	1188.6317	653.5807	.0133	3.3488
1416.9832	1189.2214	724.5423	4.9055E-03	3.4514
1488.8022	1189.4111	796.3613	1.1728E-03	3.5540
1561.432	1189.4295	868.9910	-2.9307E-04	3.6566

HORIZONTAL DYNAMIC IMPULSE (PSI-SEC) = 1.1894

Table 4

DYNAMIC PRESSURE AND IMPULSE VERSUS TIME
BASED ON PEAK OVERPRESSURES FROM BRODE [1970]

YIELD = 40 KT
HEIGHT OF BURST = .684 KFT
GROUND RANGE = 6.171 KFT
PEAK OVERPRESSURE = 2.4931 PSI (FREE AIR)
TIME OF ARRIVAL = 3575.2327 MSEC
PEAK OP (T=TA) = 5.0002 PSI
PEAK DYNAMIC PRES.= .5792 PSI
PEAK HORIZ. COMPT.= .5792 PSI
DYNAMIC POS. PHASE= 1101.7077 MSEC

TIME (MSEC)	DYN. IMPULSE(HORIZ) (PSI-MSEC)	TIME-TOA (MSEC)	DYN. HORIZ. COMPT. (PSI)	SHOCK G/R (KFT)
3580.7616	3.1617	5.5289	.5644	6.1778
3586.2916	6.2432	11.0589	.5500	6.1846
3591.8228	9.2462	16.5900	.5359	6.1915
3597.3549	12.1725	22.1222	.5221	6.1983
3608.4225	17.8018	33.1898	.4954	6.2120
3619.4943	23.1451	44.2616	.4700	6.2257
3630.5703	28.2155	55.3376	.4458	6.2393
3641.6505	33.0257	66.4178	.4227	6.2530
3652.7349	37.5877	77.5022	.4006	6.2667
3663.8235	41.9131	88.5908	.3797	6.2804
3686.0130	49.8954	110.7803	.3407	6.3077
3708.2189	57.0591	132.9862	.3053	6.3351
3730.441	63.4807	155.2082	.2733	6.3625
3752.6790	69.2303	177.4463	.2444	6.3898
3774.9329	74.3723	199.7002	.2183	6.4172
3797.2025	78.9654	221.9697	.1947	6.4445
3819.4875	83.0632	244.2548	.1735	6.4719
3841.7879	86.7145	266.5551	.1544	6.4993
3864.1034	89.9639	288.8707	.1372	6.5266
3886.4339	92.8519	311.2012	.1218	6.5540
3931.1393	97.6792	355.9066	.0955	6.6087
3975.9028	101.4610	400.6701	.0745	6.6634
4020.7232	104.4060	445.4905	.0578	6.7181
4065.5992	106.6847	490.3665	.0445	6.7729
4110.5298	108.4353	535.2971	.0340	6.8276
4155.5138	109.7698	580.2811	.0258	6.8823
4200.5501	110.7781	625.3174	.0193	6.9370
4245.6376	111.5323	670.4049	.0143	6.9917
4290.7754	112.0898	715.5426	.0105	7.0465
4335.9622	112.4961	760.7295	7.6238E-03	7.1012
4420.8167	112.9644	845.5840	3.9091E-03	7.2038
4505.8342	113.1930	930.6015	1.7725E-03	7.3064
4591.0088	113.2862	1015.7760	6.0085E-04	7.4090
4676.3346	113.3074	1101.1019	2.8437E-06	7.5116
4761.8063	113.2936	1186.5736	-2.6601E-04	7.6142

HORIZONTAL DYNAMIC IMPULSE (PSI-SEC) = .1132

Table 5

DYNAMIC PRESSURE AND IMPULSE VERSUS TIME
BASED ON PEAK OVERPRESSURES FROM BRODE [1970]

YIELD = 40 KT
HEIGHT OF BURST = .684 KFT
GROUND RANGE = 3.001 KFT
PEAK OVERPRESSURE = 8.5133 PSI (FREE AIR)
TIME OF ARRIVAL = 1209.3571 MSEC
PEAK OP (T=TA) = 14.9964 PSI
PEAK DYNAMIC PRES.= 4.7688 PSI
PEAK HORIZ. COMPT.= 4.7688 PSI
DYNAMIC POS. PHASE= 815.4375 MSEC

TIME (MSEC)	DYN. IMPULSE(HORIZ) (PSI-MSEC)	TIME-TOA (MSEC)	DYN. HORIZ. COMPT. (PSI)	SHOCK G/R (KFT)
1213.7684	20.6949	4.4112	4.6150	3.0078
1218.1844	40.7437	8.8273	4.4660	3.0146
1222.6053	60.1652	13.2481	4.3214	3.0215
1227.0308	78.9779	17.6737	4.1814	3.0283
1235.8962	114.8441	26.5390	3.9140	3.0420
1244.7803	148.4844	35.4232	3.6629	3.0557
1253.6832	180.0288	44.3260	3.4271	3.0693
1262.6045	209.6002	53.2474	3.2057	3.0830
1271.5443	237.3147	62.1872	2.9978	3.0967
1280.5024	263.2819	71.1452	2.8027	3.1104
1298.4728	310.3586	89.1156	2.4479	3.1377
1316.5147	351.6168	107.1575	2.1356	3.1651
1334.6271	387.7334	125.2700	1.8612	3.1925
1352.8091	419.3106	143.4519	1.6201	3.2198
1371.0595	446.8841	161.7023	1.4085	3.2472
1389.3775	470.9298	180.0203	1.2229	3.2745
1407.7620	491.8704	198.4049	1.0604	3.3019
1426.2122	510.0807	216.8550	.9182	3.3293
1444.7271	525.8931	235.3699	.7939	3.3566
1463.3057	539.6018	253.9486	.6854	3.3840
1500.6508	561.6652	291.2936	.5083	3.4387
1538.2404	578.0767	328.8832	.3742	3.4934
1576.0676	590.1874	366.7105	.2732	3.5481
1614.1260	599.0443	404.7688	.1976	3.6029
1652.4090	605.4548	443.0518	.1414	3.6576
1690.9105	610.0388	481.5533	.0998	3.7123
1729.6245	613.2694	520.2673	.0694	3.7670
1768.5452	615.5058	559.1880	.0472	3.8217
1807.6669	617.0190	598.3097	.0313	3.8765
1846.9842	618.0121	637.6270	.0201	3.9312
1921.2130	618.9489	711.8559	7.3506E-03	4.0338
1996.0778	619.2269	786.7206	1.2709E-03	4.1364
2071.5470	619.2034	862.1898	-1.2823E-03	4.2390

HORIZONTAL DYNAMIC IMPULSE (PSI-SEC) = .6192

Table 6

DYNAMIC PRESSURE AND IMPULSE VERSUS TIME
BASED ON PEAK OVERPRESSURES FROM BRODE [1970]

YIELD = 40 KT
HEIGHT OF BURST = .684 KFT
GROUND RANGE = 2.977 KFT
PEAK OVERPRESSURE = 8.6363 PSI (FREE AIR)
TIME OF ARRIVAL = 1193.9169 MSEC
PEAK OP (T=TA) = 15.2102 PSI
PEAK DYNAMIC PRES.= 4.8969 PSI
PEAK HORIZ. COMPT.= 4.8969 PSI
DYNAMIC POS. PHASE= 813.3632 MSEC

TIME (MSEC)	DYN. IMPULSE(HORIZ) (PSI-MSEC)	TIME-TOA (MSEC)	DYN. HORIZ. COMPT. (PSI)	SHOCK G/R (KFT)
1198.3112	21.1675	4.3943	4.7383	2.9838
1202.7104	41.6717	8.7934	4.5846	2.9906
1207.1144	61.5320	13.1975	4.4357	2.9975
1211.5232	80.7676	17.6063	4.2913	3.0043
1220.3552	117.4336	26.4383	4.0159	3.0180
1229.2063	151.8161	35.2894	3.7572	3.0317
1238.0763	184.0494	44.1593	3.5144	3.0453
1246.9651	214.2600	53.0481	3.2865	3.0590
1255.8724	242.5673	61.9555	3.0727	3.0727
1264.7983	269.0843	70.8814	2.8720	3.0864
1282.7051	317.1426	88.7882	2.5072	3.1137
1300.6844	359.2439	106.7674	2.1864	3.1411
1318.7350	396.0838	124.8181	1.9045	3.1685
1336.8560	428.2810	142.9391	1.6570	3.1958
1355.0464	456.3852	161.1295	1.4400	3.2232
1373.3052	480.8848	179.3883	1.2498	3.2505
1391.6314	502.2129	197.7145	1.0833	3.2779
1410.0241	520.7537	216.1071	.9376	3.3053
1428.4823	536.8474	234.5653	.8104	3.3326
1447.0050	550.7954	253.0881	.6993	3.3600
1484.2406	573.2328	290.3237	.5182	3.4147
1521.7238	589.9118	327.8069	.3812	3.4694
1559.4477	602.2123	365.5307	.2782	3.5241
1597.4055	611.2026	403.4885	.2011	3.5789
1635.5907	617.7060	441.6737	.1437	3.6336
1673.9971	622.3537	480.0802	.1014	3.6883
1712.6187	625.6274	518.7017	.0704	3.7430
1751.4494	627.8924	557.5324	.0479	3.7977
1790.4836	629.4242	596.5667	.0318	3.8525
1829.7158	630.4291	635.7988	.0203	3.9072
1903.7911	631.3764	709.8742	7.4461E-03	4.0098
1978.5100	631.6575	784.5931	1.2894E-03	4.1124
2053.8406	631.6341	859.9236	-1.2916E-03	4.2150

HORIZONTAL DYNAMIC IMPULSE (PSI-SEC) = .6316

Table 7

DYNAMIC PRESSURE AND IMPULSE VERSUS TIME
BASED ON PEAK OVERPRESSURES FROM BRODE [1970]

YIELD = 40 KT
HEIGHT OF BURST = .684 KFT
GROUND RANGE = 2.282 KFT
PEAK OVERPRESSURE = 13.9840 PSI (FREE AIR)
TIME OF ARRIVAL = 776.1969 MSEC
PEAK OP (T=TA) = 24.9958 PSI
PEAK DYNAMIC PRES.= 12.2128 PSI
PEAK HORIZ. COMPT.= 12.2128 PSI
DYNAMIC POS. PHASE= 833.5149 MSEC

TIME (MSEC)	DYN. IMPULSE(HORIZ) (PSI-MSEC)	TIME-TOA (MSEC)	DYN. HORIZ. COMPT. (PSI)	SHOCK G/R (KFT)
779.9936	45.4760	3.7967	11.7471	2.2888
783.7974	89.2991	7.6004	11.2993	2.2956
787.6081	131.5297	11.4112	10.8687	2.3025
791.4259	172.2258	15.2289	10.4548	2.3093
799.0822	249.2235	22.8852	9.6740	2.3230
806.7661	320.7290	30.5691	8.9519	2.3367
814.4773	387.1344	38.2804	8.2839	2.3503
822.2158	448.8026	46.0189	7.6660	2.3640
829.9813	506.0706	53.7844	7.0943	2.3777
837.7736	559.2504	61.5767	6.5652	2.3914
853.4379	654.4192	77.2409	5.6222	2.4187
869.2071	736.4600	93.0101	4.8140	2.4461
885.0796	807.1620	108.8826	4.1212	2.4735
901.0540	868.0686	124.8571	3.5270	2.5008
917.1289	920.5127	140.9319	3.0174	2.5282
933.3027	965.6456	157.1057	2.5802	2.5555
949.5740	1004.4627	173.3770	2.2053	2.5829
965.9414	1037.8246	189.7444	1.8836	2.6103
982.4034	1066.4760	206.2065	1.6078	2.6376
998.9589	1091.0611	222.7619	1.3713	2.6650
1032.3442	1130.0755	256.1473	.9949	2.7197
1066.0869	1158.6281	289.8899	.7188	2.7744
1100.1765	1179.4223	323.9796	.5169	2.8291
1134.6032	1194.4805	358.4062	.3695	2.8839
1169.3572	1205.3136	393.1602	.2624	2.9386
1204.4291	1213.0481	428.2321	.1849	2.9933
1239.8098	1218.5213	463.6129	.1290	3.0480
1275.4906	1222.3538	499.2936	.0891	3.1027
1311.4629	1225.0038	535.2659	.0606	3.1575
1347.7183	1226.8080	571.5213	.0406	3.2122
1416.4327	1228.6865	640.2357	.0179	3.3148
1486.0641	1229.4780	709.8671	6.8352E-03	3.4174
1556.5647	1229.7436	780.3677	1.7402E-03	3.5200
1627.8898	1229.7752	851.6928	-3.5055E-04	3.6226

HORIZONTAL DYNAMIC IMPULSE (PSI-SEC) = 1.2297

Table 8

DYNAMIC PRESSURE AND IMPULSE VERSUS TIME
BASED ON PEAK OVERPRESSURES FROM BRODE [1970]

YIELD = 40 KT
HEIGHT OF BURST = 2.394 KFT
GROUND RANGE = 8.065 KFT
PEAK OVERPRESSURE = 1.5272 PSI (FREE AIR)
TIME OF ARRIVAL = 5489.1631 MSEC
PEAK OP (T=TA) = 4.9991 PSI
PEAK DYNAMIC PRES.= .5790 PSI
PEAK HORIZ. COMPT.= .5790 PSI
DYNAMIC POS. PHASE= 1167.9601 MSEC

TIME (MSEC)	DYN. IMPULSE(HORIZ) (PSI-MSEC)	TIME-TOA (MSEC)	DYN. HORIZ. COMPT. (PSI)	SHOCK G/R (KFT)
5494.6581	3.1428	5.4949	.5649	8.0718
5500.154	6.2095	10.9908	.5511	8.0786
5505.6507	9.2016	16.4875	.5376	8.0855
5511.1482	12.1209	21.9851	.5244	8.0923
5522.1459	17.7468	32.9827	.4989	8.1060
5533.1469	23.1001	43.9837	.4745	8.1197
5544.1512	28.1928	54.9881	.4512	8.1333
5555.1590	33.0363	65.9958	.4290	8.1470
5566.1700	37.6419	77.0069	.4077	8.1607
5577.1844	42.0200	88.0212	.3874	8.1744
5599.2230	50.1323	110.0599	.3496	8.2017
5621.2748	57.4527	132.1116	.3151	8.2291
5643.3395	64.0521	154.1763	.2837	8.2565
5665.4171	69.9956	176.2540	.2553	8.2838
5687.5075	75.3431	198.3444	.2294	8.3112
5709.6106	80.1494	220.4474	.2060	8.3385
5731.7262	84.4648	242.5631	.1847	8.3659
5753.8543	88.3355	264.6912	.1655	8.3933
5775.9948	91.8036	286.8316	.1481	8.4206
5798.1475	94.9074	308.9843	.1324	8.4480
5842.4893	100.1525	353.3261	.1055	8.5027
5886.8789	104.3250	397.7158	.0836	8.5574
5931.3156	107.6279	442.1525	.0659	8.6121
5975.7986	110.2287	486.6355	.0517	8.6669
6020.3272	112.2649	531.1640	.0403	8.7216
6064.9006	113.8492	575.7374	.0312	8.7763
6109.5180	115.0734	620.3549	.0240	8.8310
6154.1789	116.0120	665.0157	.0183	8.8857
6198.8825	116.7253	709.7193	.0138	8.9405
6243.6281	117.2619	754.4650	.0103	8.9952
6327.6372	117.9155	838.4741	5.7673E-03	9.0978
6411.7876	118.2689	922.6244	2.9888E-03	9.2004
6496.0751	118.4427	1006.912	1.3591E-03	9.3030
6580.4959	118.5131	1091.3328	4.4597E-04	9.4056
6665.0462	118.5271	1175.8830	-3.1660E-05	9.5082

HORIZONTAL DYNAMIC IMPULSE (PSI-SEC) = .1185

Table 9

DYNAMIC PRESSURE AND IMPULSE VERSUS TIME
BASED ON PEAK OVERPRESSURES FROM BRODE [1970]

YIELD = 40 KT
HEIGHT OF BURST = 2.394 KFT
GROUND RANGE = 4.346 KFT
PEAK OVERPRESSURE = 3.6289 PSI (FREE AIR)
TIME OF ARRIVAL = 2703.1845 MSEC
PEAK OP (T=TA) = 14.9972 PSI
PEAK DYNAMIC PRES.= 4.7693 PSI
PEAK HORIZ. COMPT.= 4.7693 PSI
DYNAMIC POS. PHASE= 1025.5963 MSEC

TIME (MSEC)	DYN. IMPULSE(HORIZ) (PSI-MSEC)	TIME-TOA (MSEC)	DYN. HORIZ. COMPT. (PSI)	SHOCK G/R (KFT)
2707.7280	21.3921	4.5435	4.6479	4.3528
2712.2748	42.2540	9.0903	4.5292	4.3596
2716.8249	62.5974	13.6404	4.4133	4.3665
2721.3783	82.4340	18.1938	4.3001	4.3733
2730.4949	120.6288	27.3104	4.0815	4.3870
2739.6246	156.9293	36.4401	3.8731	4.4007
2748.7672	191.4202	45.5827	3.6743	4.4143
2757.9227	224.1828	54.7382	3.4848	4.4280
2767.0910	255.2954	63.9065	3.3043	4.4417
2776.2721	284.8331	73.0875	3.1322	4.4554
2794.6720	339.4521	91.4875	2.8124	4.4827
2813.1221	388.6008	109.9375	2.5225	4.5101
2831.6216	432.7787	128.4371	2.2601	4.5375
2850.1700	472.4445	146.9855	2.0228	4.5648
2868.7668	508.0192	165.5823	1.8085	4.5922
2887.4114	539.8888	184.2269	1.6151	4.6195
2906.1032	568.4065	202.9187	1.4407	4.6469
2924.8418	593.8952	221.6573	1.2838	4.6743
2943.6266	616.6499	240.4421	1.1426	4.7016
2962.4570	636.9394	259.2725	1.0157	4.7290
3000.2529	671.0278	297.0684	.7998	4.7837
3038.2254	697.9280	335.0409	.6266	4.8384
3076.3706	719.0438	373.1861	.4883	4.8931
3114.6848	735.5261	411.5003	.3784	4.9479
3153.1641	748.3148	449.9796	.2914	5.0026
3191.8051	758.1733	488.6205	.2229	5.0573
3230.6041	765.7193	527.4196	.1693	5.1120
3269.5578	771.4500	566.3732	.1275	5.1667
3308.6628	775.7637	605.4783	.0951	5.2215
3347.9159	778.9780	644.7313	.0702	5.2762
3421.9036	782.8434	718.7191	.0383	5.3788
3496.381	784.9034	793.1964	.0195	5.4814
3571.3287	785.9096	868.1442	8.8636E-03	5.5840
3646.7288	786.3248	943.5443	3.0753E-03	5.6866
3722.5638	786.4271	1019.3793	1.5430E-04	5.7892
3798.8172	786.3781	1095.6327	-1.1451E-03	5.8918

HORIZONTAL DYNAMIC IMPULSE (PSI-SEC) = .7863

DYNAMIC PRESSURE AND IMPULSE VERSUS TIME
BASED ON PEAK OVERPRESSURES FROM BRODE [1970]

YIELD = 40 KT
HEIGHT OF BURST = 2.394 KFT
GROUND RANGE = 1.521 KFT
PEAK OVERPRESSURE = 9.9411 PSI (FREE AIR)
TIME OF ARRIVAL = 1192.6267 MSEC
PEAK OP (T=TA) = 25.0019 PSI
PEAK DYNAMIC PRES.= 12.2183 PSI
PEAK HORIZ. COMPT.= 7.7627 PSI
DYNAMIC POS. PHASE= 800.3640 MSEC

TIME (MSEC)	DYN. IMPULSE(HORIZ) (PSI-MSEC)	TIME-TOA (MSEC)	DYN. HORIZ. COMPT. (PSI)	SHOCK G/R (KFT)
1195.2194	19.9819	2.5926	7.6518	1.5278
1197.8216	39.7507	5.1948	7.5423	1.5346
1200.4334	59.3081	7.8066	7.4343	1.5415
1203.0547	78.6555	10.4279	7.3278	1.5483
1208.3257	116.7271	15.6989	7.1192	1.5620
1213.6344	153.9794	21.0076	6.9164	1.5757
1218.9808	190.4263	26.3540	6.7192	1.5893
1224.3646	226.0816	31.7378	6.5276	1.6030
1229.7856	260.9595	37.1588	6.3414	1.6167
1235.2436	295.0738	42.6168	6.1604	1.6304
1246.2700	361.0627	53.6432	5.8136	1.6577
1257.4424	424.1574	64.8156	5.4856	1.6851
1268.7592	484.4544	76.1324	5.1746	1.7125
1280.2190	542.0392	87.5922	4.8788	1.7398
1291.8202	596.9842	99.1934	4.5965	1.7672
1303.5615	649.3484	110.9347	4.3258	1.7945
1315.4413	699.1784	122.8145	4.0655	1.8219
1327.4582	746.5114	134.8314	3.8143	1.8493
1339.6107	791.3785	146.9839	3.5716	1.8766
1351.8973	833.8093	159.2705	3.3371	1.9040
1376.8672	911.4865	184.2404	2.8930	1.9587
1402.3561	979.9036	209.7293	2.4848	2.0134
1428.3527	1039.5755	235.7259	2.1162	2.0681
1454.8455	1091.1700	262.2187	1.7892	2.1229
1481.8232	1135.4512	289.1964	1.5036	2.1776
1509.2748	1173.2112	316.6480	1.2566	2.2323
1537.1892	1205.2160	344.5624	1.0445	2.2870
1565.5556	1232.1732	372.9288	.8631	2.3417
1594.1312	1254.5409	401.5044	.7082	2.3965
1618.3710	1269.9945	425.7442	.5730	2.4512
1665.2592	1291.9046	472.6324	.3790	2.5538
1713.9298	1306.7830	521.3030	.2448	2.6564
1764.2804	1316.5786	571.6536	.1528	2.7590
1816.2177	1322.7291	623.5909	.0899	2.8616
1869.6558	1326.2847	677.0290	.0473	2.9642
1924.5157	1328.0342	731.8889	.0195	3.0668
1980.7243	1328.5894	788.0975	2.5371E-03	3.1694
2038.2135	1328.4258	845.5868	-6.5993E-03	3.2720

HORIZONTAL DYNAMIC IMPULSE (PSI-SEC) = 1.3284

Table 11

DYNAMIC PRESSURE AND IMPULSE VERSUS TIME
BASED ON NEW (EM-1) PEAK OVERPRESSURES

YIELD = 40 KT
HEIGHT OF BURST = 0 KFT
GROUND RANGE = 5.201 KFT
PEAK OVERPRESSURE = 3.3500 PSI (FREE AIR)
TIME OF ARRIVAL = 2728.1284 MSEC
PEAK OP (T=TA) = 5.0001 PSI
PEAK DYNAMIC PRES.= .5792 PSI
PEAK HORIZ. COMPT.= .5792 PSI
DYNAMIC POS. PHASE= 1043.8417 MSEC

TIME (MSEC)	DYN. IMPULSE(HORIZ) (PSI-MSEC)	TIME-TOA (MSEC)	DYN. HORIZ. COMPT. (PSI)	SHOCK G/R (KFT)
2733.5275	3.0845	5.3990	.5634	5.2078
2738.9281	6.0856	10.7996	.5480	5.2146
2744.3302	9.0053	16.2018	.5329	5.2215
2749.7339	11.8456	21.6055	.5183	5.2283
2760.5460	17.2951	32.4176	.4900	5.2420
2771.3643	22.4500	43.2358	.4632	5.2557
2782.1886	27.3247	54.0602	.4377	5.2693
2793.0191	31.9331	64.8906	.4135	5.2830
2803.8556	36.2884	75.7271	.3905	5.2967
2814.6980	40.4034	86.5696	.3687	5.3104
2836.4009	47.9572	108.2724	.3284	5.3377
2858.1273	54.6882	129.9989	.2921	5.3651
2879.8770	60.6787	151.7486	.2595	5.3925
2901.6498	66.0036	173.5213	.2303	5.4198
2923.4452	70.7309	195.3167	.2041	5.4472
2945.2630	74.9224	217.1345	.1807	5.4745
2967.1030	78.6340	238.9745	.1597	5.5019
2988.9649	81.9162	260.8364	.1410	5.5293
3010.8483	84.8149	282.7199	.1243	5.5566
3032.7532	87.3712	304.6247	.1094	5.5840
3076.6258	91.5938	348.4974	.0844	5.6387
3120.5808	94.8486	392.4524	.0647	5.6934
3164.6162	97.3412	436.4877	.0493	5.7481
3208.7299	99.2365	480.6015	.0373	5.8029
3252.9203	100.6663	524.7918	.0279	5.8576
3297.1854	101.7356	569.0569	.0207	5.9123
3341.5235	102.5272	613.3950	.0152	5.9670
3385.9329	103.1065	657.8045	.0110	6.0217
3430.4120	103.5245	702.2836	7.9276E-03	6.0765
3474.9592	103.8210	746.8307	5.5586E-03	6.1312
3558.6630	104.1472	830.5346	2.6540E-03	6.2338
3642.5908	104.2928	914.4624	1.0638E-03	6.3364
3726.7331	104.3418	998.6047	2.4443E-04	6.4390
3811.0810	104.3429	1082.9526	-1.3809E-04	6.5416

HORIZONTAL DYNAMIC IMPULSE (PSI-SEC) = .1043

Table 12

DYNAMIC PRESSURE AND IMPULSE VERSUS TIME
BASED ON NEW (EM-1) PEAK OVERPRESSURES

YIELD = 40 KT
HEIGHT OF BURST = 0 KFT
GROUND RANGE = 2.8415 KFT
PEAK OVERPRESSURE = 9.9064 PSI (FREE AIR)
TIME OF ARRIVAL = 1009.5443 MSEC
PEAK OP (T=TA) = 15.0011 PSI
PEAK DYNAMIC PRES.= 4.7716 PSI
PEAK HORIZ. COMPT.= 4.7716 PSI
DYNAMIC POS. PHASE= 800.5105 MSEC

TIME (MSEC)	DYN. IMPULSE(HORIZ) (PSI-MSEC)	TIME-TOA (MSEC)	DYN. HORIZ. COMPT. (PSI)	SHOCK G/R (KFT)
1013.9024	20.4267	4.3581	4.6038	2.8483
1018.2659	40.1586	8.7216	4.4416	2.8551
1022.6347	59.2184	13.0904	4.2850	2.8620
1027.0088	77.6282	17.4645	4.1338	2.8688
1035.7728	112.5769	26.2285	3.8466	2.8825
1044.5578	145.1722	35.0135	3.5787	2.8962
1053.3635	175.5664	43.8192	3.3288	2.9098
1062.1898	203.9018	52.6455	3.0958	2.9235
1071.0366	230.3121	61.4923	2.8785	2.9372
1079.9037	254.9224	70.3594	2.6759	2.9509
1097.6982	299.1781	88.1539	2.3109	2.9782
1115.5720	337.5509	106.0277	1.9939	3.0056
1133.5239	370.7884	123.9796	1.7187	3.0330
1151.5528	399.5463	142.0085	1.4799	3.0603
1169.6574	424.3997	160.1131	1.2729	3.0877
1187.8366	445.8525	178.2923	1.0936	3.1150
1206.0893	464.3464	196.5450	.9384	3.1424
1224.4143	480.2680	214.8700	.8041	3.1698
1242.8105	493.9553	233.2662	.6881	3.1971
1261.2769	505.7044	251.7326	.5880	3.2245
1298.4159	524.3354	288.8716	.4272	3.2792
1335.8231	537.9238	326.2788	.3082	3.3339
1373.4903	547.7561	363.9460	.2205	3.3886
1411.4100	554.8063	401.8657	.1563	3.4434
1449.5745	559.8083	440.0302	.1095	3.4981
1487.9768	563.3129	478.4325	.0757	3.5528
1526.6097	565.7314	517.0654	.0515	3.6075
1565.4666	567.3690	555.9223	.0342	3.6622
1604.5409	568.4510	594.9966	.0221	3.7170
1643.8264	569.1424	634.2821	.0137	3.7717
1718.0346	569.7634	708.4903	4.6447E-03	3.8743
1792.9256	569.9242	783.3813	5.2273E-04	3.9769
1868.4634	569.8874	858.9191	-1.0712E-03	4.0795

HORIZONTAL DYNAMIC IMPULSE (PSI-SEC) = .5698

Table 13

DYNAMIC PRESSURE AND IMPULSE VERSUS TIME
BASED ON NEW (EM-1) PEAK OVERPRESSURES

YIELD = 40 KT
HEIGHT OF BURST = 0 KFT
GROUND RANGE = 2.2275 KFT
PEAK OVERPRESSURE = 16.0127 PSI (FREE AIR)
TIME OF ARRIVAL = 642.9149 MSEC
PEAK OP (T=TA) = 25.0000 PSI
PEAK DYNAMIC PRES.= 12.2165 PSI
PEAK HORIZ. COMPT.= 12.2165 PSI
DYNAMIC POS. PHASE= 867.9666 MSEC

TIME (MSEC)	DYN. IMPULSE(HORIZ) (PSI-MSEC)	TIME-TOA (MSEC)	DYN. HORIZ. COMPT. (PSI)	SHOCK G/R (KFT)
646.6980	45.2335	3.7831	11.7025	2.2343
650.4886	88.6521	7.5737	11.2108	2.2411
654.2869	130.3303	11.3720	10.7403	2.2480
658.0926	170.3395	15.1777	10.2901	2.2548
665.7266	245.6057	22.8117	9.4470	2.2685
673.3903	314.9805	30.4754	8.6745	2.2822
681.0835	378.9336	38.1686	7.9666	2.2958
688.8060	437.8956	45.8911	7.3175	2.3095
696.5576	492.2614	53.6427	6.7223	2.3232
704.3380	542.3938	61.4230	6.1762	2.3369
719.9843	631.1895	77.0694	5.2152	2.3642
735.7432	706.7211	92.8283	4.4051	2.3916
751.6130	770.9764	108.6981	3.7216	2.4190
767.5920	825.6387	124.6771	3.1444	2.4463
783.6784	872.1354	140.7635	2.6568	2.4737
799.8706	911.6786	156.9557	2.2446	2.5010
816.1670	945.2983	173.2521	1.8959	2.5284
832.5659	973.8710	189.6510	1.6010	2.5558
849.0657	998.1428	206.1508	1.3514	2.5831
865.6649	1018.7496	222.7500	1.1402	2.6105
899.1551	1050.9496	256.2402	.8102	2.6652
933.0246	1074.0562	290.1097	.5739	2.7199
967.2617	1090.5734	324.3468	.4050	2.7746
1001.8550	1102.3256	358.9401	.2845	2.8294
1036.7937	1110.6417	393.8788	.1987	2.8841
1072.0671	1116.4885	429.1522	.1379	2.9388
1107.6650	1120.5680	464.7501	.0949	2.9935
1143.5776	1123.3891	500.6627	.0647	3.0482
1179.7953	1125.3192	536.8804	.0436	3.1030
1216.3088	1126.6227	573.3939	.0290	3.1577
1285.5381	1127.9729	642.6232	.0128	3.2603
1355.7202	1128.5503	712.8053	5.0808E-03	3.3629
1426.8025	1128.7612	783.8876	1.5751E-03	3.4655
1498.7356	1128.8102	855.8207	1.2949E-04	3.5681
1571.4732	1128.7962	928.5583	-3.6565E-04	3.6707

HORIZONTAL DYNAMIC IMPULSE (PSI-SEC) = 1.1287

Table 14

DYNAMIC PRESSURE AND IMPULSE VERSUS TIME
BASED ON NEW (EM-1) PEAK OVERPRESSURES

YIELD = 40 KT
HEIGHT OF BURST = .684 KFT
GROUND RANGE = 5.562 KFT
PEAK OVERPRESSURE = 2.9550 PSI (FREE AIR)
TIME OF ARRIVAL = 3087.6669 MSEC
PEAK OP (T=TA) = 4.9995 PSI
PEAK DYNAMIC PRES.= .5791 PSI
PEAK HORIZ. COMPT.= .5791 PSI
DYNAMIC POS. PHASE= 1070.2484 MSEC

TIME (MSEC)	DYN. IMPULSE(HORIZ) (PSI-MSEC)	TIME-TOA (MSEC)	DYN. HORIZ. COMPT. (PSI)	SHOCK G/R (KFT)
3093.0866	3.0965	5.4197	.5636	5.5688
3098.5077	6.1109	10.8408	.5485	5.5756
3103.9302	9.0452	16.2632	.5338	5.5825
3109.3541	11.9012	21.6871	.5194	5.5893
3120.2059	17.3857	32.5390	.4917	5.6030
3131.0632	22.5795	43.3963	.4653	5.6167
3141.9260	27.4966	54.2591	.4402	5.6303
3152.7942	32.1504	65.1273	.4164	5.6440
3163.6678	36.5538	76.0008	.3937	5.6577
3174.5467	40.7190	86.8798	.3722	5.6714
3196.3205	48.3787	108.6535	.3323	5.6987
3218.1153	55.2203	130.4483	.2964	5.7261
3239.9309	61.3241	152.2639	.2640	5.7535
3261.7670	66.7633	174.1000	.2349	5.7808
3283.6234	71.6043	195.9565	.2087	5.8082
3305.4999	75.9076	217.8330	.1852	5.8355
3327.3963	79.7282	239.7294	.1642	5.8629
3349.3123	83.1160	261.6454	.1454	5.8903
3371.2477	86.1161	283.5807	.1285	5.9176
3393.2023	88.7692	305.5353	.1135	5.9450
3437.1681	93.1708	349.5011	.0881	5.9997
3481.2081	96.5842	393.5411	.0680	6.0544
3525.3206	99.2150	437.6536	.0521	6.1091
3569.5039	101.2290	481.8370	.0397	6.1639
3613.7567	102.7596	526.0897	.0300	6.2186
3658.0772	103.9133	570.4103	.0225	6.2733
3702.4641	104.7750	614.7972	.0166	6.3280
3746.916	105.4117	659.2490	.0122	6.3827
3791.4313	105.8763	703.7643	8.8608E-03	6.4375
3836.0087	106.2103	748.3418	6.3038E-03	6.4922
3919.7543	106.5866	832.0874	3.1270E-03	6.5948
4003.7053	106.7633	916.0384	1.3497E-03	6.6974
4087.8537	106.8306	1000.1868	4.0651E-04	6.8000
4172.1918	106.8417	1084.5249	-5.4616E-05	6.9026

HORIZONTAL DYNAMIC IMPULSE (PSI-SEC) = .1068

Table 15

DYNAMIC PRESSURE AND IMPULSE VERSUS TIME
BASED ON NEW (EM-1) PEAK OVERPRESSURES

YIELD = 40 KT
HEIGHT OF BURST = .684 KFT
GROUND RANGE = 2.9759 KFT
PEAK OVERPRESSURE = 8.6420 PSI (FREE AIR)
TIME OF ARRIVAL = 1193.2107 MSEC
PEAK OP (T=TA) = 14.9985 PSI
PEAK DYNAMIC PRES.= 4.7701 PSI
PEAK HORIZ. COMPT.= 4.7701 PSI
DYNAMIC POS. PHASE= 813.2707 MSEC

TIME (MSEC)	DYN. IMPULSE(HORIZ) (PSI-MSEC)	TIME-TOA (MSEC)	DYN. HORIZ. COMPT. (PSI)	SHOCK G/R (KFT)
1197.6042	20.6103	4.3935	4.6132	2.9827
1202.0026	40.5640	8.7919	4.4612	2.9895
1206.4058	59.8810	13.1951	4.3139	2.9964
1210.8139	78.5803	17.6032	4.1713	3.0032
1219.6444	114.1954	26.4336	3.8994	3.0169
1228.4939	147.5566	35.2832	3.6443	3.0306
1237.3624	178.7987	44.1517	3.4051	3.0442
1246.2496	208.0484	53.0389	3.1808	3.0579
1255.1555	235.4257	61.9448	2.9706	3.0716
1264.0799	261.0432	70.8692	2.7735	3.0853
1281.9838	307.3949	88.7731	2.4159	3.1126
1299.9601	347.9111	106.7494	2.1020	3.1400
1318.0079	383.2847	124.7972	1.8269	3.1674
1336.1261	414.1307	142.9154	1.5859	3.1947
1354.3138	440.9944	161.1031	1.3751	3.2221
1372.5698	464.3589	179.3591	1.1907	3.2494
1390.8933	484.6520	197.6826	1.0297	3.2768
1409.2833	502.2522	216.0726	.8891	3.3042
1427.7389	517.4937	234.5282	.7667	3.3315
1446.2591	530.6721	253.0484	.6601	3.3589
1483.4896	551.7960	290.2789	.4868	3.4136
1520.9679	567.4234	327.7572	.3564	3.4683
1558.6870	578.8926	365.4763	.2588	3.5230
1596.6401	587.2342	403.4294	.1861	3.5778
1634.8209	593.2384	441.6102	.1324	3.6325
1673.2229	597.5080	480.0122	.0929	3.6872
1711.8402	600.5002	518.6295	.0642	3.7419
1750.6668	602.56	557.4561	.0435	3.7966
1789.6969	603.9458	596.4862	.0287	3.8514
1828.9252	604.8501	635.7145	.0182	3.9061
1902.9935	605.6964	709.7828	6.6195E-03	4.0087
1977.7056	605.9451	784.4949	1.1351E-03	4.1113
2053.0298	605.9245	859.8191	-1.1251E-03	4.2139

HORIZONTAL DYNAMIC IMPULSE (PSI-SEC) = .6059

Table 16

DYNAMIC PRESSURE AND IMPULSE VERSUS TIME
BASED ON NEW (EM-1) PEAK OVERPRESSURES

YIELD = 40 KT
HEIGHT OF BURST = .684 KFT
GROUND RANGE = 2.8415 KFT
PEAK OVERPRESSURE = 9.3882 PSI (FREE AIR)
TIME OF ARRIVAL = 1107.8909 MSEC
PEAK OP (T=TA) = 16.3732 PSI
PEAK DYNAMIC PRES.= 5.6191 PSI
PEAK HORIZ. COMPT.= 5.6191 PSI
DYNAMIC POS. PHASE= 803.9413 MSEC

TIME (MSEC)	DYN. IMPULSE(HORIZ) (PSI-MSEC)	TIME-TOA (MSEC)	DYN. HORIZ. COMPT. (PSI)	SHOCK G/R (KFT)
1112.1854	23.7219	4.2945	5.4299	2.8483
1116.4852	46.6723	8.5942	5.2468	2.8551
1120.7901	68.8751	12.8992	5.0696	2.8620
1125.1002	90.3534	17.2093	4.8982	2.8688
1133.7359	131.2205	25.8449	4.5718	2.8825
1142.3920	169.4511	34.5011	4.2663	2.8962
1151.0685	205.2070	43.1775	3.9804	2.9098
1159.7651	238.6403	51.8742	3.7128	2.9235
1168.4818	269.8943	60.5908	3.4624	2.9372
1177.2183	299.1038	69.3274	3.2281	2.9509
1194.7505	351.8595	86.8595	2.8041	2.9782
1212.3605	397.8665	104.4695	2.4334	3.0056
1230.0472	437.9438	122.1562	2.1094	3.0330
1247.8095	472.8154	139.9185	1.8266	3.0603
1265.6463	503.1211	157.7553	1.5799	3.0877
1283.5565	529.4254	175.6656	1.3648	3.1150
1301.5392	552.2267	193.6482	1.1775	3.1424
1319.5932	571.9642	211.7022	1.0146	3.1698
1337.7175	589.0248	229.8266	.8729	3.1971
1355.9112	603.7492	248.0202	.7500	3.2245
1392.5026	627.2896	284.6116	.5509	3.2792
1429.3596	644.6470	321.4687	.4018	3.3339
1466.4748	657.3461	358.5839	.2907	3.3886
1503.8410	666.5553	395.9500	.2084	3.4434
1541.4511	673.1661	433.5601	.1478	3.4981
1579.2983	677.8555	471.4073	.1034	3.5528
1617.376	681.1347	509.4850	.0713	3.6075
1655.6778	683.3880	547.7869	.0482	3.6622
1694.1976	684.9021	586.3067	.0317	3.7170
1732.9295	685.8898	625.0385	.0202	3.7717
1806.1029	686.8161	698.2120	7.3724E-03	3.8743
1879.9649	687.0940	772.0739	1.3607E-03	3.9769
1954.481	687.0808	846.5900	-1.1082E-03	4.0795

HORIZONTAL DYNAMIC IMPULSE (PSI-SEC) = .6870

Table 17

DYNAMIC PRESSURE AND IMPULSE VERSUS TIME
BASED ON NEW (EM-1) PEAK OVERPRESSURES

YIELD = 40 KT
HEIGHT OF BURST = .684 KFT
GROUND RANGE = 2.2913 KFT
PEAK OVERPRESSURE = 13.8800 PSI (FREE AIR)
TIME OF ARRIVAL = 781.3609 MSEC
PEAK OP (T=TA) = 25.0015 PSI
PEAK DYNAMIC PRES.= 12.2179 PSI
PEAK HORIZ. COMPT.= 12.2179 PSI
DYNAMIC POS. PHASE= 831.8676 MSEC

TIME (MSEC)	DYN. IMPULSE(HORIZ) (PSI-MSEC)	TIME-TOA (MSEC)	DYN. HORIZ. COMPT. (PSI)	SHOCK G/R (KFT)
785.1672	45.6056	3.8062	11.7501	2.2981
788.9805	89.5459	7.6195	11.3003	2.3049
792.8007	131.8819	11.4397	10.8679	2.3118
796.6279	172.6720	15.2669	10.4521	2.3186
804.3029	249.8249	22.9420	9.6679	2.3323
812.0055	321.4456	30.6445	8.9428	2.3460
819.7353	387.9292	38.3743	8.2721	2.3596
827.4922	449.6421	46.1312	7.6517	2.3733
835.2759	506.9244	53.9149	7.0778	2.3870
843.0863	560.0912	61.7253	6.5468	2.4007
858.7864	655.1625	77.4254	5.6007	2.4280
874.5909	737.0284	93.2299	4.7904	2.4554
890.4982	807.4963	109.1373	4.0961	2.4828
906.5070	868.1254	125.1460	3.5012	2.5101
922.6156	920.2616	141.2546	2.9914	2.5375
938.8227	965.0677	157.4617	2.5545	2.5648
955.1268	1003.5482	173.7658	2.1802	2.5922
971.5265	1036.5713	190.1656	1.8594	2.6196
988.0205	1064.8876	206.6595	1.5847	2.6469
1004.6073	1089.1462	223.2464	1.3494	2.6743
1038.0542	1127.5459	256.6932	.9757	2.7290
1071.8565	1155.5500	290.4955	.7025	2.7837
1106.0041	1175.8691	324.6432	.5032	2.8384
1140.4871	1190.5262	359.1261	.3584	2.8932
1175.2958	1201.0277	393.9348	.2534	2.9479
1210.4208	1208.4935	429.0598	.1778	3.0026
1245.8532	1213.7528	464.4922	.1235	3.0573
1281.5841	1217.4183	500.2231	.0848	3.1120
1317.6050	1219.9401	536.2440	.0575	3.1668
1353.9078	1221.6480	572.5468	.0382	3.2215
1422.7073	1223.4111	641.3464	.0167	3.3241
1492.4194	1224.1437	711.0584	6.2595E-03	3.4267
1562.9966	1224.3838	781.6356	1.5288E-03	3.5293
1634.3943	1224.4081	853.0333	-3.7616E-04	3.6319

HORIZONTAL DYNAMIC IMPULSE (PSI-SEC) = 1.2244

Table 18

DYNAMIC PRESSURE AND IMPULSE VERSUS TIME
BASED ON NEW (EM-1) PEAK OVERPRESSURES

YIELD = 40 KT
HEIGHT OF BURST = 2.394 KFT
GROUND RANGE = 7.004 KFT
PEAK OVERPRESSURE = 1.8733 PSI (FREE AIR)
TIME OF ARRIVAL = 4648.3869 MSEC
PEAK OP (T=TA) = 4.9996 PSI
PEAK DYNAMIC PRES.= .5791 PSI
PEAK HORIZ. COMPT.= .5791 PSI
DYNAMIC POS. PHASE= 1144.2719 MSEC

TIME (MSEC)	DYN. IMPULSE(HORIZ) (PSI-MSEC)	TIME-TOA (MSEC)	DYN. HORIZ. COMPT. (PSI)	SHOCK G/R (KFT)
4653.7243	3.0528	5.3373	.5648	7.0108
4659.0629	6.0310	10.6759	.5509	7.0176
4664.4027	8.9360	16.0157	.5372	7.0245
4669.7437	11.7696	21.3567	.5239	7.0313
4680.4292	17.2283	32.0422	.4980	7.0450
4691.1195	22.4199	42.7325	.4734	7.0587
4701.8145	27.3562	53.4275	.4499	7.0723
4712.5142	32.0486	64.1273	.4274	7.0860
4723.2187	36.5081	74.8317	.4060	7.0997
4733.9278	40.7451	85.5408	.3855	7.1134
4755.3599	48.5898	106.9729	.3474	7.1407
4776.8104	55.6610	128.4234	.3127	7.1681
4798.2792	62.0288	149.8922	.2812	7.1955
4819.7660	67.7574	171.3790	.2526	7.2228
4841.2708	72.9056	192.8838	.2267	7.2502
4862.7933	77.5275	214.4063	.2033	7.2775
4884.3335	81.6725	235.9465	.1820	7.3049
4905.8910	85.3859	257.5041	.1629	7.3323
4927.4659	88.7090	279.0789	.1455	7.3596
4949.0579	91.6796	300.6709	.1299	7.3870
4992.2926	96.6901	343.9056	.1032	7.4417
5035.5940	100.6659	387.2070	.0815	7.4964
5078.9609	103.8050	430.5739	.0641	7.5511
5122.3922	106.2702	474.0052	.0501	7.6059
5165.8867	108.1952	517.4997	.0389	7.6606
5209.4434	109.6888	561.0564	.0301	7.7153
5253.0610	110.8398	604.6741	.0230	7.7700
5296.7387	111.7199	648.3517	.0175	7.8247
5340.4753	112.3868	692.0883	.0132	7.8795
5384.2699	112.8872	735.8829	9.8457E-03	7.9342
5466.5375	113.4944	818.1505	5.4571E-03	8.0368
5548.9990	113.8214	900.6120	2.8158E-03	8.1394
5631.6483	113.9817	983.2614	1.2788E-03	8.2420
5714.4797	114.0468	1066.0927	4.2474E-04	8.3446
5797.4875	114.0605	1149.1005	-1.7862E-05	8.4472

HORIZONTAL DYNAMIC IMPULSE (PSI-SEC) = .1140

Table 19

DYNAMIC PRESSURE AND IMPULSE VERSUS TIME
BASED ON NEW (EM-1) PEAK OVERPRESSURES

YIELD = 40 KT
HEIGHT OF BURST = 2.394 KFT
GROUND RANGE = 3.5092 KFT
PEAK OVERPRESSURE = 4.7466 PSI (FREE AIR)
TIME OF ARRIVAL = 2175.6770 MSEC
PEAK OP (T=TA) = 15.0008 PSI
PEAK DYNAMIC PRES.= 4.7715 PSI
PEAK HORIZ. COMPT.= 4.7715 PSI
DYNAMIC POS. PHASE= 957.3576 MSEC

TIME (MSEC)	DYN. IMPULSE(HORIZ) (PSI-MSEC)	TIME-TOA (MSEC)	DYN. HORIZ. COMPT. (PSI)	SHOCK G/R (KFT)
2179.7305	19.1032	4.0534	4.6547	3.5160
2183.7887	37.7606	8.1117	4.5405	3.5228
2187.8518	55.9810	12.1748	4.4288	3.5297
2191.9197	73.7733	16.2427	4.3195	3.5365
2200.0697	108.1066	24.3927	4.1081	3.5502
2208.2386	140.8308	32.5616	3.9059	3.5639
2216.4264	172.0117	40.7494	3.7126	3.5775
2224.6329	201.7132	48.9558	3.5279	3.5912
2232.8579	229.9967	57.1809	3.3514	3.6049
2241.1014	256.9216	65.4243	3.1828	3.6186
2257.6432	306.9097	81.9662	2.8682	3.6459
2274.2575	352.1272	98.5805	2.5816	3.6733
2290.9433	392.9784	115.2663	2.3210	3.7007
2307.6998	429.8384	132.0228	2.0841	3.7280
2324.526	463.0546	148.8489	1.8692	3.7554
2341.4210	492.9483	165.7440	1.6743	3.7827
2358.3841	519.8150	182.7071	1.4977	3.8101
2375.4143	543.9369	199.7373	1.3391	3.8375
2392.511	565.5760	216.8339	1.1959	3.8648
2409.6731	584.9639	233.9961	1.0667	3.8922
2444.1908	617.7710	268.5138	.8457	3.9469
2478.9612	643.9040	303.2842	.6670	4.0016
2513.9782	664.6067	338.3012	.5232	4.0563
2549.2359	680.9124	373.5589	.4081	4.1111
2584.7285	693.6754	409.0515	.3163	4.1658
2620.4506	703.5988	444.7736	.2435	4.2205
2656.3967	711.2584	480.7197	.1860	4.2752
2692.5615	717.1233	516.8845	.1410	4.3299
2728.9401	721.5739	553.2631	.1058	4.3847
2765.5274	724.9171	589.8504	.0786	4.4394
2834.6746	728.9847	658.9975	.0434	4.5420
2904.5084	731.1886	728.8314	.0224	4.6446
2975.0001	732.2875	799.3230	.0104	4.7472
3046.1222	732.7575	870.4452	3.8223E-03	4.8498
3117.8488	732.8888	942.1718	4.4219E-04	4.9524
3190.1552	732.8531	1014.4782	-1.0941E-03	5.0550

HORIZONTAL DYNAMIC IMPULSE (PSI-SEC) = .7328

Table 20

DYNAMIC PRESSURE AND IMPULSE VERSUS TIME
BASED ON NEW (EM-1) PEAK OVERPRESSURES

YIELD = 40 KT
HEIGHT OF BURST = 2.394 KFT
GROUND RANGE = 1.4645 KFT
PEAK OVERPRESSURE = 10.1451 PSI (FREE AIR)
TIME OF ARRIVAL = 1171.5790 MSEC
PEAK OP (T=TA) = 25.0000 PSI
PEAK DYNAMIC PRES.= 12.2166 PSI
PEAK HORIZ. COMPT.= 7.4733 PSI
DYNAMIC POS. PHASE= 799.7040 MSEC

TIME (MSEC)	DYN. IMPULSE(HORIZ) (PSI-MSEC)	TIME-TOA (MSEC)	DYN. HORIZ. COMPT. (PSI)	SHOCK G/R (KFT)
1174.0919	18.6514	2.5128	7.3717	1.4713
1176.6144	37.1198	5.0353	7.2709	1.4781
1179.1467	55.4053	7.5676	7.1709	1.4850
1181.6887	73.5075	10.1097	7.0717	1.4918
1186.8017	109.1622	15.2227	6.8756	1.5055
1191.9533	144.0838	20.3742	6.6828	1.5192
1197.1432	178.2729	25.5641	6.4932	1.5328
1202.3713	211.7307	30.7922	6.3068	1.5465
1207.6374	244.4592	36.0583	6.1238	1.5602
1212.9412	276.4608	41.3622	5.9442	1.5739
1223.6616	338.2948	52.0825	5.5949	1.6012
1234.5310	397.2649	62.9519	5.2591	1.6286
1245.5479	453.4105	73.9688	4.9368	1.6560
1256.7108	506.7785	85.1317	4.6281	1.6833
1268.0182	557.4225	96.4392	4.3328	1.7107
1279.4688	605.4021	107.8897	4.0508	1.7380
1291.0609	650.7825	119.4818	3.7819	1.7654
1302.7931	693.6334	131.2140	3.5260	1.7928
1314.6639	734.0285	143.0848	3.2828	1.8201
1326.6719	772.0451	155.0928	3.0520	1.8475
1351.0936	841.2431	179.5145	2.6266	1.9022
1376.0463	901.9128	204.4672	2.2472	1.9569
1401.5186	954.7382	229.9395	1.9108	2.0116
1427.4988	1000.4085	255.9197	1.6145	2.0664
1453.9756	1039.6051	282.3965	1.3551	2.1211
1480.9378	1072.9912	309.3587	1.1294	2.1758
1508.3741	1101.2035	336.7950	.9343	2.2305
1536.2736	1124.8451	364.6945	.7669	2.2852
1564.6254	1144.4811	393.0463	.6287	2.3400
1593.3516	1161.3552	421.7726	.5444	2.3947
1639.2109	1182.3629	467.6318	.3777	2.4973
1686.9132	1196.9555	515.3341	.2434	2.5999
1736.3508	1206.373	564.7717	.1464	2.7025
1787.4253	1212.0088	615.8463	.0813	2.8051
1840.0471	1215.0785	668.4681	.0403	2.9077
1894.1335	1216.5191	722.5544	.0162	3.0103
1949.6081	1216.9961	778.0290	3.0831E-03	3.1129
2006.4002	1216.9528	834.8212	-3.3292E-03	3.2155

HORIZONTAL DYNAMIC IMPULSE (PSI-SEC) = 1.2169

REFERENCES

Brode, Harold L., *Height of Burst Effects at High Overpressures*, The Rand Corporation, RM-6301-DASA, 1970 (DASA report 2506).

-----, *Theoretical Description of the Blast and Fireball for a Sea Level Megaton Explosion*, The Rand Corporation, RM-2248, 1959.

Needham, Charles E., Martin L. Havens, and Carolyn S. Knauth, *Nuclear Blast Standard (1 kT)*, Air Force Weapons Laboratory, Report AFWL-TR-73-55 (rev.), April 1975.

APPENDIX

NEW ANALYTIC FIT FOR REVISED EM-1 CURVES

The new fit takes advantage of the similarities evident in the family of HOB curves from 1.0 to 10,000 psi. The behavior along the x-axis (zero HOB) is that of a surface burst, for which overpressure can be expressed as a simple function of ground range:

$$PD = \frac{6.48}{x^{1.2518}} + \frac{3.9727}{x^{2.924}} \quad \text{psi} . \tag{A.1}$$

Along the vertical axis (zero ground range), the behavior is approximated by

$$PK = \frac{11.049}{y^{1.3069}} + \frac{6.0481}{y^{3.4793}} \quad \text{psi} , \tag{A.2}$$

in which x and y are in $kft/kT^{1/3}$.

Along a curve through the maximum horizontal range for each isobar (y = RA in Fig. A.1), the pressure is expressed by

$$PE = \frac{1.7934}{x^{3.4227}} + \frac{441,830\ x^{8.7266}}{1 + 28,242\ x^{9.661}}$$

$$- \frac{5(RA)^{2.2643}}{1 + 1.0453(RA)^{4.8336}} - 0.21915RA , \tag{A.3}$$

where the curve

$$y = RA = 0.00009686\ x^{2.045} + 0.6857\ x^{0.4906}$$

$$- \frac{0.1176\ x^{0.01869}}{1 + 296.5\ x^{3.962}} - 0.02255 . \tag{A.4}$$

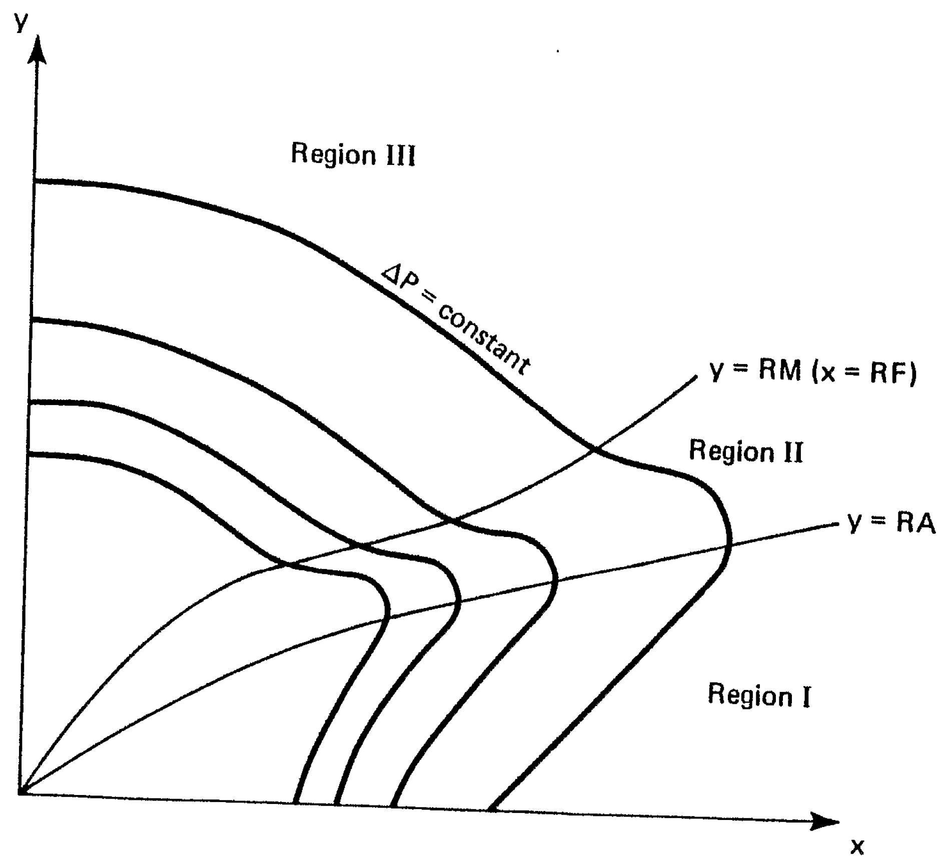

Figure A.1. Typical isobars and fit regions.

Along a curve through the relative minimum above the knees (y = RM in Fig. A.1), the pressure is approximated as

$$PJ = \frac{14.35}{(RI)^{1.45}} + 0.056 + \frac{4}{(RI)^{3.71}} - \frac{0.171}{(RI)^{4.716}} , \qquad (A.5)$$

in which $RI = [(RF)^2 + y^2]^{1/2}$, with

$$RF = 4.106\ y^{0.7555} - 2.317\ y^{0.3074} + \frac{10.3\ y^{1.803}}{1 + 230.8\ y^{2.132}}$$

$$- \frac{2.286\ y^{1.291}}{1 + 1.006\ y^{2.236}} + 0.5642 . \qquad (A.6)$$

Interpolating between the pressures along the four curves y = 0, x = 0, y = RA(x), and x = RF(y) defines peak overpressure for any height of burst (y) and range (x).

The interpolation is not linear and differs in each region. In region I, between y = 0 and y = RA,

$$\Delta P_s \simeq (1 - FC)PD + FC \cdot PE , \qquad (A.7)$$

where

$$FC = \frac{FB(0.433 + 1.011FB)}{1 + 0.444(FB)^5}$$

and

$$FB = \frac{y}{RA} .$$

In region II, between y = RA(x) and x = RF(y),

$$\Delta P_s \simeq FO \cdot PL + (1 - FP) \cdot FC \cdot PE , \qquad (A.8)$$

where

$$FO = 0.7717(FN)^{2.743} + 0.2283(FN)^{0.7} ,$$

$$FN \simeq \frac{y(y - RA)}{RM(RM - RA)} ,$$

$$FP = FO\left[1+0.00594\left(\sqrt{x^2+y^2}\right)^{2.565}\right] ,$$

$$PL \simeq (1 - FH)PK + FH \cdot PJ ,$$

$$FH = 0.09284(FG)^{1.0286} + \frac{7.696(FG)^{2.513}}{1 + 7.4836(FG)^{2.151}} ,$$

$$FG = \frac{x}{RF} ,$$

and

$$RM = \frac{-0.09175\,x^{-0.3896}}{1 + 31.31\,x^{3.106}} + 0.003582 + \frac{0.6907\,x^{0.4597}}{1 - 0.2021\,x^{0.4696}} + \frac{0.005963}{x^{1.106}} .$$

In region III,

$$\Delta P_s \simeq PL . \qquad (A.9)$$

This fit provides a continuous analytic approximation to the new (and improved) peak overpressure curves recommended for EM-1.

CHAPTER 8

CAVITY DECOUPLING OF UNDERGROUND NUCLEAR EXPLOSIONS

Robert M. Henson
Eugene T. Herrin
William E. Ogle
Frank J. Thomas

DECOUPLING FACTOR

Two definitions for the seismic decoupling factor are as follows:

- Experimental. The decoupling factor is the ratio of the amplitude of the teleseismic p-wave from a tamped shot to that from a cavity-decoupled shot of the same yield, both signals observed at the same distance from the source.
- Theoretical. The decoupling factor is the ratio of the reduced displacement potential (RDP) for an equivalent elastic source for a tamped shot to that for a cavity-decoupled shot. The RDP is the proper measure of source strength for generating teleseismic p-waves, based on the theory of elastic-wave propagation. The log to the base 10 of the RDP is directly proportional to the teleseismic magnitude m_b of the event.

The optimum decoupling ratio (the ratio for a "fully" decoupled shot) is defined as the decoupling ratio obtained when the following two conditions are met:

(b)(2)

[redacted]

From calculations that assume an "ideal granite" medium and experimental results in a salt dome, the optimum decoupling ratio is [redacted] The shape of the curve relating decoupling ratio to scaled cavity radius is based on calculations for "ideal granite" and is shown in Fig. 1.

(b)(2)

At practical depths of about 1 km, the required cavity sizes are as follows:

(b)(2)

[redacted]

where R is the cavity radius required for optimum decoupling and W is the yield in kilotons. In Fig. 1, for "ideal granite" the ordinate is the RDP or equivalent source size for generating teleseismic waves.

(b)(2)

[redacted]

(b)(2)

[redacted]

Figure 1. Final RDP vs. scaled initial source size.

SIGNIFICANCE OF CAVITY DECOUPLING TO TREATY VERIFICATION

To calculate the pertinent yields for possible evasion of a Comprehensive Test Ban Treaty (CTBT) using cavity decoupling, we assume that

(b)(2) [redacted]

(b)(2) [redacted]

The above conclusions are illustrated in Fig. 2, which shows the relationships between yield, magnitude, and cavity radius for optimum decoupling. Reducing the cavity size or increasing the yield beyond the given values would result in a higher detection probability and might be unacceptable to a careful evader.

(b)(2) Mining [redacted] in salt is a major undertaking. [redacted]

(b)(2)

We conclude from the stated assumptions and criteria that a yield [redacted] (b)(2) could be fired in a decoupling cavity in salt

(b)(2)

Figure 2. Magnitude-yield relations for tamped and decoupled explosions.

with an "acceptable" probability of seismic detection, depending on the time and effort expended in constructing the cavity.

(b)(2) [redacted]

NONSEISMIC TECHNIQUES

Electromagnetic Pulse (EMP)

A decoupling cavity is likely to enhance the electromagnetic signal from an underground nuclear test. That is, the EMP source should be larger than that from a tamped explosion with the same yield.

(b)(2) [redacted]

We conclude that this subject requires additional theoretical analysis and perhaps numerical calculations for realistic salt dome models, but that no requirement currently exists for an underground nuclear explosion in order to study the phenomenon.

Ionospheric Shock

The surface motion directly above an underground test in a decoupling cavity and its effect on the ionosphere should be subject (b)(2) [redacted]

Figure 3. Schematic of decoupling cavity in a salt dome.

to decoupling factors similar to those associated with teleseismic signals. It is expected that the ground surface displacements for an optimum decoupling cavity will be reduced below those for a normal tamped shot [redacted] (b)(2) The phenomenon can probably be studied at reasonable cost by adding on experiments to future underground nuclear tests.

RECOMMENDATIONS

(b)(2) [redacted] Results from an additional decoupled nuclear experiment in salt—or any other medium—should not significantly change that conclusion. We make the following specific recommendations:

1. DNA should not invest in a nuclear cavity decoupling experiment at this time.
2. DNA should support, and cooperate with DARPA, in high-explosive tests directed toward understanding the phenomenology of earth motion from decoupled shots.
3. Should DNA field an underground nuclear test to explore coupling of near-surface bursts, add-on experiments should be included that relate particularly to nonseismic techniques that might improve our capability for detecting decoupled explosions.

CHAPTER 9

TESTING RESPONSE TO FIREBALL ENVIRONMENTS: NEEDS AND TECHNIQUES

Harold L. Brode

PREFACE

Many structures, military systems, and vehicles are targeted for nuclear attack, yet few have been exposed to nuclear explosions--though most have clear vulnerabilities to blast and thermal effects. In no case has a complete system been demonstrated as "hardened"--able to resist the full impact at design levels of a nuclear threat. Hardened elements are nevertheless associated with all strategic systems, such as the silos that protect land-based missiles and the communication links for control and communications centers. High levels of protection are required for all egresses and communications for underground command centers, and they would be important for superhard reserve missile storage sites. Many aspects of air defense and antiballistic missile defense systems also require hardening.

In virtually all cases, designs for survival of surface elements remain untested in the nuclear environment. Such a heavy dependence on theory and hypothesis in ensuring the nuclear hardness of vital military equipment or structures has no precedent in other military (nonnuclear) systems. Ample field-testing and realistic exposure to threat weapons is the least we can expect in the certification process for a nonnuclear system.

Generally, passive survival for systems with exposed elements depends on hardening and wide separation between redundant elements; that is, system survival depends on dispersal* and numbers as well as on hardness. While the number and separation of elements (whether missile silos or communications tie-points to a superhard center) are both important, the achievable hardness for individual elements usually governs system feasibility and cost. With regard to survivable communications for a facility deep underground, if antennas,

*Some suggested basing modes, particularly the MX concept, rely on location uncertainty as a partial substitute for dispersal and hardness; even so, appreciable hardness is necessary to limit the deployment area. An ordinary transport vehicle or truck can be damaged at 2 psi (14 kPa), and it is within current Soviet capabilities to cover the entire western United States with more than 14 kPa.

cable tie-ins, or repeater stations cannot be hardened at or near the surface to the 1000 psi (7 MPa) level, but can be guaranteed only to the 100 psi (700 kPa) level, then wider separations requiring much longer connections, tunnels, or cable drill-holes must be constructed; the consequent system costs rise significantly. Longer tunnels and drill-holes increase the chances of crossing major earthquake faults or other abrupt geologic discontinuities, accompanied by a greater chance of gross displacements that can cause tunnel disruption and cable breaks. In the end, however, it is important to ensure that all the hard-surface tie-points are at least as difficult to destroy as the central (sometimes deep) facility.

How can we test surface features? As the overpressure levels rise from hundreds to thousands of pounds per square inch, blast simulation with high explosives rapidly becomes impractical, and ultimately impossible. At present, only a shock tube driven by a large volume of exceedingly high-temperature air appears able to create a nuclear fireball environment on a scale appropriate for full-scale (or even scaled-down model) structure exposures. A nuclear explosive device promises the only known practical means of providing an adequate volume of air plasma at temperatures and pressures high enough to simulate blast waves from a nuclear fireball.

The response of structures in fireball environments is complex, and theoretical treatments are too sketchy to be credible without experimental verification. Exposures on past nuclear tests have been too limited to extrapolate to relevant materials and configurations. No proposed simulators driven by chemical explosives can hope to create either the high dynamic pressures or the high fireball gas temperatures of a nuclear explosion; but a nuclear-driven shock tube in an underground tunnel could generate a realistic large-yield, high-overpressure blast environment.

It remains to be demonstrated that such a facility could function adequately. Questions of containment and safety are of paramount importance. Massive wall losses and early tunnel collapse could preclude useful tests. Adequately designed and tested instrumentation must be available to accurately record both fireball phenomena and structure response. Such instruments and techniques have not yet been verified.

What follows is a paper (first prepared more than 12 years ago and subsequently rewritten at least twice) drafted to support the concept of an underground nuclear test for fireball exposures. The need continues, and the techniques are now better known. The question we address here is, What are the current prospects?

SECTION 1

INTRODUCTION

Many modern military systems are intended to withstand the effects of nuclear bursts. The present missile-basing systems and most ICBMs are designed to survive at very high blast and radiation levels. Current missile silos already provide protection from hundreds to thousands of pounds per square inch (at megapascal levels) of peak overpressure from nuclear blasts. Some follow-on missile systems have been planned or designed to withstand thousands of psi. We also conceive of active defense systems that can continue to operate during a nuclear attack, and believe they must have an appreciable degree of protection from nuclear effects.

High-level nuclear attack survival is particularly pertinent to command and control facilities and other military contexts in which hardness counts because opportunities for redundancy or mobility are limited. It is important that communication links and intelligence facilities be made to survive, along with the commanders and communicators who will operate the surviving weapon systems. Even tactical systems in a nuclear warfare environment must often rely on high-level protection to gain survivability.

In all these military systems, some surface structures and some near-surface mechanisms or connections must be designed to withstand exposure to close-in nuclear weapon effects, often at megapascal blast levels (thousands of psi). At short range, they will also experience thousands to tens of thousands of calories per square centimeter of thermal or X-ray radiation (20 to 40 cal/cm^2 of thermal radiation will ignite most combustibles), and tens of thousands to millions of radians of nuclear radiation (450 rads is a lethal dose for man). They may also be subjected to megapascal blast-wind pressures and to impacts with fast-moving debris or crater ejecta. Ground motion may be violent, with displacement of as much as a meter, velocities of many meters per second, and permanent damage. At the same time, much of the equipment must remain operative and undamaged during exposure to extreme electromagnetic transients (running to fields of tens of thousands of volts per meter).

Surviving high levels of blast pressure from a nuclear explosion means withstanding a fireball environment. Current hardened missile-basing systems, principally the Minuteman, have been examined long and carefully to determine if there is any reason to doubt the design level for survival. A direct and convincing test using a series of nuclear explosions on a complex of silos, launch-control centers, and connected facilities was once planned; but it has not been possible to carry out the test since the atmospheric test-ban treaty went into effect. However, much of the nuclear environment has been reproduced and applied piecemeal to operational or scaled test structures. Nuclear radiation and electromagnetic pulse (EMP) sources have been provided for testing systems. Overpressure loads have been simulated using the high-explosive simulation test (HEST) technique and have been applied to full-scale hardened structures.

Such simulations are very helpful, and have contributed impressively to our understanding of and confidence in the survival of hardened facilities. Some of these tests are, however, very expensive; a nuclear test would not necessarily be much costlier or more time-consuming than a simulation test. Of course, only underground nuclear tests are currently possible, so even such tests can provide only partial atmospheric burst environments.

More important, piecemeal simulation of specific effects, no matter how well done, will leave unanswered many questions about combined effects. EMP without ground shock or nuclear radiation may miss some vulnerabilities. Structure response to overpressure loads without accompanying drag forces may be misleading. Unfortunately, none of the simulation techniques offers complete verisimilitude. In some cases, the nuclear phenomena are not known well enough to be sure what to simulate (e.g., direct ground shock or debris characteristics). Some phenomena still defy simulation at all, especially the very intense blast and thermal regime of the nuclear fireball.

Below, in support of further investigations of the effects of fireball exposure, we briefly review close-in nuclear burst phenomena (the fireball environment) and the expected effects on exposed structures. We list outstanding close-in vulnerability questions, compare alternative fireball simulation and investigation techniques, and suggest advantages and disadvantages of each. The nuclear-shock-tube concept is given particular attention. The use of "get-lost holes" for disposing of nuclear fission products from nuclear explosive devices is proposed as a feasible method of reducing postshot radiation hazards, thus aiding reentry and the recovery of experimental information.

SECTION 2

FIREBALL ENVIRONMENT

Since successful designs for survival inside nuclear fireballs must rely on our incomplete knowledge of close-in phenomenology, they must demonstrate an insensitivity to the expected variations in fireball features. Test observations from earlier atmospheric bursts combined with theoretical calculations of radiation transport and dynamic motions have provided a fairly detailed and presumably accurate picture of free-air bursts; yet those descriptions of close-in phenomena are by no means complete.

In most cases, the greatest uncertainty lies not in the phenomena themselves but in the response of exposed materials and in the mechanisms by which damage is done. For example, free-air fireball temperatures and pressures may be fairly well predicted by detailed calculations and confirmed from observations made during previous atmospheric tests; but the responses of such material as concrete and steel to high heat and stress loads are not well known because they are so hard to calculate and difficult to measure. In fact, few of the boundary phenomena at surfaces--of either earth or structures--are understood or can be predicted. More important, the basic reflection phenomena from bursts on or near the earth's surface are only partly understood.

The table below suggests some levels of environmental effects within a fireball in the absence of surface interaction complications. The levels represent exposures generally not achievable using conventional nonnuclear simulation techniques, even for small-scale model structures or instruments. Reproduction of the indicated pressures, temperatures, and flow rates becomes essential in testing to confirm the survivability of structures or facilities within fireballs--that is, for peak overpressure exposures above 1 MPa.

As an example, consider what can be expected a quarter mile (0.40 km) from a 1 MT burst. The peak overpressure is around 1600 psi

Close-in weapon effect levels.

Effect	1/4 mi Range			1/2 mi Range			1 mi range		
Yield (surface burst)	100 kT	1 MT	10 MT	100 kT	1 MT	10 MT	100 kT	1 MT	10 MT
Peak overpressure (psi)	180	1,600	15,000	32	224	1,900	7.3	38	270
Overpressure impulse (psi-sec)	12	70	320	5	27	160	2.2	11	60
Blast duration (sec)	0.43	1.3	3.2	0.53	1	2.8	1	1.1	2.1
Peak wind velocity (ft/sec)	3,000	9,300	28,000	1,000	3,400	10,000	300	900	3,700
Peak dynamic pressure (psi)	250	4,800	70,000	18	370	6,000	1.1	23	430
Drag impulse (psi-sec)	7.4	28	95	2.3	17.5	62	0.32	6	40
Wind duration (sec)	1.2	2.4	5.2	1.3	2.5	5.2	1.3	2.8	5.4
Shock-temperature rise (°C)	600	3,800	15,000	130	770	4,300	34	150	860
Maximum air temperature rise (°C)	2,400	43,000	110,000	130	3,700	50,000	34	150	4,800
γ-ray dose (R)[a]	5.5^{+5}	3.5^{+7}	4.1^{+9}	3.5^{+4}	2.3^{+6}	3.1^{+8}	580	3.8^{+4}	7.2^{+6}
Neutron dose (rad)[a]	4.5^{+5}	4.5^{+6}	4.5^{+7}	1.7^{+4}	1.7^{+5}	1.7^{+6}	100	1,000	10,000
Soil (C_L = 400 ft/sec)									
U_s/C_L	1.25	3.5	10.8	0.62	1.4	3.9	0.44	0.66	1.5
Maximum vertical acceleration (g)	21	180	1,700	2.1	25	220	0.52	2.4	31
Maximum vertical velocity (ft/sec)	2.3	20	180	2.1	2.8	24	0.52	2.4	3.4
Maximum vertical displacement (ft)	0.13	1.3	12	0.14	0.33	3.3	0.036	0.36	0.83
Maximum horizontal displacement (ft)	0.07	0.7	6	0.14	0.17	1.6	0.036	0.36	0.4
Rock (C_L = 15,000 ft/sec)									
U_s/C_L	0.25	0.70	2.15	0.12	0.28	0.78	0.09	0.13	0.3
Maximum vertical acceleration (g)	1.6	7.6	334	0.41	1.9	9.0	0.10	0.48	2.2
Maximum vertical velocity (ft/sec)	1.2	5.7	27	0.31	1.4	6.6	0.08	0.35	1.6
Maximum vertical displacement (ft)	0.08	0.85	1.8	0.02	0.21	2	0.005	0.05	0.5
Maximum horizontal displacement (ft)	0.08	0.85	0.9	0.02	0.21	2	0.005	0.05	0.5

[a]Hot day (97°F) near sea level or cold day (46°F) at 3,600 ft; ρ_a = 1.1 kg/m^3.

(11 MPa), with a positive phase impulse of about 70 psi-sec (0.5 MPa-sec), lasting 1.3 sec; a peak blast wind of 9300 ft/sec (2.8 km/sec); a peak dynamic pressure of 4800 psi (33 MPa); and a drag impulse of 28 psi-sec (0.2 MPa-sec) over 2.4 sec of positive blast wind. The shock-temperature rise at this range (1/4 mi from 1 MT) is 3800°C, increasing to 43,000°C as the fireball expands beyond that range. A gamma-ray dose of about 35 million R (~350 thousand grey) and a neutron dose of around 4.5 million rad (45 thousand grey) can be expected. Ground motions in soil of 180 g, 20 ft/sec (6 m/sec) maximum vertical velocity, and vertical displacements of 1.3 ft (40 cm) are possible.

Each explosive level listed in the table occurs within one or two seconds, so that as high pressures are applied, high temperatures, large ground motions, and high doses of nuclear radiation are experienced. Combined effects may be more serious than any single exposure, so that the integrated environment should be contemplated in assessing response, and possibly in designing simulators.

SECTION 3

QUESTIONS ABOUT SURVIVAL AND OPERATION IN FIREBALL ENVIRONMENT

There have been exceedingly few attempts to measure the blast, heat, radiation, and debris impacts inside the fireball. In contrast, about 70 nuclear tests have carried blast measurements at peak levels below 100 psi (~700 kPa, outside the fireball) during the more than 20 years of atmospheric testing. Consequently, many questions about the survival of equipment and installations at the close fireball ranges remain unanswered.

As noted, the strong shock of the fireball can be well described for a free-air burst. Unfortunately, the fireball blast cannot be so accurately described when it strikes the ground, and its features are even less predictable when the burst itself is on, near, or under the surface. The lone "good" record of a blast near 1000 psi (7 MPa) from a megaton surface burst [Meszaros et al., 1962] is not so good that it can be definitely compared with calculations. Although some kiloton-yield records extend into thousands of pounds per square inch, there are very few time-histories above a megapascal [Ellis and Wells, 1966], and very few peak values have been recorded near 1000 psi (7 MPa).

The lack of data does not stem from a lack of interest in the high-pressure region; rather, the nearest gauges were often destroyed in nuclear tests before records could be made. Although the old test reports catalog the reasons for the failures, the unhappy fact is that early equipment performed poorly at high levels. Extreme heat, enormous dynamic forces, violent ground motion, paralyzingly high voltages (EMP), and deadly flying debris combined to destroy or invalidate records from even the most rugged blast gauges. One gains little assurance of the survival of extensive, complex structures in a region where simple measurements of the environment have proven so difficult.

It is true, however, that the very high pressures (~10 MPa) of [redacted] underground cavity experiment were measured with slightly more success [redacted] the results lending some credence to the claim that future nuclear tests could provide more and better measurements of blast pressures in the tens of megapascals. However, the very low yield [redacted] should be recognized as causing small displacements and thus making gauge survival easier.

A number of sophisticated calculations agree on predictions of temperatures, densities, and velocities as well as pressures in an air-burst fireball; but there are only indirect experimental observations (mostly photographs) for confirming or checking the predictions. More important, calculations for surface bursts or low heights of burst have not yet proven realistic or reliable.

Direct measurements of dynamic pressure, temperature, sound speed, and other free-field fireball phenomena pertinent to hard-site survival do not yet exist. Instrumentation for the ranges in question grow out of simulator efforts; but the lack of success on nuclear events leaves some question as to their survivability or reliability. The response of structures and materials to the fireball environment has been observed for only a few tests and for even fewer exposures of materials. For all test objects, exposure was influenced by blast interactions with nearby surfaces--interactions of uncertain nature and extent.

This old evidence contained many surprises and mysteries not completely understood or resolved even today, 20 to 30 years later. Much careful calculation of both the fireball environment and the material response for each exposure must precede any confident understanding of the few observations. On the basis of such confirmation, we may be able to predict what other materials might do in other locations on other shots using improved and extended calculations. But, as always, ex post "predictions" lack the credibility of verified, true predictions; without further confirmation through realistic testing, therefore, the former will remain quite uncertain.

At a half-mile from 10 MT (see the table above), overpressure is 1900 psi (13 MPa), but peak dynamic pressure is 6000 psi (41 MPa) and peak wind velocity, 10,000 ft/sec (~3 km/sec). In such a dynamic flow, can any projecting structures, no matter how small, survive? Will doors, footings, or collars forced up above the surface a few inches--or even only a fraction of an inch (by differential ground motion)--experience loads for which they were not designed?

At a 13 MPa (2000 psi) level, the shock temperature is 4600°K; but the hot air behind the shock makes the temperature at that range rise to a maximum of 50,000°K in less than 0.10 sec and persist at that level for another fraction of a second. The combined high-speed airflow and high rates of material vaporization at such elevated temperatures make the response of sizable exposed surfaces doubly difficult to predict. No currently envisaged laboratory or chemical-explosive test facility can reproduce such a high-pressure, high-flow-rate, high-temperature environment over any useful area.

Since superhot gas flows themselves constitute the blast load, simulating the static overpressures alone cannot--even when given the expected time-history of pressure relief--create the same blast environment that a silo door, hardened antenna, or intake valve would be exposed to at the 10 or 20 MPa level in a nuclear fireball.

At such high levels of blast and heat exposure, only installations wholly below ground--having no surface appurtenances, openings, closure mechanisms, plenums, pop-up antennas, etc.--can be assured of survival without more careful testing. Even for the below-grade portions of surface installations, lesser questions about the influence of the superhot, fast-flowing air of the fireball on structure and contents may not be answered without testing. What will be the effect of high-temperature fireball gases intruding into cracks temporarily opened by the passing ground shock? Could the fast-flowing gas lubricate the cracks to reduce shear resistance in large rock joint systems, thereby amplifying the hazards of block motion? These and related questions peculiar to survival in fireball environments could be answered much more confidently by means of a nuclear test. Only underground testing is currently possible, but a fireball-sized underground chamber is impractical. Can a shock-tube configuration driven by the superheated air from a cavity nuclear explosion provide the appropriate fireball environment? Is a nuclear-driven shock tube practical in both construction time and cost?

Carpenter, Gilmore, and Mills [1976] examined both mechanical and thermal mechanisms that might lead to serious failures following exposure to a fireball. Mechanical or structural failures included seal blowout by airblast, seal ports opened by structural distortion, leak ports opened by cracking and eroding of material, inadequate geometrical expansion for leakage, and insufficient shielding from hot jets through cracks. Thermal mechanisms were closure weldup and torching. The enlarging effect of erosion and ablation on a crack or hole through which hot gases penetrated was also considered. Their report did not answer all the important questions, however, and further resolution by means of experiments with a 100 MW plasma arc was recommended, along with renewed study of the nuclear-driven shock tube.

SECTION 4

SIMULATION FOR SYSTEM AND COMPONENT TESTING

The atmospheric test-ban treaty precludes direct testing of hardened systems in nuclear fireball environments. High-explosive simulation of fireball environments has been attempted successfully with a number of different techniques, however. The high-explosive simulation test (HEST)--which uses distributed charges of primacord or other distributed explosives that are arrayed, tamped, and detonated over a structure so as to reproduce the early portion of a static overpressure blast history--has been used successfully up to 35 MPa.

A kind of self-destructing, high-explosive-driven shock tube, the DABS facility, creates not only the overpressure but also the dynamic flow for pressures up to perhaps 3 MPa. The DABS has serious limitations in both cost and accuracy of simulation, however, since the high-explosive products are blown over the test structures.

The so-called BOSS or shaped-charge simulator uses a converging wedge configuration of high explosives without a metal liner to shock-squeeze the contained air to very high temperatures and high velocities. The BOSS also, unfortunately, cannot be used to test full-scale structures without exposing them to a later flow of explosion products. In addition, its use of explosives is extremely inefficient, and it becomes very expensive on a large scale. It does, however, create higher temperatures and higher pressures than can ordinarily be obtained with simple charges of high explosive [Physics International, 1968].

If the loading due to very high blast pressures is understood, then it is possible to recreate the loads using a shaped HEST or distributed charges of explosives arrayed over the surfaces of a test structure. The high temperatures could be simulated on a small scale with a plasma torch, so that some studies of ablative erosion and boundary-layer behavior could be carried out--but the simultaneous pressure and velocity of flow effects would be lacking.

Again, however, high-explosive gases do not behave like air, and none of the flow of fireball hot gases is adequately simulated by a shaped HEST. To simulate ground motion, either as induced by the air blast or directly caused by cratering, it is possible to use a set of explosive charges buried in a line or an array in the ground--what is known as the DI-HEST concept. If the actual cratering motions are to be recreated, the Mine-Throw concept applies, in which the detonation of a distributed high-explosive charge simulates the actual earth stresses leading to nuclear-cratering motions.

Of all these possibilities, only the BOSS concept, with a shaped charge creating superheated airflows, comes close to recreating the fireball environment accompanying megapascal shocks. Even it falls short of reproducing the hot air and temperatures in the tens of thousands of degrees Kelvin at high velocities that follow such shocks, and it showers test structures with the expanding explosion products.

Superheated airflow could be the critical factor in causing damage or malfunctioning in the blast valves, plenums, delay lines, closure seals, antenna ports, or exposed faces of any hardened structure. Failure to simulate the full high-speed, high-temperature plasma flows means less than full credibility in the simulation or testing of structural survivability at fireball levels under megapascal pressures.

A sure way of obtaining the required fireball temperatures and pressures is to explode a nuclear device in an underground cavity. However, the cavity required for any reasonable explosion would be inordinately large. But there is still the possibility of driving the hot air created by a nuclear explosion down a tube. The next section describes such a nuclear-driven shock tube.

SECTION 5

NUCLEAR-EXPLOSION SHOCK TUBE

The most direct way of achieving air temperatures up to 100,000°K--predicted in a nuclear fireball at the 70 MPa (10,000 psi) peak overpressure distance--is with a nuclear explosion. (b)(2) Nuclear bursts in large underground cavities have been successfully contained [redacted] (b)(2) [redacted] Furthermore, the restraining walls of a rock cavern leading into a tunnel are not unlike the geometry of a conventional shock tube, which allows testing at considerable distances from a source of high pressure, and makes it easier to generate the long durations typical of large-yield explosions. In fact, the shock-tube configuration, with an explosively loaded driver section and a controlled test section, has long been a useful blast-simulation technique. A nuclear-explosive driver is, however, an innovation--necessary in this case to generate a large volume of driver gas (air) at elevated temperatures (~10 eV).

One possible mechanism would detonate a small-yield nuclear device in an air-filled cavity to pressurize and heat the air. That hot, high-pressure volume would represent a shock-tube driver section. When allowed to blow into a tunnel with a variable (possibly expanding) cross section, the hot air could create the flow time-history typical of the strong blast from a large-yield weapon. A large-yield environment might thus be provided using a small-yield nuclear source.

An increasing number of successful tests suggest that a valid structure-response test can be conducted when the scale of test structures (as well as the scale of the blast) is substantially reduced. In that case, the overall facility need not be on a scale of a full multimegaton burst. Structural design, construction, and analysis have reached a point where modestly reduced dimensions still allow dynamic similitude in structure response. For instance, model silos and hardened structures in high-explosive simulations, when scaled down to one-quarter (all dimensions reduced to one-fourth of those of the original structure), have responded dynamically almost like a full-scale structure [Johnson et al., 1965]. Obviously, if quarter-scale tests can be convincing, then the requirements for an underground test facility can be dramatically reduced. With all dimensions reduced by 1/4, the blast energy--and hence the yield to be simulated--is reduced by $(1/4)^3$ or 1/64*th*, so that a 16 kT yield represents the effect of 1 MT on a quarter-scale structure.

In addition, by channeling the blast energy down a tunnel, just a fraction of the 16 kT yield is needed to develop the blast time-history. Simply, the requisite fraction of energy can be estimated as the fraction of total solid angle formed by the tunnel cone interacting with a spherical driver section. Thus, a test section 80 ft wide at a distance of 250 ft from the 16 kT burst (3000 psi) would subtend a solid angle of ~0.080 sr, or 0.0064 of the total sphere. That fraction of the 16 kT yield is 100 tons. It is far less difficult or costly to build a cavity to contain 100 tons of nuclear yield than it is to build one for a yield of several kilotons.

Many questions arise in developing this concept. How big must the driver section be to avoid gross wall motions? If a spherical driver chamber blows into a conical test section, will the adjacent walls shear off in the driver chamber and spoil the shock-tube geometry or cause excessive debris? Must the driver section have a volume comparable to the shock-tube volume? Must the tube be conical to produce a decaying blast wave?

Some of those questions have been previously investigated by the Defense Nuclear Agency, with answers encouraging enough to make the concept's general feasibility apparent [Lewis, 1968]. The design becomes more uncertain when effects additional to the high-level blast wave are to be modeled simultaneously. It is conceivable to simultaneously create prompt radiation, direct and air-induced ground shock, and even EMP and thermal radiation with the same (or another) nuclear source. But to do so would require further modification as well as much more sophisticated analysis and theoretical calculations in support of planning.

Our first objective in investigating the feasibility of a nuclear shock tube has been to show that some reasonable configuration should produce the desired blast history. Although many further improvements are likely, the simplest configuration for calculation is a nearly spherical driver chamber feeding a cylindrical or conical tube and test section. The first calculations were for a driver chamber about 11 m in radius, centered on a 100-ton-yield nuclear device (a spherical model). Subsequent calculations investigated the effects of yield and cavity-size changes. While more calculations followed (sponsored by DNA at The Rand Corporation and Physics International [Physics International, 1968]), the feasibility of a facility to test component and structure response to a true fireball environment seemed already established.

The concerns sometimes raised over the rate of growth of boundary layers and the consequent choked flow in the test section were alleviated by the analysis of Carpenter, Gilmore, and Mills [1976];

(b)(2)

SECTION 6

PRETESTS

Serious questions arise concerning the novel nuclear test configuration proposed. To answer some of them, we suggest that a small preliminary nuclear shot in a similar geometry be considered, and a study be made of the most questionable features and the potential difficulties identified. Some questions to consider (not necessarily in order) are, How serious is wall ablation? What is the effect of wall smoothness on strong shock propagation? How can the test section be protected from rock failures upstream in the shock tube or in the driver chamber (shot room)? How can the upstream walls (rock) be controlled and kept from interfering with the fireball exposure experiments downstream?

Further questions are, Would lining and rock-bolting add measurably to rock control, or would they contribute to the hazards? What late-time problems exist for stemming or for preventing cavity collapse or further extraneous damage to the test section? Can the shock propagation and radiation flow reproduce the predicted environment in the test section? What reflected shock perturbations can be expected? How well can the radioactive debris be prevented from contaminating the test structures? What are the problems in ensuring reentry into and postshot examination of the test sections?

In addition, what measurements can be made? Can overpressure, dynamic pressure, velocity, and temperature measurements be made with sufficient accuracy to improve our understanding of fireballs? What instrument development and testing is necessary or desirable?

Clearly, the experiment would be of limited use if the data derived from it were no more accurate or reliable than previous measurements or the results of detailed calculations. However, even a poorly instrumented test promises to provide a benchmark for theoretical work on both environment and response.

(b)(2)

Since the earlier efforts at measuring fireball levels, much has been accomplished in instrument development and verification/calibration--virtually all relevant to the concept of underground-cavity nuclear tests. Questions remain, however: Can we expect significantly improved knowledge of the fireball environment? Can the responses be measured accurately enough to justify the expense and effort involved?

SECTION 7

TEST OBJECTIVES

The obvious goal of a nuclear-shock-tube test is to expose scale-model or prototype missile shelters or silos and surface elements of similar superhard systems to nuclear effects. A more general but perhaps equally valuable set of test objects would include blast valves, doors or closures, antennas, sensors, plenums, and delay lines for any hardened system hopeful of survival and operation at high blast levels. Basic response tests should be considered for various types of metal, rock, metal/rock interfaces, concrete, moving parts and bearing surfaces, and components requiring controlled dimensions (such as radar or communications antennas and some types of sensors). Of additional great value would be experiments on the physical effects of heat and pressure on both natural and constructed materials--experiments that lead to extreme temperature and pressure transient loads.

The physics of fireballs--particularly in the presence of surfaces and solid objects--is uncertain, and could be studied in such a test. In fact, some measurements might be carried out quite reliably and simply underground, outside the burst chamber (down the shock-tube drift). Such measurements have proven extremely difficult in above-ground tests.

SECTION 8

METHODS FOR REDUCING RADIOACTIVE CONTAMINATION OF TEST SECTION

Twenty-three years ago, it was common to conceive and carry out atmospheric tests for both weapon development and research on weapon effects. However, the problems in modeling atmospheric bursts are formidable, and underground nuclear tests have been used for only limited simulations, mostly of exoatmospheric X-ray effects. A full-scale nuclear surface burst is best for "simulating" the effects of a nuclear surface burst; but a nuclear surface burst in an underground cavity requires such a large excavation that it is impractical. One possible mechanism for making such an underground cavity test more useful and more appropriate for exposing structures in an adjacent shock tube would be to include a "get-lost hole"—a tube or drill-hole behind the nuclear device into which most of the radioactivity can be driven and within which it can be contained.

(b)(2) The rudimentary concept was demonstrated [redacted] in which a drill-hole below an underground test accepted and trapped a great fraction of the radioactive debris from the device. The concept can be elaborated to the extent that a special test device can be designed to not only produce a nuclear explosion but direct most of the radioactive fission fragments into a pipe that leads below ground. The pipe can then be closed by techniques already common in "down-hole" or vertical line-of-sight, open-hole experiments.

The task of containing the debris and a small fraction of the energy of a nuclear blast—with the bulk of the energy already outside to assist in closure—should be much simpler than that of closing off conventional explosions, where most of the explosion energy works to blow out the closures. Obviously, an underground demonstration of such a device is desirable before its use as a surface-burst simulator is approved. An underground test with backup containment could further confirm the feasibility of the "get-lost hole" concept and demonstrate the adequacy of instrumentation as well as verify theoretical calculations. A successful test of the "get-lost hole" in connection with a shock-tube test would ensure an uncontaminated test section, and allow earlier reentry and data recovery.

The design details of such a device are the proper business of Department of Energy weapon designers. Preliminary discussions with Lawrence Livermore Laboratory staff (some of whom originated the "get-lost hole" concept) suggest that a special design is within present capabilities and could be worked out in timely fashion if desired (that is, if money and official sanction were forthcoming).

Beyond its considerable importance to a nuclear-shock-tube test, a surface-burst simulation capability with reduced residual radiation could lead directly to repeated and simultaneous testing of many structures in fireball environments. More important, it offers an otherwise unattainable opportunity to simulate the prompt nuclear radiation and the close-in EMP fields, important aspects of which are not now calculable. The return currents in the ground and the dynamics of intense close-in nuclear radiation heating with induced activity or (n, γ) reactions in solid and construction materials need experimental investigation and confirmation.

Not all aspects of cloud rise, dust, debris, and ejecta phenomena from nuclear bursts can be simulated with chemical-explosive bursts. At the same time, realistic calculations are extremely difficult to both formulate and accomplish--yet are usually incomplete and unreliable. Such phenomena are beyond the simulation ability of current underground test concepts. The cratering from an underground nuclear device cannot be said to reproduce the initial conditions of an operational weapon delivery or a real warhead. Even so, it will yield radiation levels and reproduce energy densities much more like those of a "real" burst than any high-explosive charge could generate. X-rays can be made to shine from such a source device, and hundreds to thousands of megabars of pressure can be delivered to the ground surface in the immediate vicinity. Any chemical explosive is limited to fractions of a megabar and to temperatures of a few thousand degrees. Although detailed replication of yields, masses, and geometries of interest to coupling studies is thus unlikely, the general features of nuclear bursts important to coupling can be reproduced and studied in greater realism than by any other simulation, short of full-scale operational weapon tests.

BIBLIOGRAPHY

Air Force Systems Command, *Systems Applications of Nuclear Technology, Effects of Air Blast, Ground Shock, and Cratering on Hardened Structures,* Air Force Systems Command Manual AFSCM 500-8, 1 March 1967.

Brode, H. L., *A Review of Nuclear Explosion Phenomena Pertinent to Protective Construction,* The Rand Corporation, R-425-PR, May 1964.

-----, "Review of Nuclear Weapons Effects," *Ann. Rev. Nuc. Sci.,* Vol. 18, 1968.

Carpenter, H. J., F. R. Gilmore, and A. F. Mills, *Sealing Facilities against Nuclear Fireball Effects,* R & D Associates, RDA Report TR-2006-007, November 1976.

Ellis, P. A., and P. B. Wells, *High Pressure Surface Airblast Phenomena,* Kaman Nuclear, KN Report 66-207(R), 13 May 1966.

Glasstone, S., and P. J. Dolan (eds.), *The Effects of Nuclear Weapons,* 3d ed., U.S. Department of Defense and U.S. Department of Energy, 1977.

Johnson, J. E., et al., *Simulation of Air-Blast-Induced Ground Motions, Phase II,* Vol. II, Air Force Weapons Laboratory, AFWL Report TR-65-26, May 1965.

Lewis, J., Defense Atomic Support Agency, personal communication, 1968.

Meszaros, H., et al., *Airblast Phenomena and Instrumentation of Structures, Oper. Hardtack,* Ballistic Research Laboratory, Report WT-1612, 16 July 1962.

Moulton, J. F., Jr. (ed.), *Nuclear Weapons Blast Phenomena,* Defense Atomic Support Agency, DASA Report 1200, March 1960.

Physics International, informal discussions and papers for the Defense Atomic Support Agency, 1968.

(b)(2) [redacted]

Sauer, F. M., 3d, *Nuclear Geoplosics: Vol. IV, Empirical Analysis of Ground Motion and Cratering,* Defense Atomic Support Agency, DASA Report 1285, May 1964.

(b)(2) [redacted]

DISTRIBUTION LIST

DEPARTMENT OF DEFENSE

(b)(6) Assistant to the Secretary of Defense
Atomic Energy
ATTN: Mil Appl, [redacted]

Defense Advanced Rsch Proj Agency
ATTN: TTO

Defense Nuclear Agency
ATTN: SPTD
ATTN: SPSS
ATTN: SPAS
4 cy ATTN: TITL

Defense Tech Info Ctr
2 cy ATTN: DD

Field Command
(b)(6) Defense Nuclear Agency
ATTN: FCTT, [redacted]
ATTN: FCTT, [redacted]

Field Command
Defense Nuclear Agency
Livermore Br
ATTN: FC-1

Field Command
Defense Nuclear Agency
Los Alamos Br
ATTN: MS-635, FC-2

Interservice Nuclear Weapons School
ATTN: TTV, 3416th TTSQ

DEPARTMENT OF THE ARMY

Harry Diamond Labs
(b)(6) ATTN: DELHD-NW-RA
ATTN: DELHD-TD, [redacted]
ATTN: DELHD-NW-P, [redacted]

US Army Ballistic Rsch Labs
ATTN: DRDAR-BLV

US Army Materiel Dev & Readiness Cmd
ATTN: DRCDE-DM, Spec Mun Sys Dev
ATTN: DRCNC, Nuc-Chem Ofc

US Army Materiel Sys Analysis Actvy
ATTN: DRXSY-DS
ATTN: DRXSY-CR
ATTN: DRXSY-S

US Army Nuclear & Chemical Agency
ATTN: Library for MONA-SAL
(b)(6) ATTN: Library for MONA-ZB
ATTN: MONA-OPS, [redacted]
ATTN: Library

US Army TRADOC Sys Analysis Actvy
ATTN: ATAA-TDC, [redacted]

(b)(6) US Army Training and Doctrine Comd
ATTN: ATCD-NN
ATTN: ATOO-NCO

DEPARTMENT OF THE ARMY (Continued)

(b)(6) US Army War College
ATTN: AWCI, [redacted]

DEPARTMENT OF THE NAVY

David Taylor Naval Ship R&D Ctr
ATTN: Code 174, Code 186

Joint Cruise Missiles Project Ofc
ATTN: JCM-G

Naval Air Systems Cmd
ATTN: AIR-54/33D

Naval Material Cmd
ATTN: MAT-OON

Naval Ocean Systems Ctr
ATTN: Rsch Library

Naval Postgraduate School
ATTN: Code 1424, Library

Naval Sea Systems Cmd
ATTN: SEA-643

(b)(6) Naval Surface Weapons Ctr
ATTN: Code F32, [redacted]
ATTN: Code X211
ATTN: Code F31

Naval War College
ATTN: I2
ATTN: Ctr for War Gaming

Naval Weapons Evaluation Facility
ATTN: Code 70

Office of Naval Rsch
ATTN: Code 713

(b)(6) Theater Nuclear Warfare Prj Ofc
ATTN: PM-23, [redacted]

DEPARTMENT OF THE AIR FORCE

Air Force Weapons Lab
ATTN: SUL
ATTN: NSSB
ATTN: AFWL, SA
ATTN: NTN

Air University Library
ATTN: AUL-LSE

(b)(6) Headquarters
Air Force Systems Cmd
ATTN: [redacted]

Deputy Chief of Staff
Rsch, Dev, & Acq
ATTN: AFRDQI

(b)(6)

DEPARTMENT OF ENERGY

Department of Energy
ATTN: OMA,

OTHER GOVERNMENT AGENCY

Central Intelligence Agency
ATTN: OSWR/NED

DEPARTMENT OF ENERGY CONTRACTORS

University of California
Lawrence Livermore National Lab
ATTN: L-9, [redacted]
ATTN: L-21 [redacted]
ATTN: L-9, [redacted]

Los Alamos National Lab
ATTN: [redacted]

Sandia National Lab
ATTN: 5613, R. Stratton
ATTN: 5612, J. Keizur

(b)(6)

DEPARTMENT OF DEFENSE CONTRACTORS

Kaman Sciences Corp
ATTN: [redacted]

Kaman Tempo
ATTN: DASIAC

Mission Rsch Corp
ATTN: Tech Library

DEPARTMENT OF DEFENSE CONTRACTORS (Continued)

Pacific-Sierra Rsch Corp
3 cy ATTN: [redacted] Chairman SAGE

R & D Associates
ATTN: [redacted]
3 cy ATTN: [redacted]

Rand Corp
ATTN: Library
ATTN: [redacted]

S-CUBED
ATTN: [redacted]

(b)(6)

Santa Fe Corp
ATTN: [redacted]

Science Applications, Inc
ATTN: [redacted]
ATTN: [redacted]

Science Applications, Inc
ATTN: [redacted]

SRI International
ATTN: [redacted]
ATTN: [redacted]

SRI International
ATTN: [redacted]